

THE FEDERAL DEMOCRATIC REPUBLIC OF ETHIOPIA  
GEOLOGICAL SURVEY OF ETHIOPIA (GSE)

DATA COLLECTION SURVEY FOR  
GEOTHERMAL DEVELOPMENT  
IN ETHIOPIA

FINAL REPORT (APPENDIX)

JUNE 2017

JAPAN INTERNATIONAL COOPERATION AGENCY (JICA)

NIPPON KOEI CO., LTD.  
JMC GEOTHERMAL ENGINEERING CO., LTD.  
SUMIKO RESOURCES EXPLORATION AND  
DEVELOPMENT CO., LTD.

## **Appendices**

Appendix-1: Geological Reconnaissance Survey

Appendix-2: MT/TEM Survey

Appendix-3: Gravity Survey

Appendix-4: Micro-seismic Monitoring

Appendix-5: Temperature Survey

Appendix-6: Environmental, Social Impact Assessment

Appendix-7: Drilling Program

Appendix-8: Minutes of Meetings

Appendix-9: Improvement of Calculating Formulas for Geothermal Volumetric Assessment

Appendix-10: An Outline of Countermeasures against Scale

Appendix-11: Civil Works (Access Road, Drilling Pad, and Water Supply System)



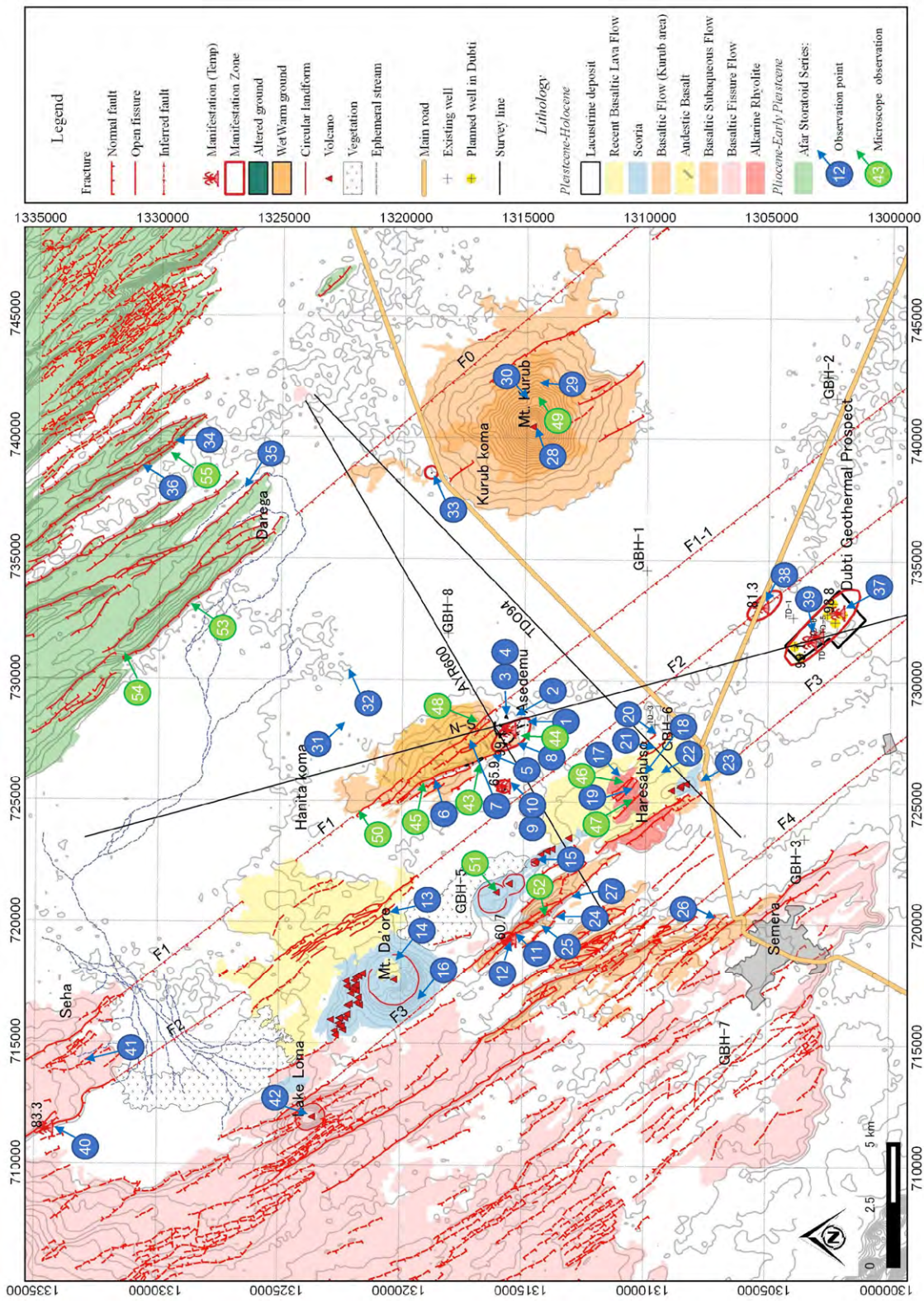
## **APPENDIX-1**

### **Geological Reconnaissance Survey**



## Appendix-1 Geological Surface Survey

### A1.1 Geological reconnaissance survey in Tendaho-2



Source: JICA Survey Team

Figure A1.1.1 Tendaho-2 Location Map of Photo Recording

## Tendaho-2 (Ayrobera)



1. Wet/warm grounds with temperature over 50 °C aligned in NNE-SSW direction in Asedemu area. Due to wet condition, glass covers around the wet/warm ground
2. Fumarole with maximum temperature 99.1 °C in Asedemu area. Gas sample was collected in MP study. Dry steam is dominated.



3. White-colored calcite alteration in alluvium deposit around Asedemu area, which is supposed to be wet/warm ground. Shrub grows around the altered ground.
4. Close-up of calcite alteration. Univalve shell fossil and sand is cemented with calcite.



5. Small hill along fault F1 composed of silica-gypsum altered rocks
6. Fault cliff and rift along fault F1-2. Rift has around 150 km width and covered with sand.

	
7. Pillow structure observed in subaqueous basalt in Asedemu basaltic plateau.	8. Sedimentary layer composed of sand, silt, and clay with clear stratified structure in Asedemu area. Basaltic flow covers on the top of the layer. Lamination can be observed in the layer.
	
9. White colored and consolidated Calcite alternation surrounding basaltic eruption center.	10. Wet/warm ground with maximum temperature 65.9 °C around the basaltic eruption center. Glass also grows in wet/warm ground.
	
11. Fumaroles along fault F3 with maximum temperature 60.7 °C. Dry steam is dominated.	12. Horst topography between faults near the fumaroles. Sedimentary layer is interbedded in basalts.

	
13. Fresh and deep open fissure without displacement in recent basaltic lava flow.	14. Recent basaltic lava flow in dark brown scoria cone located in spreading main axis.
	
15. Maar with spring water with normal temperature 27.5 °C in the center of cone. Scoria, pumice, and basaltic lava are observed in the maar.	16. Scoria and pumice layer with clear stratified structure observed gully in Da'ore volcanic mountain showing tuff ring.
	
17. Rhyolite surrounded and partially covered by basaltic flows, which has clear flow structure.	18. Plateau composed of Rhyolite is cut and displaced by several normal faults. Rhyolite is weathered and brown-colored.

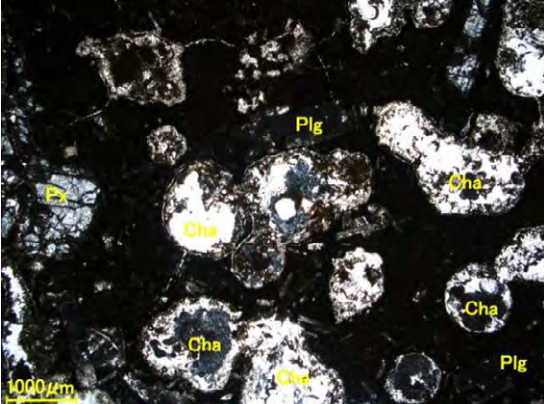
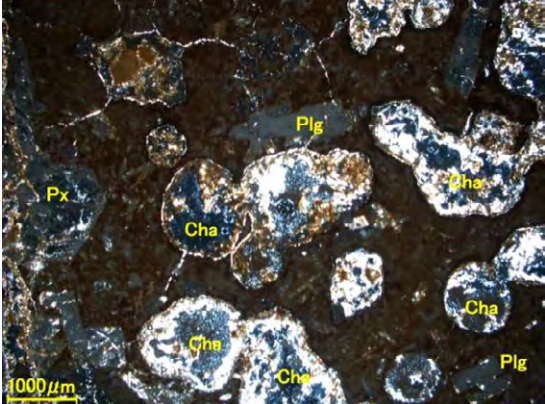
	
19. Fault plane with slickenside in rhyolite with steep (85~90 degree dipping to east)	20. Termination of site survey due to bad road condition.
	
21. Ropy texture in pahoehoe lava. Due to fault movement, surface of the lava was tilting.	22. Fissure eruption of basaltic lava along open crack of the elder basaltic flow.
	
23. Pyroclastic deposit including tuff, scoria, and pumice with clear stratified structure.	24. Stratified silt and clay sedimentary layer. Basaltic lava covers on the top of the layer.

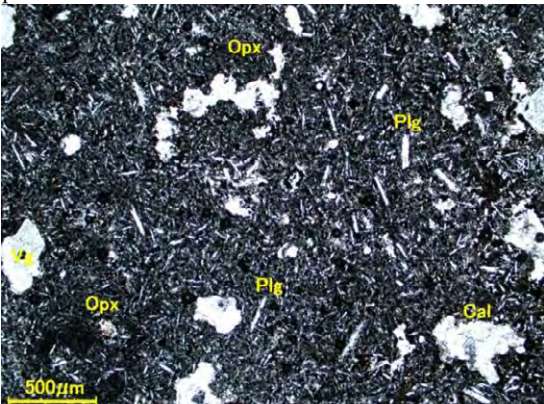
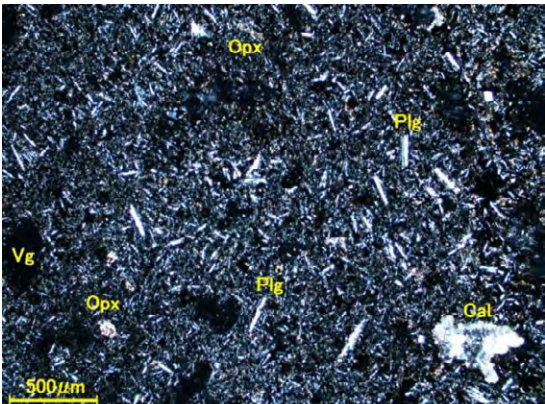
25. High and rectilinear fault cliff. Displacement of the layer by echelon pattern normal fault can be observed in the center of the photo. On the toe of the slope, there is a green bush due to spring water.	26. NNW-SSE oriented fault cliff composed of slightly weathered basalt.
27. Highly fractured and weathered fissure basalt.	28. Old volcanic vent at the top of Mt. Kurub, covered by sand and soil.
29. Small lateral volcano in Mr. Kurub.	30. Columnar joint in basaltic flow in Mt. Kurub

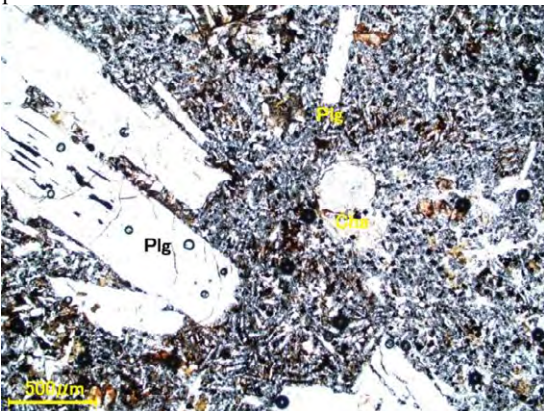
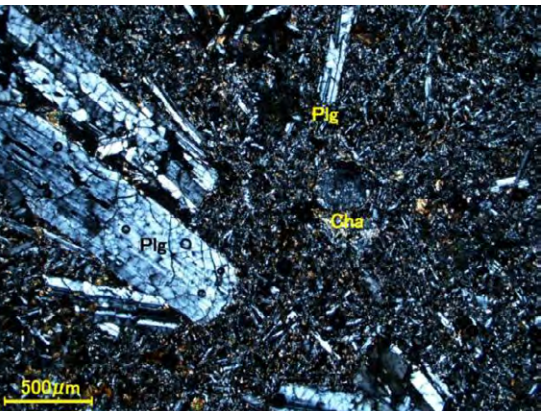
	
31. Sand dune in flat area of alluvium deposit east of Asedemu area	32. Overview of alluvium deposit area covered with sand and soil east of Asedemu area. 4WD vehicle can run throughout the desert.
	
33. "Geothermal Glass", which is commonly observed in geothermal manifestation. Calcite alternation can be observed near the glass.	34. Clear and rectilinear fault along fault F0, exposed with basalt in Afar stratoid series.
	
35. Fault cliff and alluvium deposit plane. White part in the plane shows assembly of univalve shell fossils.	36. Close-up of basalt of Afar stratoid series. The rock is hard and dense. Vesicles are aligned in some direction.

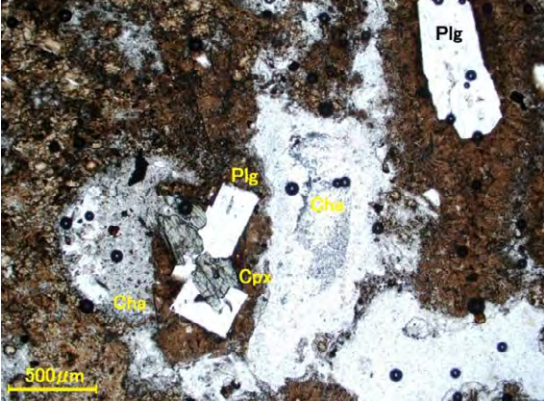
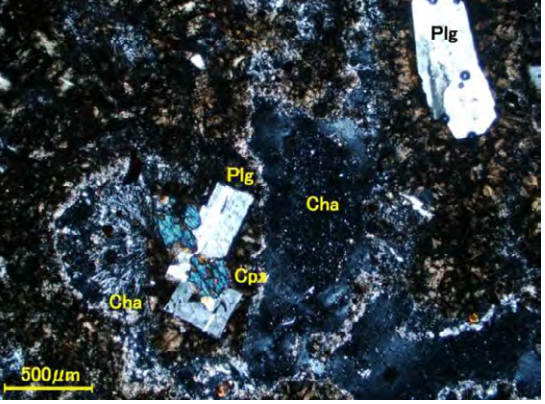
	
37. Hot spring in Dubti; the hot water contains mud and bubbles.	38. Wet/warm ground on alluvium deposit along fault F2.
	
39. Tilting wellhead valve of TD-6, due to deformation of ground.	40. Hot spring in Seha, with maximum temperature is 83.3 °C. *Photo was taken in the Master Plan study.
	
41. Weak fumarole found at cavity in basalt. *Photo was taken in the Master Plan study.	42. Caldera lake named Lake Loma. Low temperature spring water was found. *Photo was taken in the Master Plan study.

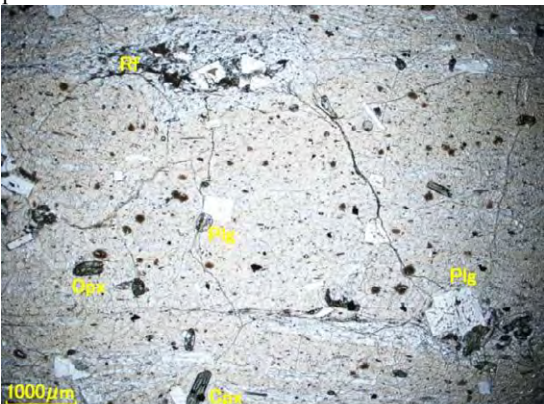
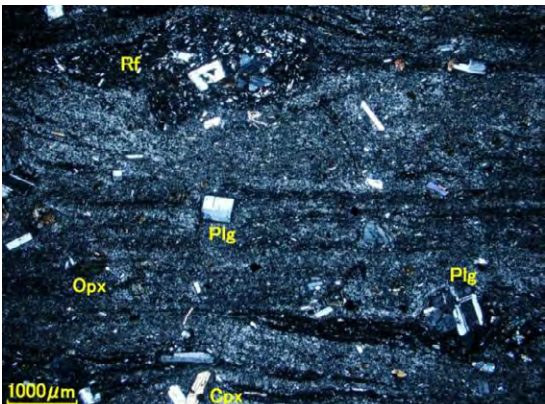
## Microscope observation

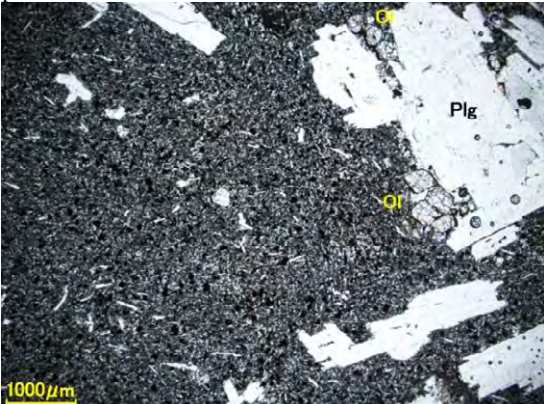
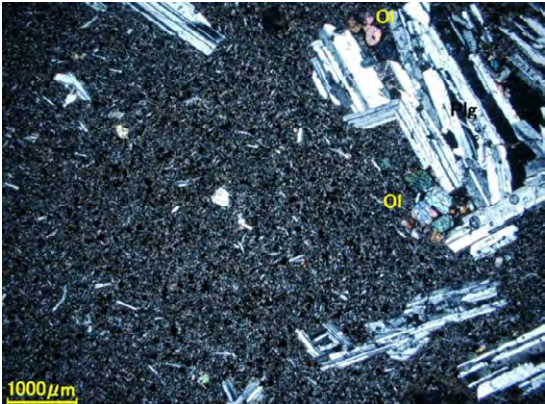
Site No.	43	Rock name	Highly altered basalt																		
Open			Crossed																		
																					
			Plg: Plagioclase, Px: pyroxene, Cha: chalcedony																		
Mineral composition:			Note: Totally high alteration. Ground mass composed of volcanic glass, which is devitrified to chalcedony. Phenocrysts are plagioclase and pyroxene.																		
<table border="1"> <thead> <tr> <th>Mineral</th> <th>Modal (%)</th> <th>Texture</th> </tr> </thead> <tbody> <tr> <td>Volcanic glass</td> <td>55</td> <td></td> </tr> <tr> <td>Plagioclase</td> <td>20</td> <td>Anhedral</td> </tr> <tr> <td>Pyroxene</td> <td>18</td> <td>Anhedral</td> </tr> <tr> <td>Calcite</td> <td>5</td> <td>Anhedral</td> </tr> <tr> <td>Chalcedony</td> <td>2</td> <td>Radial fibrous</td> </tr> </tbody> </table>			Mineral	Modal (%)	Texture	Volcanic glass	55		Plagioclase	20	Anhedral	Pyroxene	18	Anhedral	Calcite	5	Anhedral	Chalcedony	2	Radial fibrous	
Mineral	Modal (%)	Texture																			
Volcanic glass	55																				
Plagioclase	20	Anhedral																			
Pyroxene	18	Anhedral																			
Calcite	5	Anhedral																			
Chalcedony	2	Radial fibrous																			

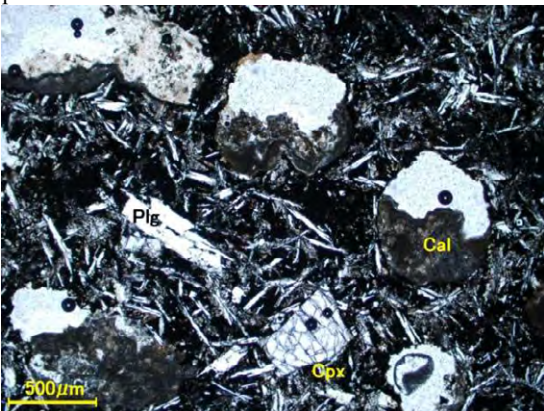
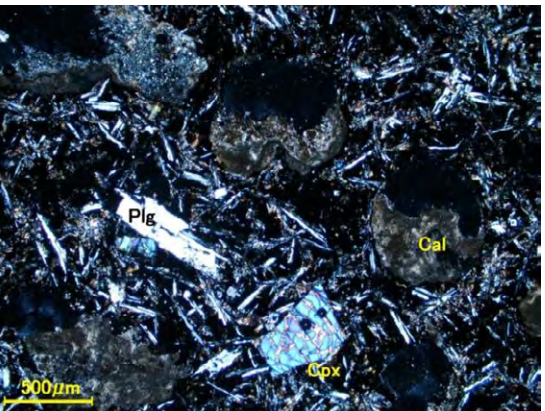
Site No.	44	Rock name	Intergranular vesicular basalt																								
Open			Crossed																								
																											
			Plg: Plagioclase, Opx: orthopyroxene, Vg: Volcanic glass, Cal: Calcite																								
Mineral composition:			Note: Ground mass is composed of colored mineral (pyroxene) and opaque mineral which fill between lath plagioclase phenocrysts. Phenocrysts are plagioclase and orthopyroxene. Some of vesicles are filled with calcite.																								
<table border="1"> <thead> <tr> <th>Mineral</th> <th>Modal (%)</th> <th>Texture</th> </tr> </thead> <tbody> <tr> <td>Microlite plagioclase</td> <td>35</td> <td>Microlitic</td> </tr> <tr> <td>Pyroxene</td> <td>20</td> <td>Fine, Anhedral</td> </tr> <tr> <td>Opaque (Fe-oxide)</td> <td>17</td> <td>Fine, Anhedral</td> </tr> <tr> <td>Calcite</td> <td>8</td> <td>Anhedral</td> </tr> <tr> <td>Chalcedony</td> <td>2</td> <td>Radial fibrous</td> </tr> <tr> <td>Volcanic glass</td> <td>15</td> <td></td> </tr> <tr> <td>Zeolite</td> <td>3</td> <td></td> </tr> </tbody> </table>			Mineral	Modal (%)	Texture	Microlite plagioclase	35	Microlitic	Pyroxene	20	Fine, Anhedral	Opaque (Fe-oxide)	17	Fine, Anhedral	Calcite	8	Anhedral	Chalcedony	2	Radial fibrous	Volcanic glass	15		Zeolite	3		
Mineral	Modal (%)	Texture																									
Microlite plagioclase	35	Microlitic																									
Pyroxene	20	Fine, Anhedral																									
Opaque (Fe-oxide)	17	Fine, Anhedral																									
Calcite	8	Anhedral																									
Chalcedony	2	Radial fibrous																									
Volcanic glass	15																										
Zeolite	3																										

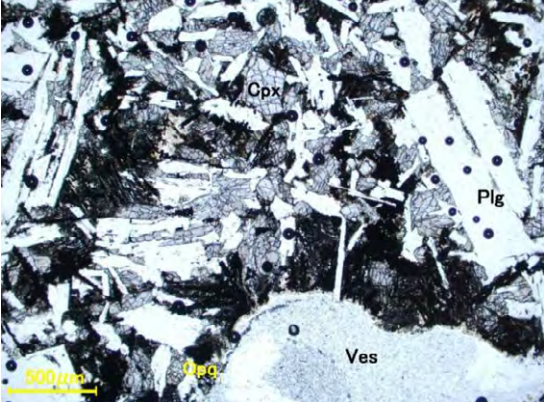
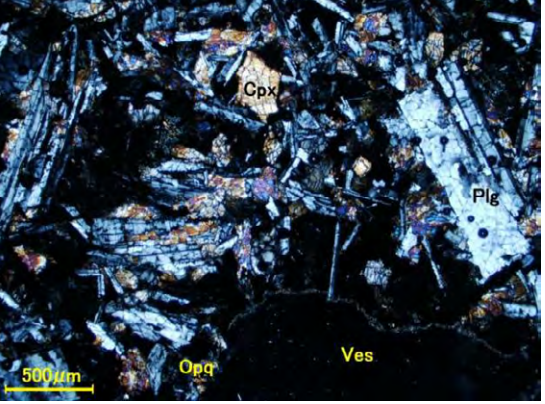
Site No.	45	Rock name	Intergranular and porphyritic basalt
Open			
			
Crossed			
			
Plg: Plagioclase, Cha: chalcedony			
Mineral composition:			
Mineral	Modal (%)	Texture	
Plagioclase	42	Lath, Tabular	
Pyroxene	25	Fine, Anhedral	
Devitrified volcanic glass	20		
Opaque (Fe-oxide)	7	Anhedral	
Chalcedony	6	Radial fibrous	

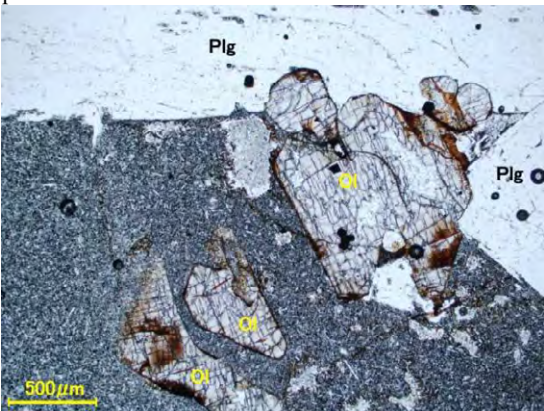
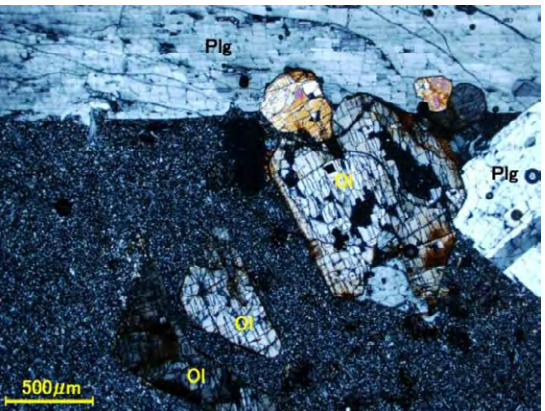
Site No.	46	Rock name	Vitrophyric rhyolitic tuff
Open			
			
Crossed			
			
Plg: Plagioclase, Cpx: clinopyroxene, Cha: chalcedony			
Mineral composition:			
Mineral	Modal (%)	Texture	
Volcanic glass	50		
Plagioclase	20	Anhedral	
Pyroxene	15	Anhedral	
Calcite	10	Anhedral	
Opaque (Fe-oxide)	3	Anhedral	
Chalcedony	2	Radial fibrous	

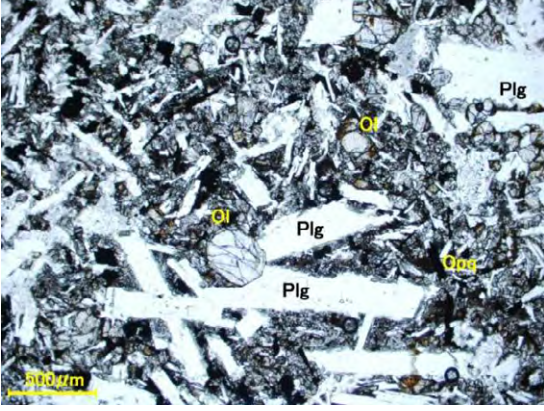
Site No.	47	Rock name	Vitrophyric and lithic rhyolitic tuff																					
Open			Crossed																					
																								
Plg: Plagioclase, Cpx: clinopyroxene, Opx: orthopyroxene, Rf: rock fragment																								
Mineral composition: <table border="1"> <thead> <tr> <th>Mineral</th> <th>Modal (%)</th> <th>Texture</th> </tr> </thead> <tbody> <tr> <td>Volcanic glass</td> <td>48</td> <td></td> </tr> <tr> <td>Plagioclase</td> <td>22</td> <td>Tabular</td> </tr> <tr> <td>Chalcedony</td> <td>14</td> <td>Radial fibrous</td> </tr> <tr> <td>Pyroxene</td> <td>8</td> <td>Euhedral</td> </tr> <tr> <td>Rock fragment</td> <td>6</td> <td></td> </tr> <tr> <td>Opaque (Fe-oxide)</td> <td>2</td> <td>Euhedral</td> </tr> </tbody> </table>			Mineral	Modal (%)	Texture	Volcanic glass	48		Plagioclase	22	Tabular	Chalcedony	14	Radial fibrous	Pyroxene	8	Euhedral	Rock fragment	6		Opaque (Fe-oxide)	2	Euhedral	Note: Matrix composed of volcanic glass shows lamella structure. Plagioclase, pyroxene, and rock fragment lie on the matrix.
Mineral	Modal (%)	Texture																						
Volcanic glass	48																							
Plagioclase	22	Tabular																						
Chalcedony	14	Radial fibrous																						
Pyroxene	8	Euhedral																						
Rock fragment	6																							
Opaque (Fe-oxide)	2	Euhedral																						

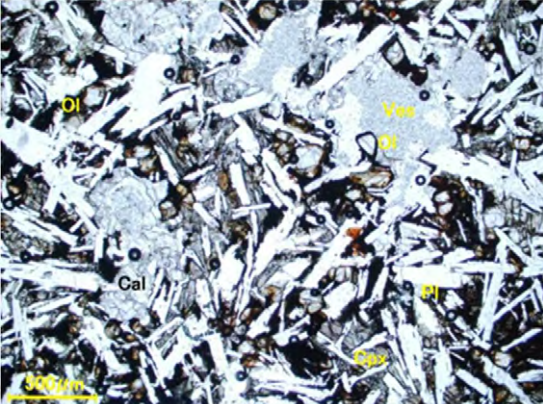
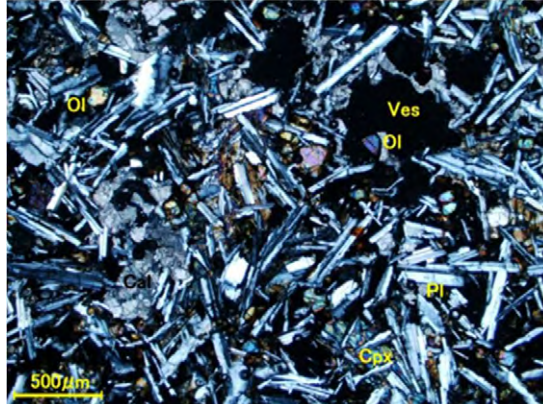
Site No.	48	Rock name	Vesicular and glomeroporphyritic basalt																								
Open			Crossed																								
																											
Plg: Plagioclase, Ol: Olivine																											
Mineral composition: <table border="1"> <thead> <tr> <th>Mineral</th> <th>Modal (%)</th> <th>Texture</th> </tr> </thead> <tbody> <tr> <td>Plagioclase</td> <td>40</td> <td>Lath, Tabular</td> </tr> <tr> <td>Pyroxene</td> <td>30</td> <td>Anhedral-Euhedral</td> </tr> <tr> <td>Opaque (Fe-oxide)</td> <td>10</td> <td>Anhedral-Euhedral</td> </tr> <tr> <td>Olivine</td> <td>7</td> <td>Euhedral</td> </tr> <tr> <td>Calcite</td> <td>5</td> <td>Anhedral</td> </tr> <tr> <td>Volcanic glass</td> <td>5</td> <td></td> </tr> <tr> <td>Chalcedony</td> <td>3</td> <td>Radial fibrous</td> </tr> </tbody> </table>			Mineral	Modal (%)	Texture	Plagioclase	40	Lath, Tabular	Pyroxene	30	Anhedral-Euhedral	Opaque (Fe-oxide)	10	Anhedral-Euhedral	Olivine	7	Euhedral	Calcite	5	Anhedral	Volcanic glass	5		Chalcedony	3	Radial fibrous	Note: Ground mass is composed of fine plagioclase, pyroxene, and opaque mineral. Phenocrysts are plagioclase and olivine. Plagioclase phenocrysts shows glomeroporphyritic texture. Some vesicles are filled with calcite and chalcedony.
Mineral	Modal (%)	Texture																									
Plagioclase	40	Lath, Tabular																									
Pyroxene	30	Anhedral-Euhedral																									
Opaque (Fe-oxide)	10	Anhedral-Euhedral																									
Olivine	7	Euhedral																									
Calcite	5	Anhedral																									
Volcanic glass	5																										
Chalcedony	3	Radial fibrous																									

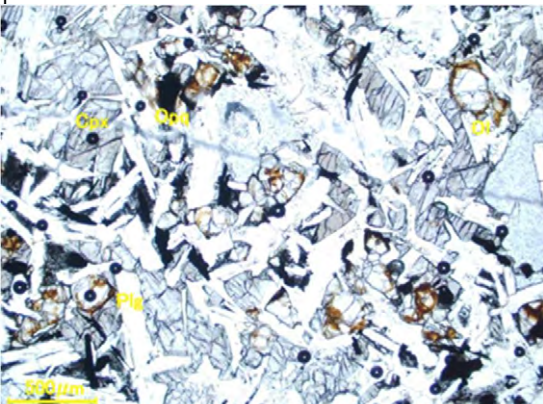
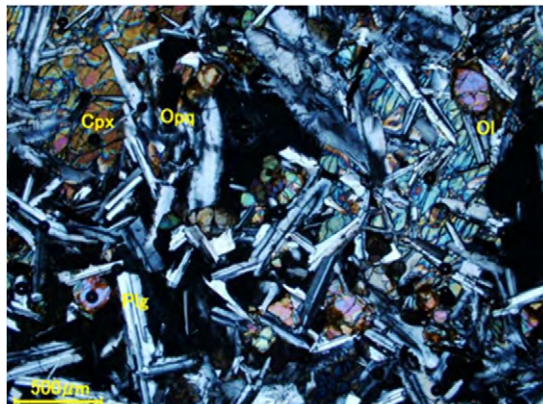
Site No.	49	Rock name	Vesicular and intergranular basalt																					
Open	Crossed																							
																								
Plg: Plagioclase, Cpx: clinopyroxene, Cal: Calcite																								
Mineral composition:			Note: Ground mass in composed of colored mineral (pyroxene) and opaque mineral, which fill intergranular of lath plagioclase. Phenocrysts of plagioclase and clinopyroxene is observed. Calcite fills some vesicle.																					
<table border="1"> <thead> <tr> <th>Mineral</th> <th>Modal (%)</th> <th>Texture</th> </tr> </thead> <tbody> <tr> <td>Plagioclase</td> <td>38</td> <td>Anhedral</td> </tr> <tr> <td>Pyroxene</td> <td>36</td> <td>Anhedral</td> </tr> <tr> <td>Calcite</td> <td>10</td> <td>Anhedral</td> </tr> <tr> <td>Opaque (Fe-oxide)</td> <td>15</td> <td>Anhedral</td> </tr> <tr> <td>Volcanic glass</td> <td>5</td> <td></td> </tr> <tr> <td>Olivine</td> <td>Trace</td> <td>Anhedral</td> </tr> </tbody> </table>			Mineral	Modal (%)	Texture	Plagioclase	38	Anhedral	Pyroxene	36	Anhedral	Calcite	10	Anhedral	Opaque (Fe-oxide)	15	Anhedral	Volcanic glass	5		Olivine	Trace	Anhedral	
Mineral	Modal (%)	Texture																						
Plagioclase	38	Anhedral																						
Pyroxene	36	Anhedral																						
Calcite	10	Anhedral																						
Opaque (Fe-oxide)	15	Anhedral																						
Volcanic glass	5																							
Olivine	Trace	Anhedral																						

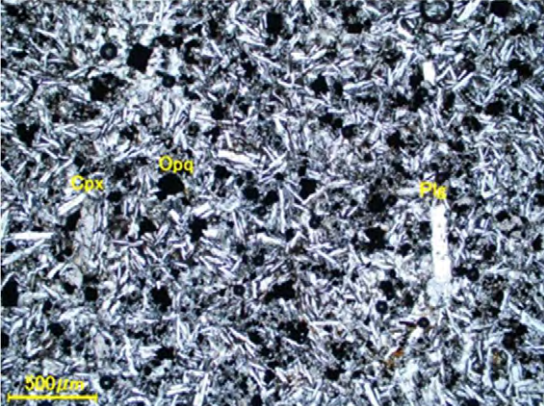
Site No.	50	Rock name	Vesicular and seriate basalt																		
Open	Crossed																				
																					
Plg: Plagioclase, Cpx: clinopyroxene, Opq: Opaque, Ves: vesicle																					
Mineral composition:			Note: Clinopyroxene and opaque mineral fill intergranular of strip form or lath plagioclases, which shows seriate texture that has several grain size of phenocryst from coarse to fine. Vesicle is also observed.																		
<table border="1"> <thead> <tr> <th>Mineral</th> <th>Modal (%)</th> <th>Texture</th> </tr> </thead> <tbody> <tr> <td>Plagioclase</td> <td>40</td> <td>Lath</td> </tr> <tr> <td>Pyroxene</td> <td>38</td> <td>Anhedral</td> </tr> <tr> <td>Volcanic glass</td> <td>12</td> <td></td> </tr> <tr> <td>Opaque (Fe-oxide)</td> <td>8</td> <td>Euhedral-Anhedral</td> </tr> <tr> <td>Calcite</td> <td>2</td> <td>Anhedral</td> </tr> </tbody> </table>			Mineral	Modal (%)	Texture	Plagioclase	40	Lath	Pyroxene	38	Anhedral	Volcanic glass	12		Opaque (Fe-oxide)	8	Euhedral-Anhedral	Calcite	2	Anhedral	
Mineral	Modal (%)	Texture																			
Plagioclase	40	Lath																			
Pyroxene	38	Anhedral																			
Volcanic glass	12																				
Opaque (Fe-oxide)	8	Euhedral-Anhedral																			
Calcite	2	Anhedral																			

Site No.	51	Rock name	Porphyritic olivine basalt																		
Open			Crossed																		
																					
			Plg: Plagioclase, Ol: Olivine																		
Mineral composition:			Note: Ground mass is observed very fine. Phenocrysts are plagioclase and olivine. Major axis of plagioclase phenocryst is maximum approx. 7mm.																		
<table border="1"> <thead> <tr> <th>Mineral</th> <th>Modal (%)</th> <th>Texture</th> </tr> </thead> <tbody> <tr> <td>Microlite plagioclase</td> <td>50</td> <td>Microlitic</td> </tr> <tr> <td>Pyroxene</td> <td>24</td> <td>Fine, Anhedral</td> </tr> <tr> <td>Opaque (Fe-oxide)</td> <td>20</td> <td>Fine,Euhedral-Anhedral</td> </tr> <tr> <td>Olivine</td> <td>5</td> <td>Euhedral</td> </tr> <tr> <td>Chalcedony</td> <td>1</td> <td>Radial fibrous</td> </tr> </tbody> </table>			Mineral	Modal (%)	Texture	Microlite plagioclase	50	Microlitic	Pyroxene	24	Fine, Anhedral	Opaque (Fe-oxide)	20	Fine,Euhedral-Anhedral	Olivine	5	Euhedral	Chalcedony	1	Radial fibrous	
Mineral	Modal (%)	Texture																			
Microlite plagioclase	50	Microlitic																			
Pyroxene	24	Fine, Anhedral																			
Opaque (Fe-oxide)	20	Fine,Euhedral-Anhedral																			
Olivine	5	Euhedral																			
Chalcedony	1	Radial fibrous																			

Site No.	52	Rock name	Intergranular basalt															
Open			Crossed															
																		
			Plg: Plagioclase, Ol: Olivine, Opq: Opaque															
Mineral composition:			Note: Ground mass is composed of colored mineral (pyroxene) and opaque mineral filling intergranular of lath plagioclases. Phenocrysts are plagioclase and olivine.															
<table border="1"> <thead> <tr> <th>Mineral</th> <th>Modal (%)</th> <th>Texture</th> </tr> </thead> <tbody> <tr> <td>Plagioclase</td> <td>40</td> <td>Lath</td> </tr> <tr> <td>Pyroxene</td> <td>38</td> <td>Anhedral</td> </tr> <tr> <td>Olivine</td> <td>14</td> <td>Euhedral</td> </tr> <tr> <td>Opaque (Fe-oxide)</td> <td>8</td> <td>Euhedral-Anhedral</td> </tr> </tbody> </table>			Mineral	Modal (%)	Texture	Plagioclase	40	Lath	Pyroxene	38	Anhedral	Olivine	14	Euhedral	Opaque (Fe-oxide)	8	Euhedral-Anhedral	
Mineral	Modal (%)	Texture																
Plagioclase	40	Lath																
Pyroxene	38	Anhedral																
Olivine	14	Euhedral																
Opaque (Fe-oxide)	8	Euhedral-Anhedral																

Site No.	53	Rock name	Intergranular basalt																					
Open			Crossed																					
																								
Plg: Plagioclase, Ol: Olivine, Cpx: Clinopyroxene, Cal: Calcite, Ves: Vesicle																								
Mineral composition: <table border="1"> <thead> <tr> <th>Mineral</th> <th>Modal (%)</th> <th>Texture</th> </tr> </thead> <tbody> <tr> <td>Plagioclase</td> <td>33</td> <td>Lath</td> </tr> <tr> <td>Pyroxene</td> <td>32</td> <td>Anhedral</td> </tr> <tr> <td>Olivine</td> <td>17</td> <td>Euhedral</td> </tr> <tr> <td>Calcite</td> <td>7</td> <td>Anhedral</td> </tr> <tr> <td>Volcanic glass</td> <td>7</td> <td></td> </tr> <tr> <td>Opaque (Fe-oxide)</td> <td>4</td> <td>Euhedral-Anhedral</td> </tr> </tbody> </table>			Mineral	Modal (%)	Texture	Plagioclase	33	Lath	Pyroxene	32	Anhedral	Olivine	17	Euhedral	Calcite	7	Anhedral	Volcanic glass	7		Opaque (Fe-oxide)	4	Euhedral-Anhedral	Note: Colored mineral (pyroxene and olivine) and opaque mineral fill intergranular of lath plagioclases. Plagioclase phenocryst is observed approx. 2mm in major axis. Some vesicles are filled with calcite.
Mineral	Modal (%)	Texture																						
Plagioclase	33	Lath																						
Pyroxene	32	Anhedral																						
Olivine	17	Euhedral																						
Calcite	7	Anhedral																						
Volcanic glass	7																							
Opaque (Fe-oxide)	4	Euhedral-Anhedral																						

Site No.	54	Rock name	Intergranular and porphyritic olivine basalt																		
Open			Crossed																		
																					
Plg: Plagioclase, Ol: Olivine, Cpx: Clinopyroxene, Opq: Opaque																					
Mineral composition: <table border="1"> <thead> <tr> <th>Mineral</th> <th>Modal (%)</th> <th>Texture</th> </tr> </thead> <tbody> <tr> <td>Plagioclase</td> <td>38</td> <td>Lath, Tabular</td> </tr> <tr> <td>Pyroxene</td> <td>36</td> <td>Anhedral</td> </tr> <tr> <td>Olivine</td> <td>16</td> <td>Euhedral</td> </tr> <tr> <td>Opaque (Fe-oxide)</td> <td>7</td> <td>Euhedral-Anhedral</td> </tr> <tr> <td>Volcanic glass</td> <td>3</td> <td></td> </tr> </tbody> </table>			Mineral	Modal (%)	Texture	Plagioclase	38	Lath, Tabular	Pyroxene	36	Anhedral	Olivine	16	Euhedral	Opaque (Fe-oxide)	7	Euhedral-Anhedral	Volcanic glass	3		Note: Colored mineral (pyroxene and olivine) and opaque mineral fill intergranular of lath plagioclases. Plagioclase phenocryst is observed approx. 5mm in major axis.
Mineral	Modal (%)	Texture																			
Plagioclase	38	Lath, Tabular																			
Pyroxene	36	Anhedral																			
Olivine	16	Euhedral																			
Opaque (Fe-oxide)	7	Euhedral-Anhedral																			
Volcanic glass	3																				

Site No.	55	Rock name	Intergranular basalt																					
Open	Crossed																							
																								
Plg: Plagioclase, Cpx: Clinopyroxene, Opq: Opaque																								
<table border="1"> <thead> <tr> <th colspan="3">Mineral composition:</th> </tr> <tr> <th>Mineral</th> <th>Modal (%)</th> <th>Texture</th> </tr> </thead> <tbody> <tr> <td>Plagioclase</td> <td>40</td> <td>Lath</td> </tr> <tr> <td>Pyroxene</td> <td>39</td> <td>Anhedral</td> </tr> <tr> <td>Opaque (Fe-oxide)</td> <td>11</td> <td>Euhedral-Anhedral</td> </tr> <tr> <td>Volcanic glass</td> <td>7</td> <td></td> </tr> <tr> <td>Calcite</td> <td>3</td> <td>Anhedral</td> </tr> </tbody> </table>			Mineral composition:			Mineral	Modal (%)	Texture	Plagioclase	40	Lath	Pyroxene	39	Anhedral	Opaque (Fe-oxide)	11	Euhedral-Anhedral	Volcanic glass	7		Calcite	3	Anhedral	Note: Ground mass is composed of colored mineral (pyroxene) and opaque mineral filling intergranular of lath plagioclases. Phenocryst is not almost observed.
Mineral composition:																								
Mineral	Modal (%)	Texture																						
Plagioclase	40	Lath																						
Pyroxene	39	Anhedral																						
Opaque (Fe-oxide)	11	Euhedral-Anhedral																						
Volcanic glass	7																							
Calcite	3	Anhedral																						

## A1.2 Geological reconnaissance survey in Boseti

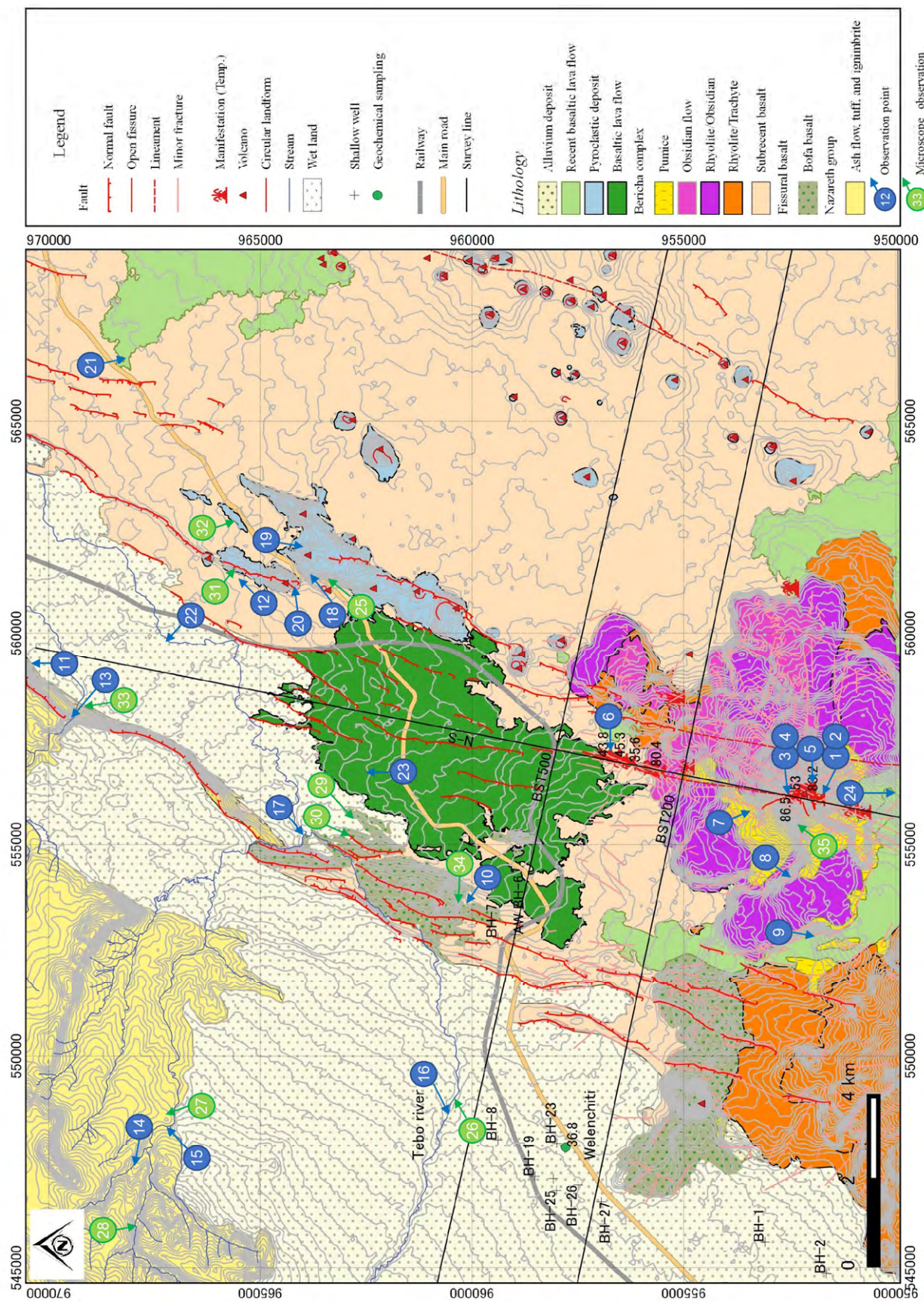


Figure A1.2.1 Boseti Location Map of Photo Recording

## Boseti

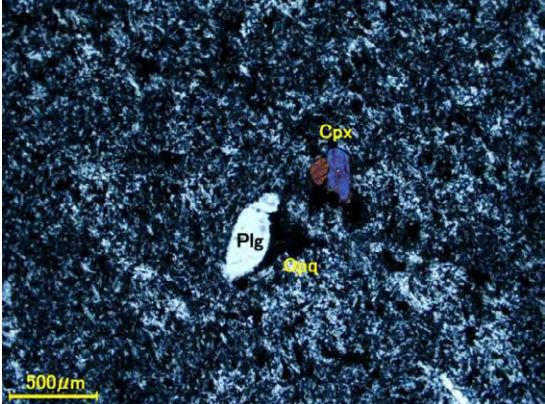
	
1. Old volcanic vent on the top of Mt. Bericha. There are fumaroles around the vent. Lava flowed northward (upward of the photograph).	2. Fumaroles with dry steam of maximum temperature 82.8°C from altered pumice layer around the volcanic vent.
	
3. Open flank fissure with 5-10m deep near the top of Mt. Bericha. There are fumaroles from the fissure, and steam filled in the fissure.	4. Fumaroles in the flank fissure. Maximum temperature is 86.5 °C.
	
5. Fumaroles in the gully near the top of Mt. Bericha. *Photo was taken in the Master Plan study.	6. One of fumaroles at the northern foot of the mountain. Hot steam from cavity in basaltic flow is utilized for sauna for local people. Temperature is from 35.6 to 80.4 °C.

	
7. Overview of Mt. Bericha, the flank fissure can be clearly observed on northern slope of the mountain.	8. Fresh and unconsolidated pumice layer on western side of Mt.Bericha.
	
9. Fresh recent basaltic lava flow filled in the valley, covered with green low glasses.	10. Hard and intact Bofa basalt in the quarry.
	
11. Fault cliff with about 200m height on the north of the survey area. Tuff layer can be observed on upper part of the cliff.	12. NNE-SSW oriented fault F1-1, dipping to west cuts scoria layer.

	
13. Dried-up water fall continuing fault cliff of fault F2. Tuff layer above ignimbrite can be observed on the slope.	14. Weathered ignimbrite interbedded with tuffaceous silt in dried-up valley.
	
15.. Calcite vein( near the hummer) with NNE-SSW and E-W direction in the highly weathered ignimbrite.	16. Fresh and clearly stratified ash deposit including pumice, observed on the undercut slope of river.
	
17. Basaltic flow observed on river bed. Highly fractured but dense and intact Aphyric basalt.	18. Rhyolite dome near the scoria cones. Rhyolite is highly weathered and fractured.

	
19. Silica vein in rhyolite dome.	20. Brown to reddish stratified volcanic ash layer including pumice coarse fragment and black scoria above light brown rhyolite with flow structure.
	
21. Aa lava at the tip of recent basaltic flow.	22. Stratified sedimentary layer of sand, silt, and clay..
	
23. National highway build in the basaltic flows. Fault cliff continues back side of the basalt.	24. Overview of Mt.Gudda, view form Mt.Bericha.

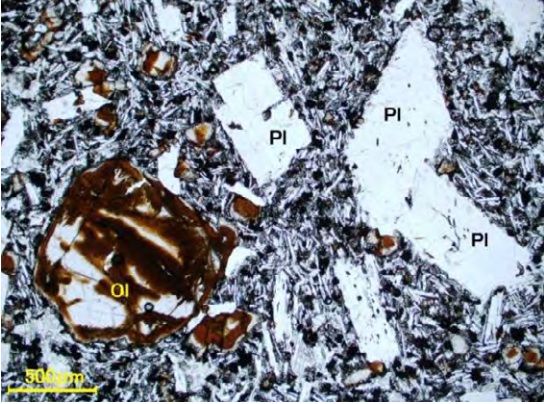
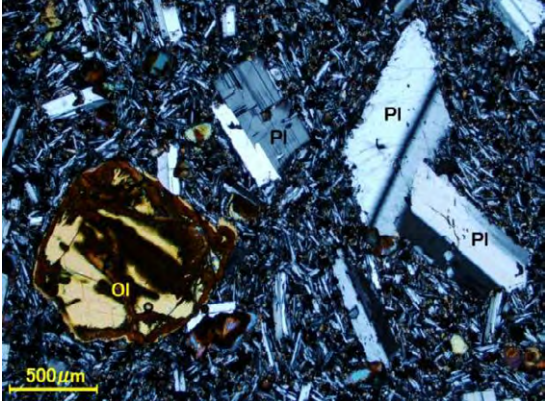
### Microscope observation

Site No.	25	Rock name	Rhyolite
Open			Crossed
			
Plg: Plagioclase, Cpx: Clinopyroxene, Opq: Opaque			

Mineral composition:		
Mineral	Modal (%)	Texture
Plagioclase	58	Lath, Anhedral
Pyroxene	25	Anhedral
Opaque (Fe-oxide)	10	Euhedral- Anhedral
Volcanic glass	7	

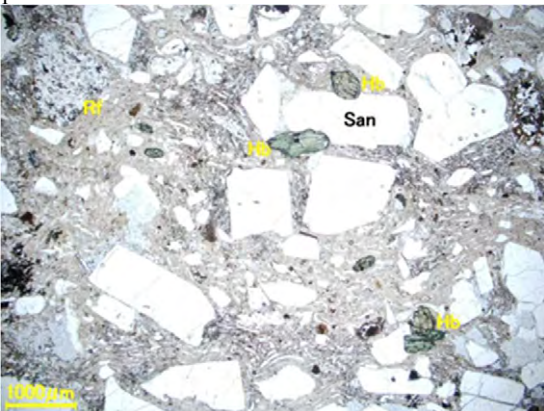
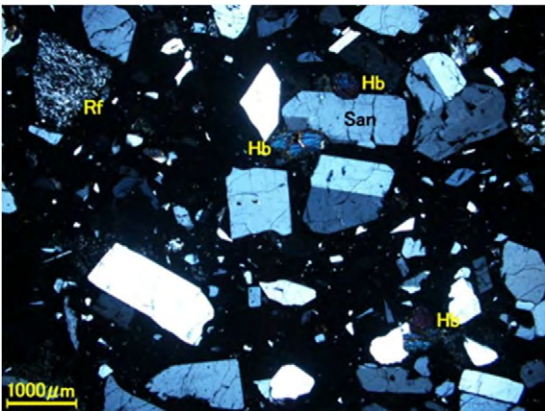
Note:  
 Ground mass is composed of very fine plagioclase, colored mineral (pyroxene), and opaque mineral, which slightly show preferred orientation. Phenocrysts of plagioclase and clinopyroxene are observed.

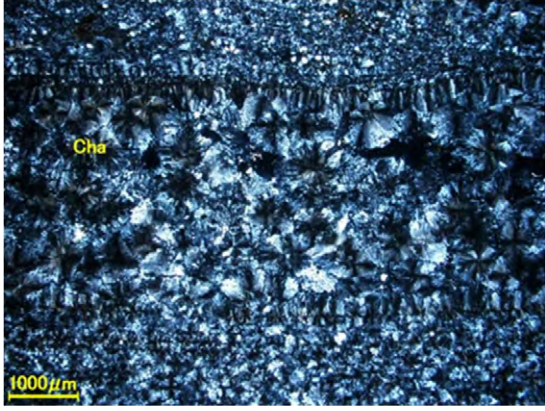
Site No.	26	Rock name	Intergranular and porphyritic basalt
Open			Crossed
			
Plg: Plagioclase, Ol: Olivine			

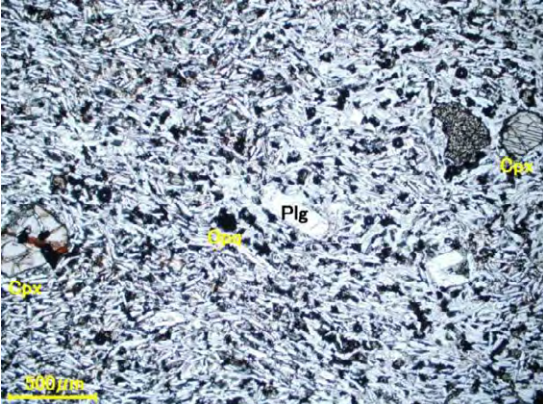
  

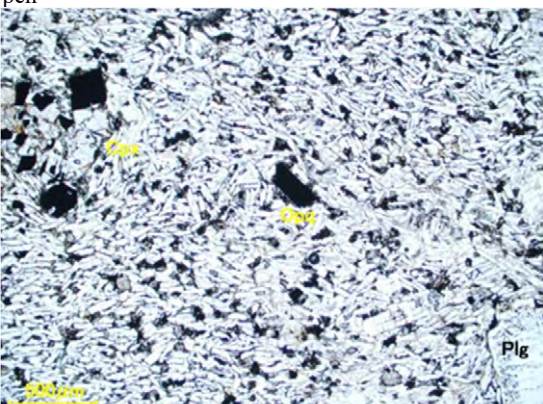
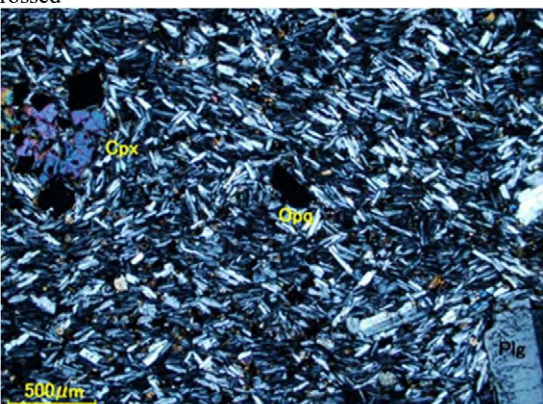
Mineral composition:		
Mineral	Modal (%)	Texture
Plagioclase	46	Lath, Anhedral
Pyroxene	39	Anhedral
Opaque (Fe-oxide)	10	Anhedral
Olivine	5	Anhedral

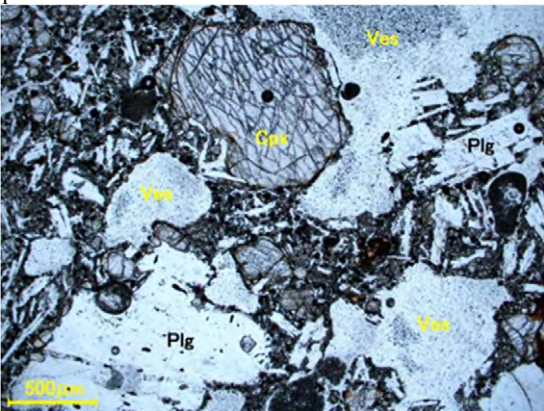
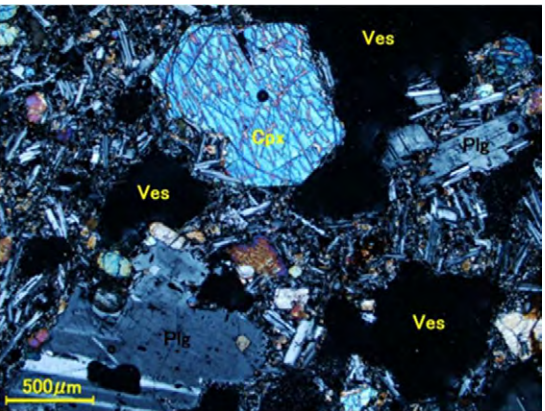
Note:  
 Ground mass is composed of colored mineral (pyroxene) and opaque mineral filling intergranular of lath plagioclases. Reddish brown colored olivine and plagioclase phenocryst are often observed.

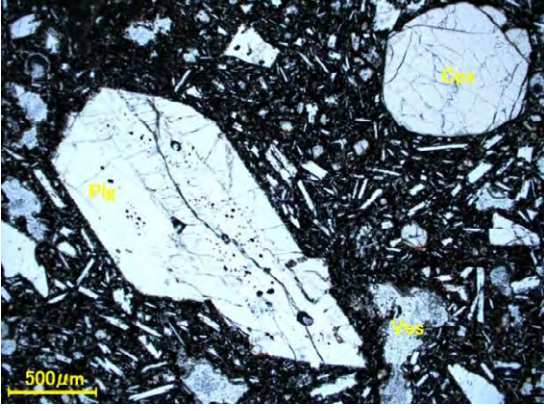
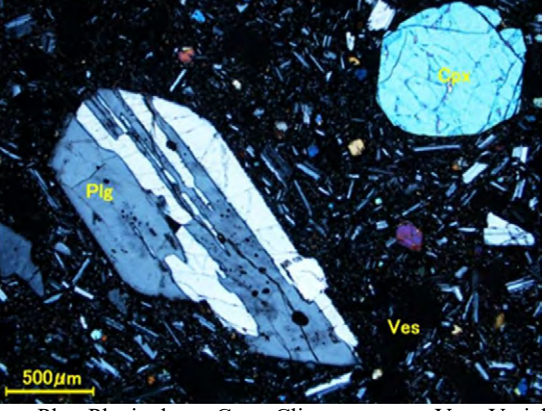
Site No.	27	Rock name	Vitrophyric rhyolitic tuff																								
Open			Crossed																								
																											
			San: Sanidine, Hb: Hornblende, Rf: Rock fragment																								
Mineral composition:			Note: Sanidine, hornblende, and volcanic rock fragment lie on glassy matrix.																								
<table border="1"> <thead> <tr> <th>Mineral</th> <th>Modal (%)</th> <th>Texture</th> </tr> </thead> <tbody> <tr> <td>Volcanic glass</td> <td>48</td> <td></td> </tr> <tr> <td>Sanidine</td> <td>25</td> <td>Anhedral</td> </tr> <tr> <td>Plagioclase</td> <td>12</td> <td>Anhedral</td> </tr> <tr> <td>Quarts</td> <td>10</td> <td>Anhedral</td> </tr> <tr> <td>Opaque (Fe-oxide)</td> <td>3</td> <td>Euhedral-Anhedral</td> </tr> <tr> <td>Hornblende</td> <td>2</td> <td>Anhedral</td> </tr> <tr> <td>Biotite</td> <td>Trace</td> <td>Anhedral</td> </tr> </tbody> </table>			Mineral	Modal (%)	Texture	Volcanic glass	48		Sanidine	25	Anhedral	Plagioclase	12	Anhedral	Quarts	10	Anhedral	Opaque (Fe-oxide)	3	Euhedral-Anhedral	Hornblende	2	Anhedral	Biotite	Trace	Anhedral	
Mineral	Modal (%)	Texture																									
Volcanic glass	48																										
Sanidine	25	Anhedral																									
Plagioclase	12	Anhedral																									
Quarts	10	Anhedral																									
Opaque (Fe-oxide)	3	Euhedral-Anhedral																									
Hornblende	2	Anhedral																									
Biotite	Trace	Anhedral																									

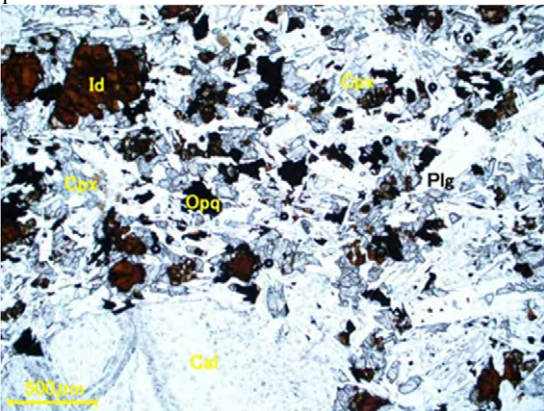
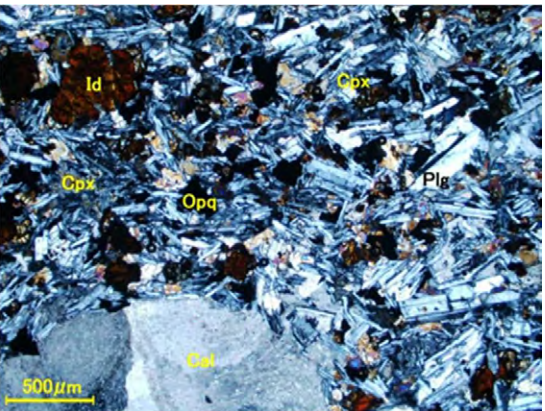
Site No.	28	Rock name	Rhyolite																					
Open			Crossed																					
																								
			Cha: Chalcedony																					
Mineral composition:			Note: This rock is observed that rhyolite with flow structure was silicified completely. Quarts are sometimes find on the center of chalcedony with radial and fibrous texture.																					
<table border="1"> <thead> <tr> <th>Mineral</th> <th>Modal (%)</th> <th>Texture</th> </tr> </thead> <tbody> <tr> <td>Chalcedony</td> <td>35</td> <td>Radial fibrous</td> </tr> <tr> <td>Quarts</td> <td>30</td> <td>Anhedral</td> </tr> <tr> <td>Volcanic glass</td> <td>25</td> <td></td> </tr> <tr> <td>Plagioclase</td> <td>5</td> <td>Tabular</td> </tr> <tr> <td>Opaque (Fe-oxide)</td> <td>5</td> <td>Anhedral</td> </tr> <tr> <td>Biotite</td> <td>Trace</td> <td>Anhedral</td> </tr> </tbody> </table>			Mineral	Modal (%)	Texture	Chalcedony	35	Radial fibrous	Quarts	30	Anhedral	Volcanic glass	25		Plagioclase	5	Tabular	Opaque (Fe-oxide)	5	Anhedral	Biotite	Trace	Anhedral	
Mineral	Modal (%)	Texture																						
Chalcedony	35	Radial fibrous																						
Quarts	30	Anhedral																						
Volcanic glass	25																							
Plagioclase	5	Tabular																						
Opaque (Fe-oxide)	5	Anhedral																						
Biotite	Trace	Anhedral																						

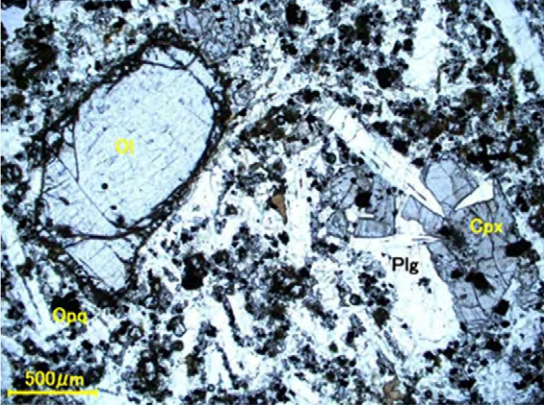
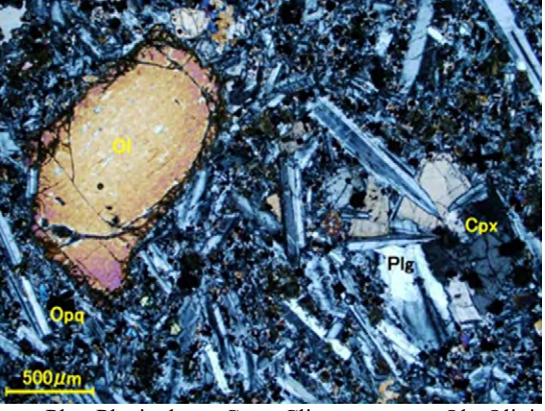
Site No.	29	Rock name	Pilotaxitic and porphyritic basalt												
Open			Crossed												
															
			Plg: Plagioclase, Cpx: Clinopyroxene, Opq: Opaque												
Mineral composition:			Note: Ground mass is composed of colored mineral (pyroxene) and opaque mineral, which fill intergranular of strip form or lath plagioclases. Phenocrysts of plagioclase and clinopyroxene lie on the ground mass.												
<table border="1"> <thead> <tr> <th>Mineral</th> <th>Modal (%)</th> <th>Texture</th> </tr> </thead> <tbody> <tr> <td>Plagioclase</td> <td>55</td> <td>Anhedral</td> </tr> <tr> <td>Pyroxene</td> <td>35</td> <td>Anhedral</td> </tr> <tr> <td>Opaque (Fe-oxide)</td> <td>10</td> <td>Anhedral</td> </tr> </tbody> </table>			Mineral	Modal (%)	Texture	Plagioclase	55	Anhedral	Pyroxene	35	Anhedral	Opaque (Fe-oxide)	10	Anhedral	
Mineral	Modal (%)	Texture													
Plagioclase	55	Anhedral													
Pyroxene	35	Anhedral													
Opaque (Fe-oxide)	10	Anhedral													

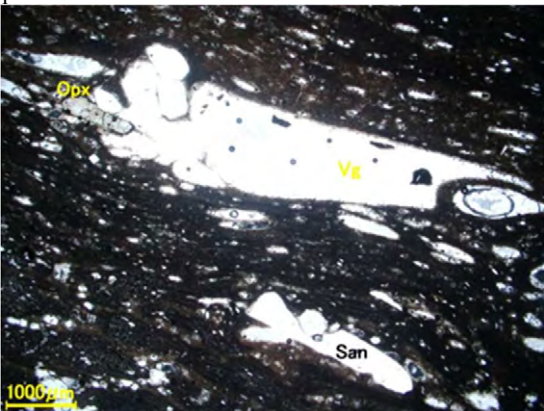
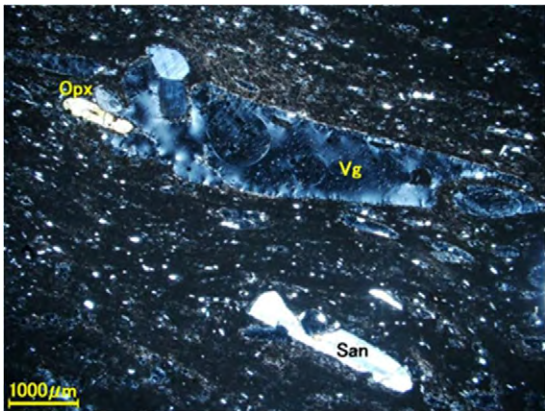
Site No.	30	Rock name	Pilotaxitic and porphyritic basalt												
Open			Crossed												
															
			Plg: Plagioclase, Cpx: Clinopyroxene, Opq: Opaque												
Mineral composition:			Note: Ground mass is composed of colored mineral (pyroxene) and opaque mineral, which fill intergranular of strip form or lath plagioclases with preferred orientation. Phenocrysts of plagioclase and clinopyroxene lie on the ground mass. Vesicle is also observed.												
<table border="1"> <thead> <tr> <th>Mineral</th> <th>Modal (%)</th> <th>Texture</th> </tr> </thead> <tbody> <tr> <td>Plagioclase</td> <td>56</td> <td>Anhedral</td> </tr> <tr> <td>Pyroxene</td> <td>35</td> <td>Anhedral</td> </tr> <tr> <td>Opaque (Fe-oxide)</td> <td>9</td> <td>Anhedral</td> </tr> </tbody> </table>			Mineral	Modal (%)	Texture	Plagioclase	56	Anhedral	Pyroxene	35	Anhedral	Opaque (Fe-oxide)	9	Anhedral	
Mineral	Modal (%)	Texture													
Plagioclase	56	Anhedral													
Pyroxene	35	Anhedral													
Opaque (Fe-oxide)	9	Anhedral													

Site No.	31	Rock name	Intergranular and porphyritic vesicular basalt															
Open			Crossed															
																		
Plg: Plagioclase, Cpx: Clinopyroxene, Ves: Vesicle																		
<b>Mineral composition:</b> <table border="1"> <thead> <tr> <th>Mineral</th> <th>Modal (%)</th> <th>Texture</th> </tr> </thead> <tbody> <tr> <td>Plagioclase</td> <td>46</td> <td>Anhedral</td> </tr> <tr> <td>Pyroxene</td> <td>42</td> <td>Anhedral</td> </tr> <tr> <td>Opaque (Fe-oxide)</td> <td>9</td> <td>Anhedral</td> </tr> <tr> <td>Olivine</td> <td>3</td> <td>Euhedral-Anhedral</td> </tr> </tbody> </table>			Mineral	Modal (%)	Texture	Plagioclase	46	Anhedral	Pyroxene	42	Anhedral	Opaque (Fe-oxide)	9	Anhedral	Olivine	3	Euhedral-Anhedral	<b>Note:</b> Ground mass is composed of colored mineral (pyroxene) and opaque mineral, which fill intergranular of lath plagioclases. Phenocrysts of plagioclase and clinopyroxene are often observed. Vesicle is also observed.
Mineral	Modal (%)	Texture																
Plagioclase	46	Anhedral																
Pyroxene	42	Anhedral																
Opaque (Fe-oxide)	9	Anhedral																
Olivine	3	Euhedral-Anhedral																

Site No.	32	Rock name	Intergranular and porphyritic vesicular basalt															
Open			Crossed															
																		
Plg: Plagioclase, Cpx: Clinopyroxene, Ves: Vesicle																		
<b>Mineral composition:</b> <table border="1"> <thead> <tr> <th>Mineral</th> <th>Modal (%)</th> <th>Texture</th> </tr> </thead> <tbody> <tr> <td>Plagioclase</td> <td>45</td> <td>Anhedral, Lath</td> </tr> <tr> <td>Pyroxene</td> <td>40</td> <td>Anhedral</td> </tr> <tr> <td>Opaque (Fe-oxide)</td> <td>12</td> <td>Anhedral</td> </tr> <tr> <td>Olivine</td> <td>3</td> <td>Anhedral</td> </tr> </tbody> </table>			Mineral	Modal (%)	Texture	Plagioclase	45	Anhedral, Lath	Pyroxene	40	Anhedral	Opaque (Fe-oxide)	12	Anhedral	Olivine	3	Anhedral	<b>Note:</b> Ground mass is composed of colored mineral (pyroxene) and opaque mineral, which fill intergranular of lath plagioclases. Phenocrysts of plagioclase and clinopyroxene are often observed.
Mineral	Modal (%)	Texture																
Plagioclase	45	Anhedral, Lath																
Pyroxene	40	Anhedral																
Opaque (Fe-oxide)	12	Anhedral																
Olivine	3	Anhedral																

Site No.	33	Rock name	Intergranular basalt															
Open	Crossed																	
																		
Plg: Plagioclase, Cpx: Clinopyroxene, Id: Iddingsite, Opq: Opaque, Cal: Calcite																		
<table border="1"> <thead> <tr> <th>Mineral composition:</th> <th>Modal (%)</th> <th>Texture</th> </tr> </thead> <tbody> <tr> <td>Plagioclase</td> <td>42</td> <td>Anhedral, Lath</td> </tr> <tr> <td>Pyroxene</td> <td>39</td> <td>Anhedral</td> </tr> <tr> <td>Opaque (Fe-oxide)</td> <td>12</td> <td>Euhedral-Anhedral</td> </tr> <tr> <td>Olivine</td> <td>5</td> <td>Anhedral</td> </tr> </tbody> </table>			Mineral composition:	Modal (%)	Texture	Plagioclase	42	Anhedral, Lath	Pyroxene	39	Anhedral	Opaque (Fe-oxide)	12	Euhedral-Anhedral	Olivine	5	Anhedral	<p>Note: Clinopyroxene and opaque mineral fill intergranular of strip form or lath plagioclases showing preferred orientation. Reddish brown minerals are iddingsite which is altered from olivine. Calcite fills vesicles.</p>
Mineral composition:	Modal (%)	Texture																
Plagioclase	42	Anhedral, Lath																
Pyroxene	39	Anhedral																
Opaque (Fe-oxide)	12	Euhedral-Anhedral																
Olivine	5	Anhedral																

Site No.	34	Rock name	Intergranular and porphyritic basalt															
Open	Crossed																	
																		
Plg: Plagioclase, Cpx: Clinopyroxene, Ol: Olivine																		
<table border="1"> <thead> <tr> <th>Mineral composition:</th> <th>Modal (%)</th> <th>Texture</th> </tr> </thead> <tbody> <tr> <td>Plagioclase</td> <td>44</td> <td>Lath, Tubular</td> </tr> <tr> <td>Pyroxene</td> <td>41</td> <td>Anhedral</td> </tr> <tr> <td>Opaque (Fe-oxide)</td> <td>12</td> <td>Anhedral</td> </tr> <tr> <td>Olivine</td> <td>3</td> <td>Euhedral-Anhedral</td> </tr> </tbody> </table>			Mineral composition:	Modal (%)	Texture	Plagioclase	44	Lath, Tubular	Pyroxene	41	Anhedral	Opaque (Fe-oxide)	12	Anhedral	Olivine	3	Euhedral-Anhedral	<p>Note: Ground mass is composed of colored mineral (pyroxene) and opaque mineral, which fill intergranular of lath plagioclases. Phenocrysts are plagioclase, clinopyroxene, and olivine.</p>
Mineral composition:	Modal (%)	Texture																
Plagioclase	44	Lath, Tubular																
Pyroxene	41	Anhedral																
Opaque (Fe-oxide)	12	Anhedral																
Olivine	3	Euhedral-Anhedral																

Site No.	35	Rock name	Vitrophyric rhyolitic welded tuff																												
Open			Crossed																												
																															
			San: Sanidine, Opx: Orthopyroxene, Vg: Volcanic glass																												
Mineral composition:			Note: Ground mass is composed of colored mineral (pyroxene) and opaque mineral filling intergranular of lath plagioclases. Plagioclase, clinopyroxene, and olivine are observed as phenocryst.																												
<table border="1"> <thead> <tr> <th>Mineral</th> <th>Modal (%)</th> <th>Texture</th> <th></th> </tr> </thead> <tbody> <tr> <td>Volcanic glass</td> <td>53</td> <td></td> <td></td> </tr> <tr> <td>Quartz</td> <td>15</td> <td>Anhedral</td> <td></td> </tr> <tr> <td>Sanidine</td> <td>11</td> <td>Anhedral</td> <td></td> </tr> <tr> <td>Pyroxene</td> <td>10</td> <td>Anhedral</td> <td></td> </tr> <tr> <td>Opaque (Fe-oxide)</td> <td>6</td> <td>Anhedral</td> <td></td> </tr> <tr> <td>Plagioclase</td> <td>5</td> <td>Lath, Anhedral</td> <td></td> </tr> </tbody> </table>				Mineral	Modal (%)	Texture		Volcanic glass	53			Quartz	15	Anhedral		Sanidine	11	Anhedral		Pyroxene	10	Anhedral		Opaque (Fe-oxide)	6	Anhedral		Plagioclase	5	Lath, Anhedral	
Mineral	Modal (%)	Texture																													
Volcanic glass	53																														
Quartz	15	Anhedral																													
Sanidine	11	Anhedral																													
Pyroxene	10	Anhedral																													
Opaque (Fe-oxide)	6	Anhedral																													
Plagioclase	5	Lath, Anhedral																													

**APPENDIX-2**

**MT/TEM Survey**

**Methodology and Survey Data**



## Appendix-2 Methodology of MT and TEM survey and results data

### A2.1 MT Method

#### (1) Principle of Method

MT (Magnetotellurics) method observes the earth's magnetic field and telluric current in nature with magnetic and electric sensors to investigate underground structures. MT method can investigate more than 10,000 m deep.

The term "MT method" is an abbreviation for magnetotellurics method, derived from the combination of the earth's magnetism and telluric currents. It denotes a survey method using the earth's telluric currents produced in the ground by variations of the earth's magnetic field (Figure 1). The earth's magnetic field changes naturally and is thought to be due to the earth's magnetic oscillation, less than 1Hz, driven by solar activity and the earth's magnetic pulsation, more than 1Hz, produced by lightning. MT method observes these activities in the frequency range between 0.001Hz and 1,000Hz. Observation is commonly carried out overnight when the noise level is low. The remote reference method eliminates the noise at survey points. It uses an observation result at a reference station more than 50 km away from the subject site.

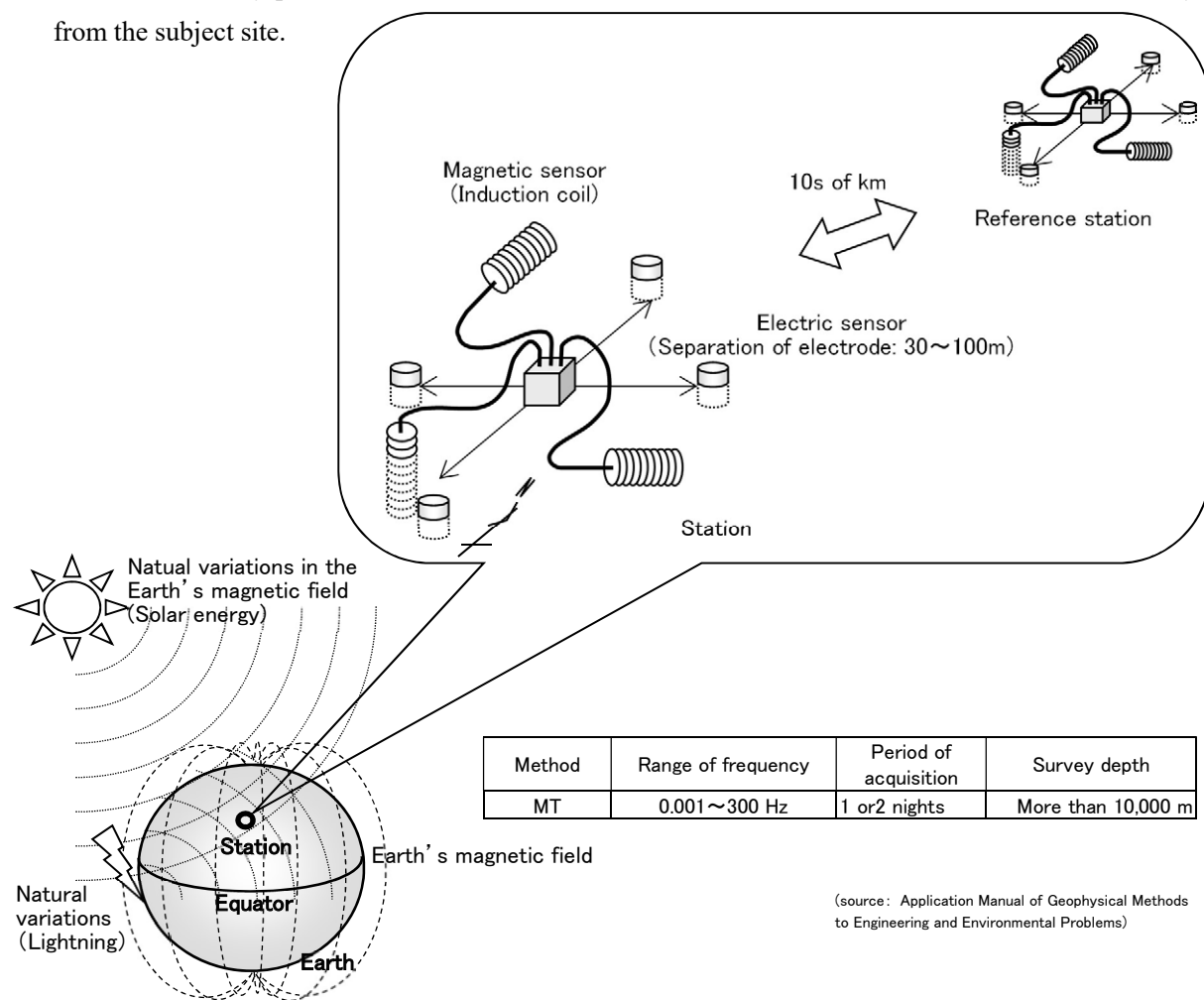


Figure A2.1.1 Schematic diagram of principles of MT method

The electromagnetic wave is attenuated gradually while it enters ground surface and penetrates underground. MT method is some of the

The skin depth where the energy intensity decreases to 1/e (about 0.37time) of the intensity at ground surface is regarded as a rule of thumb of the exploration depth for MT method.

The skin depth  $\delta$  (m) depends on resistivity of ground  $\rho$  (ohm-m) and frequency  $f$  (Hz) of electromagnetic wave and is estimated as the following equation.

$$\delta = \sqrt{\frac{\rho}{\pi f \mu}} \approx 503 \sqrt{\frac{\rho}{f}}$$

Where  $\mu$  is electric permeability.

This equation shows that the higher the resistivity and the lower the frequency, the deeper the exploration depth into the ground. About MT method in the frequency range of 300 ~ 0.001Hz, the resistivity of 10ohm-m indicates the skin depth of about from 92m to 50km. It is said that the exploration depth of MT method is about 2-1/2 ( $\approx 0.707$ ) of the skin depth.

As the variations of the earth's magnetism and telluric currents in low frequencies like the micropulsation affected by solar activity are observed for MT method, the measurement has to be carried out overnight when the culture noise level is low at least for one night. However, at MT measurement, the variations of the earth's magnetism and telluric currents are small and it is difficult to distinguish those signals from noises. The remote reference station is set up at the far place from the survey site and where noise is low and the measurement is carried out at the survey station and the remote reference station simultaneously. The variations of observed signals at the survey station which have the correlation with data at the remote reference station are recognized as correct signals and those signals reduce affection of noise to acquired data. This technique is called the remote reference method.

The resistivity is the electrical property obtained from the electromagnetic or electric surveys including MT method. The definition of resistivity is electric resistance per unit of length with electric current flowing through the unit cross section area. This means, the apparent resistivity value is different depending on the directions of the measurements in case of layered underground or fracture rock. In other words, the resistivity shows anisotropy. MT method routinely measure this apparent anisotropy of resistivity differently from electromagnetic surveys except for MT method or electric surveys. For example, in case of the survey for fault, the resistivity in parallel with the strike direction of fault is TE mode and that of the orthogonal direction of the strike is TM mode.

In MT method, generally **Hx** as magnetic field and **Ex** as electric field in NS direction (x axis) and **Hy** and **Ey** in EW direction (y axis) are observed. Bold characters mean complex number. The definition of impedance tensor **Z** is expressed as the next equation with the relationship of magnetic and electric field.

$$\begin{pmatrix} \mathbf{E}_x \\ \mathbf{E}_y \end{pmatrix} = \mathbf{Z} \begin{pmatrix} \mathbf{H}_x \\ \mathbf{H}_y \end{pmatrix} = \begin{pmatrix} \mathbf{Z}_{xx} & \mathbf{Z}_{xy} \\ \mathbf{Z}_{yx} & \mathbf{Z}_{yy} \end{pmatrix} \begin{pmatrix} \mathbf{H}_x \\ \mathbf{H}_y \end{pmatrix}$$

The resistivity is related to the mutually-perpendicular components Z<sub>xy</sub> and Z<sub>yx</sub> of impedance tensor. Therefore 2 orthogonal directions of the resistivity are obtained in MT method. If x axis is rotated from NS direction to another, each component value of impedance tensor Z is varied. It means that by using the impedance tensor Z calculated from the observed data at NS and EW directions, the resistivity at arbitrary direction can be estimated.

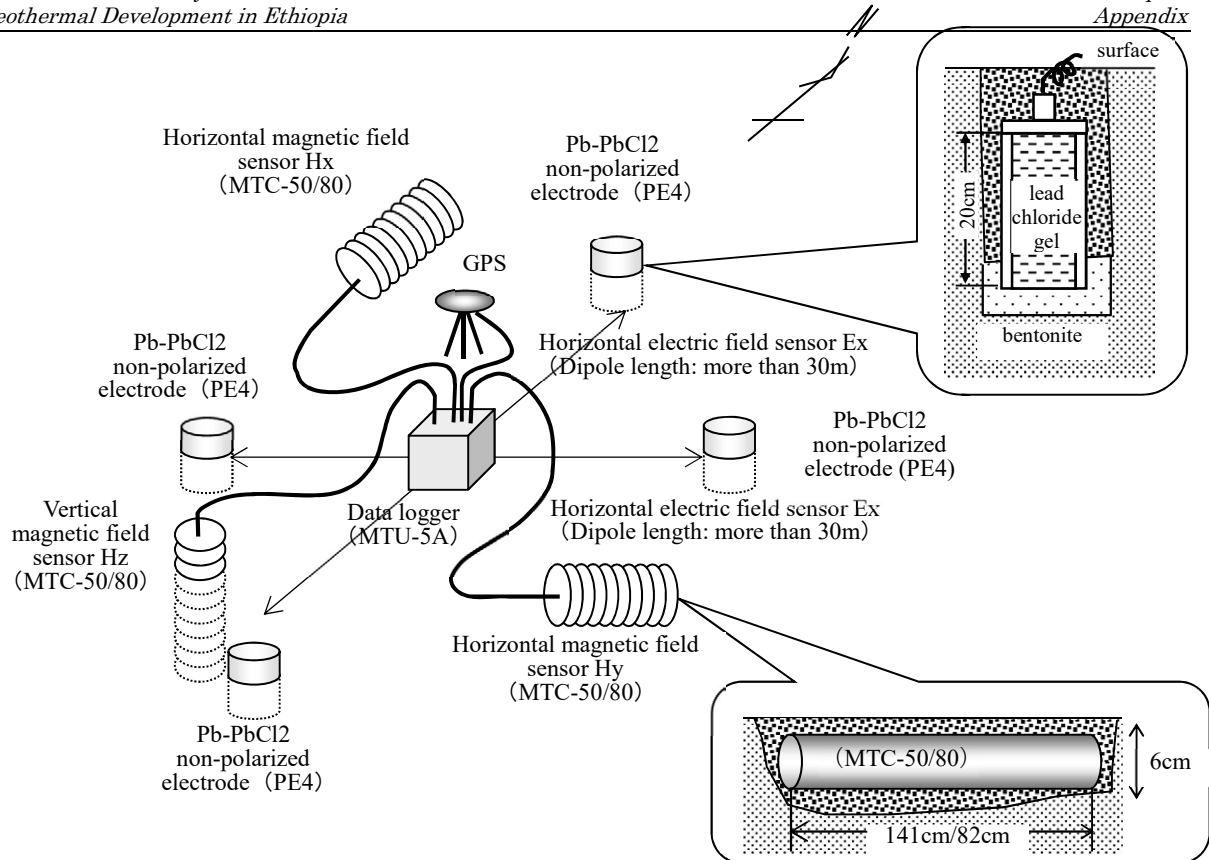
## (2) Measurement Method

Figure 2 shows the schematic drawing for deployment of MT data acquisition system in the project. For data acquisition, MTU-5A system of Phoenix Geophysics (compatible with MT/AMT) was used and 2 components of the electric field and 3 components of the magnetic field were observed as time series. at each station.

The Pb-PbCl<sub>2</sub> non-polarized electrodes PE4 of Phoenix Geophysics were used at the measurement of the telluric current and according to the condition of each station, the dipole of 50~100m range was selected. The 2 directions of the dipole were NS and EW direction referring the magnetic north as standard. The electrodes were buried with water and bentonite to reduce contact resistivity in the hole of about 30m depth.

At the measurement of the magnetic field, the induction coils MTC-50/80 of Phoenix Geophysics were used to observe the magnetic field in the direction of NS and EW (magnetic north as standard) and verticality.

The remote reference stations were set up at more than 60 km far from the survey sites. The measurements were conducted simultaneously at the survey station and the remote reference station for more than 14 hours overnight and the survey equipment were moved and set up at next station during daytime. At the beginning of each survey, the calibration was executed to test magnetic sensors and decide coil coefficients.



**Figure A2.1.2 Schematic drawing for deployment of MT data acquisition system**

### (3) Data Processing

The time series data including 3 components of magnetic field and 2 components of electric field acquired by data logger were moved to the laptop computer soon in the field after finishing the measurement. each component of the time series data was processed by Fourier transform and each power spectrum at every frequency  $f$  (Hz) was obtained. The spectral ratios of horizontal magnetic field  $H_x(f)$  and  $H_y(f)$ , electric field  $E_x(f)$  and  $E_y(f)$  compose each component of impedance tensor  $Z(f)$  at every frequency. The mutually-perpendicular resistivity  $\rho_{xy}(f)$ ,  $\rho_{yx}(f)$  and phase difference  $\Delta\phi_{xy}(f)$ ,  $\Delta\phi_{yx}(f)$  were computed from the impedance tensor  $Z(f)$  using the next equation.

$$\rho_{xy}(f) = \frac{1}{2\pi f \mu} |Z_{xy}(f)| = \frac{1}{5f} \frac{|E_x(f)|}{|H_y(f)|}, \quad \Delta\phi_{xy}(f) = \phi\{H_y(f)\} - \phi\{E_x(f)\}$$

$$\rho_{yx}(f) = \frac{1}{2\pi f \mu} |Z_{yx}(f)| = \frac{1}{5f} \frac{|E_y(f)|}{|H_x(f)|}, \quad \Delta\phi_{yx}(f) = \phi\{H_y(f)\} - \phi\{E_x(f)\}$$

Where,

$f$ : frequency (Hz),  $\pi$ : the ratio of the circumference of a circle to its diameter,  $\mu$ : magnetic permeability

$|E_x(f)|$ 、 $|E_y(f)|$ : intensity of electric field (V/m),  $|H_x(f)|$ ,  $|H_y(f)|$ : intensity of magnetic field (nT)

$\phi\{E_x(f)\}$ ,  $\phi\{E_y(f)\}$ : phase of electric field (degree),  $\phi\{H_x(f)\}$ ,  $\phi\{H_y(f)\}$ : phase of magnetic field (degree)

Calculated resistivity  $\rho_{xy}(f)$  and  $\rho_{yx}(f)$  mean exact resistivity in case that the ground resistivity is equal. Actually, as they mean approximate resistivity because of the unequal ground resistivity, it is called “apparent resistivity” in MT method. Phase difference is called “phase”  $\phi_{xy}(f)$ ,  $\phi_{yx}(f)$ . An example of apparent resistivity and phase curve is shown in Figure 3.

In the project, the observed time series data were divided to 20 segments and each apparent resistivity and phase is calculated at every segment. 20 processed values were obtained at every frequency and statistically

mean and variance are calculated and variance is expressed as error bar on apparent resistivity curve or phase curve. Generally, it is desirable and means high quality to have low scatter, moderate curvature and well-joined frequency-band curve segments. Data processing by using only the observation data at survey station is called local processing. In the project, after downloading data to the laptop computer, the local processing was done and data quality of the observed data was estimated with the apparent resistivity and phase curve.

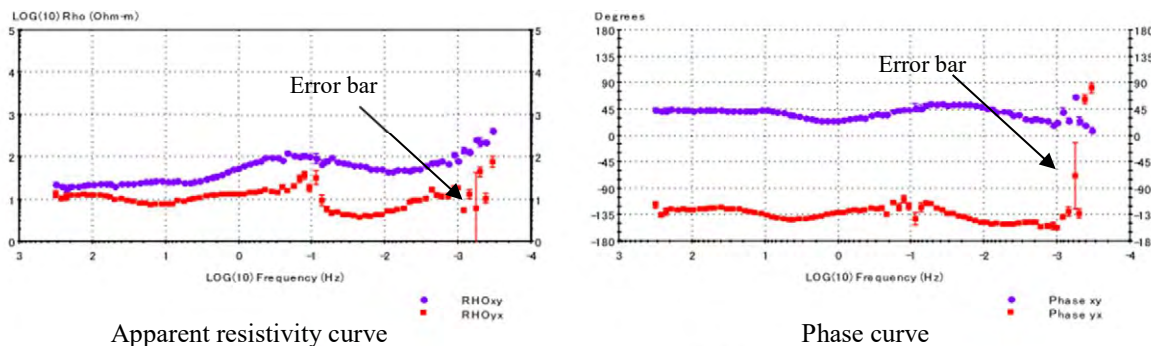


**Figure A2.1.3 An example of an apparent resistivity and phase curve**

About data processing of this survey, at 80 frequencies in the range between 320Hz ~ 0.00034Hz of MT data, each impedance tensor  $Z(f)$  was computed.

After the field survey finishing, by using the acquired data at remote reference station, the remote reference processing technique was applied to the acquired data at survey stations to remove local noises. A concept of remote reference processing is given in Figure 4. Both the observed data and the remote reference data have artificial electromagnetic noises generated by power lines, residences, and traffic of vehicles etc. in circles of Figure. If the distance between the survey site and the remote reference station is fully far, the correlation of the signal is good and at the same time, noise shows no correlation. Therefore after cross-correlation data processing, the processed data without noise are created.

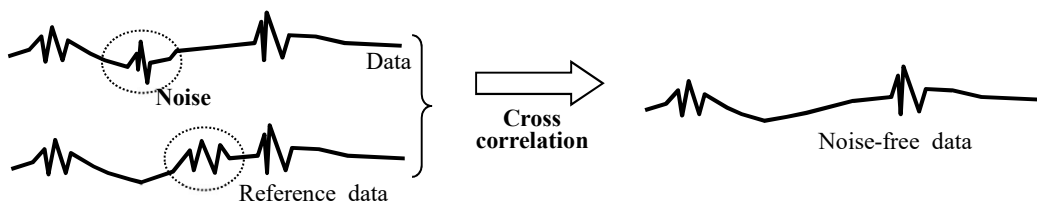


Figure A2.14 A concept of remote reference processing

SSMT2000 software of Phoenix Geophysics was used for a series of remote reference data processing technique. The processed data were edited by selecting the segment with high S/N at every frequency so that the apparent resistivity and phase curves have small error bar and smooth curvature. For edit, MT-editor software of Phoenix Geophysics was used.

#### (4) Data Analysis

##### 1) Dimensionality analysis

Impedance tensor obtained by MT measurement can be rotated to any other coordinate system by the rotation matrix. In case of 1 dimensional layered resistivity structure,  $Z_{xx}=Z_{yy}=0$  and  $Z_{xy}=-Z_{yx}(\neq 0)$  are satisfied at arbitrary direction. In case of 2 dimensionality structure,  $Z_{xx}=Z_{yy}=0$  and  $Z_{xy}\neq-Z_{yx}(\neq 0)$  are satisfied when the strike direction of the resistivity structure is parallel to x axis and perpendicular to y axis. Therefore, by the rotation of impedance tensor, the strike direction of the resistivity structure and the index of the structure complexity can be obtained.

Impedance polar diagram is the drawn trace when  $Z_{xy}$  and  $Z_{xx}$  are rotated mathematically. In 1 dimensional structure,  $Z_{xy}$  diagram is should be circle and  $Z_{xx}$  diagram is should be minimal. In 2 dimensional structure,  $Z_{xy}$  is peanut shape or elliptic shape. The long axis is parallel to the strike direction if the station is at conductive side or is perpendicular to the strike direction if the station is at resistive side. In 3 dimensional structure,  $Z_{xy}$  and  $Z_{xx}$  change shape largely to cloverleaf shape. The qualitative interpretation of the resistivity structure can be conducted by impedance polar diagram.

The vertical magnetic field Hz shows large value near the vertical structure. Then, Hz correlates well with the horizontal magnetic field Hr. Tipper strike is defined as  $r + 90$  degrees and the parameter of the strike direction. In case that the station is far from the discontinuity of the structure, the vertical magnetic field Hz becomes small drastically so that it is difficult to determine tipper strike precisely.

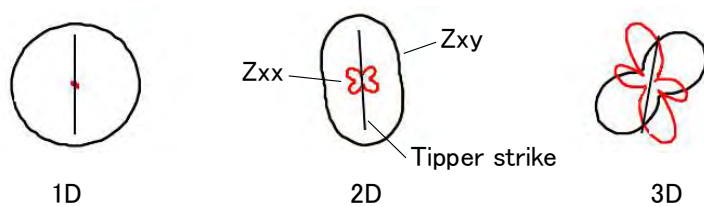


Figure A2.15 Impedance polar diagram and tipper strike

Tipper magnitude is the calculated parameter from 3 components of the magnetic field and indicates dimensionality. In case that the magnitude is almost zero (or less than 0.2), it indicates the presence of 1 dimensional subsurface resistivity structure. In case that the magnitude is more than 0.5, 2 dimensional or 3 dimensional structure may present. Tipper magnitude becomes large around the boundary of the resistivity structure.

$$TipMag = (A^2 + B^2)^{1/2}$$

## 2) 2D analysis

As mentioned above, the apparent resistivity  $\rho_{xy}(f)$  and  $\rho_{yx}(f)$  computed through data processing just indicate the mean value of resistivity to the exploration depth (about 0.707 times skin depth). 2D analysis was executed using apparent resistivity and phase curves to infer the resistivity structure.

For data analysis, considering dimensional parameters and the comprehensive geological strike direction of the survey site, profiles were set up and y axis was put in the direction of the profile and x axis was put in the perpendicular direction of the profile.

Impedance tensor was rotated and the apparent resistivity from the combination of electric field of x direction and magnetic field of y direction as TE mode (parallel to structure) and the apparent resistivity from the combination of electric field of y direction and magnetic field of x direction as TM mode (perpendicular to structure) are computed respectively and used for 2D inversion as input data.

In 2D analysis, under the assumption that the resistivity structure doesn't change and continue infinitely in the direction perpendicular to profile, 2D resistivity model is computed automatically so that the response of 2D resistivity model fits to the observed impedance. The resistivity value of each cell in the resistivity model is calculated from all apparent resistivities of the profile by non-linear least squares method. As apparent resistivity of adjacent survey station and adjacent resistivity cell are considered, a relatively continuous model is obtain as reasonable analysis result.

In the project, 2D resistivity inversion analysis was executed using WinGLink of GEOSYSTEM SRL which has a function of 2D inversion. The cross section of profile is composed by the elements of finite difference method for model calculation and resistivity cells combined by elements. The size of the element and the resistivity cell are made enough fine at shallow zone and larger to the direction of marginal and deep zone.

And next, the homogeneous model of 100 ohm-m resistivity is used as initial model and the response of resistivity model by finite element method was computed at each survey station. Comparing the calculated apparent resistivity with the observed apparent resistivity, the iteration of correcting resistivity was continued until RMS (abbreviation of Root Mean Square) error becomes less than the threshold.

## 3) 3D analysis

In 3D analysis, the electric and the magnetic field are calculated by the resistivity structure of every direction to obtain the resistivity structure model which explains well apparent resistivity and phase calculated from the observed data. Apparent resistivity ( $\rho_{xy}$ ,  $\rho_{yx}$ ) and phase (Phase $xy$ , Phase $yx$ ) data were not rotated to use for analysis as the strike direction didn't need to be assumed.

In this project, 3D resistivity inversion analysis was executed using EMVision® of TechnoImaging. The resistivity model for data analysis is divided to the cells with size of 184 m x 184 m in horizontal direction evenly. The size of the cells in vertical direction varies logarithmically from 25 m to 3162 m. In the deeper zone, the size is large as sensitivity per unit (MT response to change of resistivity) is low. Though the special resolution becomes low because of the large cell in size, the parameters of the resistivity structure converge stably.

The analysis area is 18 km (East-West) x 27 km (South-North) and 32 km depth from the surface. Data of 199 stations were used for data analysis and the frequency range for calculation is from 0.001 Hz to 100 Hz.

## A2.2 TEM Method

### (1) Principle of Method

TEM method is an abbreviation for transient electromagnetic method. It means a method that observes the transients of magnetic field after turning off an input artificial magnetic field (Figure 6)

An artificial magnetic field is transmitted in a vertical direction when an electric current flows in an electric square loop on the ground (transmission loop). The loop may be rectangle or circle. When the electric current is turned off, a secondary electric current starts in the ground in a circle to maintain the input magnetic field. This current gradually spreads under the ground further. This current is called the eddy current, or often called “smoke ring” comparing to the smoke loop from cigar. The input artificial magnetic field decays in time and its rate is less where the resistivity is low. The resistivity of the subsurface is estimated by measuring the decay of the artificial magnetic field by an induction (receiver) coil. The decay immediately after stopping the current signal (early time response) indicates resistivity at shallow ground and the late time response resistivity at deeper parts.

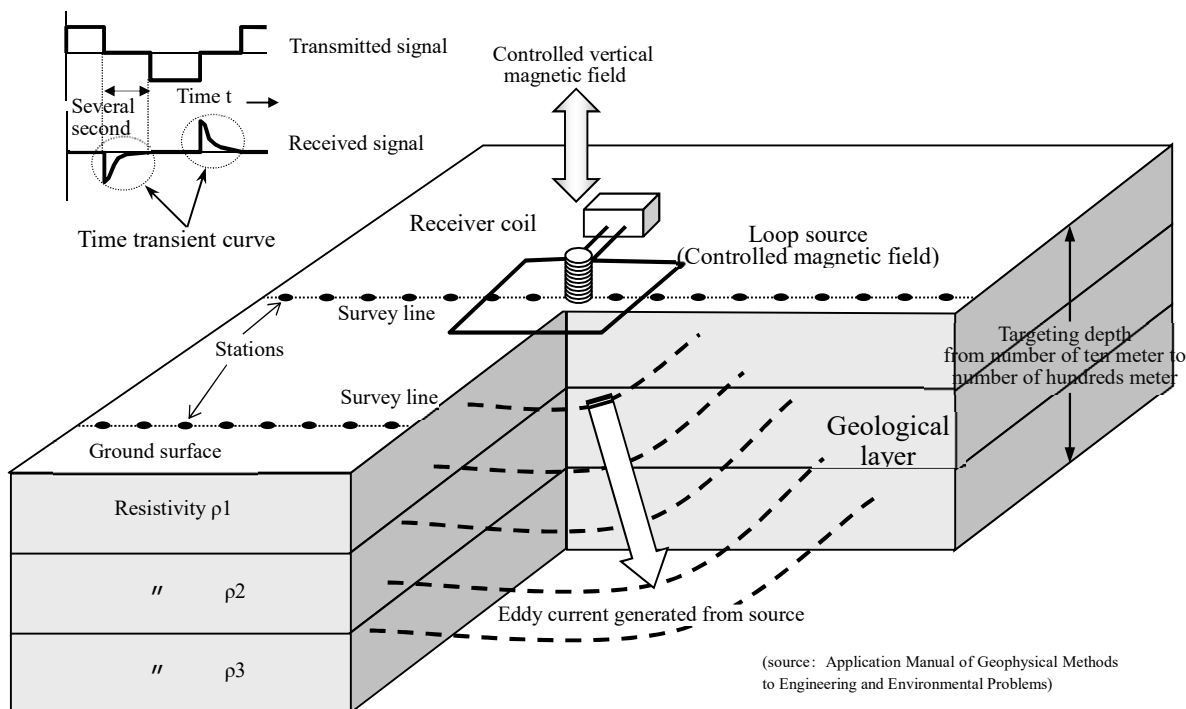


**Figure A2.2.1 Schematic diagram of principles of TEM method**

Especially, TEM method is useful to the structure which shows low resistivity (high conductance) due to groundwater, argillation, weathered deep layer, alteration etc.

The diffusion depth  $\delta$  (m) is regarded as a rule of thumb of the exploration depth for TEM method and it is estimated as the following equation.

$$\delta = \sqrt{\frac{2t\rho}{\mu}}$$

Where,  $\rho$ : ground resistivity (ohm-m),  $t$ : time after turning off the primary field (sec),  $\mu$ : magnetic permeability

This equation shows that the higher the resistivity and the longer the time, the deeper the exploration depth into the ground.

It is difficult to investigate the structure under the distribution of low resistivity with electric methods at the survey site where low resistivity distributes such as argillation or alteration at the shallower zone. But TEM method is available to investigate deeper zone. Especially, in the survey site where argillation or saline groundwater exists at the surface layer TEM method is suitable.

## (2) Measurement Method

In the project, TEM method is used for static correction of MT data. As about 100m is needed as exploration depth, 40m square loop was set up on the ground and the current was passed by the portable transmitter to induce magnetic field. After turning off the current, the transient response of magnetic field was measured by the induction coil in the center of the loop for a few times in central loop system. Figure 7 shows the survey schematic drawing for deployment of TEM data acquisition system in the project. PROTEM CM HP system of Geonics Limited was used and the transient response of vertical magnetic field was measured at each station. The transmitter current is about 2A, the number of time windows is 20, the number of stacks is more than 10 times and 3 kinds of the repeat rate 237.5Hz, 62.5Hz and 25.0Hz were mainly used.

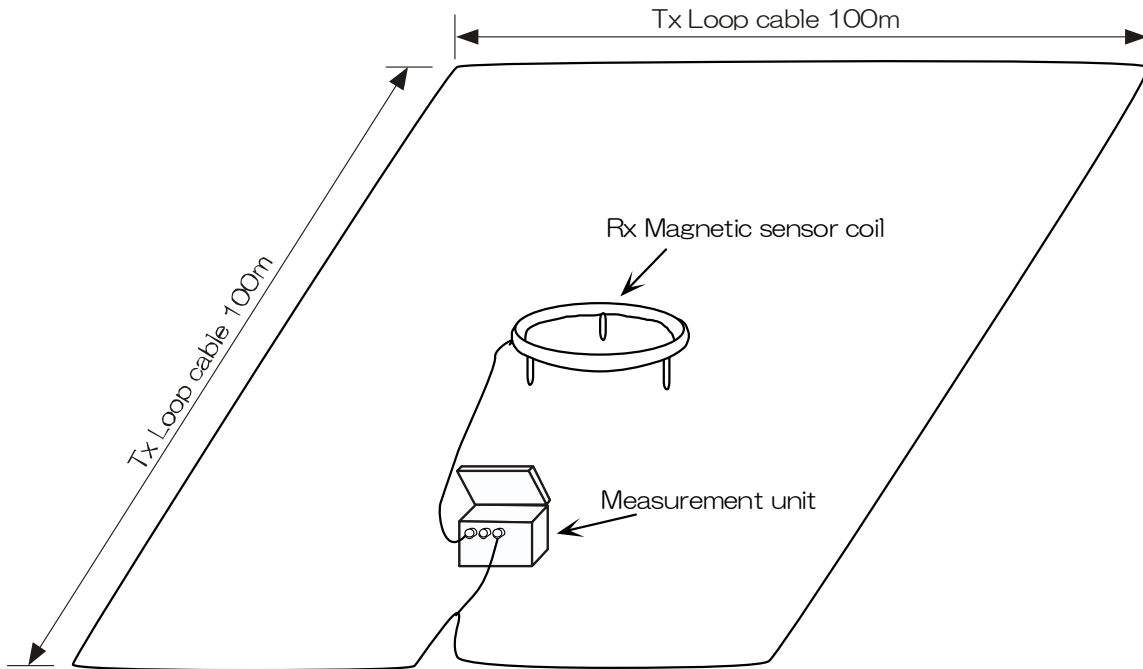
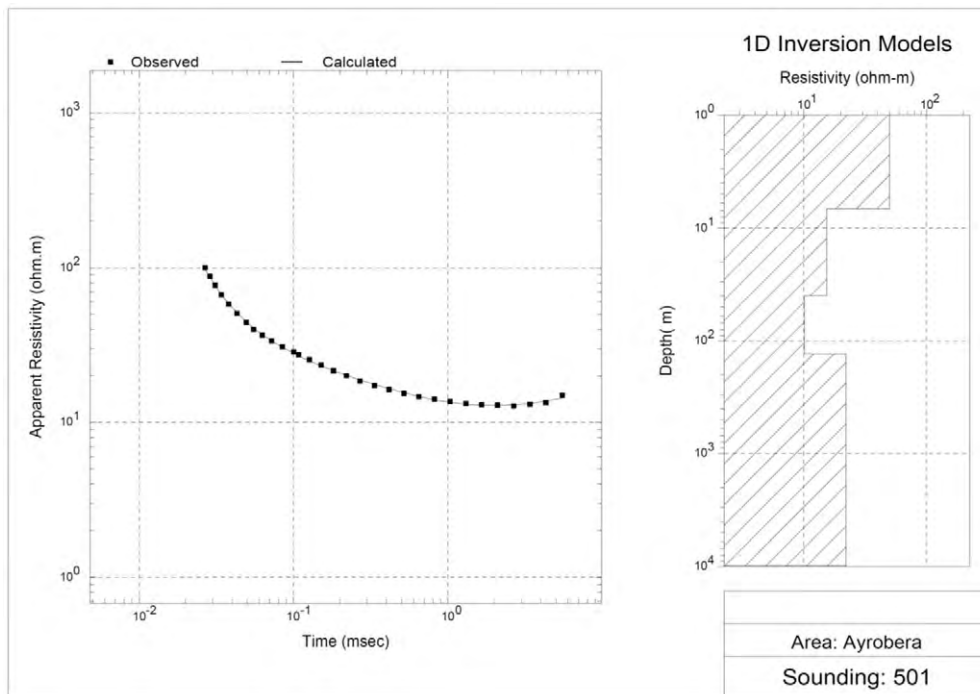


**Figure A2.2.2 Schematic drawing for deployment of TEM data acquisition system**

### (3) Data Processing and Analysis

The 1D inversion analysis was carried out from the acquired TEM data. The analysis software is WinGLink of GEOSYSTEM SRL. At each survey station, 5 or 6 layers' structure was assumed and the values of resistivity and layer's thickness of the 1D layered model was obtained by 1D inversion analysis so that the transient response of the 1D layered model fitted the observed transient response. An example of the acquired TEM data and the result of 1D layered inversion analysis are shown in Figure 8.



Observed data: □ and calculated curve: solid line (left) and 1D inversion result (right)

**Figure A2.2.3 An example of TEM data analysis**

#### (4) Static Correction of MT data

An important feature in the data processes with MT method is static shift. The apparent resistivity curve in Figure 9 contains a static shift caused by a local resistivity anomaly in the shallow ground near the survey station. Before starting the analysis, it is necessary to move the apparent resistivity curve back to its normal position, where it would be without the anomaly. A qualitative process is used for this purpose, incorporating shallow resistivity information by resistivity or other electromagnetic methods like TEM, or the difference in a pair of apparent resistivity of higher frequency band.

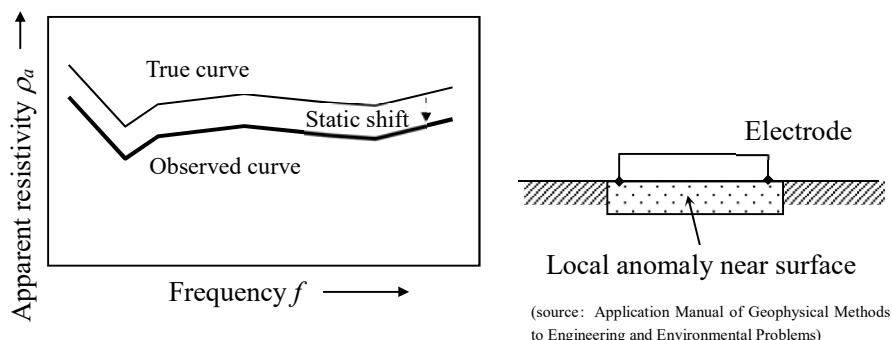


**Figure A2.2.4 Static-shift due to a near-surface anomaly**

In the project, TEM measurement was taken at the same station as MT measurement in the southern part of the survey site and 1D analysis for TEM data was executed. By using the result of the 1D analysis, the static correction was applied to MT data. MT response of the analyzed 1D model was calculated and

the apparent resistivity curve of MT data was shifted so that the curve of MT data in the highest frequency match MT response curve of 1D model from TEM. The list of shift value for each station is at the back of the report.

### **A2.3     MT/TEM Survey Results**

Results of MT/TEM survey carried out in this project are shown as follows.

### Coordinate of measuring stations (1/2) (Tendaho-2 Ayrobera)

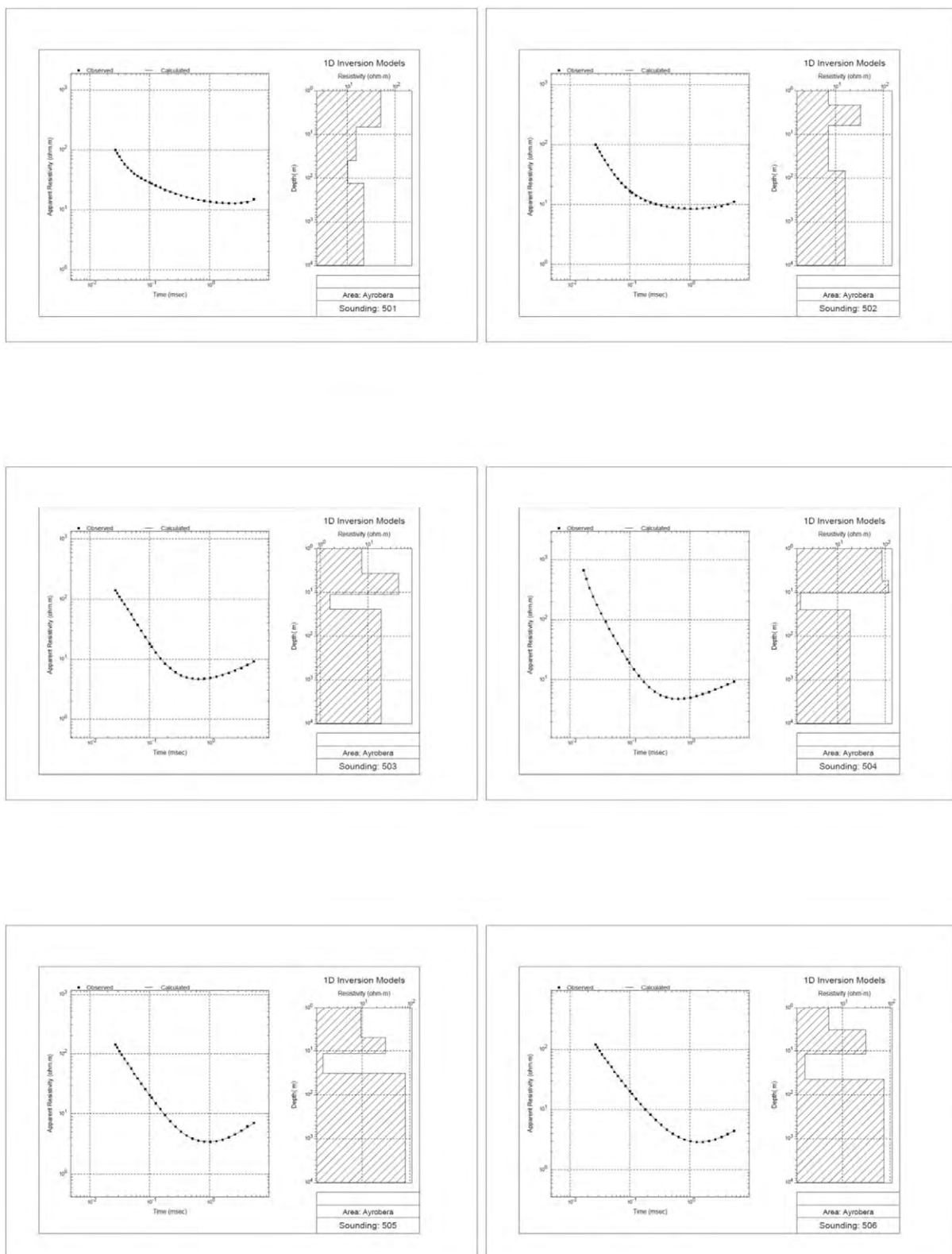
Station	Coordinate (WGS84)		Elevation (m)
	Latitude	Longitude	
AYR-301	11°55'19.9"	41°5'37.1"	389
AYR-302	11°55'39.5"	41°6'8.89"	374
AYR-303	11°55'56.4"	41°6'37.0"	373
AYR-304	11°56'13.1"	41°7'4.89"	372
AYR-305	11°56'30.4"	41°7'33.3"	371
AYR-306	11°56'48.9"	41°8'3.39"	372
AYR-307	11°57'4.50"	41°8'29.2"	372
AYR-397	11°53'28.7"	41°3'20.1"	364
AYR-398	11°53'44.8"	41°3'46.2"	372
AYR-399	11°54'0.90"	41°4'12.4"	372
AYR-400	11°54'16.9"	41°4'38.4"	378
AYR-401	11°55'4.60"	41°5'57.7"	384
AYR-402	11°55'12.8"	41°6'11.2"	377
AYR-403	11°55'21.5"	41°6'25.8"	373
AYR-404	11°55'30.3"	41°6'40.2"	373
AYR-405	11°55'39.1"	41°6'54.7"	373
AYR-406	11°55'47.9"	41°7'9.19"	372
AYR-407	11°55'56.6"	41°7'23.7"	373
AYR-408	11°56'5.40"	41°7'38.4"	374
AYR-409	11°56'14.0"	41°7'52.5"	372
AYR-410	11°56'22.9"	41°8'7.09"	373
AYR-411	11°56'31.6"	41°8'21.6"	373
AYR-412	11°56'40.4"	41°8'36.0"	373
AYR-501	11°54'39.0"	41°6'3.29"	391
AYR-502	11°54'59.5"	41°6'36.5"	373
AYR-503	11°55'16.4"	41°7'4.89"	372
AYR-504	11°55'33.1"	41°7'32.6"	374
AYR-505	11°55'50.6"	41°8'1.19"	372
AYR-506	11°56'9.10"	41°8'31.3"	373
AYR-507	11°56'24.7"	41°8'57.4"	373
AYR-599	11°53'2.90"	41°4'6.49"	366
AYR-600	11°53'13.2"	41°4'24.7"	367
AYR-601	11°53'22.9"	41°4'43.3"	370
AYR-602	11°53'35.8"	41°5'3.59"	372
AYR-603	11°53'44.0"	41°5'21.5"	377
AYR-604	11°54'3.50"	41°5'52.9"	378
AYR-605	11°54'13.3"	41°6'13.9"	382
AYR-606	11°54'23.7"	41°6'29.4"	376
AYR-607	11°54'32.5"	41°6'44.9"	373
AYR-608	11°54'41.3"	41°7'0.59"	372
AYR-609	11°54'50.2"	41°7'15.9"	372
AYR-610	11°54'59.2"	41°7'31.5"	372
AYR-611	11°55'7.90"	41°7'47.1"	372
AYR-612	11°55'16.9"	41°8'2.79"	373
AYR-613	11°55'25.7"	41°8'18.2"	373
AYR-614	11°55'34.6"	41°8'33.7"	373
AYR-615	11°55'43.6"	41°8'49.4"	374
AYR-616	11°55'52.3"	41°9'4.89"	373
AYR-617	11°56'1.10"	41°9'20.3"	373
AYR-700	11°52'57.3"	41°4'33.8"	367
AYR-701	11°53'10.1"	41°5'4.69"	372
AYR-702	11°53'26.1"	41°5'34.3"	373
AYR-703	11°53'42.1"	41°6'5.99"	377
AYR-704	11°53'58.3"	41°6'36.4"	375
AYR-705	11°54'14.6"	41°7'6.79"	373
AYR-706	11°54'39.1"	41°7'52.5"	372
AYR-707	11°54'59.0"	41°8'29.6"	373
AYR-708	11°55'9.10"	41°8'48.6"	373
AYR-709	11°55'29.9"	41°9'27.4"	374
AYR-799	11°52'22.7"	41°4'35.1"	368

### Coordinate of measuring stations (2/2) (Tendaho-2 Ayrobera)

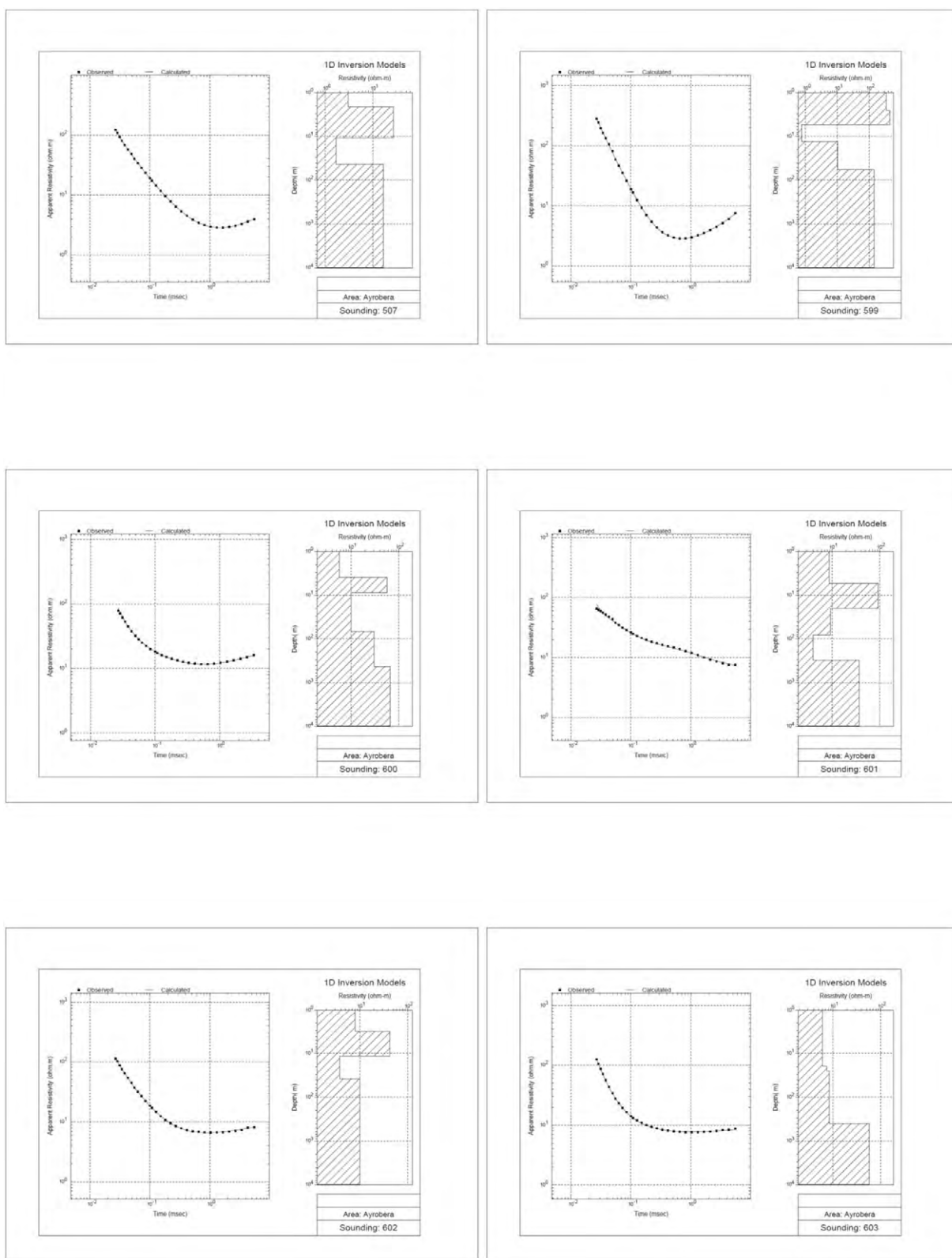
Station	Coordinate (WGS84)		Elevation (m)
	Latitude	longitude	
AYR-800	11°52'33.0"	41°4'53.6"	368
AYR-801	11°52'42.2"	41°5'12.7"	371
AYR-802	11°52'53.8"	41°5'30.0"	374
AYR-803	11°53'4.60"	41°5'47.3"	377
AYR-804	11°53'15.7"	41°6'58.9"	376
AYR-805	11°53'26.6"	41°6'23.8"	376
AYR-806	11°53'37.6"	41°6'41.8"	373
AYR-807	11°53'48.4"	41°6'59.7"	371
AYR-808	11°53'58.3"	41°7'16.9"	374
AYR-809	11°54'8.40"	41°7'35.1"	373
AYR-810	11°54'18.5"	41°7'53.3"	374
AYR-811	11°54'28.8"	41°8'11.4"	373
AYR-812	11°54'38.9"	41°8'29.6"	373
AYR-813	11°54'49.1"	41°8'47.7"	372
AYR-814	11°54'59.2"	41°9'6.09"	373
AYR-815	11°55'9.40"	41°9'24.1"	373
AYR-816	11°55'19.6"	41°9'42.2"	374
AYR-899	11°52'5.00"	41°4'49.2"	369
AYR-900	11°52'15.2"	41°5'7.49"	369
AYR-901	11°52'25.7"	41°5'25.8"	371
AYR-902	11°52'36.6"	41°5'43.8"	374
AYR-903	11°52'47.6"	41°6'1.79"	377
AYR-904	11°52'58.5"	41°6'19.6"	377
AYR-905	11°53'9.50"	41°6'37.6"	374
AYR-906	11°53'20.3"	41°6'55.5"	373
AYR-907	11°53'31.4"	41°7'13.4"	371
AYR-908	11°53'40.9"	41°7'30.9"	374
AYR-909	11°53'50.8"	41°7'49.2"	374
AYR-910	11°54'1.10"	41°8'7.39"	373
AYR-911	11°54'11.0"	41°8'25.2"	373
AYR-912	11°54'21.5"	41°8'44.2"	373
AYR-913	11°54'31.7"	41°9'1.79"	373
AYR-914	11°54'41.9"	41°9'19.9"	373
TDH-900 (MT-Ref: Mille)	11°16'37.0"	40°42'16.0"	512

### Static shift correction value

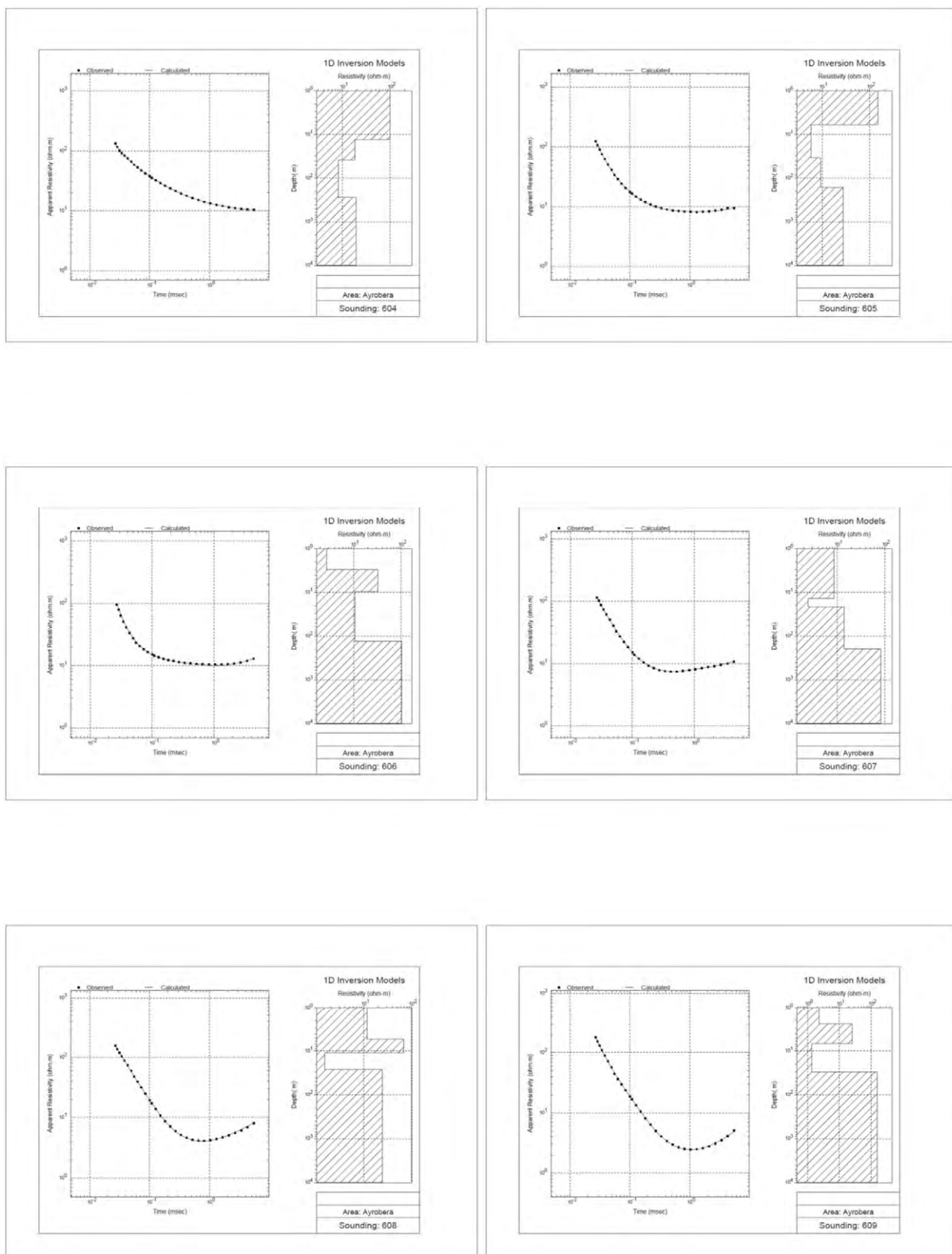
Station	Static Shift (xy)	Static Shift (yx)	Station	Static Shift (xy)	Static Shift (yx)
AYR-501	1.000	1.162	AYR-803	1.152	0.832
AYR-502	1.000	0.825	AYR-804	1.000	1.137
AYR-503	1.117	1.108	AYR-805	1.131	1.073
AYR-504	1.120	1.182	AYR-806	1.110	1.000
AYR-505	1.192	1.108	AYR-807	1.000	1.000
AYR-506	1.215	1.088	AYR-808	1.000	1.189
AYR-507	1.149	1.000	AYR-809	55.61	1.409
AYR-599	1.534	1.224	AYR-810	1.895	1.943
AYR-600	1.000	1.000	AYR-811	1.121	1.189
AYR-601	1.437	0.796	AYR-812	1.457	1.201
AYR-602	1.269	1.041	AYR-813	1.179	1.106
AYR-603	1.221	1.000	AYR-814	1.227	1.089
AYR-604	1.000	1.000	AYR-815	1.130	1.130
AYR-605	1.000	1.000	AYR-816	1.145	1.078
AYR-606	1.384	1.136	TDO9701	1.000	1.000
AYR-607	1.257	1.075	TDO9702	1.049	1.128
AYR-608	1.146	1.410	TDO9703	1.232	1.433
AYR-609	1.208	1.244	TDO9705	1.000	1.000
AYR-610	2.241	1.985	TDO9706	0.846	0.702
AYR-611	1.387	0.736	TDO9707	1.392	1.066
AYR-612	1.000	0.729	TDO9708	1.000	1.183
AYR-613	1.470	1.000	TDO9709	1.540	1.178
AYR-614	1.328	1.151	TDO9710	2.126	1.766
AYR-615	1.000	1.000	TDO9711	1.992	2.090
AYR-616	1.245	1.146	TDO9712	1.000	1.000
AYR-617	1.159	1.140	TDO9713	1.000	1.289
AYR-700	1.000	0.656	TDO9714	0.890	1.270
AYR-701	0.707	1.000	TDO9801	1.503	1.459
AYR-702	1.229	1.085	TDO9802	1.000	1.625
AYR-703	1.112	1.004	TDO9803	1.752	0.734
AYR-704	1.280	1.094	TDO9804	1.097	1.103
AYR-705	1.457	1.000	TDO9805	1.923	1.051
AYR-706	0.874	0.854	TDO9806	1.000	1.000
AYR-707	1.432	1.000	TDO9807	1.326	1.780
AYR-708	1.000	0.727	TDO9808	1.569	1.364
AYR-709	1.082	1.131	TDO9809	1.316	1.000
AYR-799	1.249	1.137	TDO9810	1.140	0.699
AYR-800	1.131	1.110	TDO9811	1.167	1.207
AYR-801	1.102	0.857	TDO9812	1.405	0.901
AYR-802	1.217	1.074	TDO9813	1.101	1.217



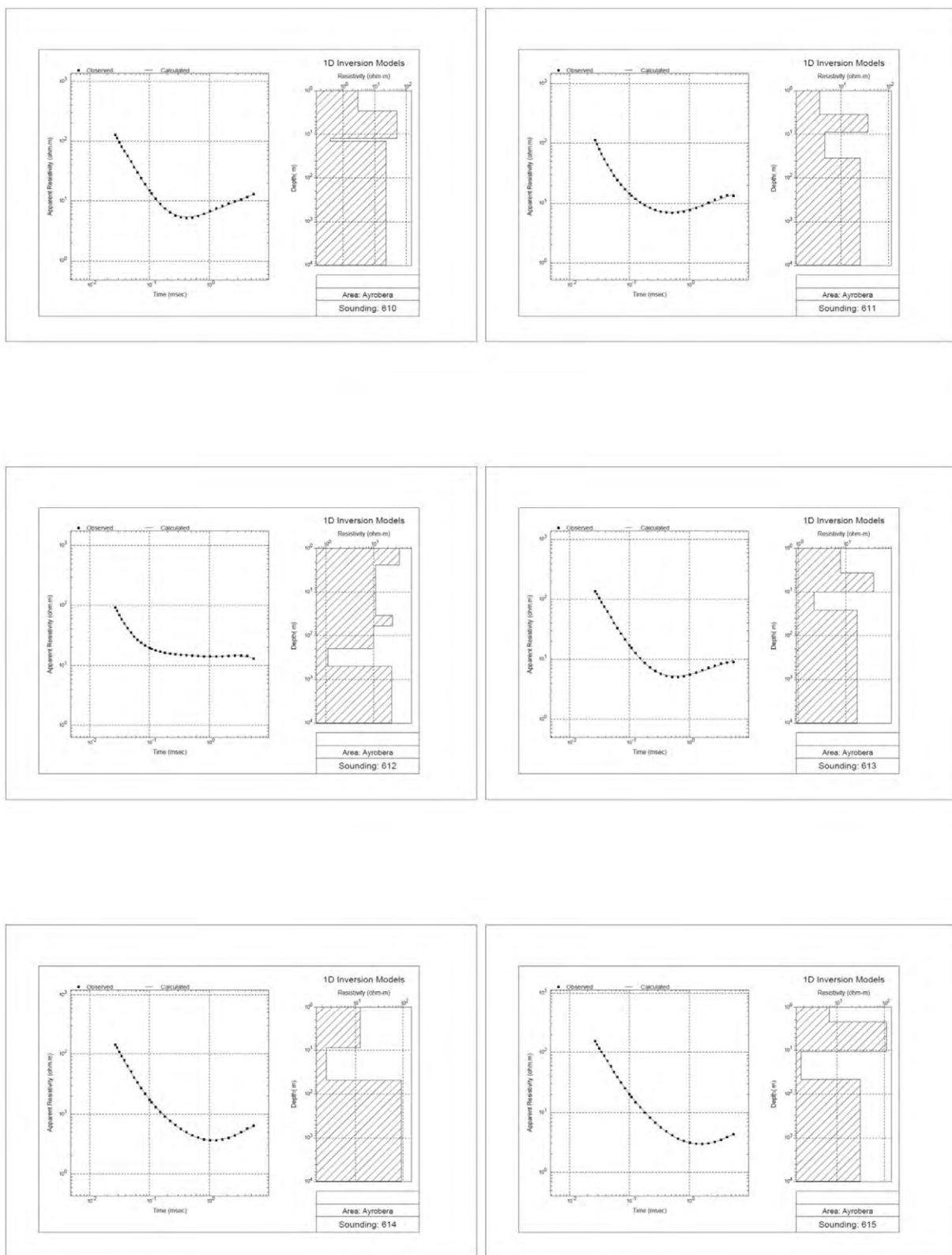
One-dimensional analysis result of TEM survey (1/14)



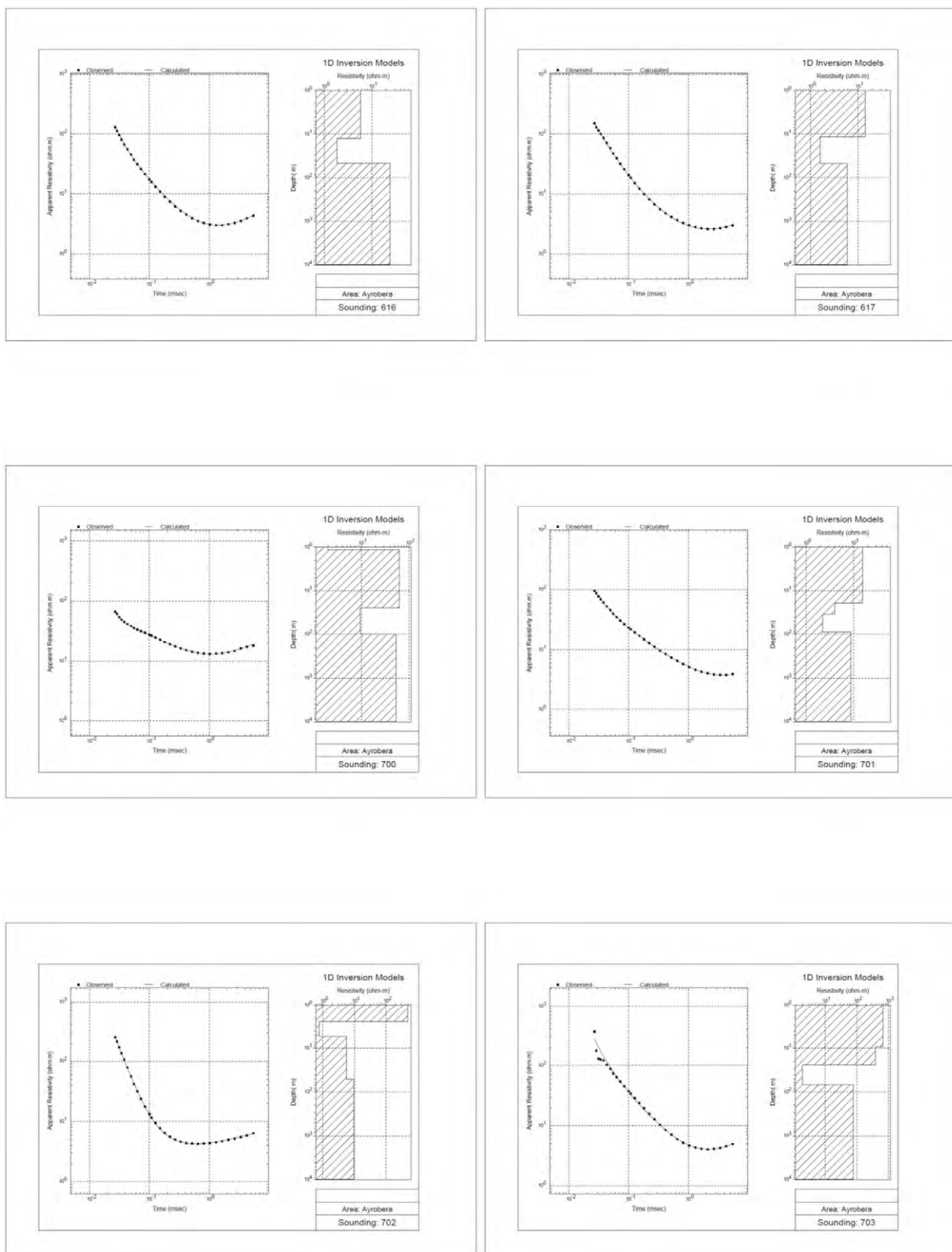
One-dimensional analysis result of TEM survey (2/14)



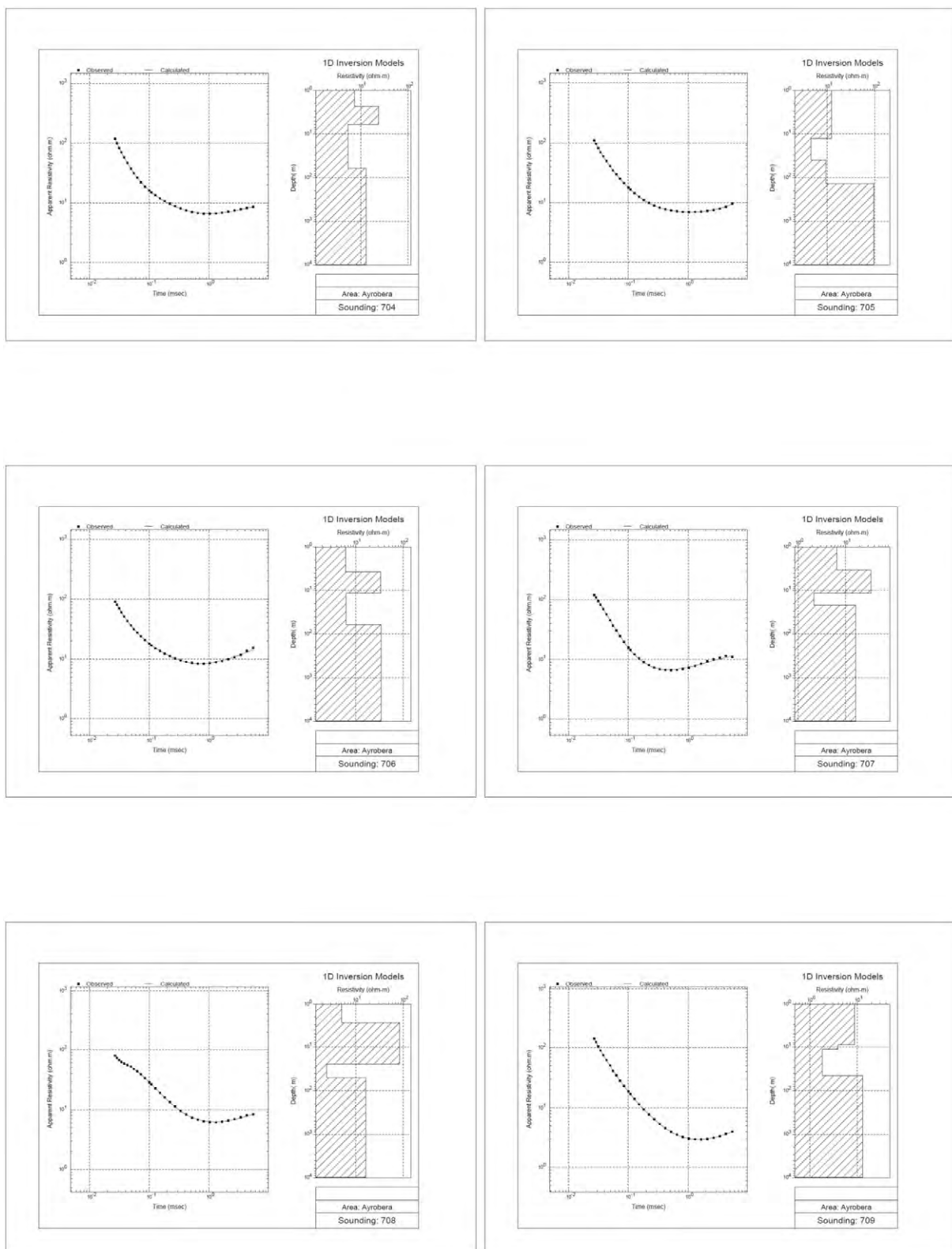
One-dimensional analysis result of TEM survey (3/14)



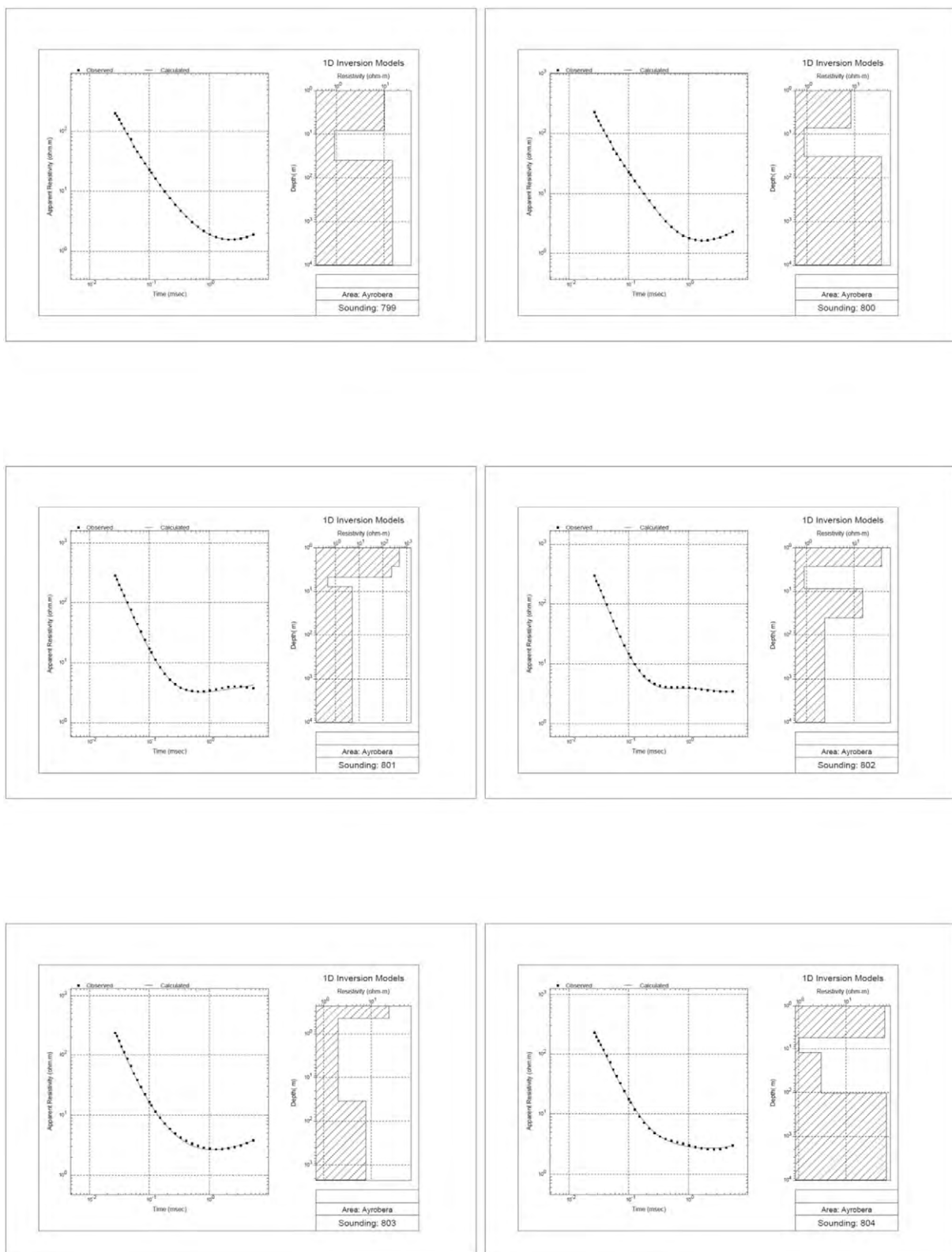
One-dimensional analysis result of TEM survey (4/14)



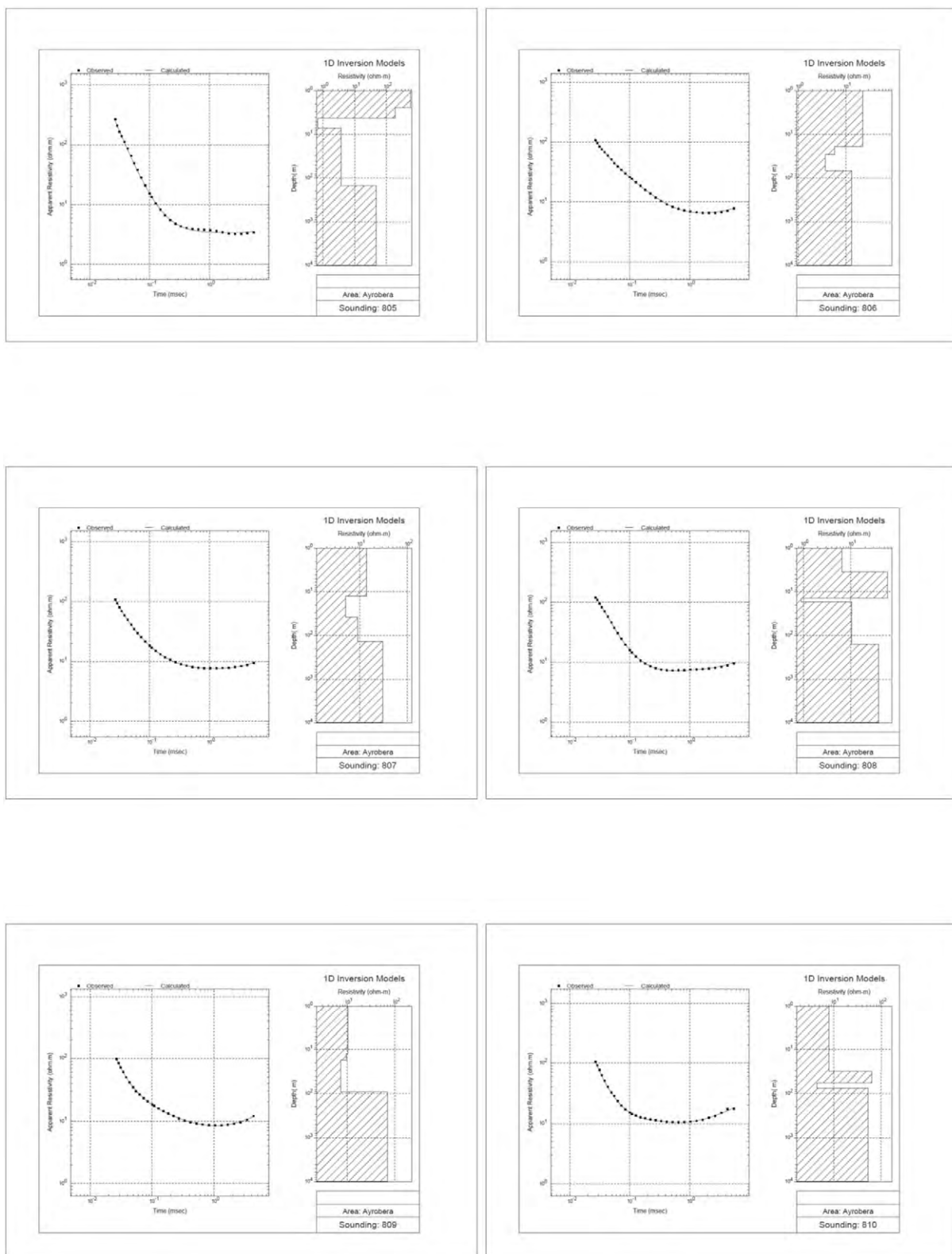
One-dimensional analysis result of TEM survey (5/14)



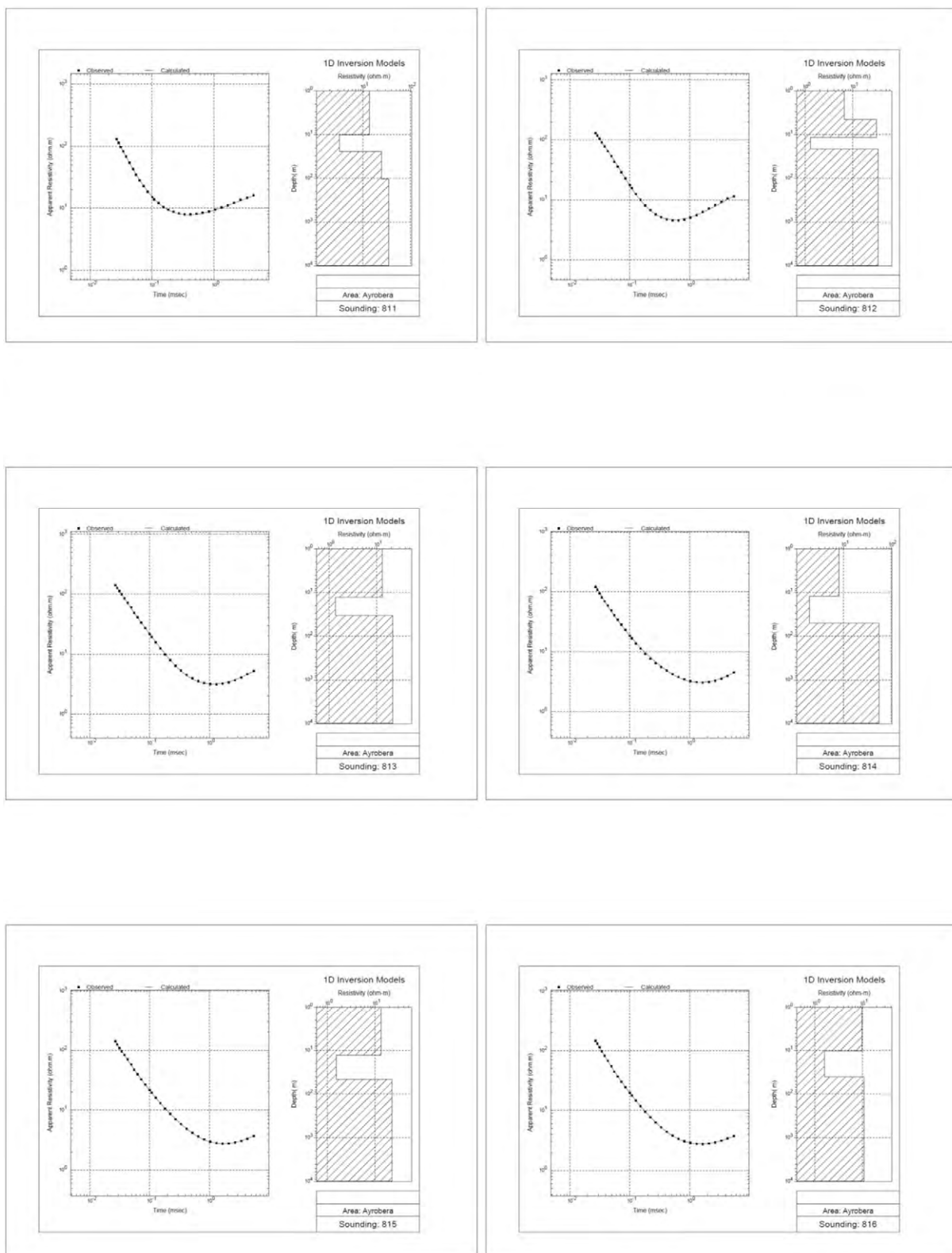
One-dimensional analysis result of TEM survey (6/14)



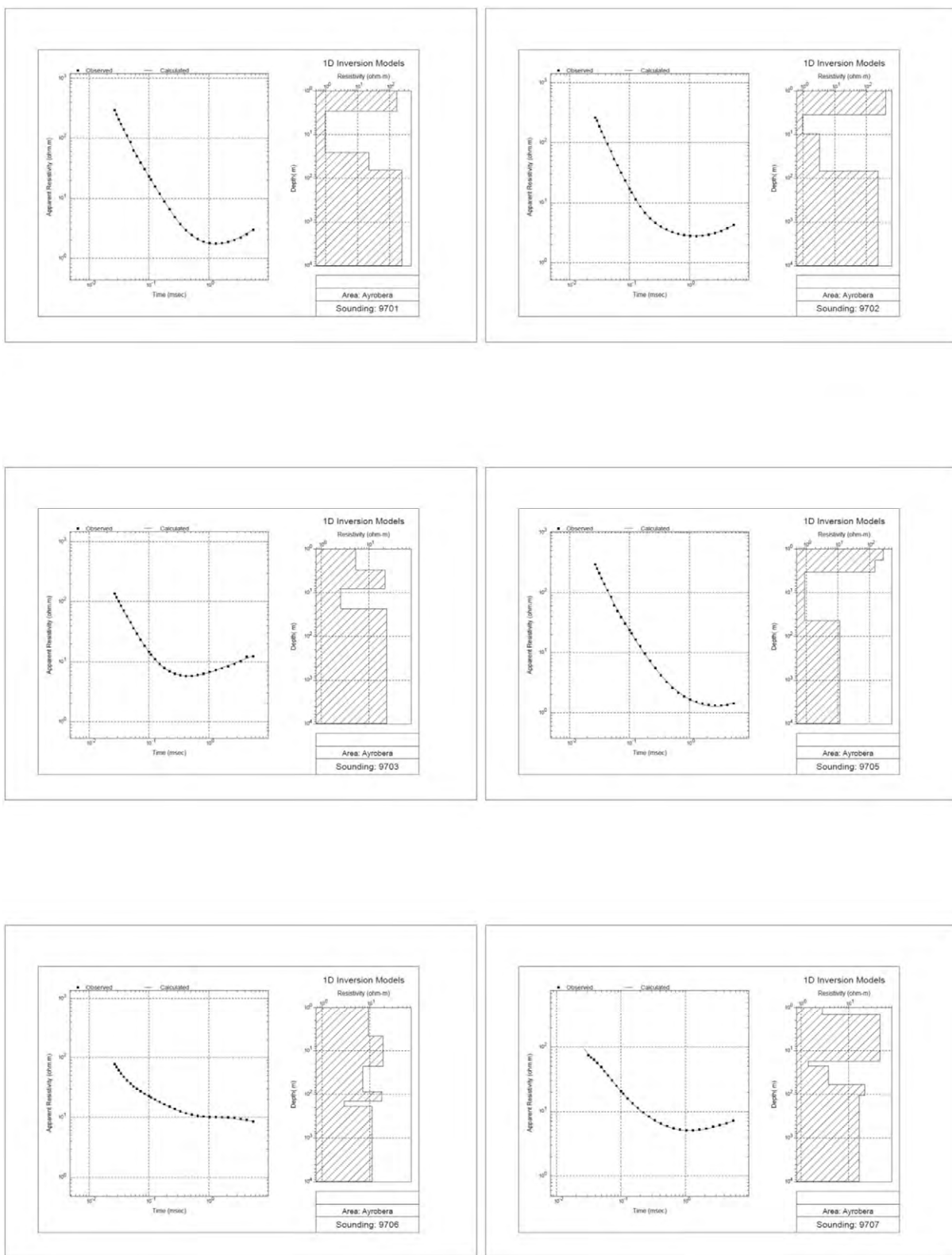
One-dimensional analysis result of TEM survey (7/14)



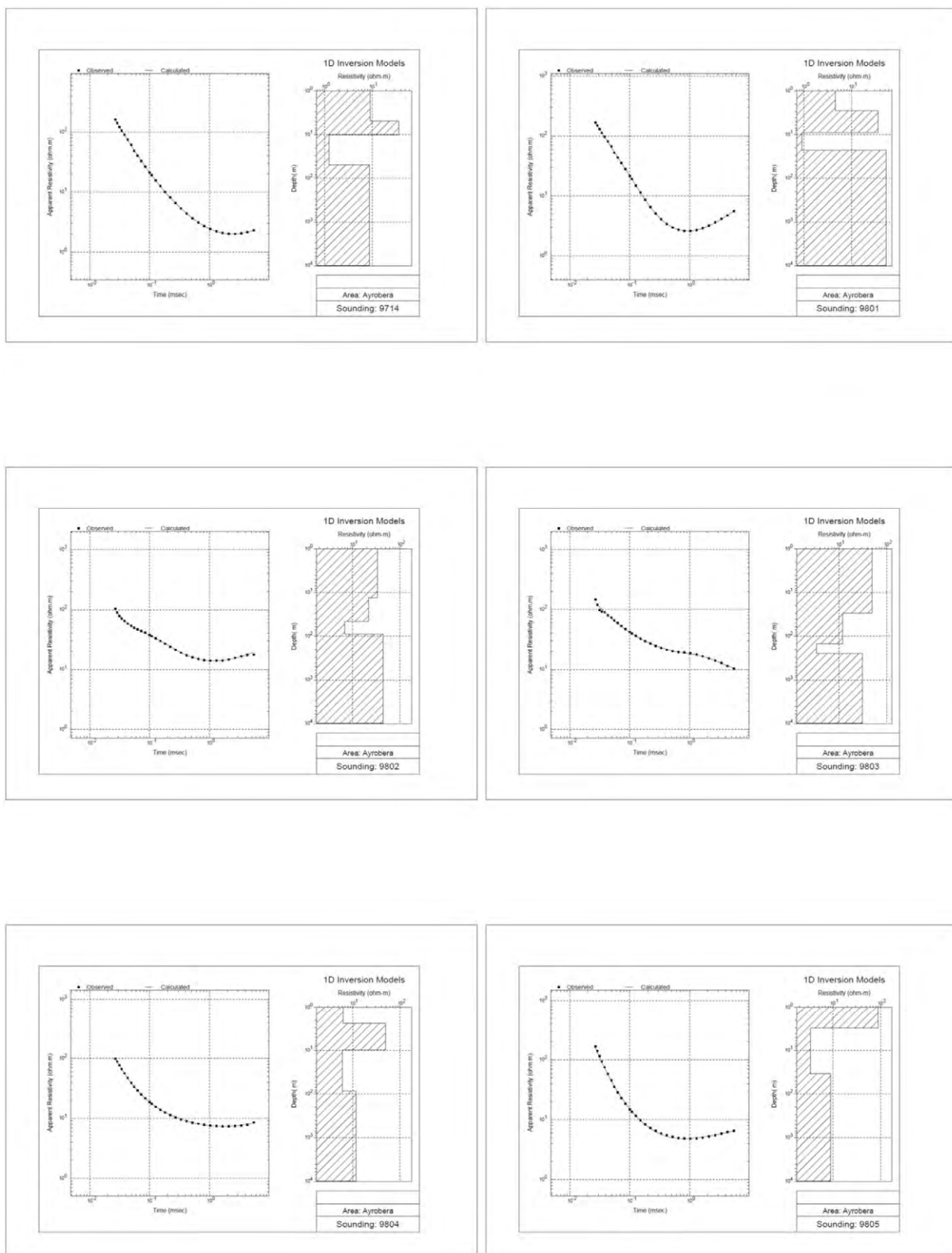
One-dimensional analysis result of TEM survey (8/14)



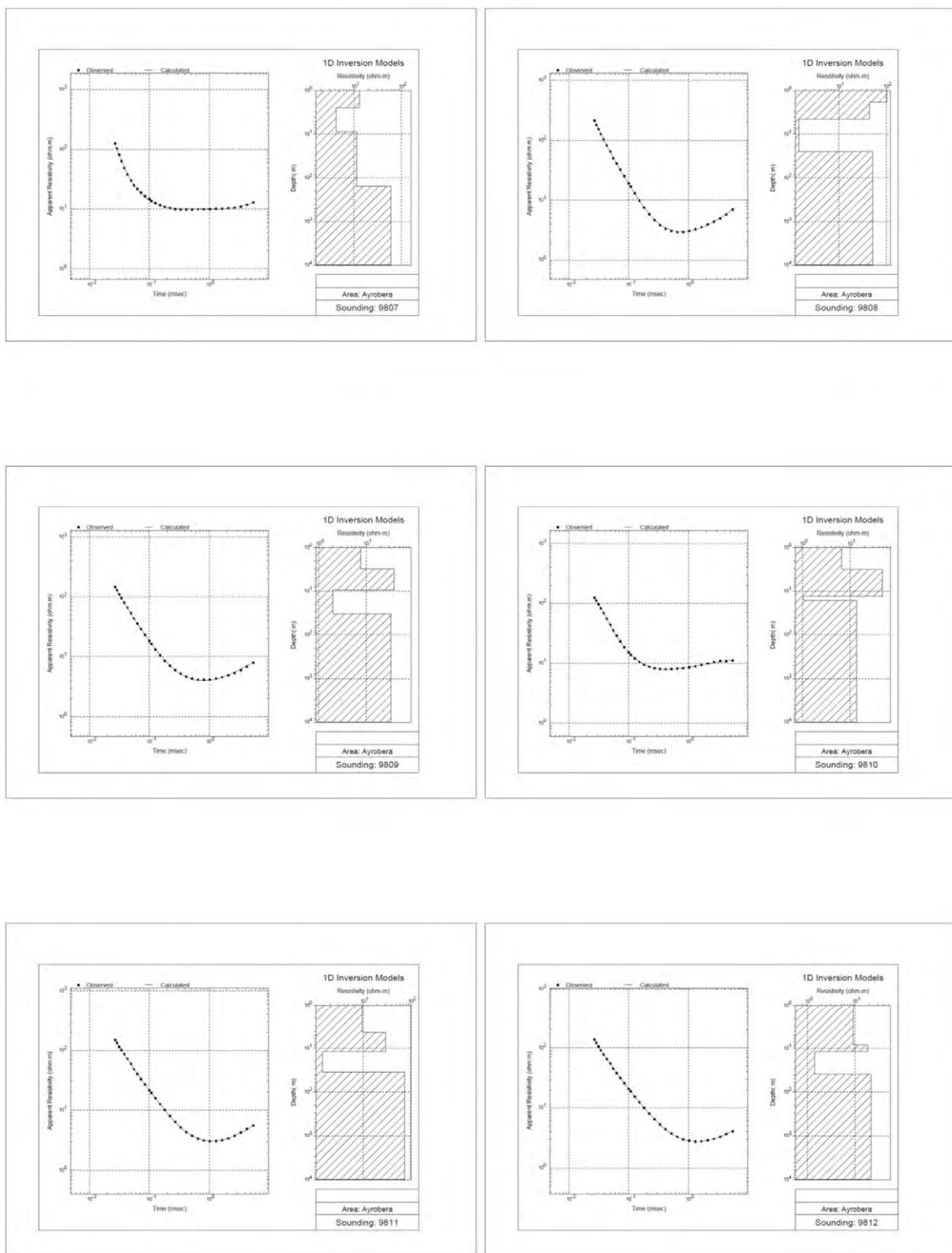
One-dimensional analysis result of TEM survey (9/14)



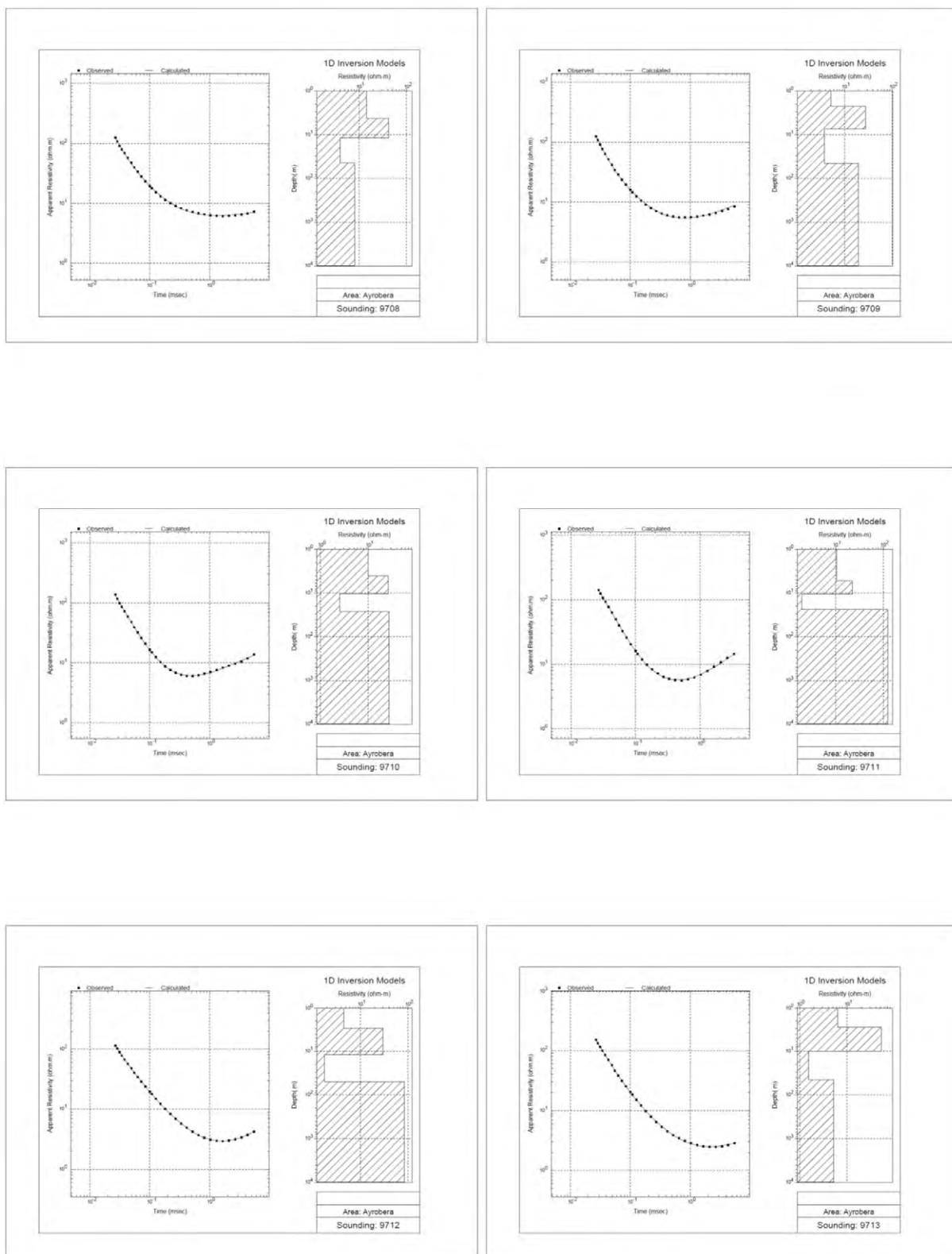
One-dimensional analysis result of TEM survey (10/14)



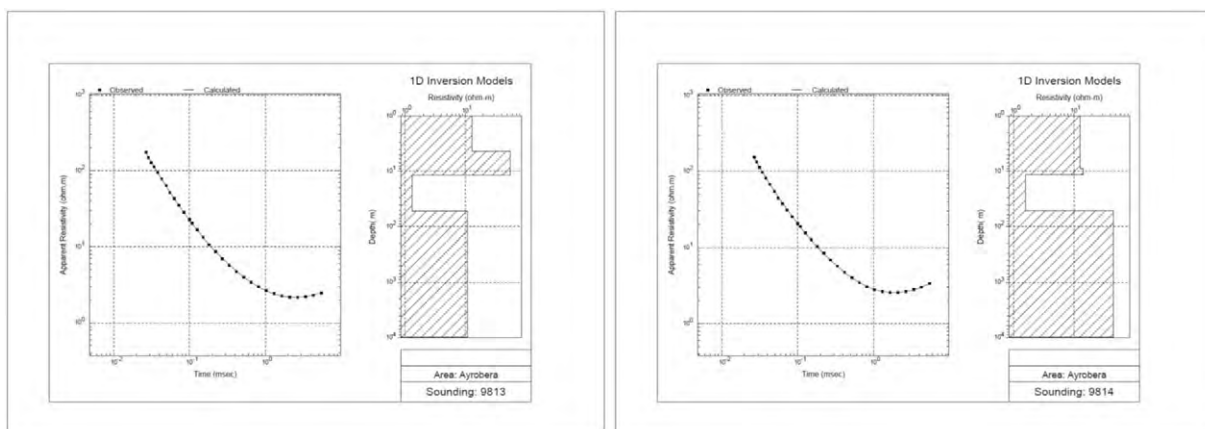
One-dimensional analysis result of TEM survey (11/14)



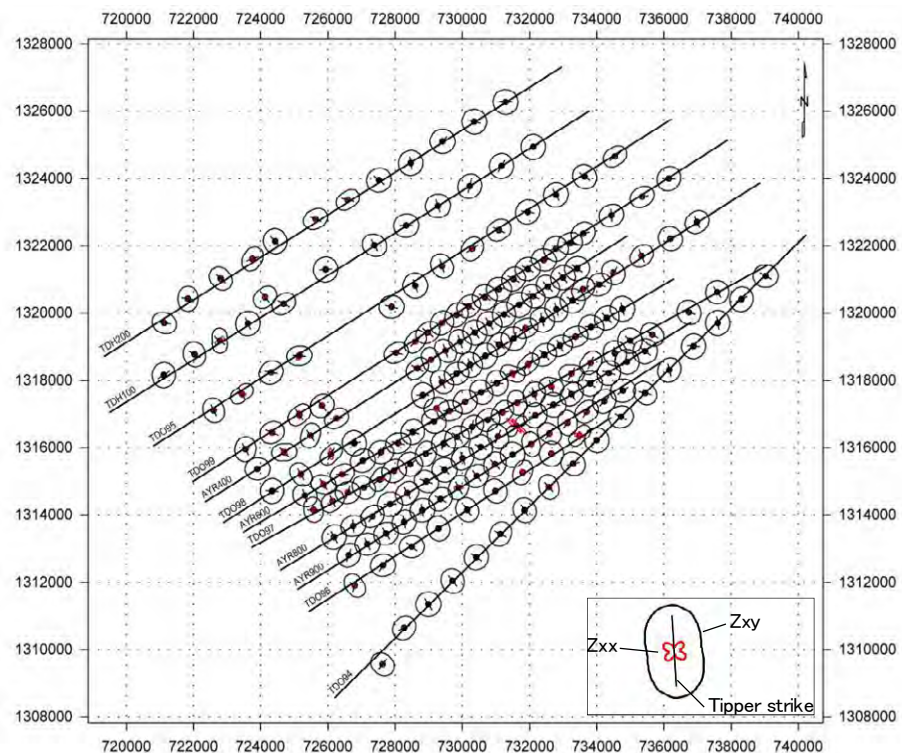
One-dimensional analysis result of TEM survey (12/14)



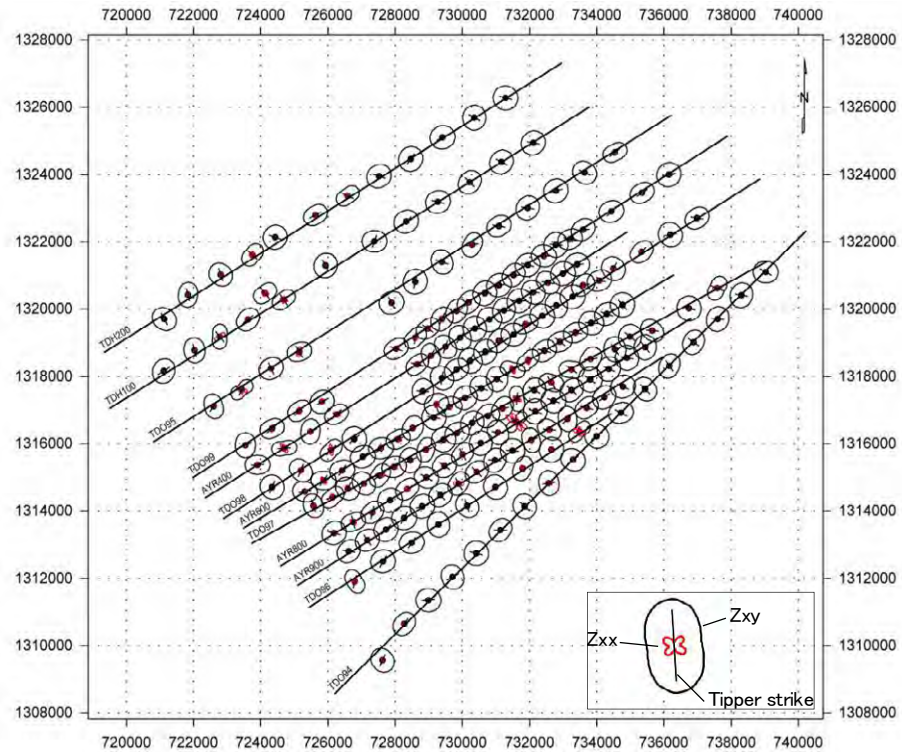
One-dimensional analysis result of TEM survey (13/14)



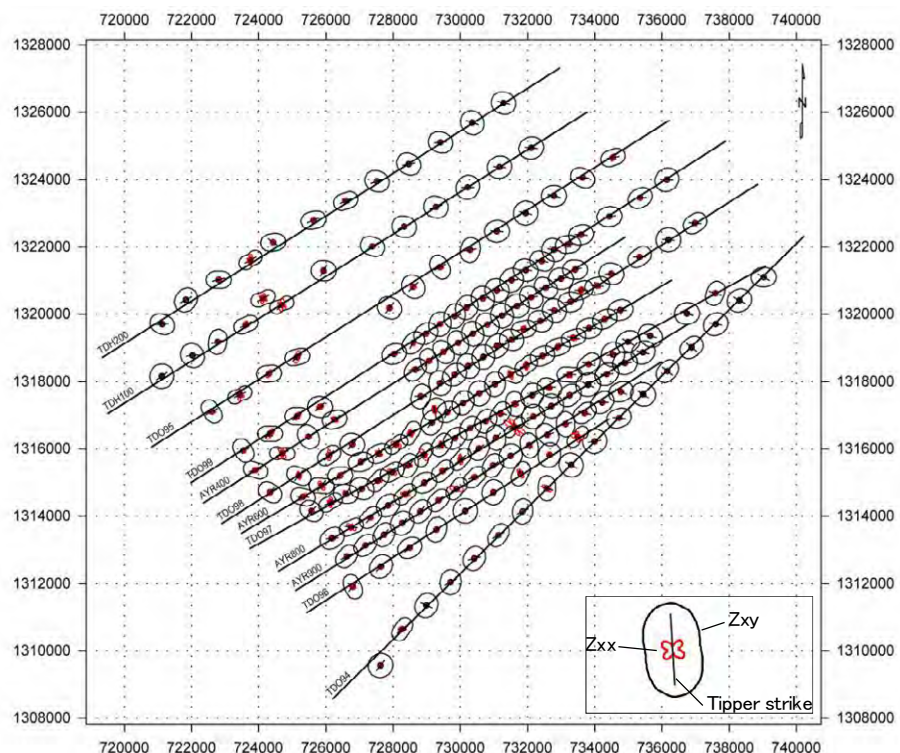
### One-dimensional analysis result of TEM survey (14/14)



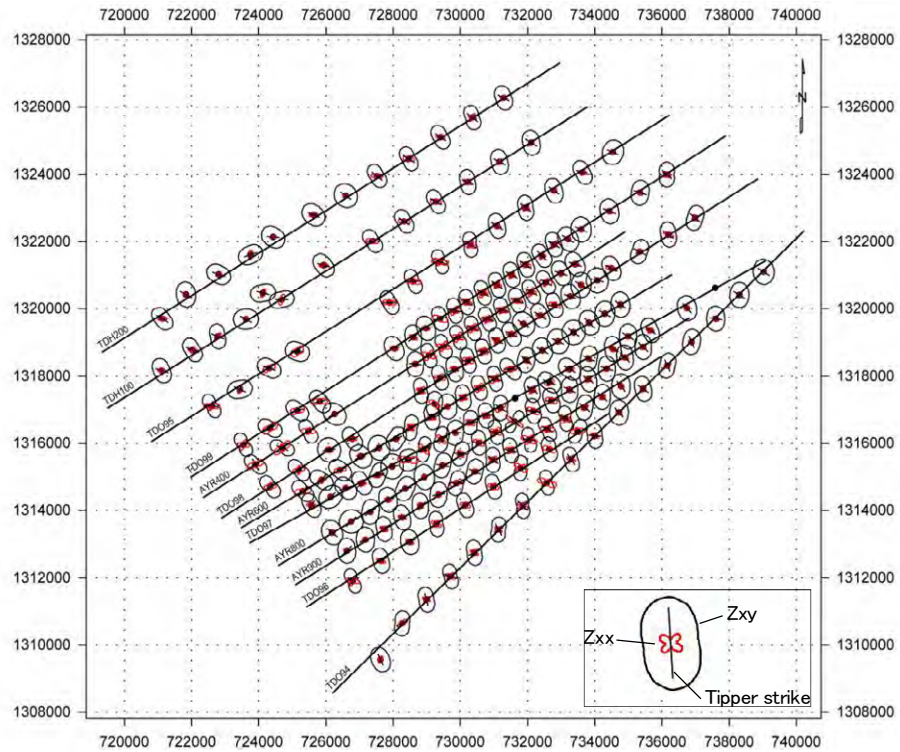
**Impedance polar diagram and tipper strike (10Hz)**



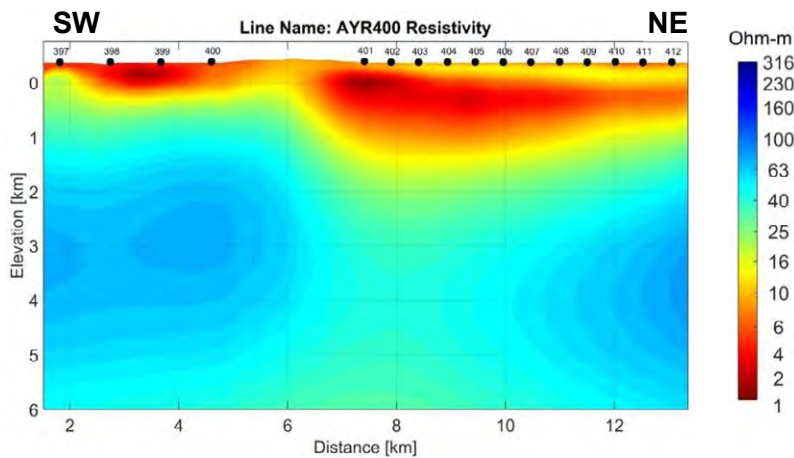
**Impedance polar diagram and tipper strike (1Hz)**



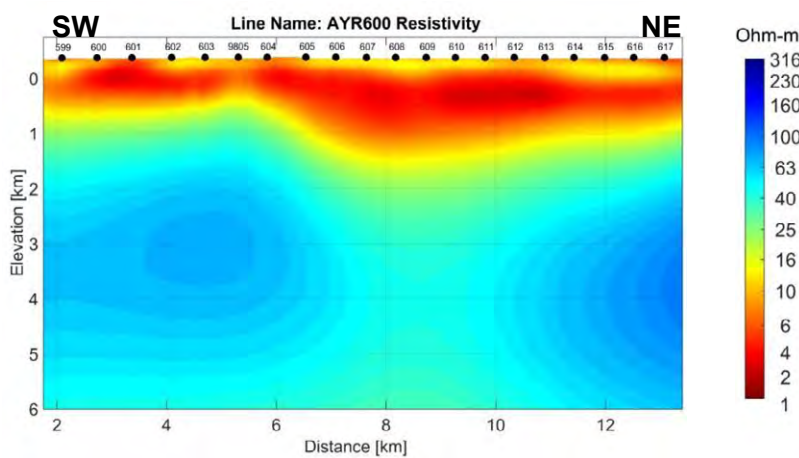
**Impedance polar diagram and tipper strike (0.1Hz)**



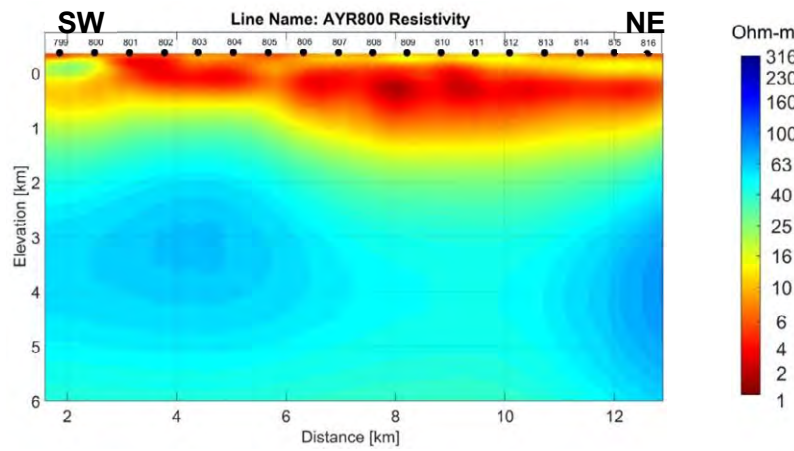
**Impedance polar diagram and tipper strike (0.01Hz)**



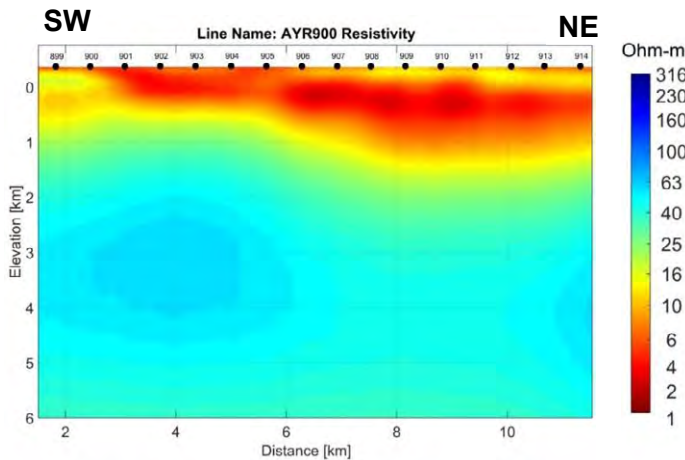
Resistivity cross section map (3D model) (AYR400)



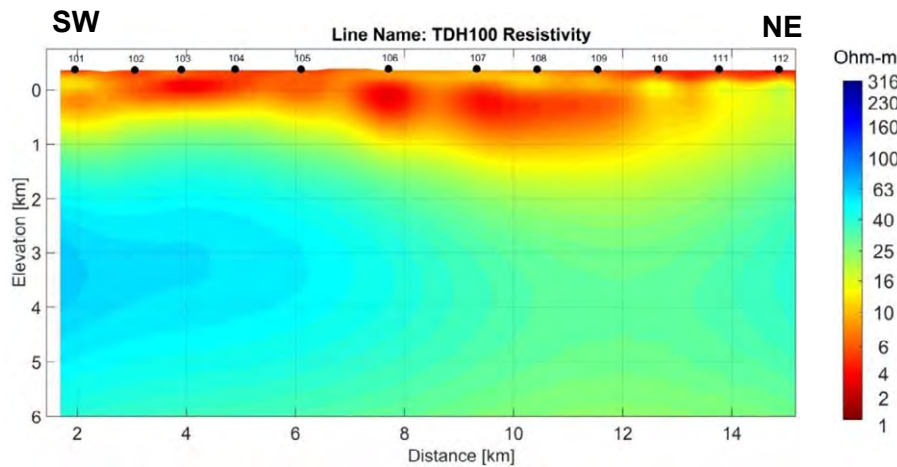
Resistivity cross section map (3D model) (AYR600)



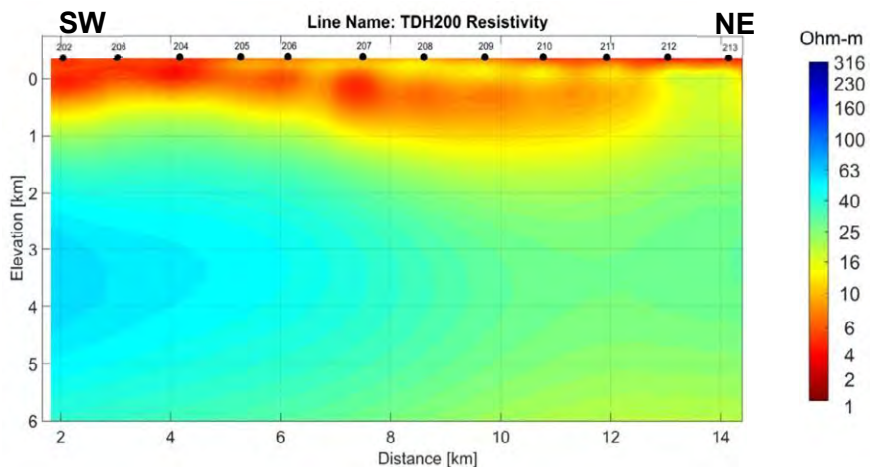
Resistivity cross section map (3D model) (AYR800)



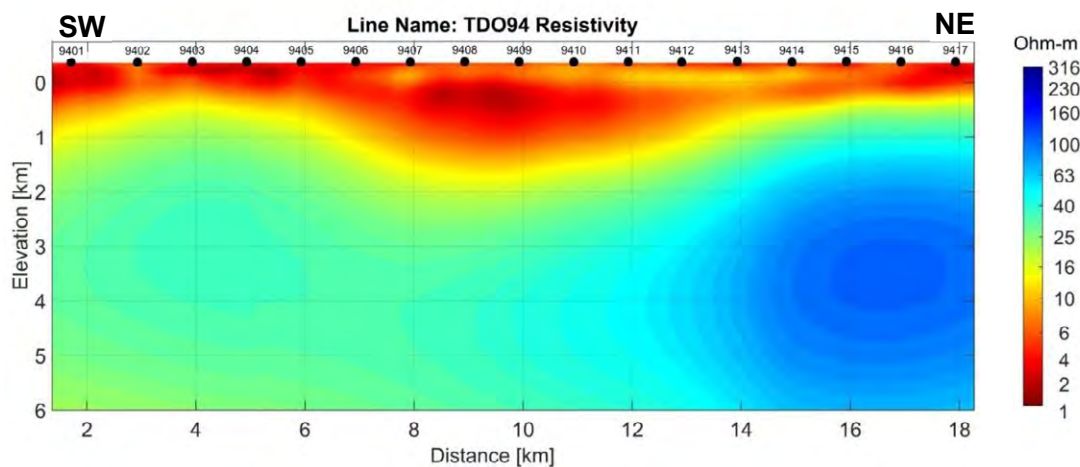
Resistivity cross section map (3D model) (AYR900)



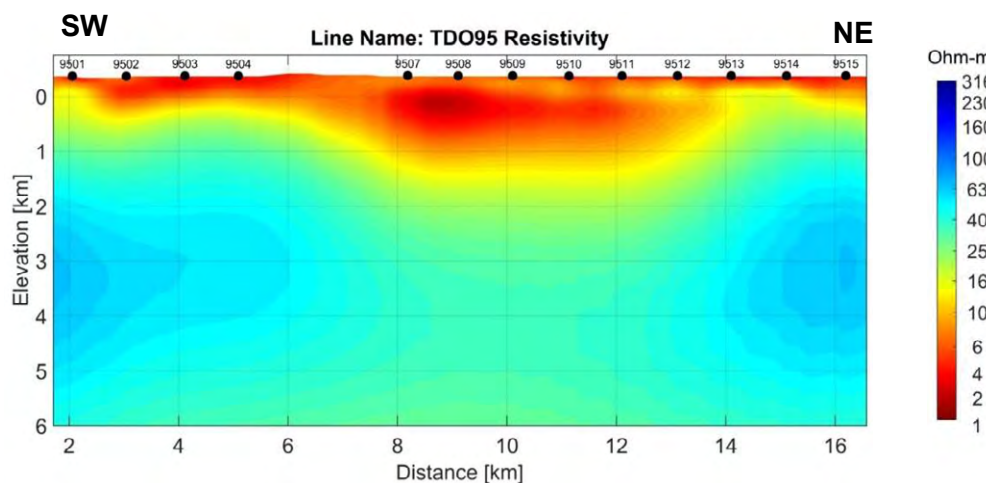
Resistivity cross section map (3D model) (TDH100)



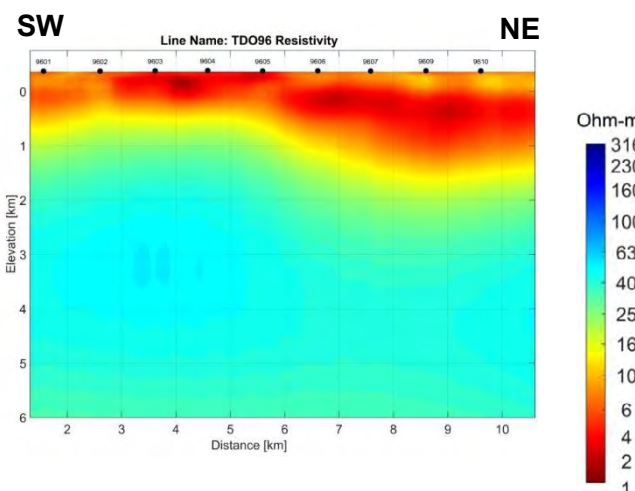
Resistivity cross section map (3D model) (TDH200)



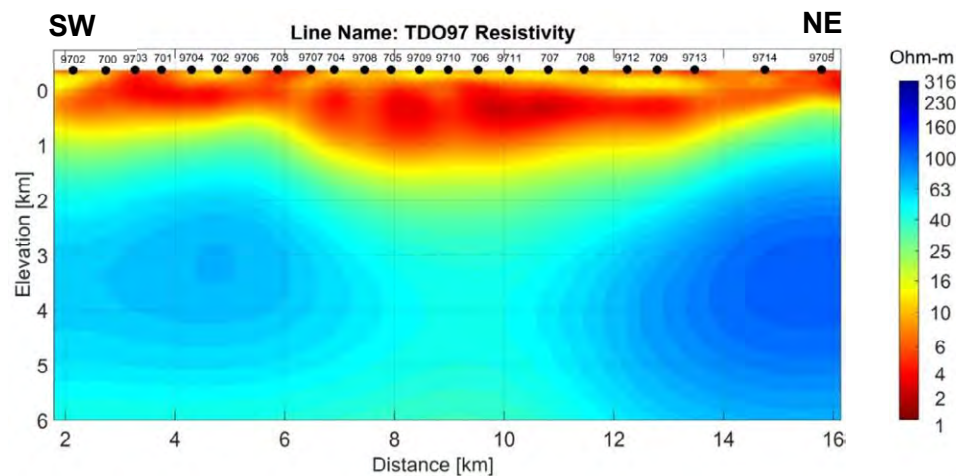
Resistivity cross section map (3D model) (TDO94)



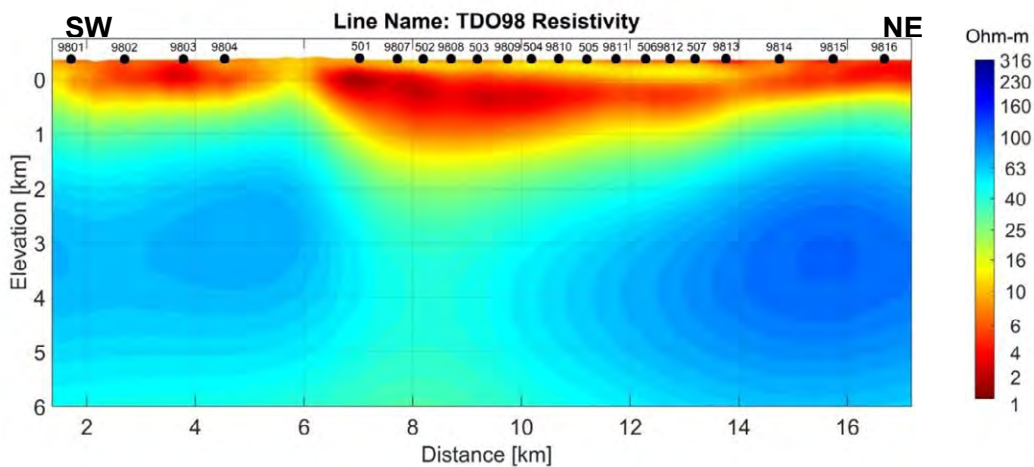
Resistivity cross section map (3D model) (TDO95)



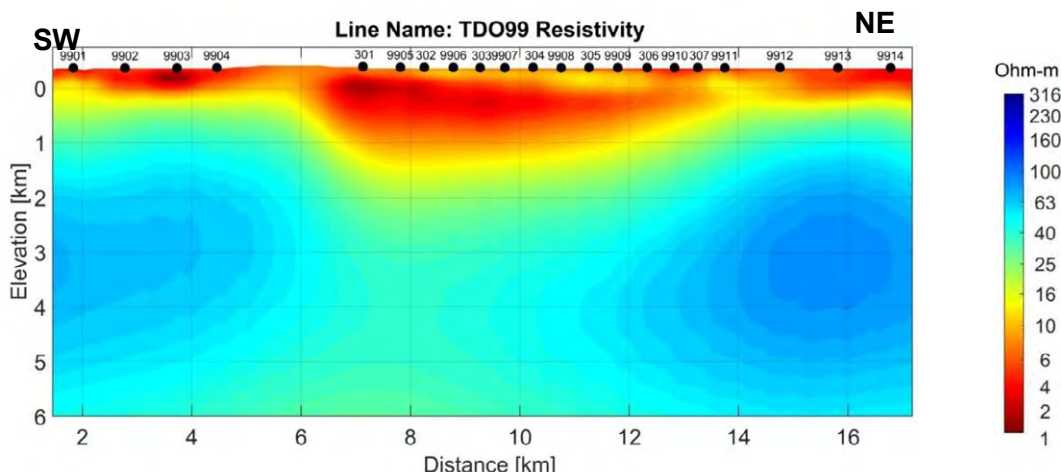
Resistivity cross section map (3D model) (TDO96)



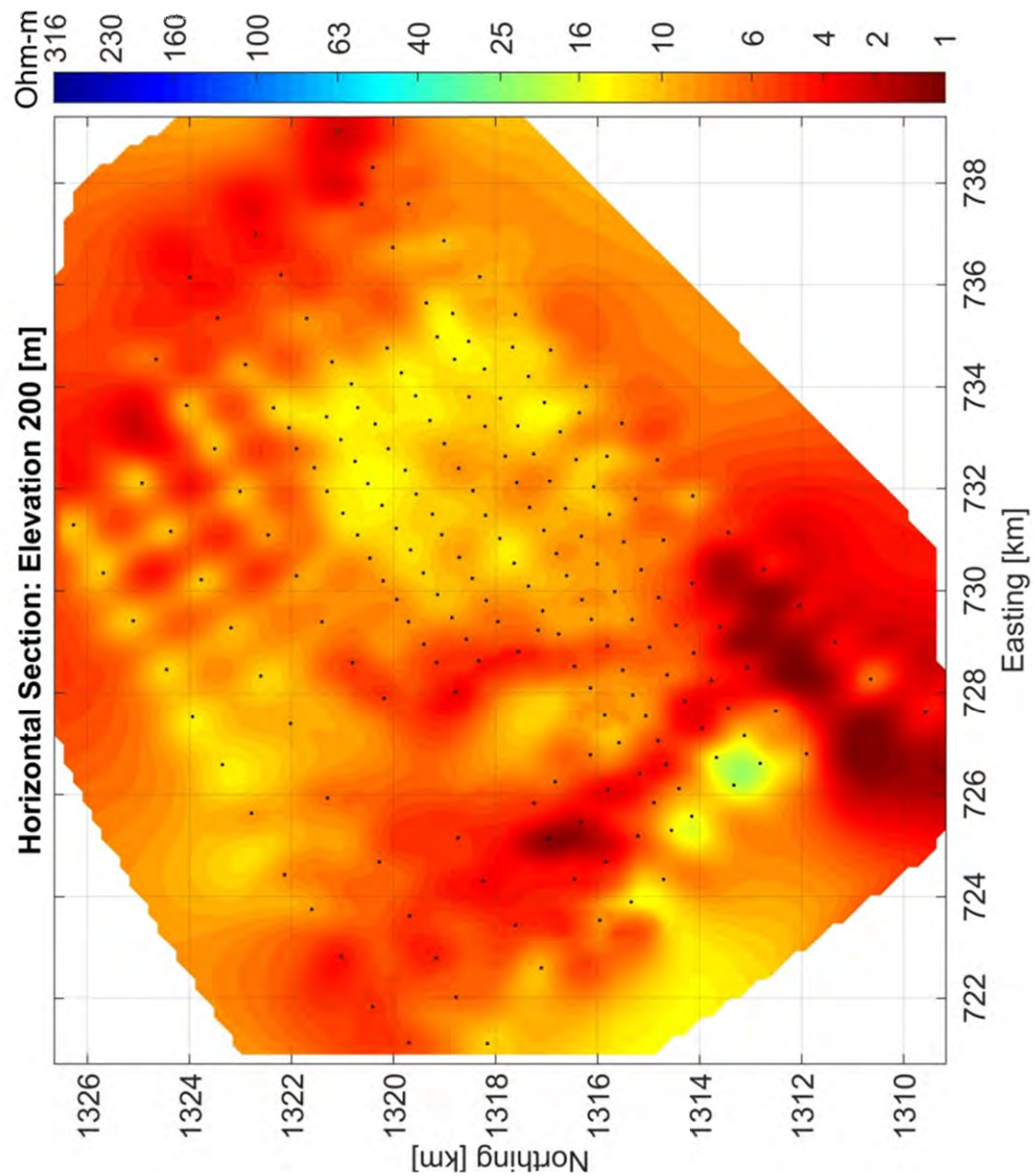
Resistivity cross section map (3D model) (TDO97)



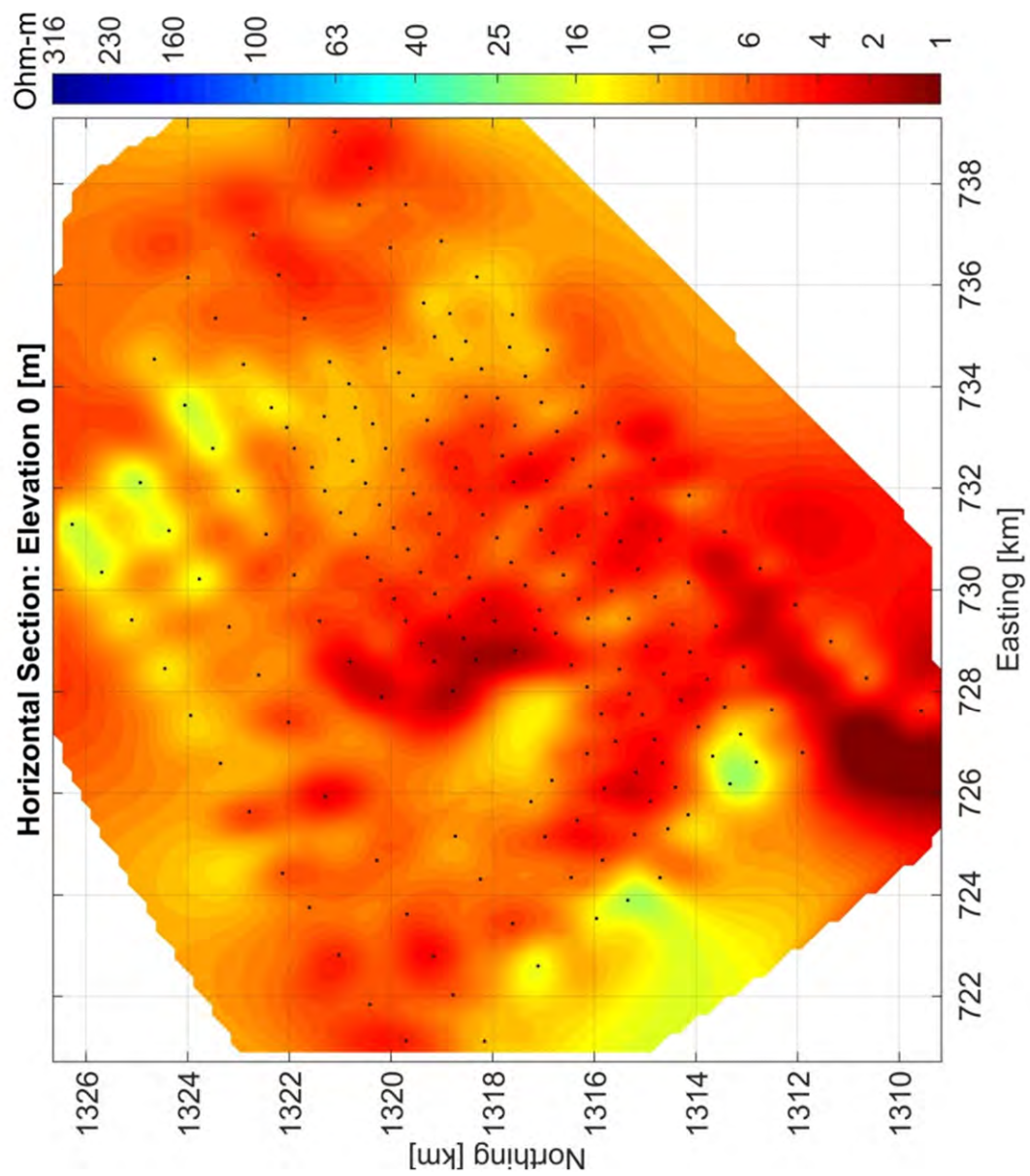
Resistivity cross section map (3D model) (TDO98)



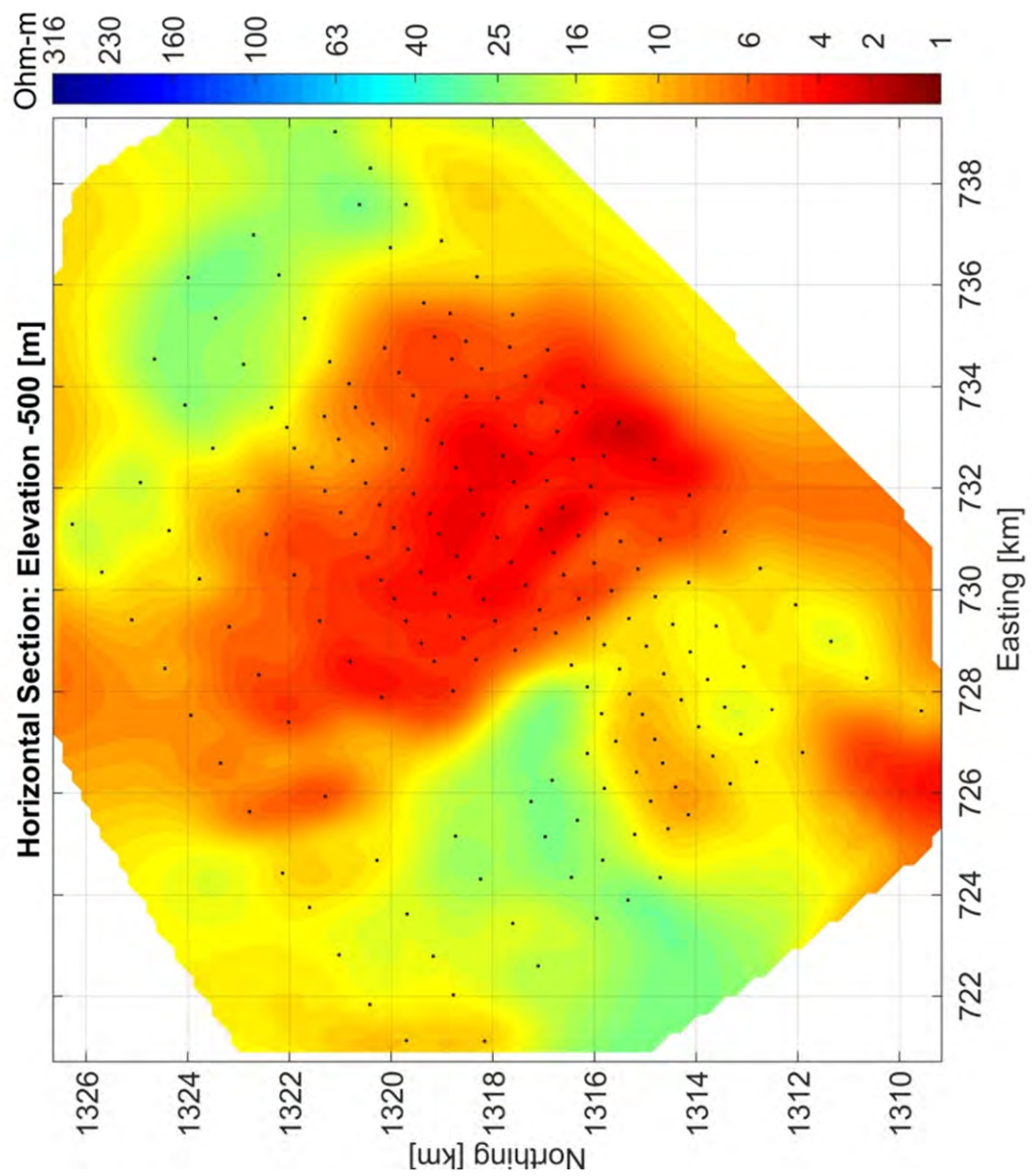
Resistivity cross section map (3D model) (TDO99)



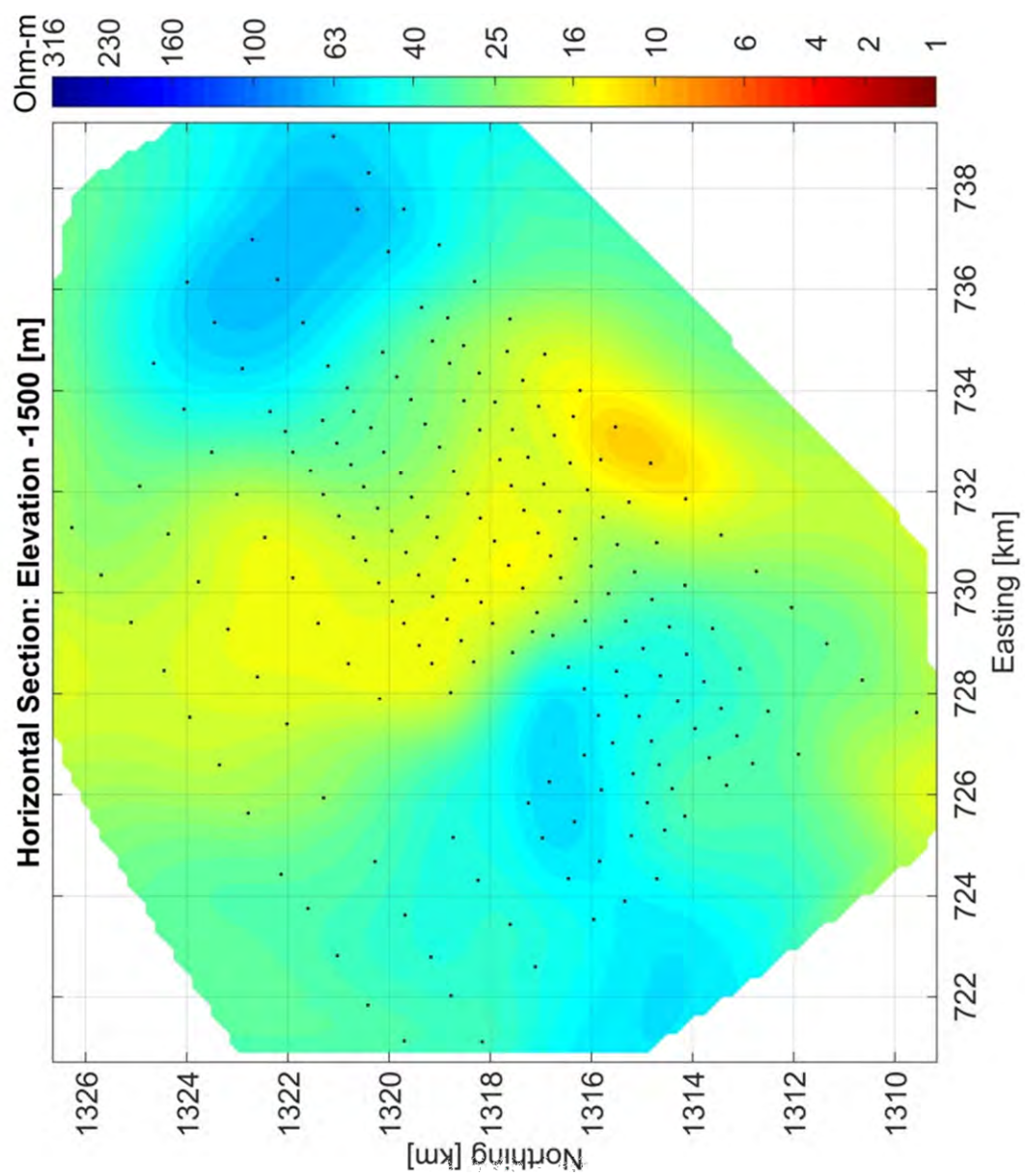
Resistivity plan view map (3D model) (Elevation 200m)



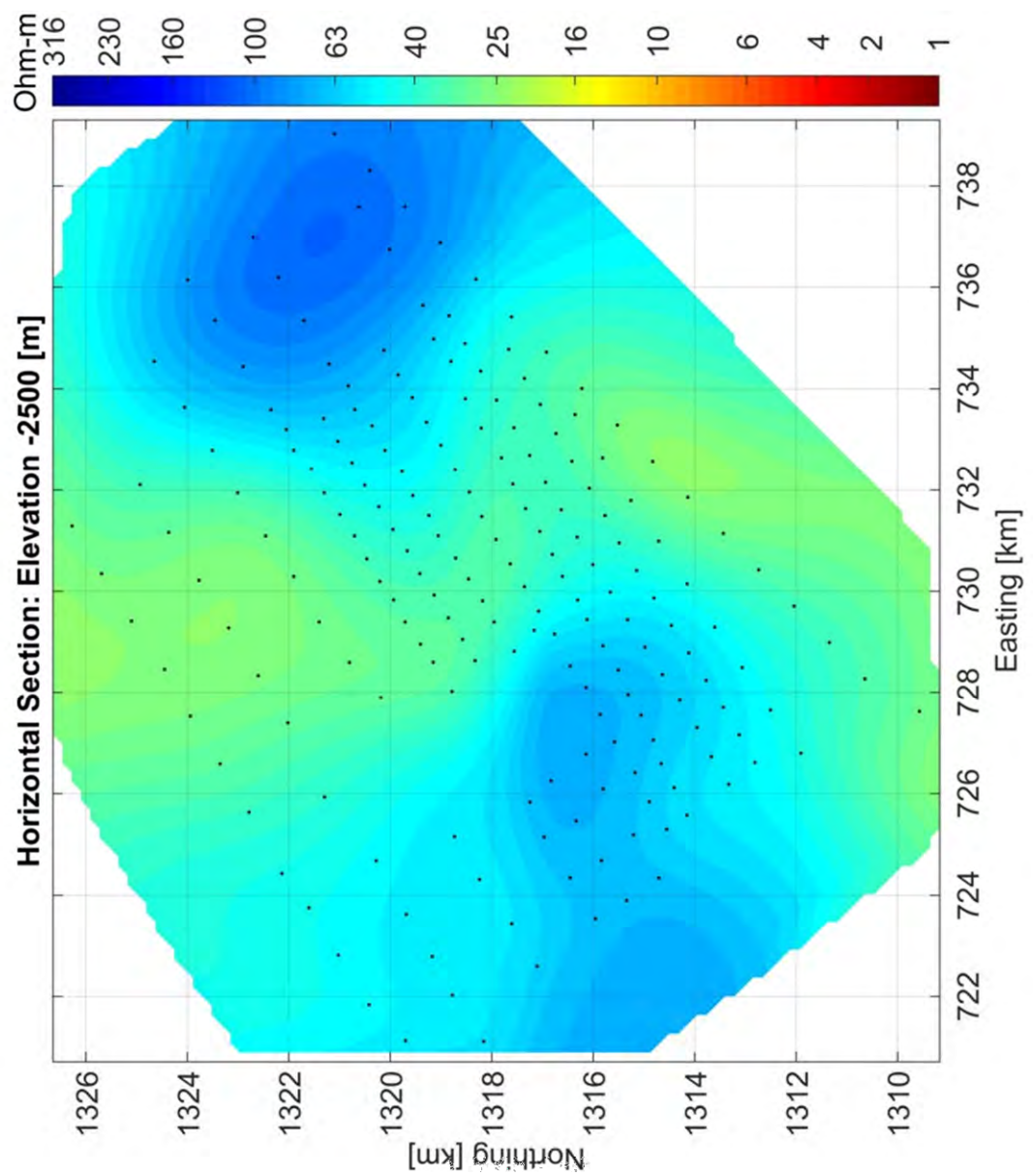
**Resistivity plan view map (3D model) (Elevation 0m)**



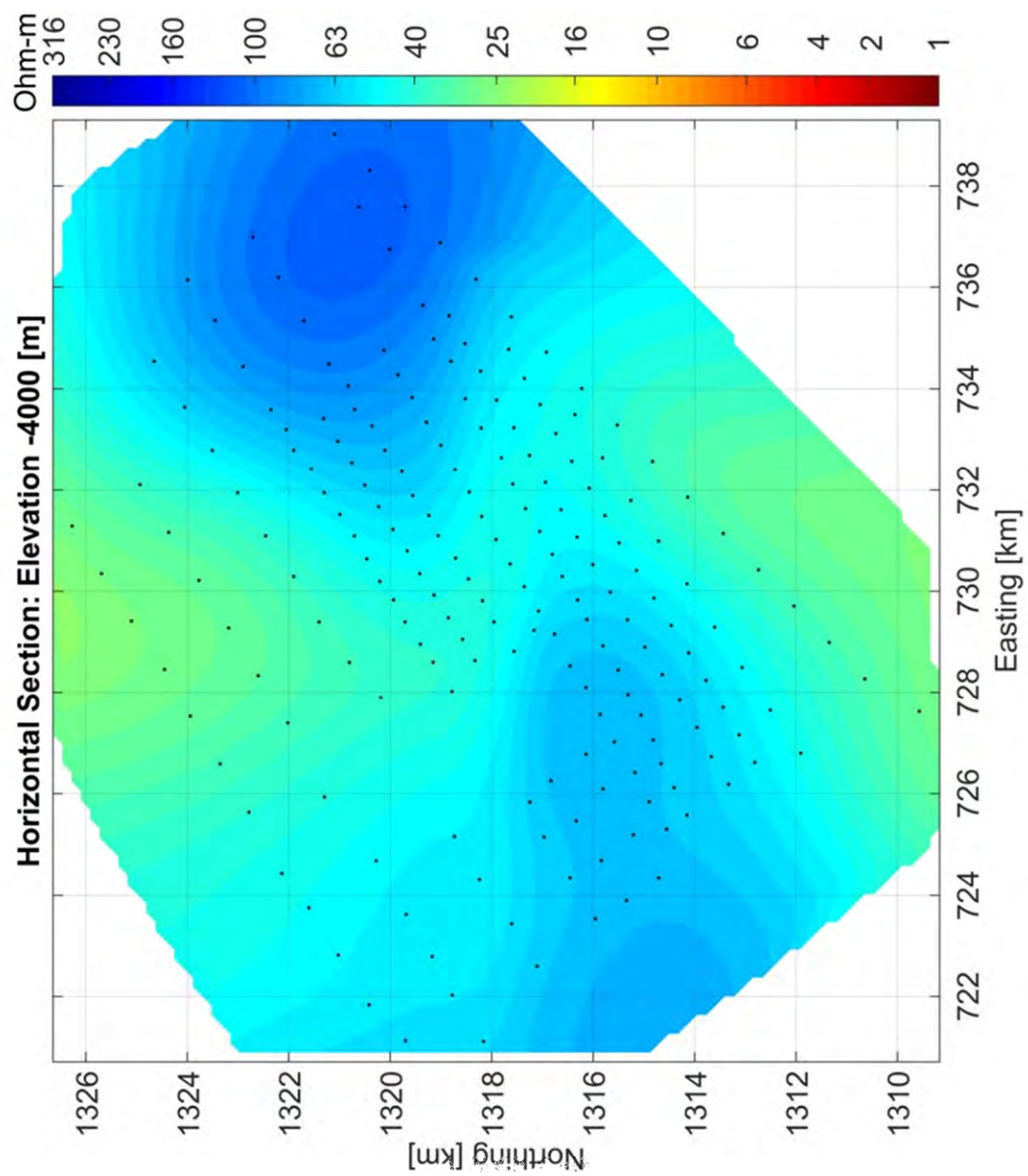
Resistivity plan view map (3D model) (Elevation 500m)



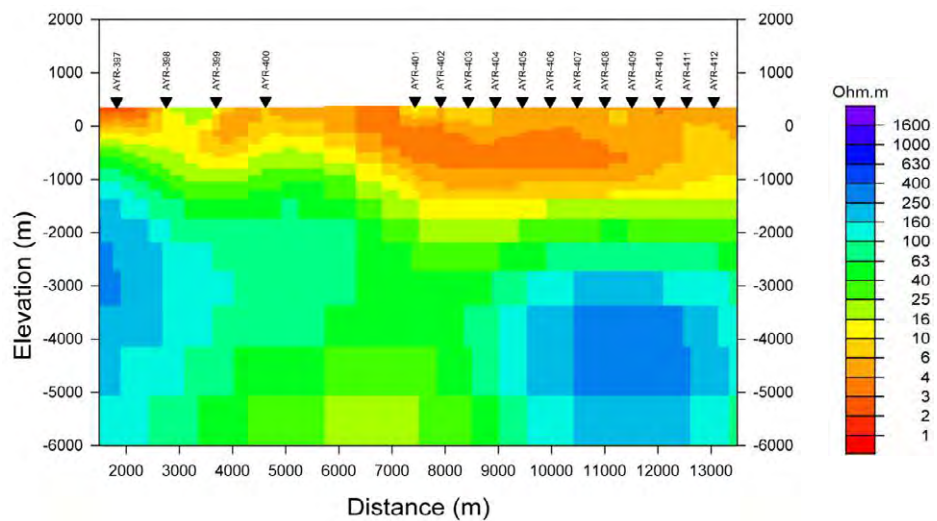
**Resistivity plan view map (3D model) (Elevation 1500m)**



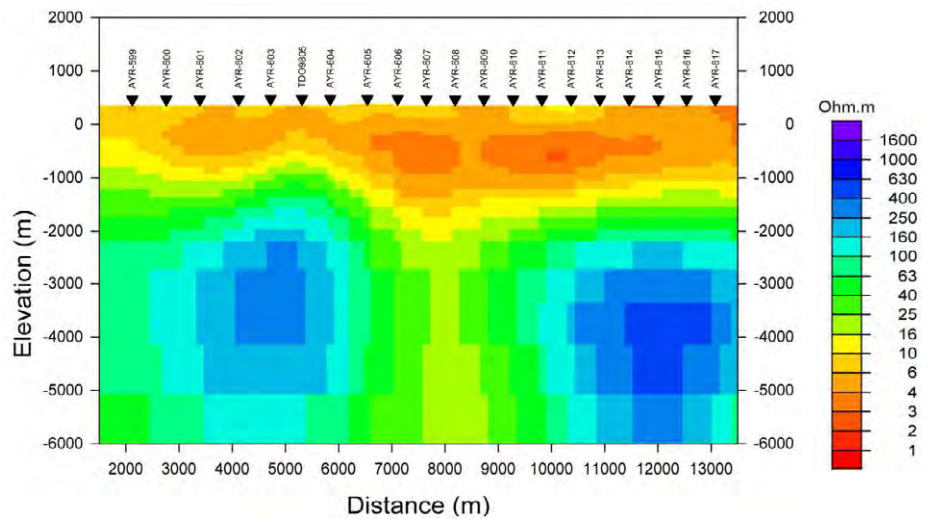
**Resistivity plan view map (3D model) (Elevation 2500m)**



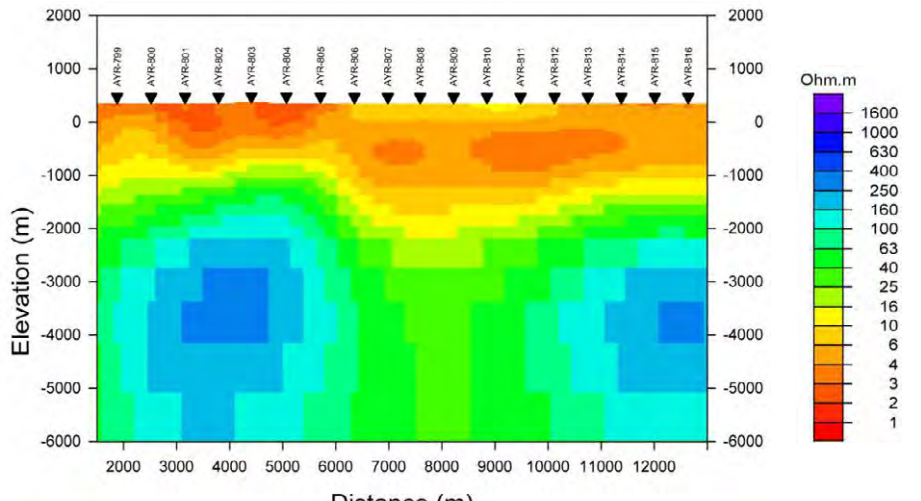
**Resistivity plan view map (3D model) (Elevation 4000m)**



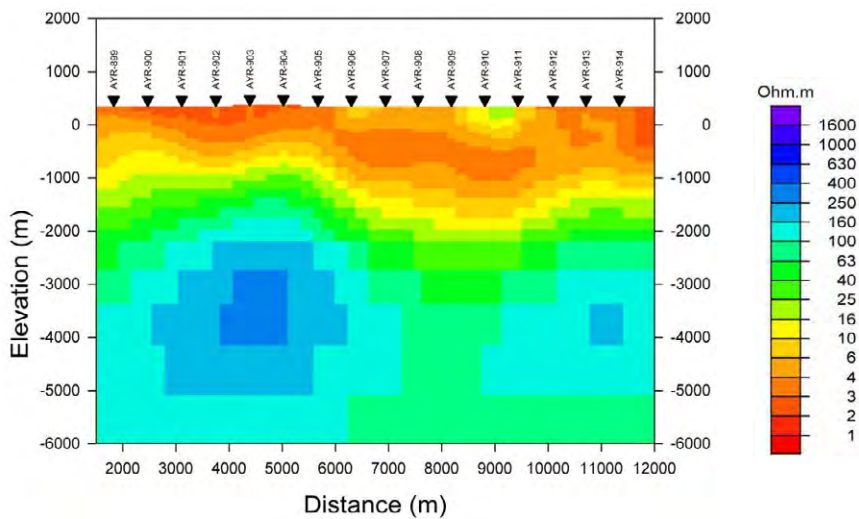
**Resistivity cross section map (2D model) (AYR400)**



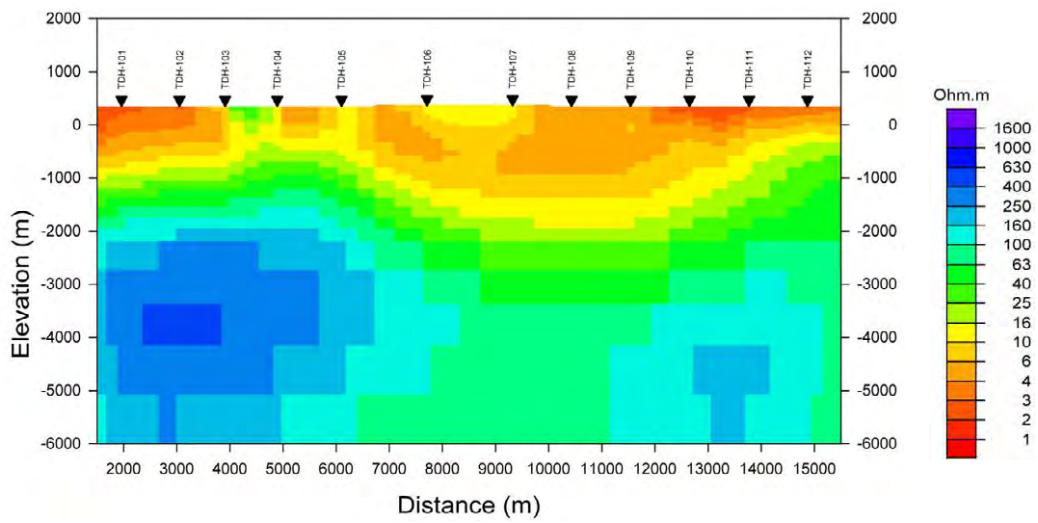
**Resistivity cross section map (2D model) (AYR600)**



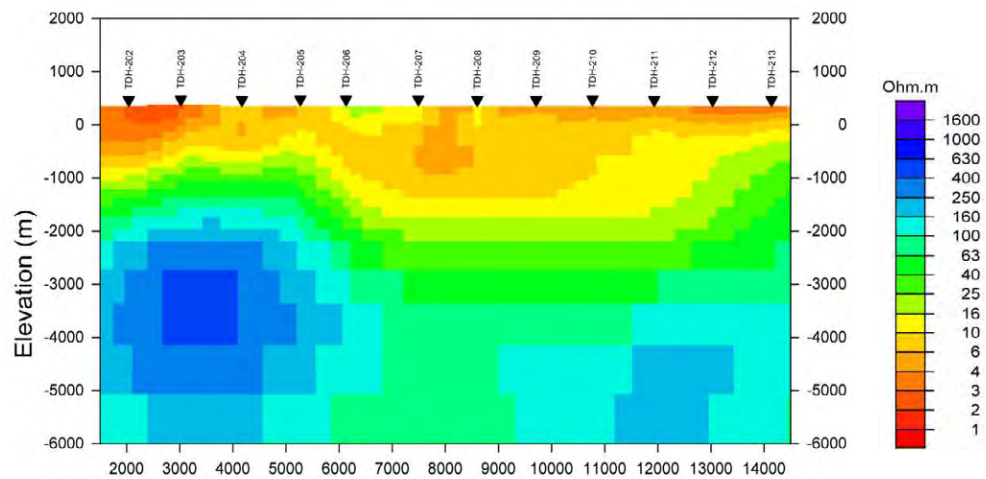
**Resistivity cross section map (2D model) (AYR800)**



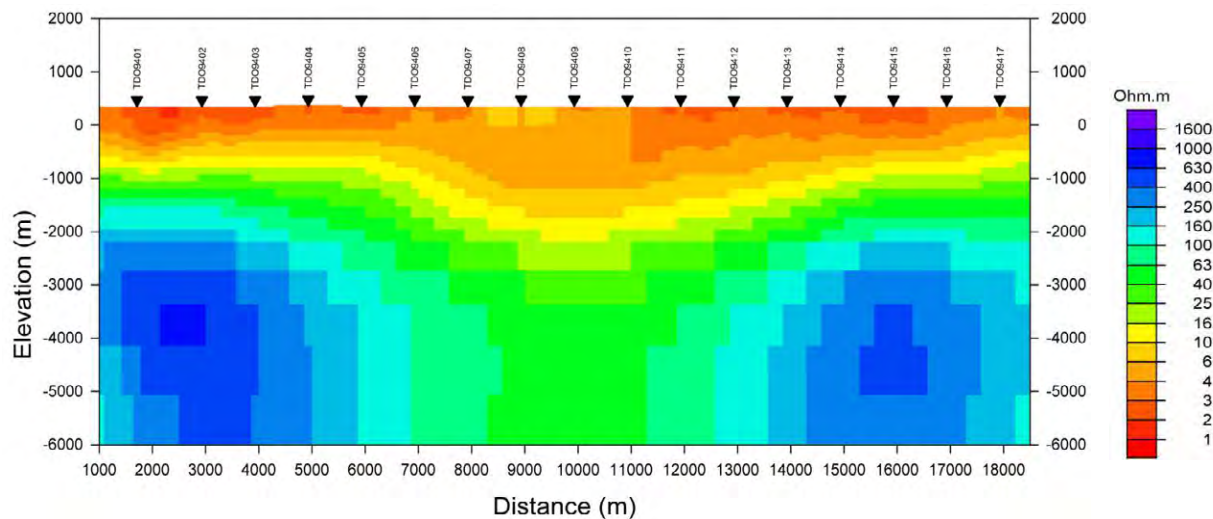
**Resistivity cross section map (2D model) (AYR900)**



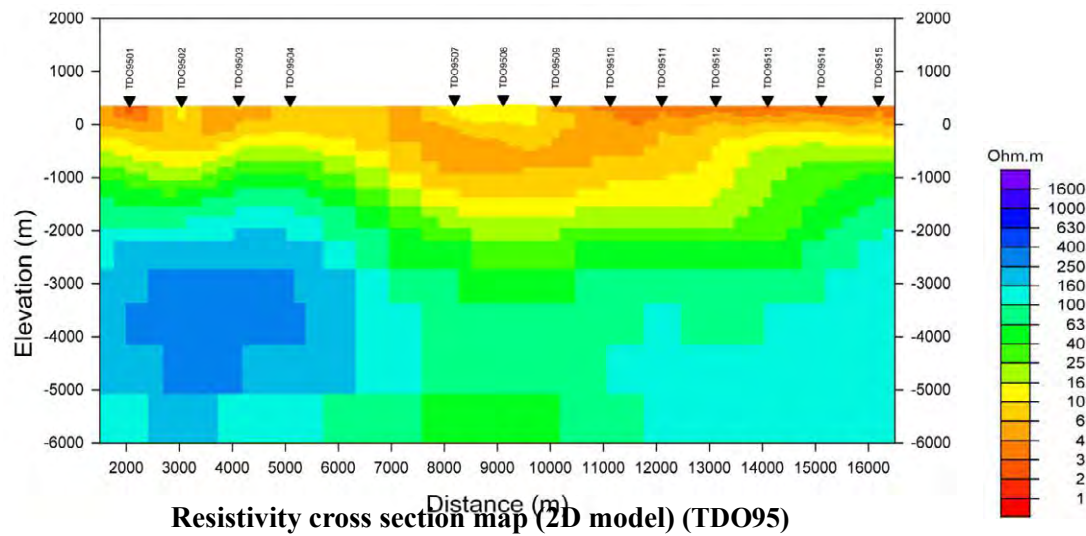
**Resistivity cross section map (2D model) (TDH100)**



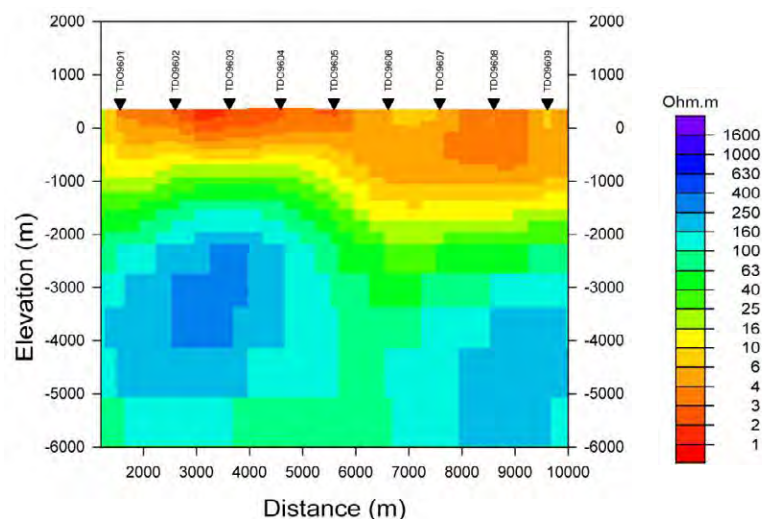
**Resistivity cross section map (2D model) (TDH200)**



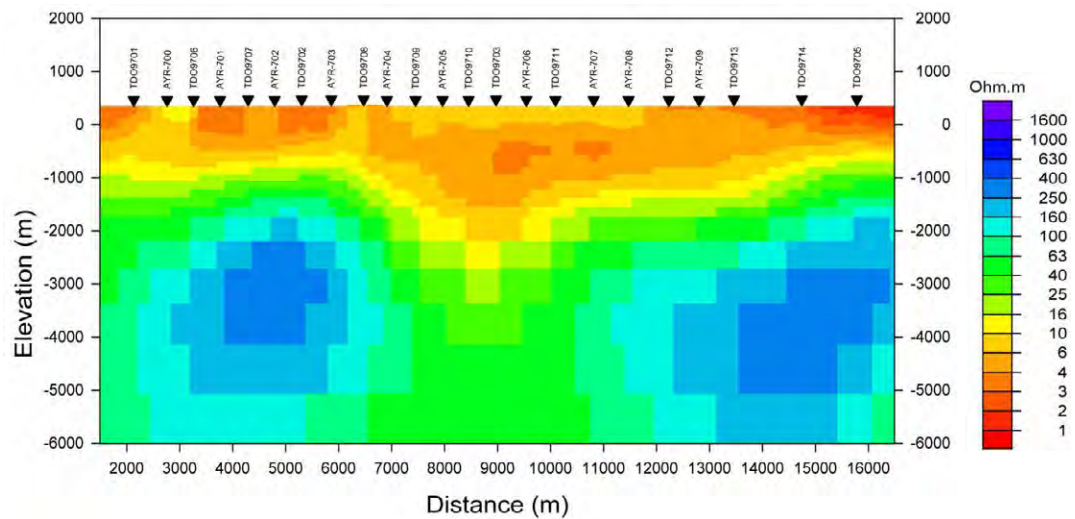
**Resistivity cross section map (2D model) (TDO94)**



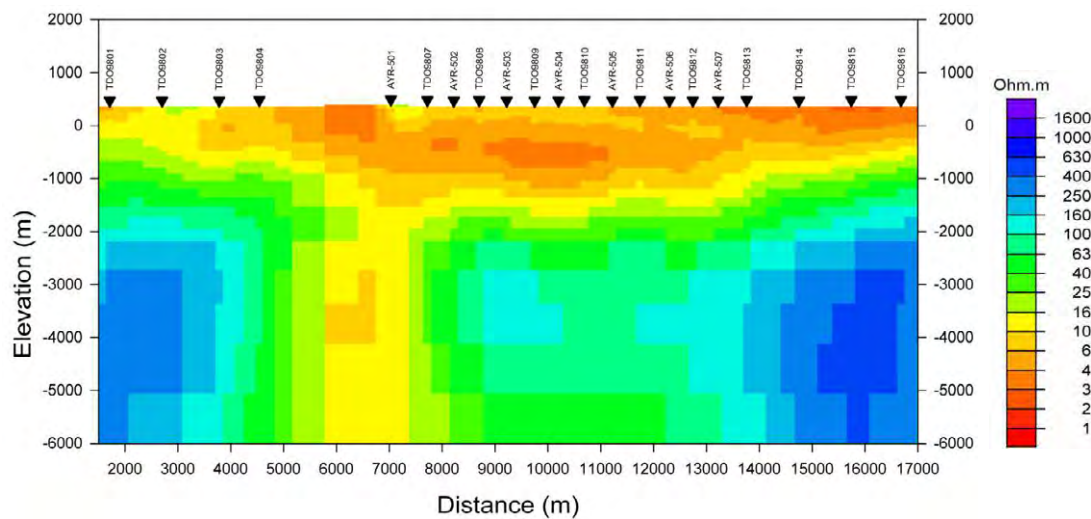
**Resistivity cross section map (2D model) (TDO95)**



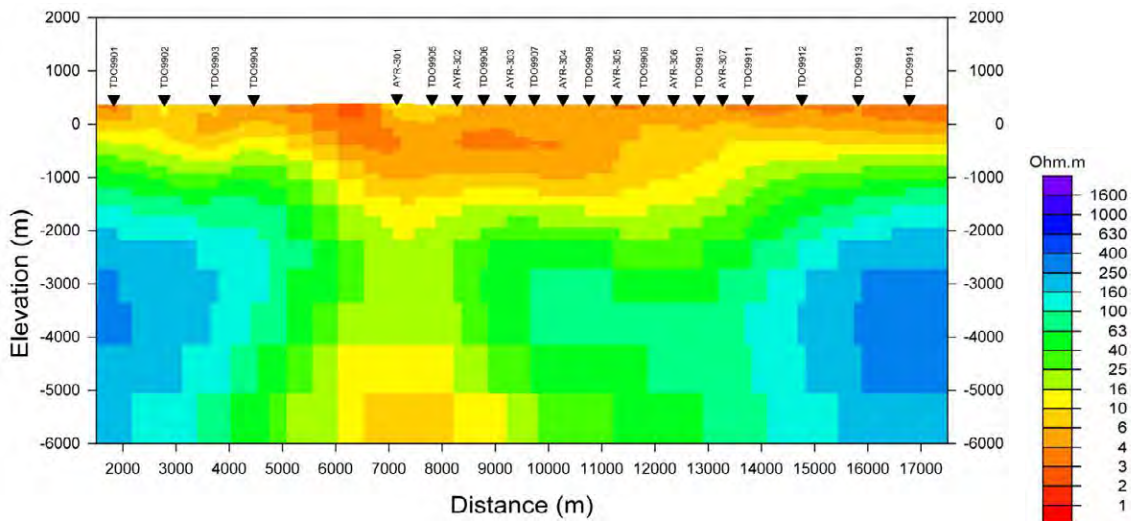
**Resistivity cross section map (2D model) (TDO96)**



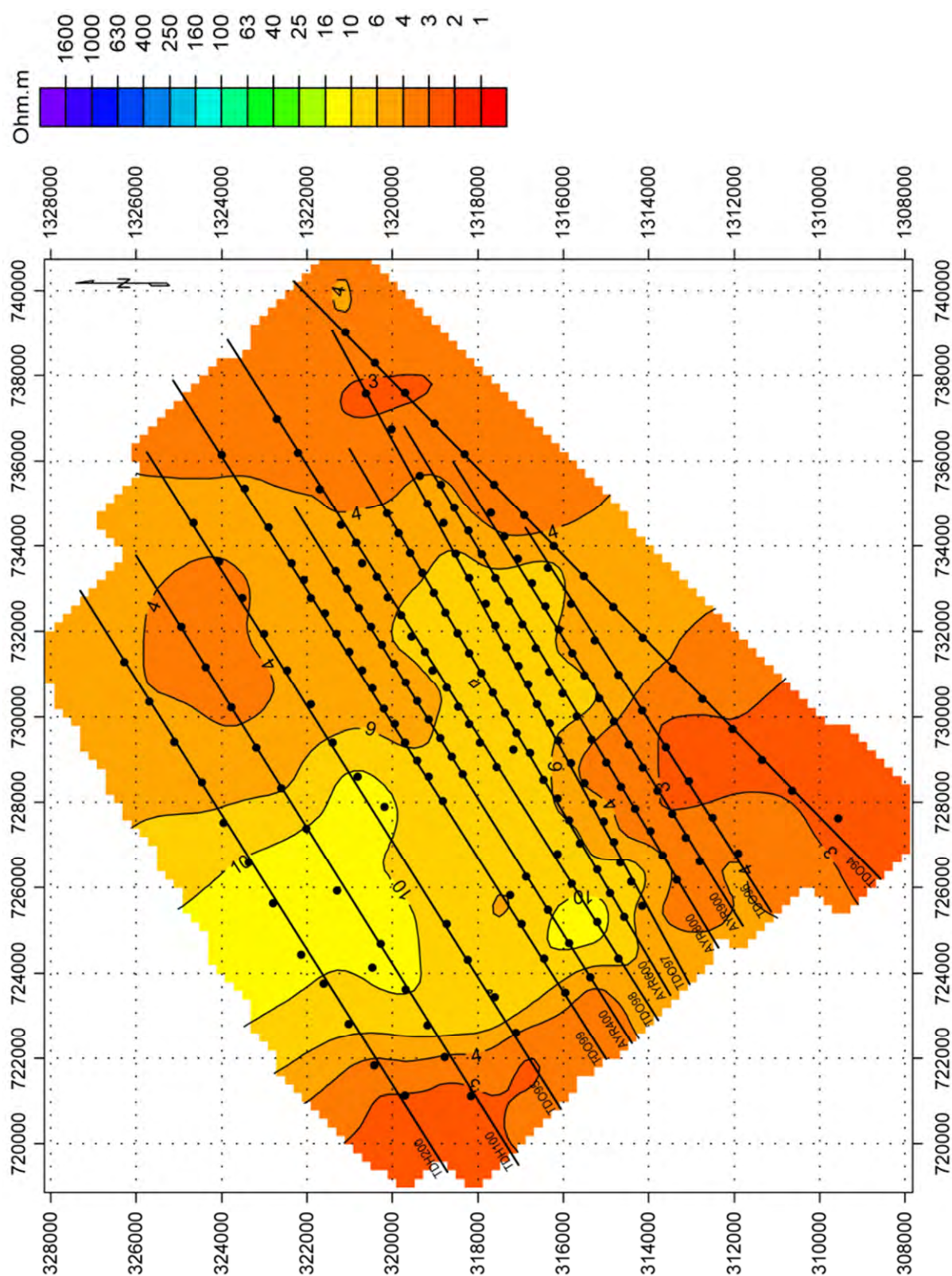
**Resistivity cross section map (2D model) (TDO97)**



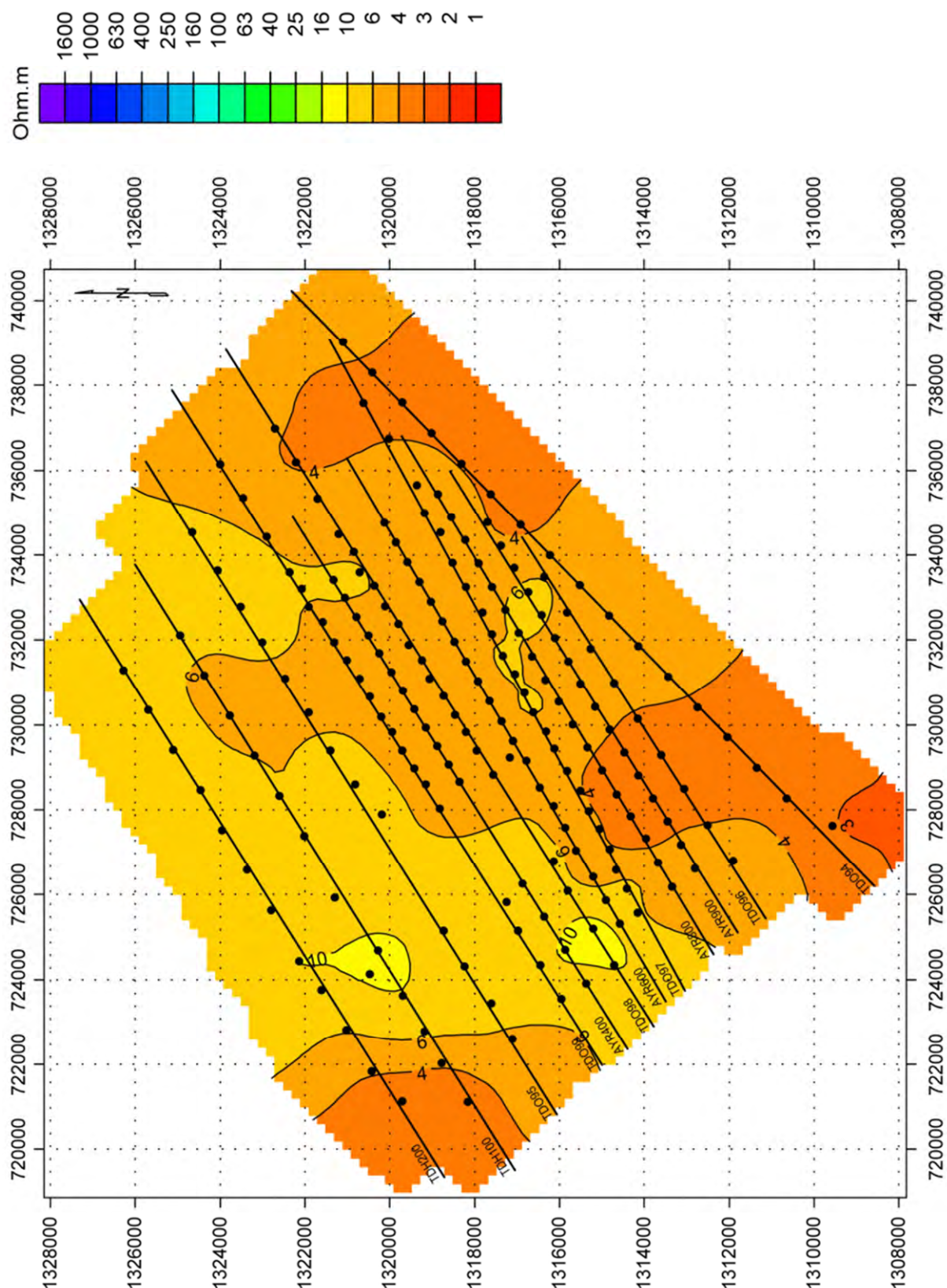
**Resistivity cross section map (2D model) (TDO98)**



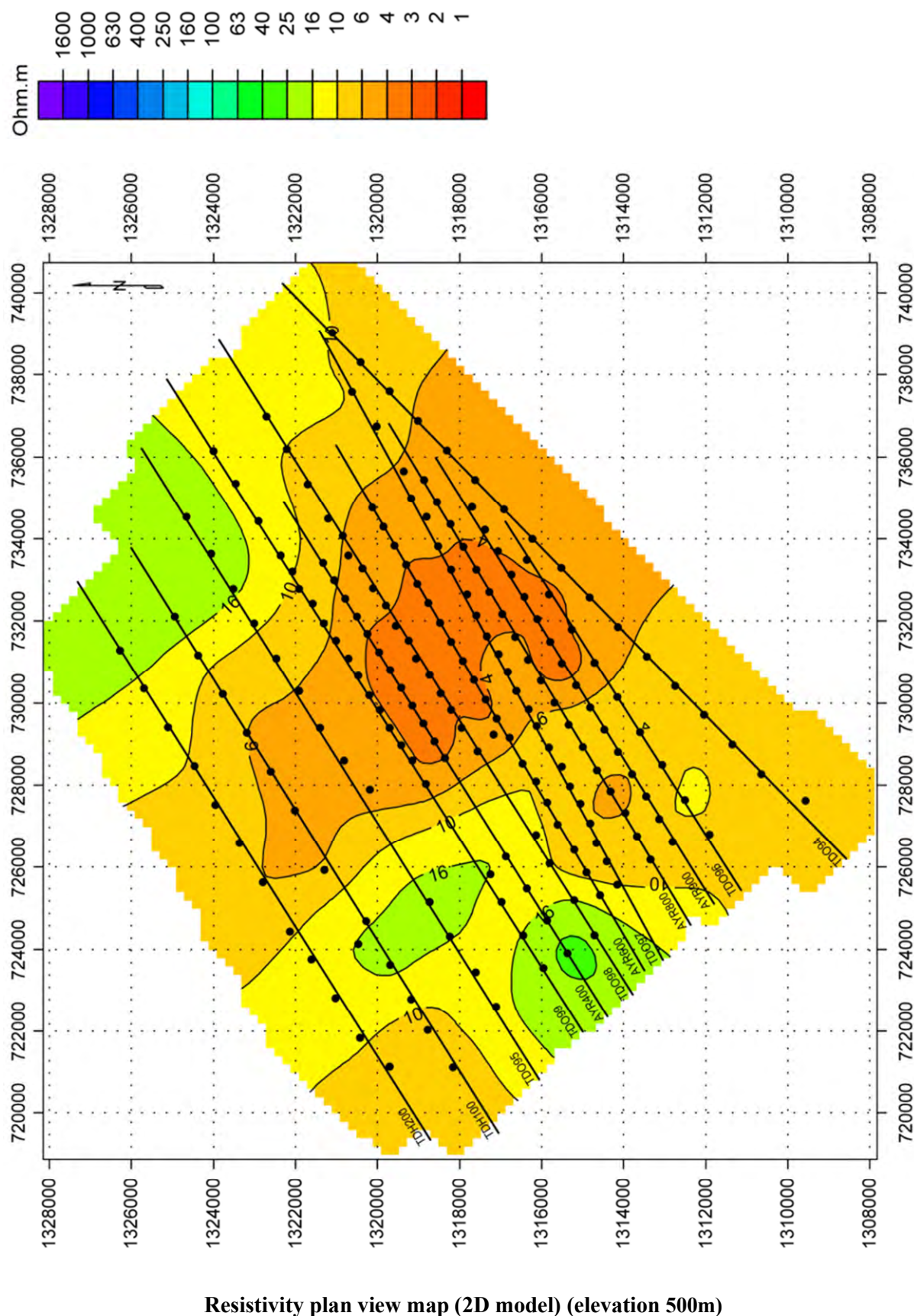
**Resistivity cross section map (2D model) (TDO99)**



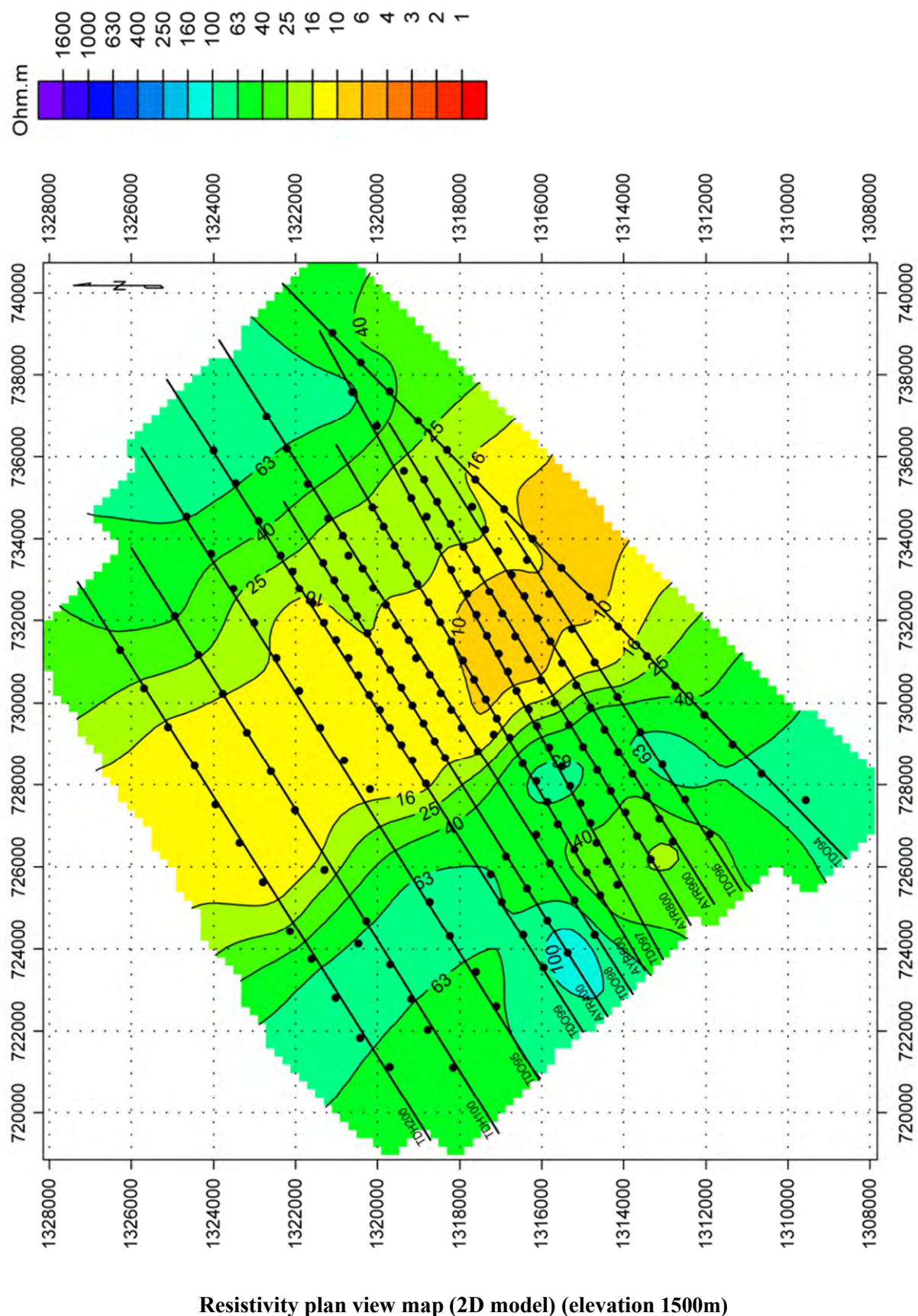
**Resistivity plan view map (2D model) (elevation 200m)**



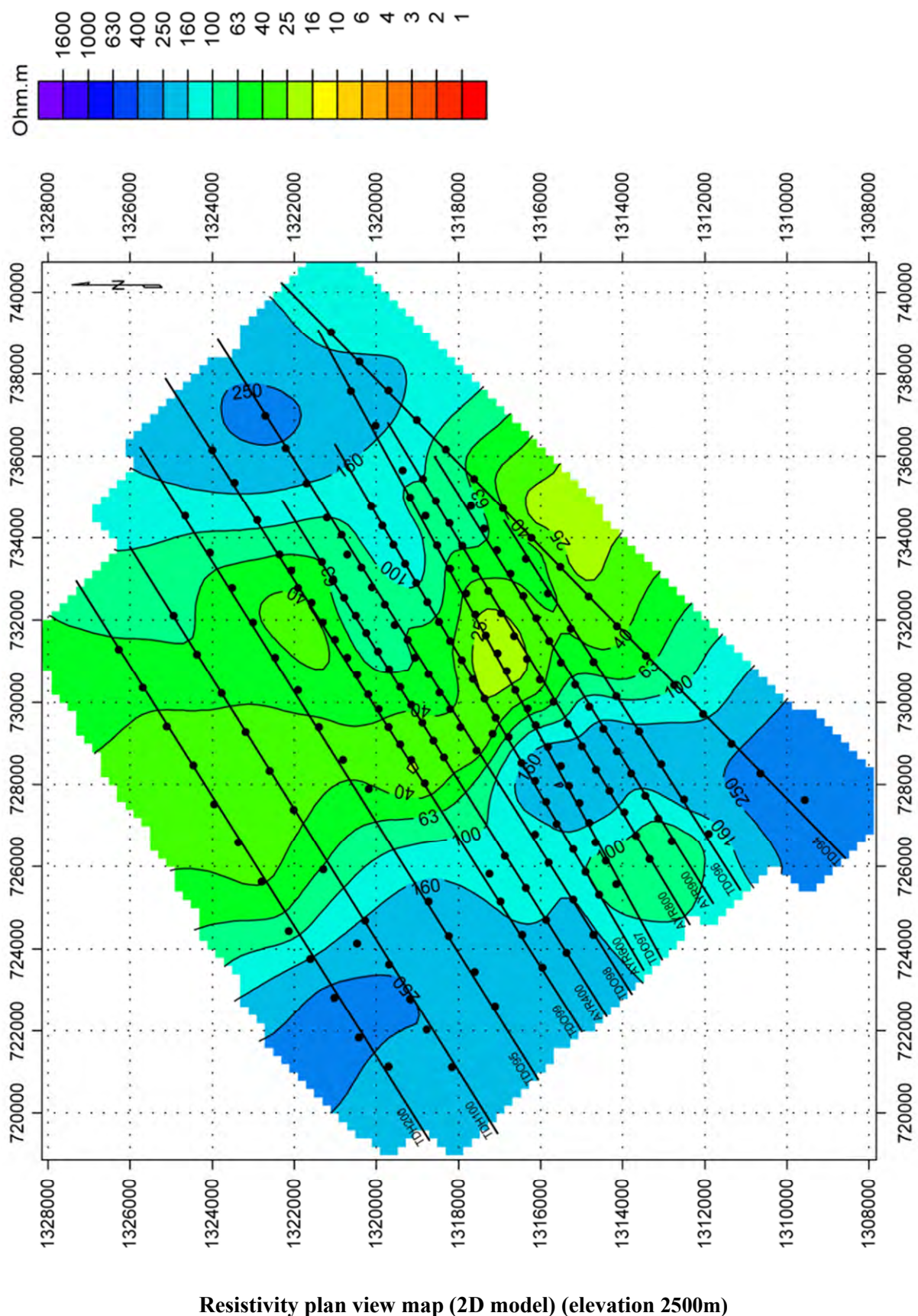
**Resistivity plan view map (2D model) (elevation 0m)**



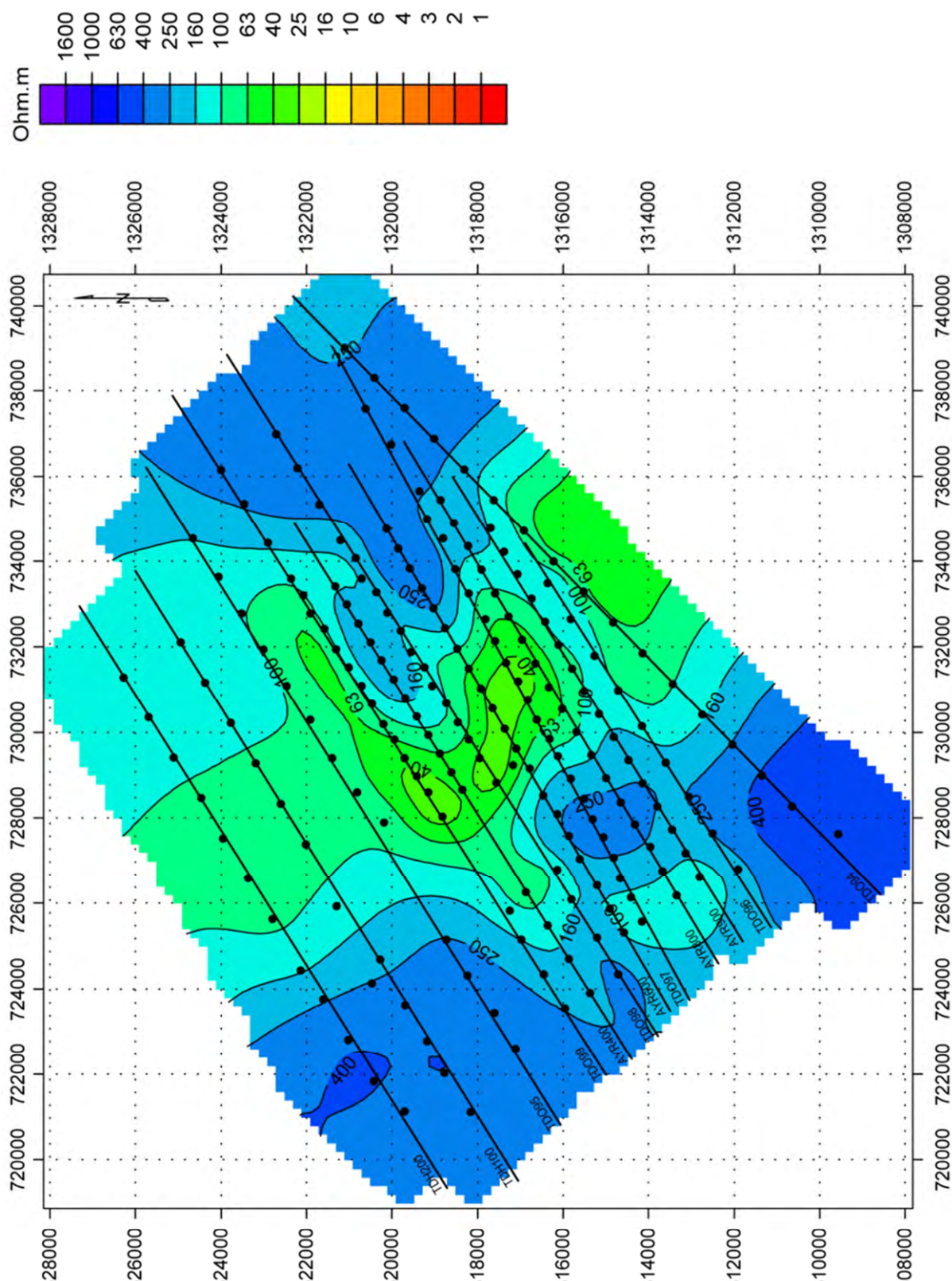
Resistivity plan view map (2D model) (elevation 500m)



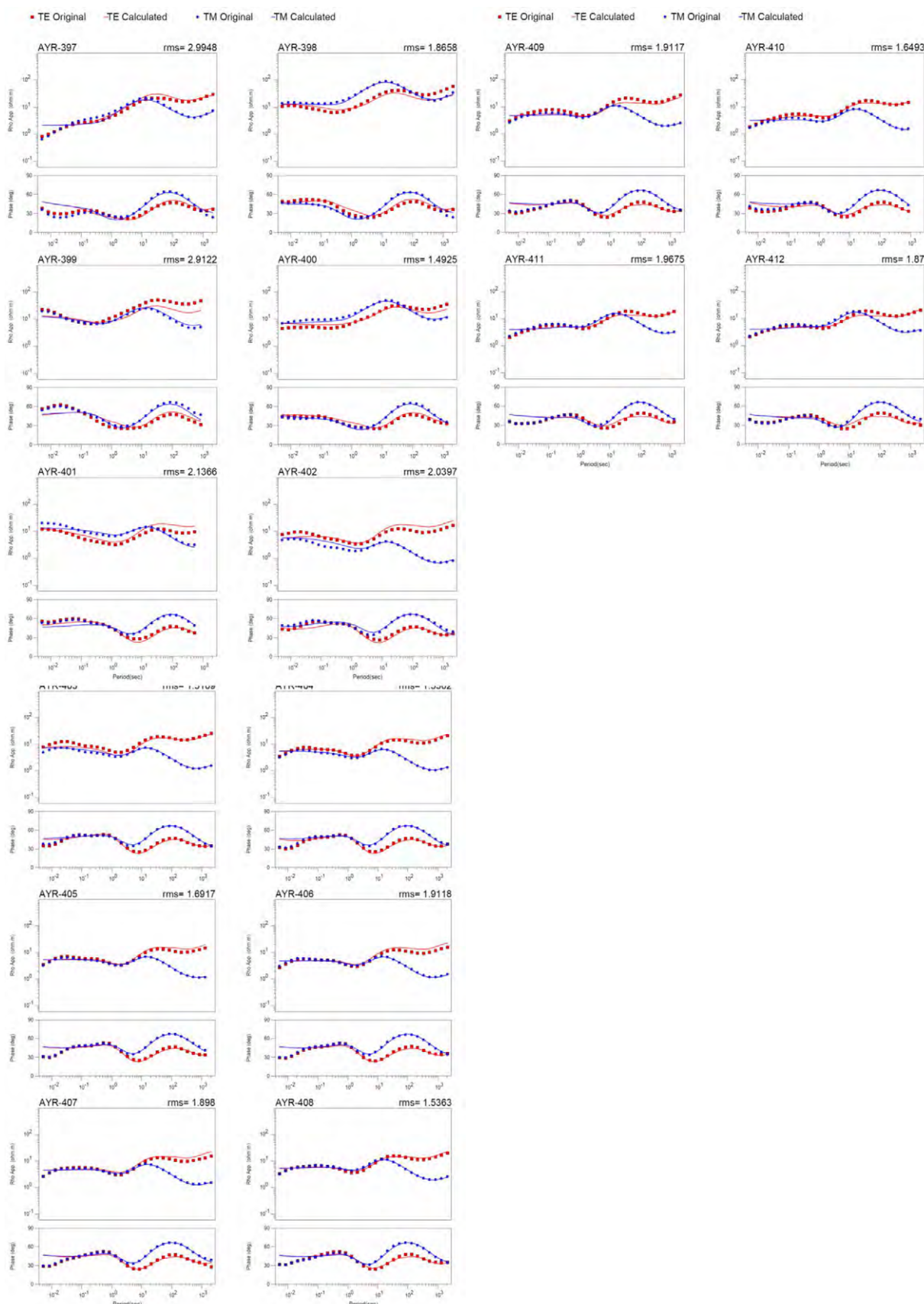
Resistivity plan view map (2D model) (elevation 1500m)



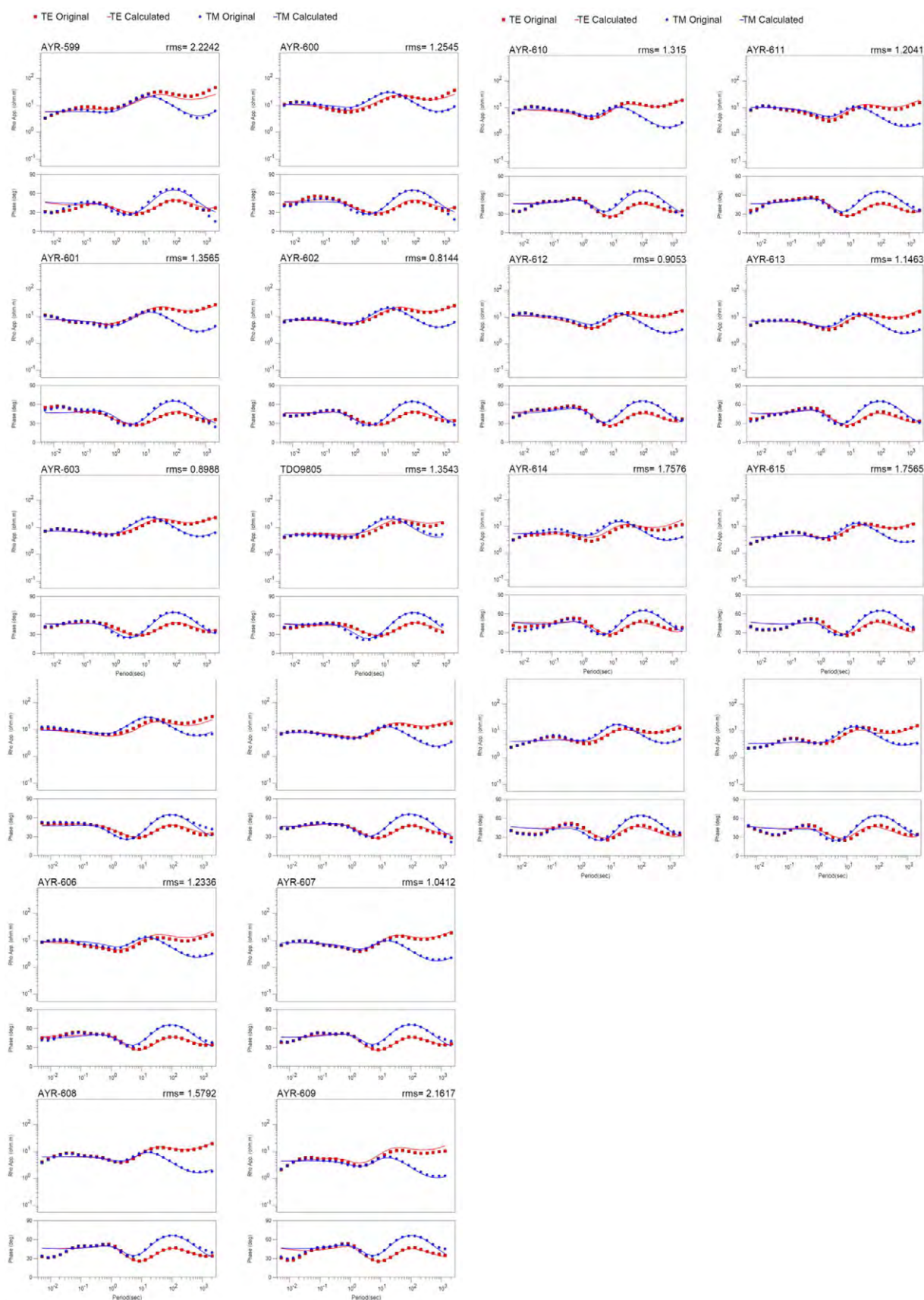
Resistivity plan view map (2D model) (elevation 2500m)



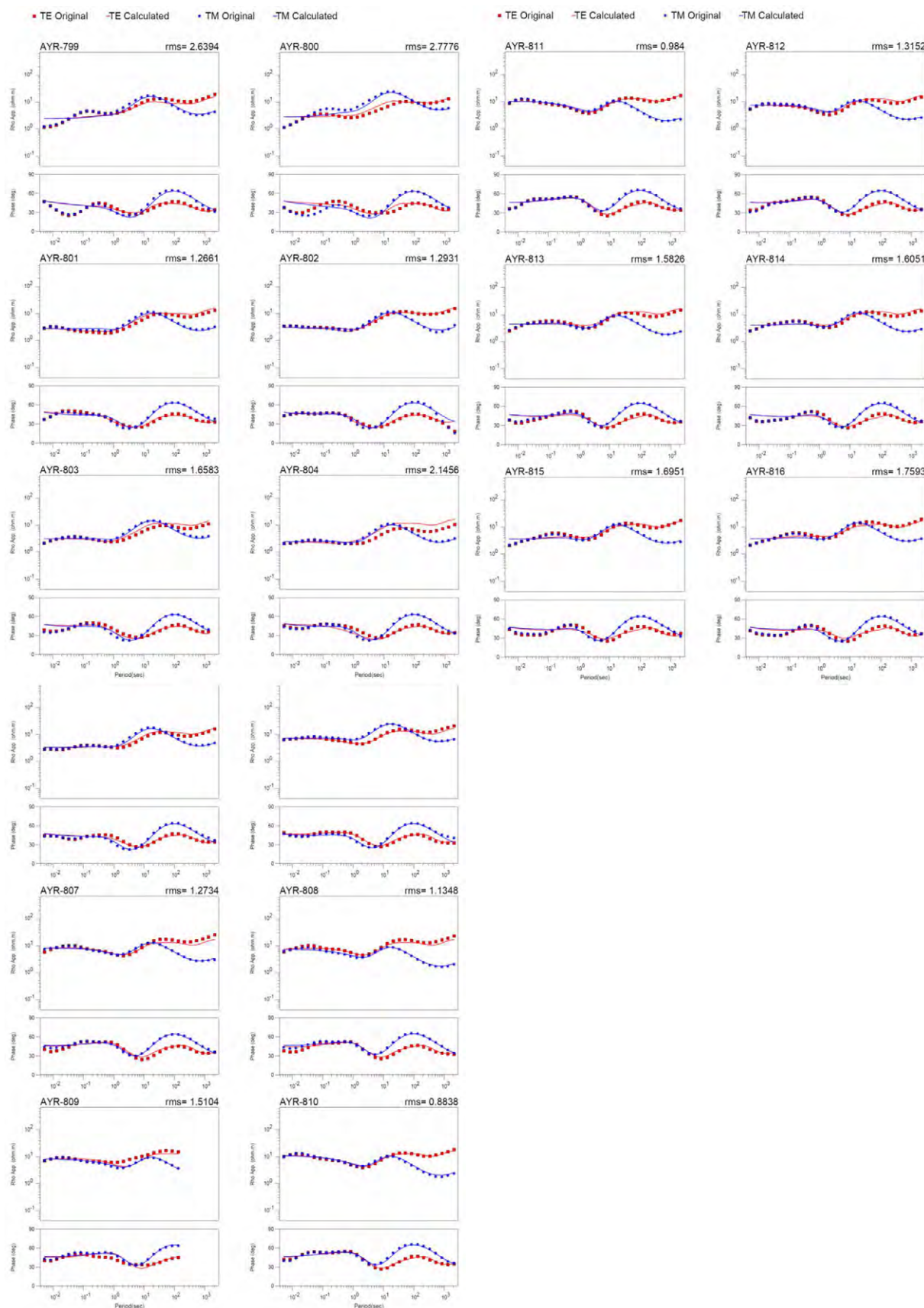
Resistivity plan view map (2D model) (elevation 4000m)



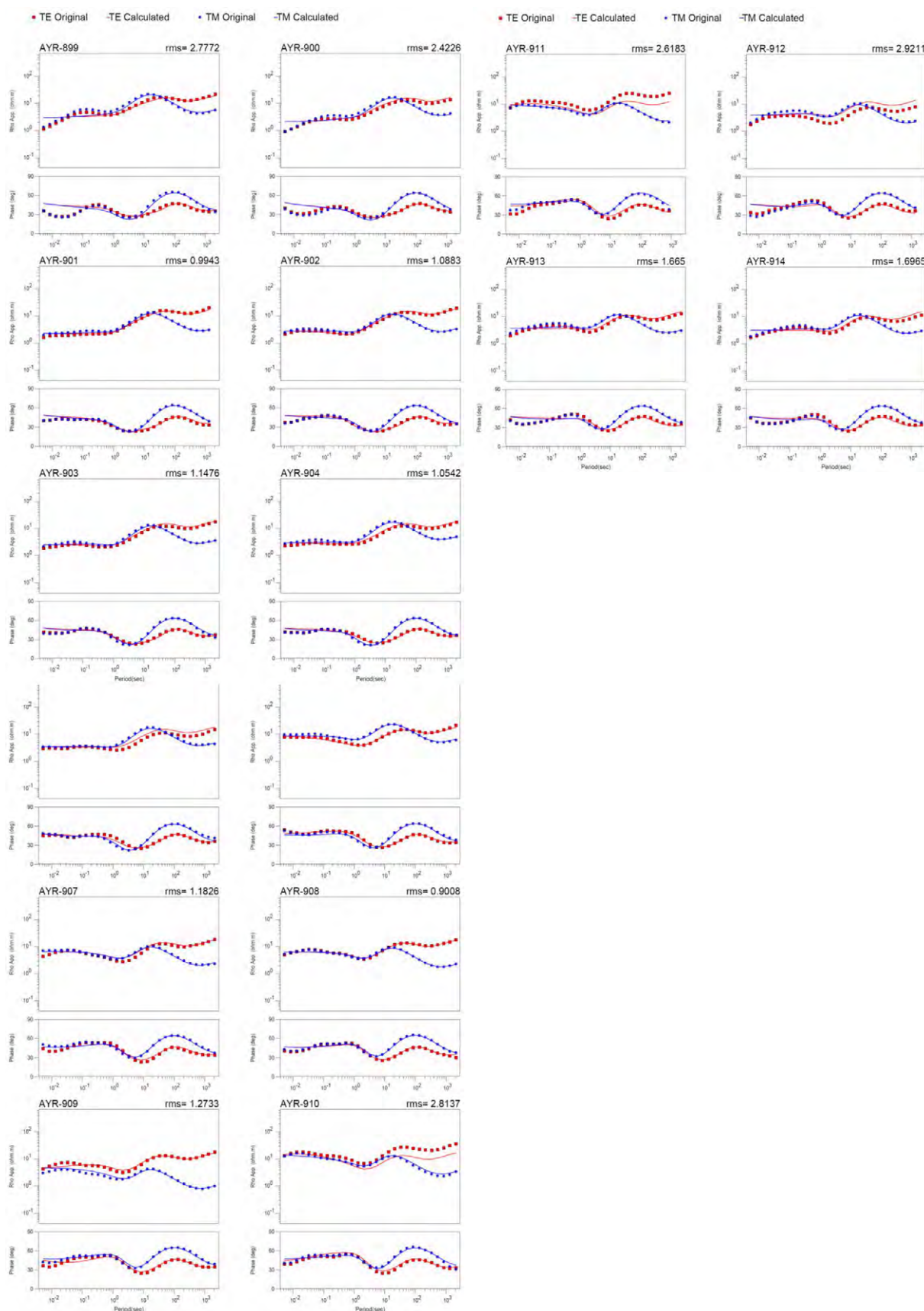
## 2D analysis results - Calculated and observed value of apparent resistivity and phase curve (AYR400)



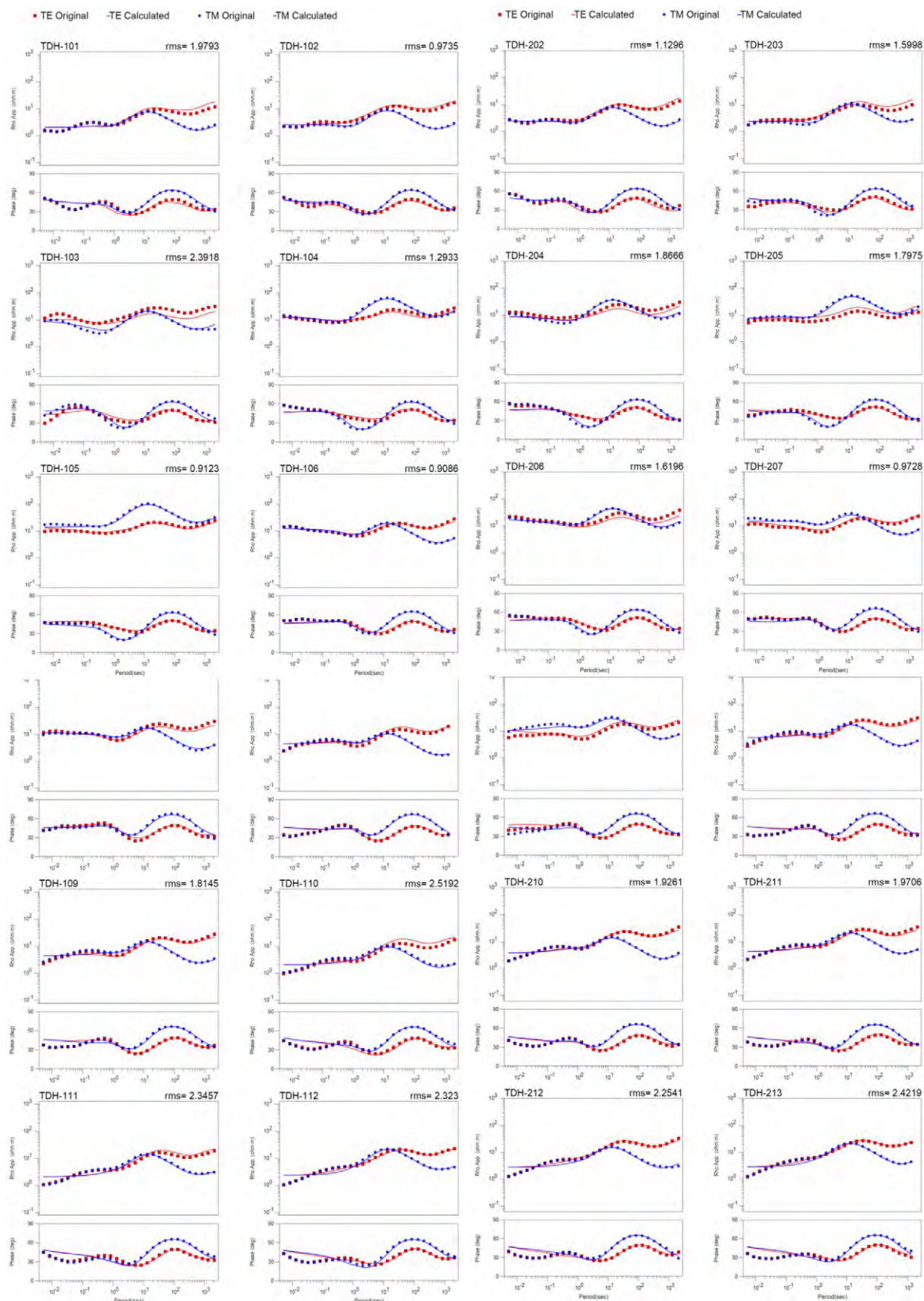
## 2D analysis results - Calculated and observed value of apparent resistivity and phase curve (AYR600)



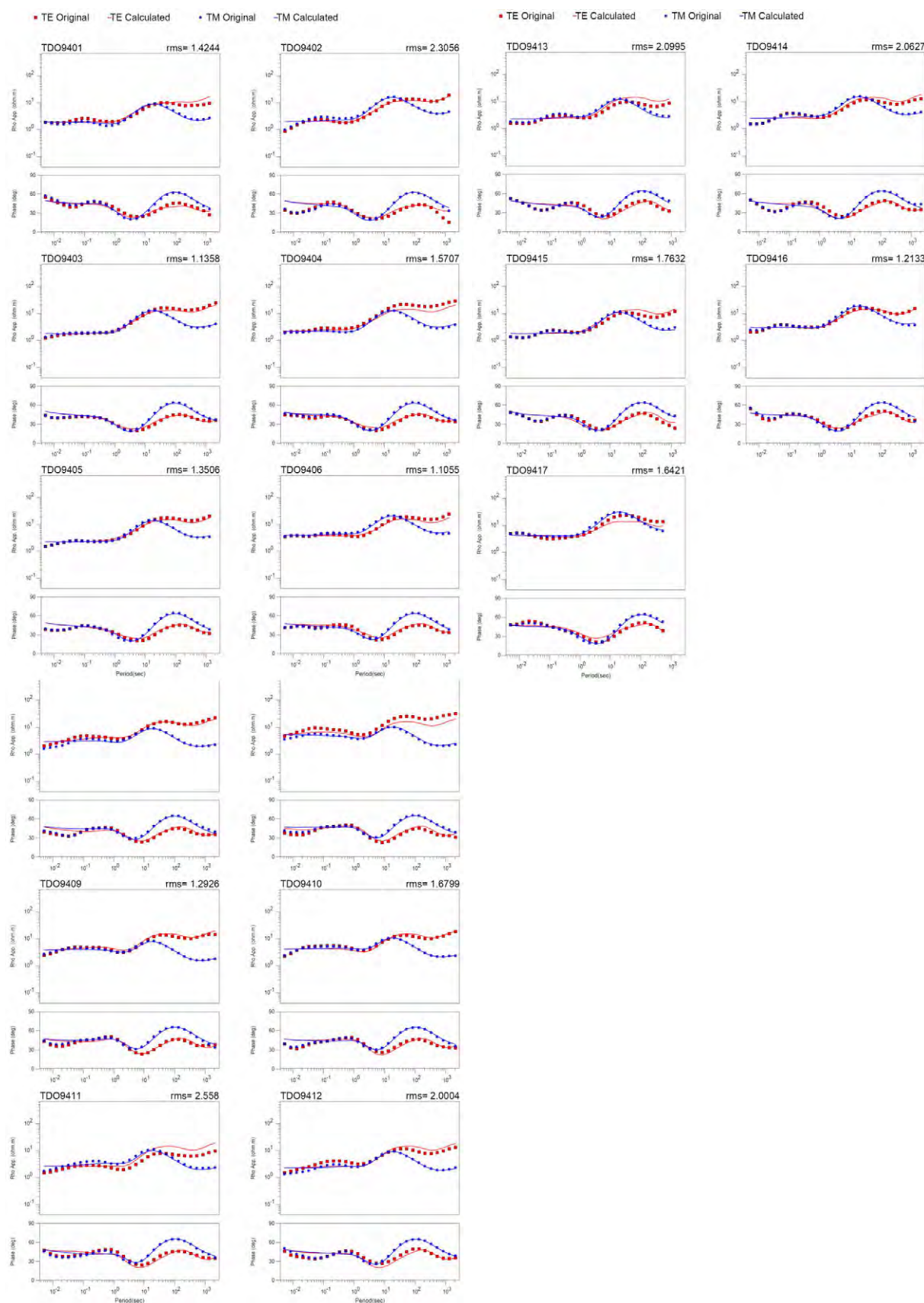
## 2D analysis results - Calculated and observed value of apparent resistivity and phase curve (AYR800)



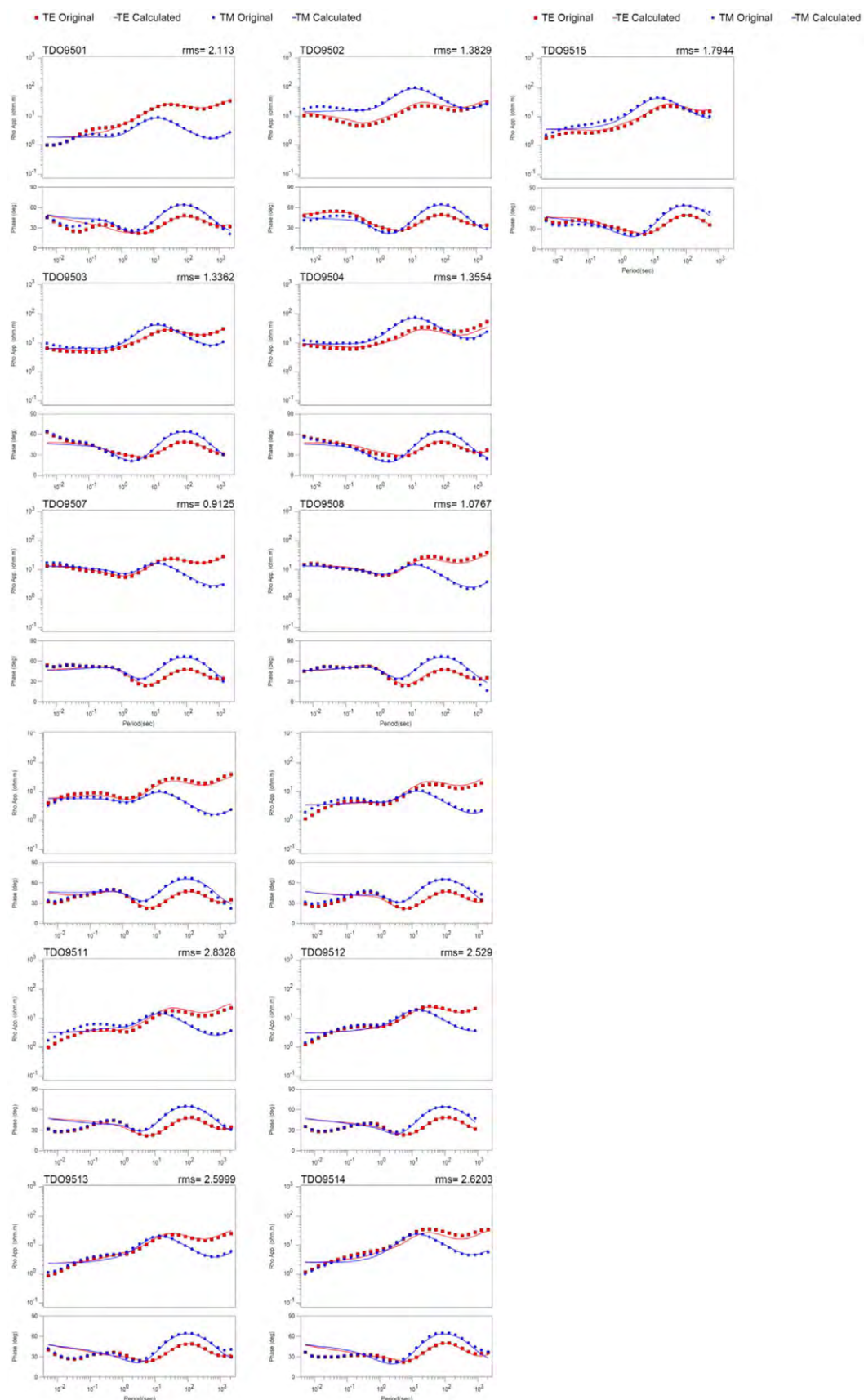
## 2D analysis results - Calculated and observed value of apparent resistivity and phase curve (AYR900)



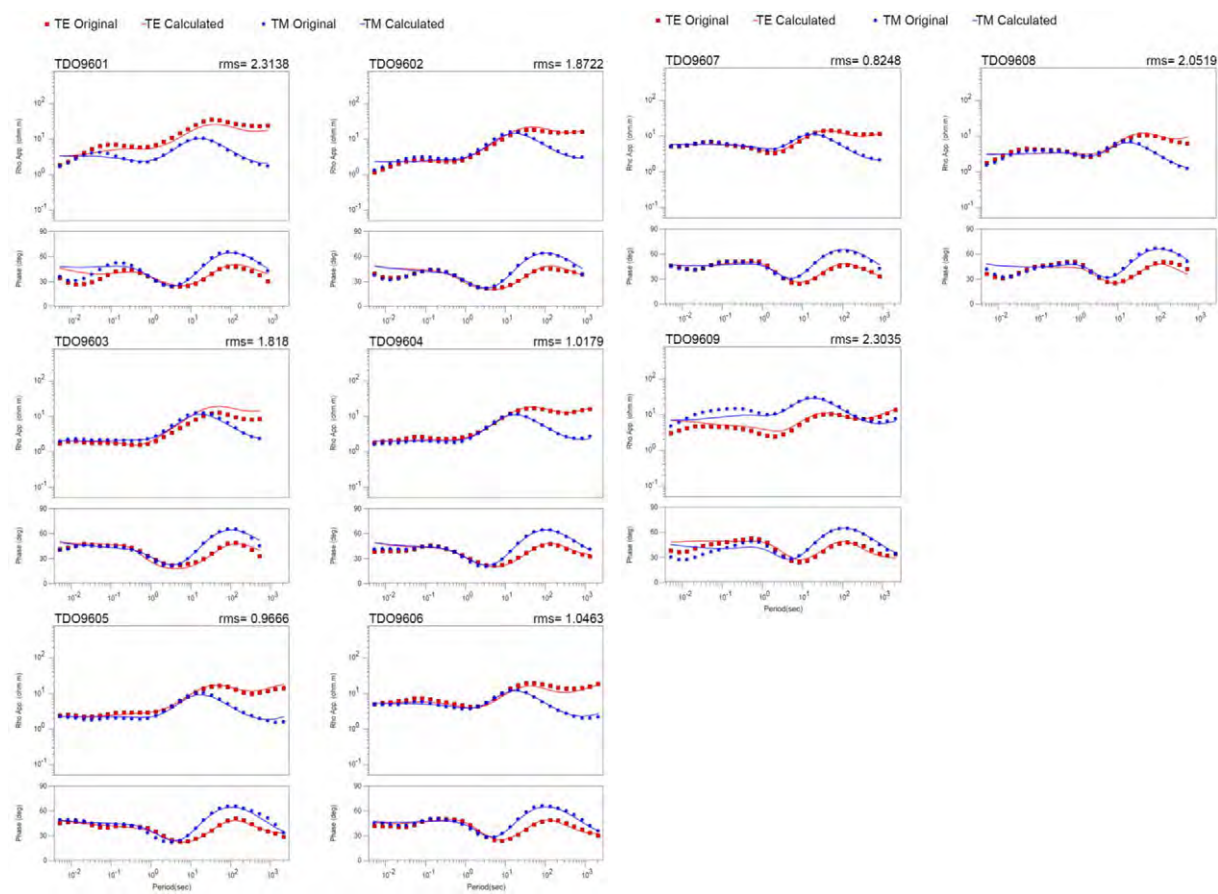
2D analysis results - Calculated and observed value of apparent resistivity and phase  
curve (TDH100, TDH200)



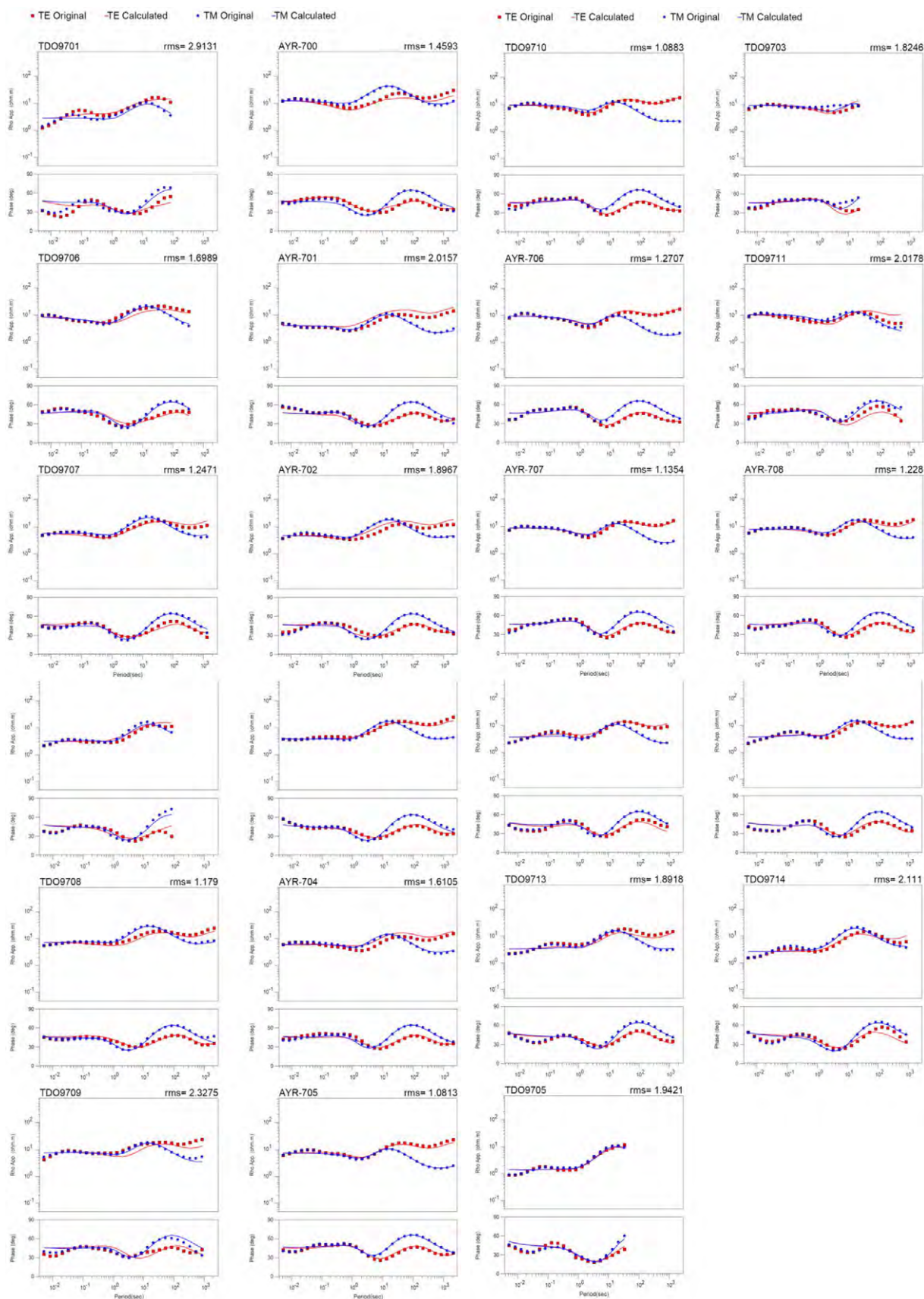
## 2D analysis results - Calculated and observed value of apparent resistivity and phase curve (TDO94)



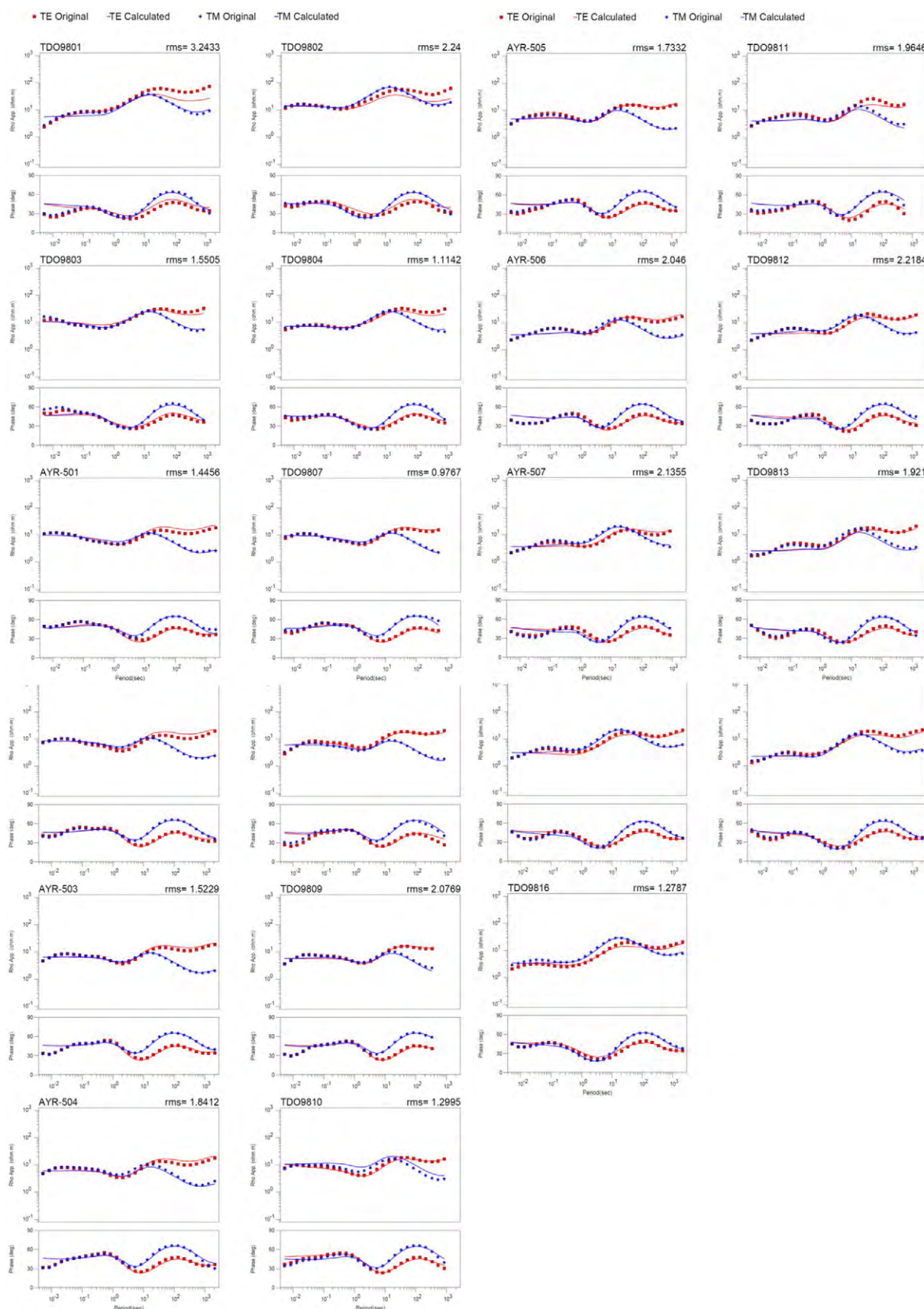
## 2D analysis results - Calculated and observed value of apparent resistivity and phase curve (TDO95)



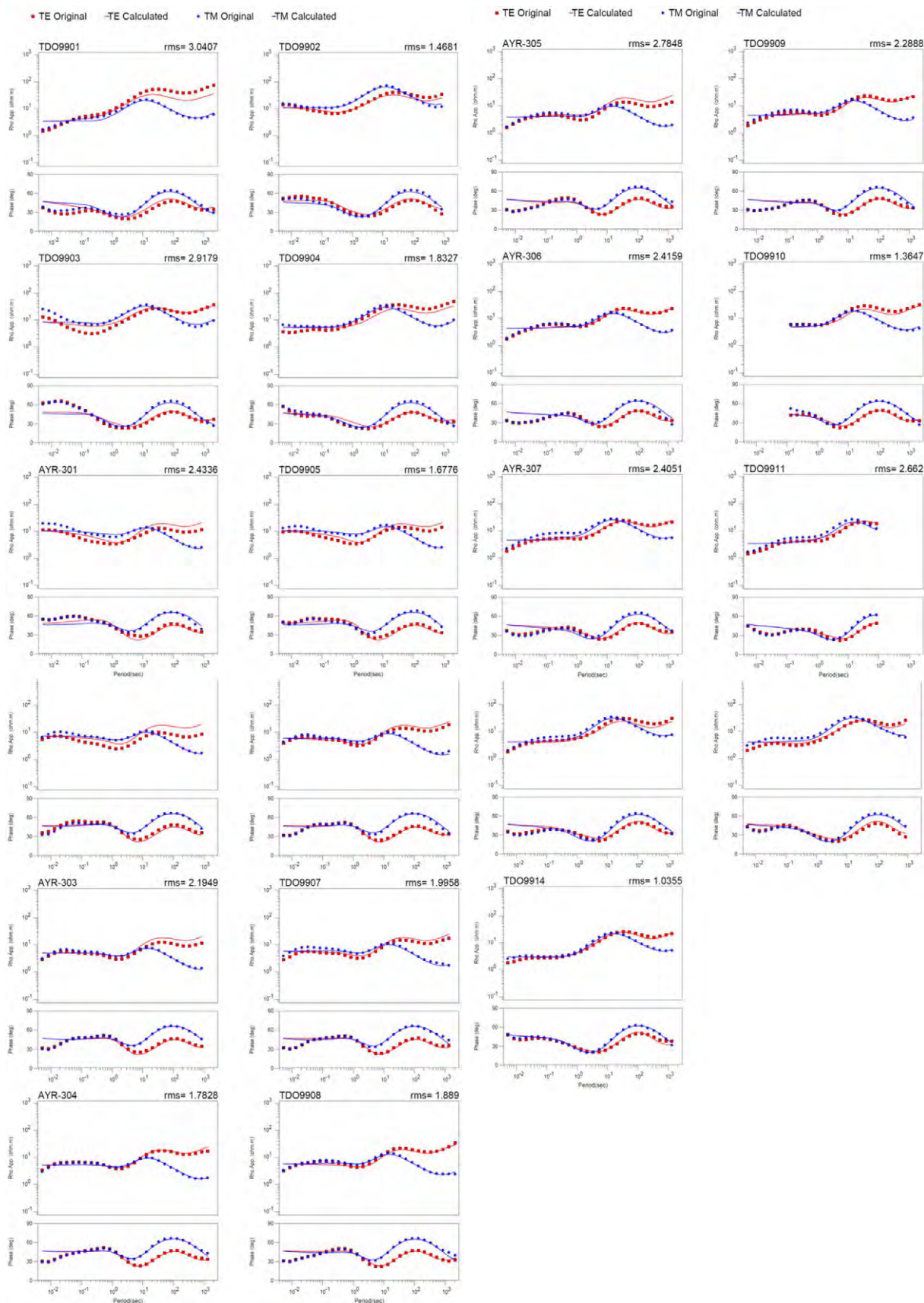
**2D analysis results - Calculated and observed value of apparent resistivity and phase curve (TDO96)**



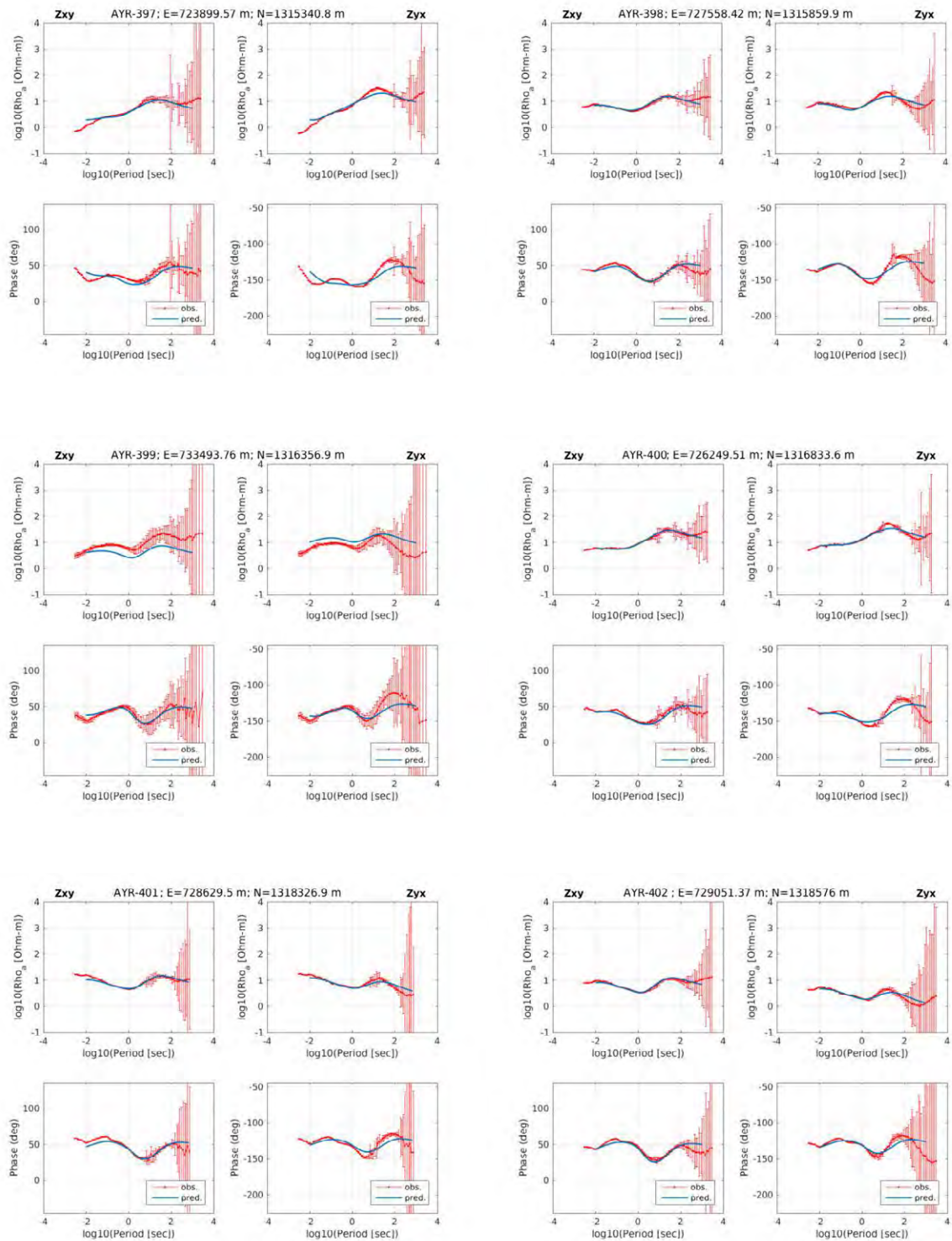
## 2D analysis results - Calculated and observed value of apparent resistivity and phase curve (TDO97)



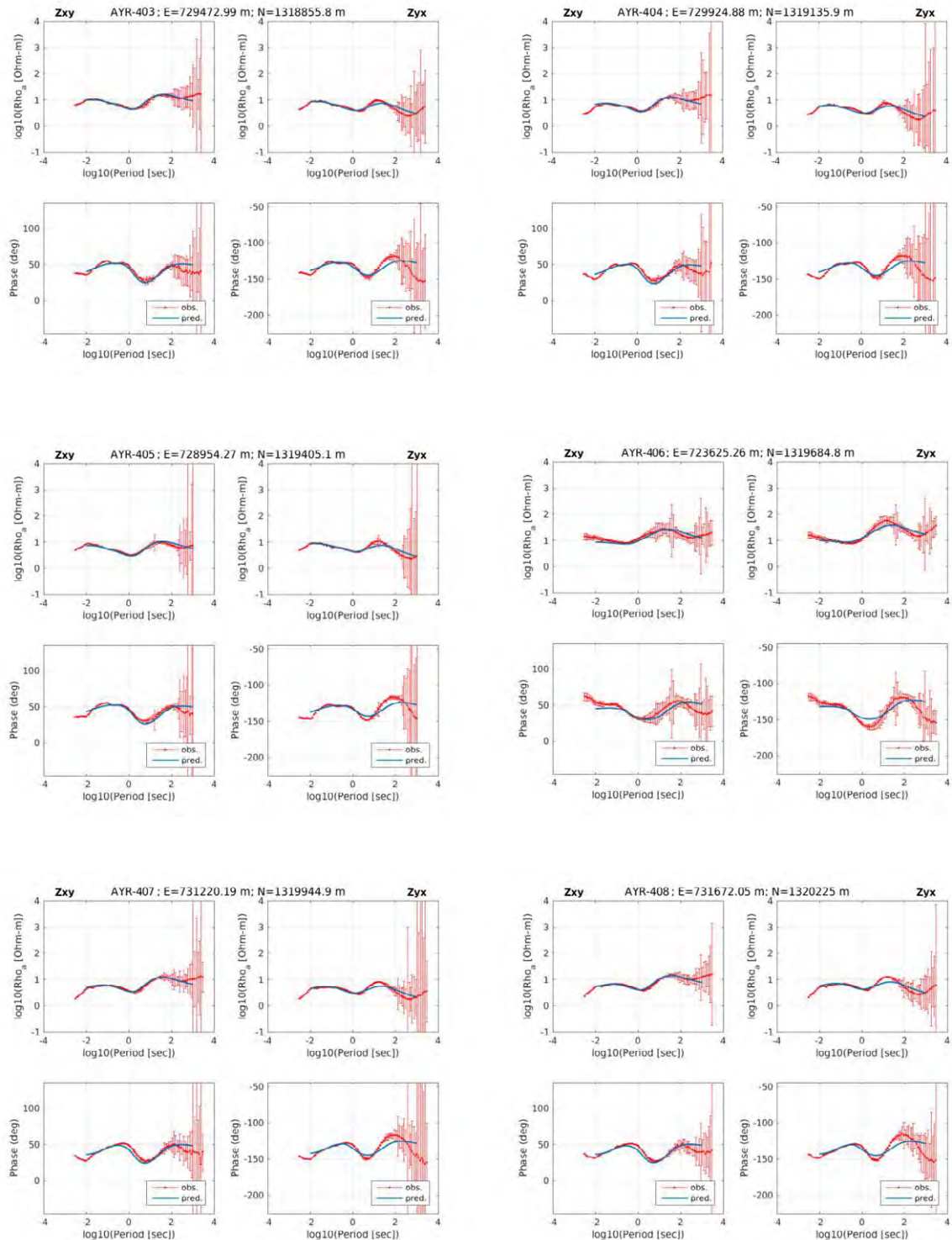
## 2D analysis results - Calculated and observed value of apparent resistivity and phase curve (TDO98)



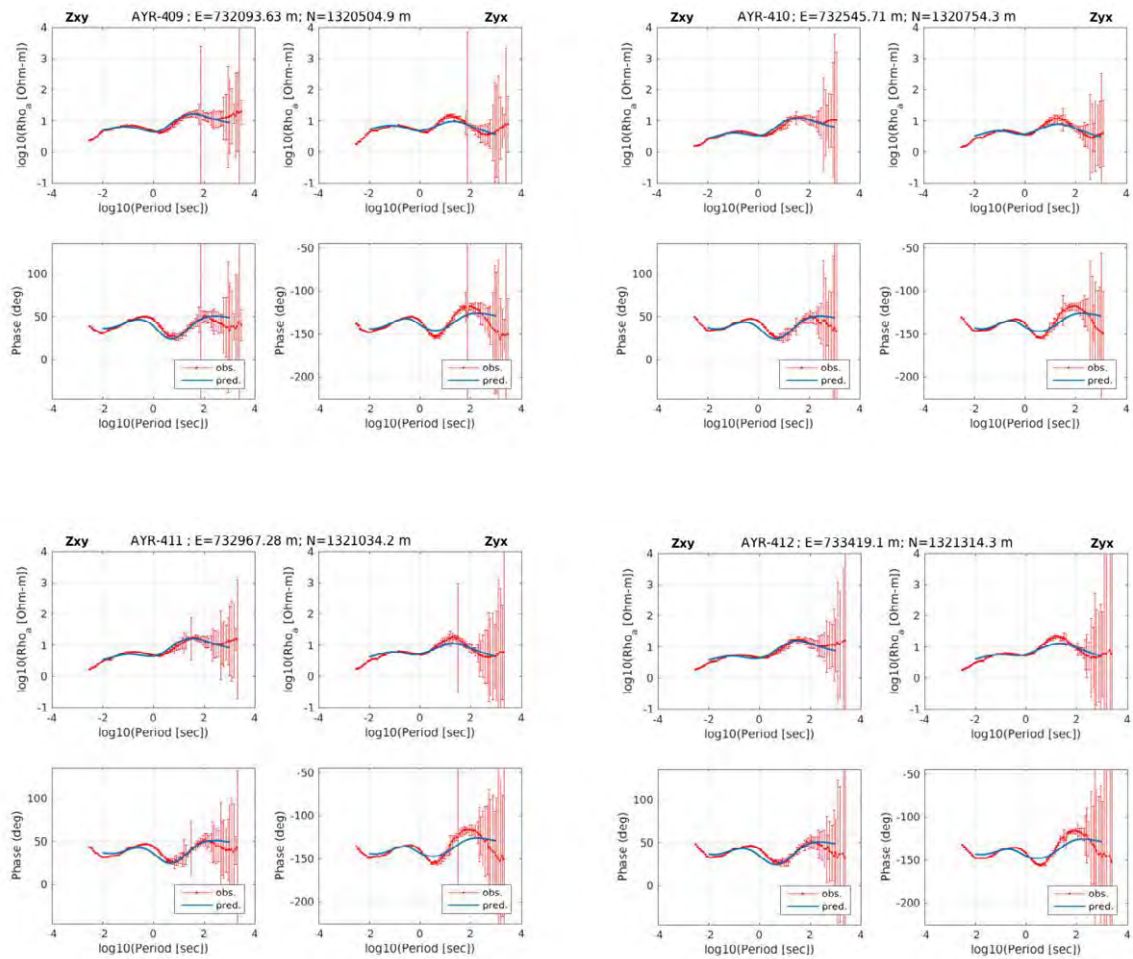
## 2D analysis results - Calculated and observed value of apparent resistivity and phase curve (TDO99)



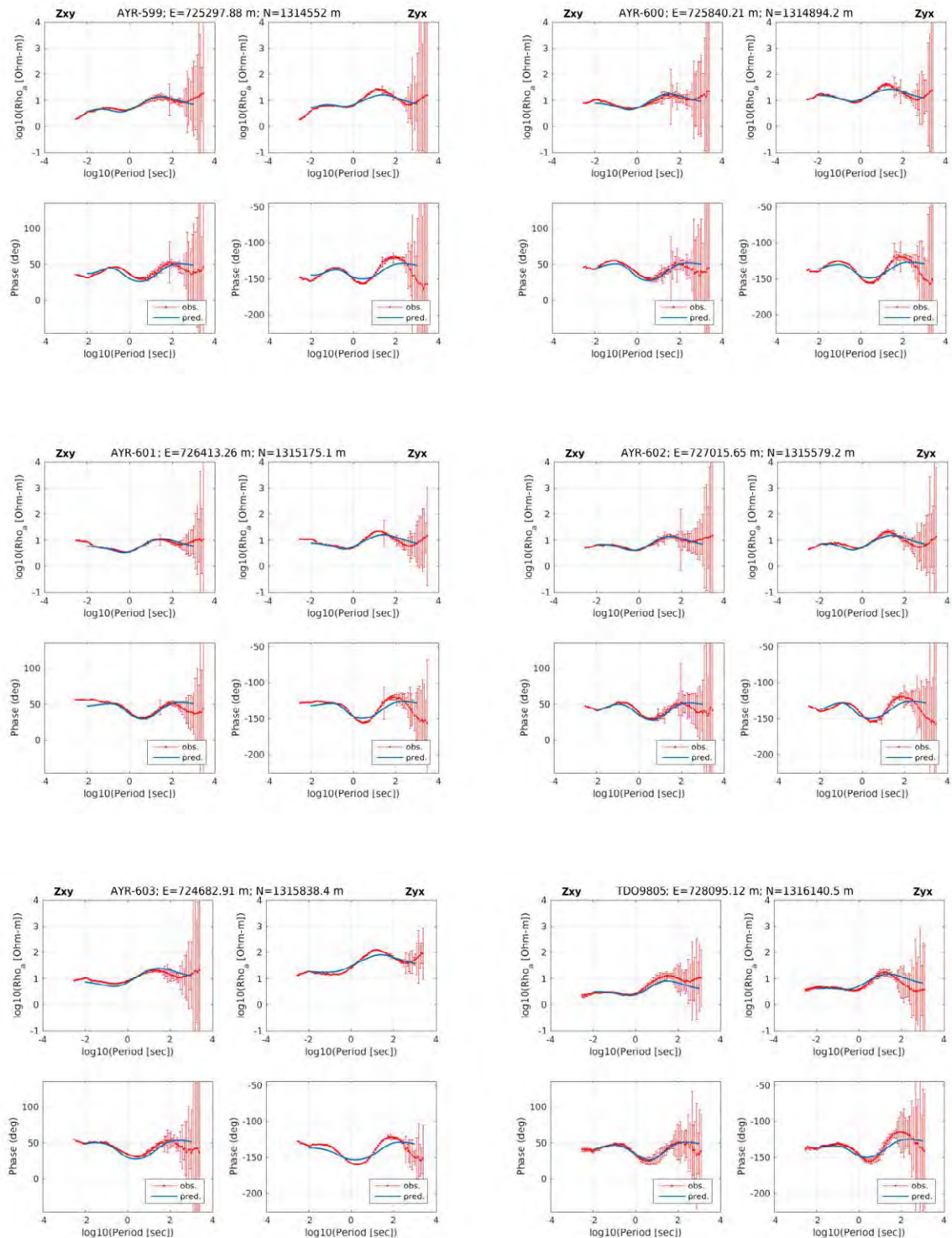
**3D analysis results - Calculated and observed value of apparent resistivity and phase curve (AYR400 1/3)**



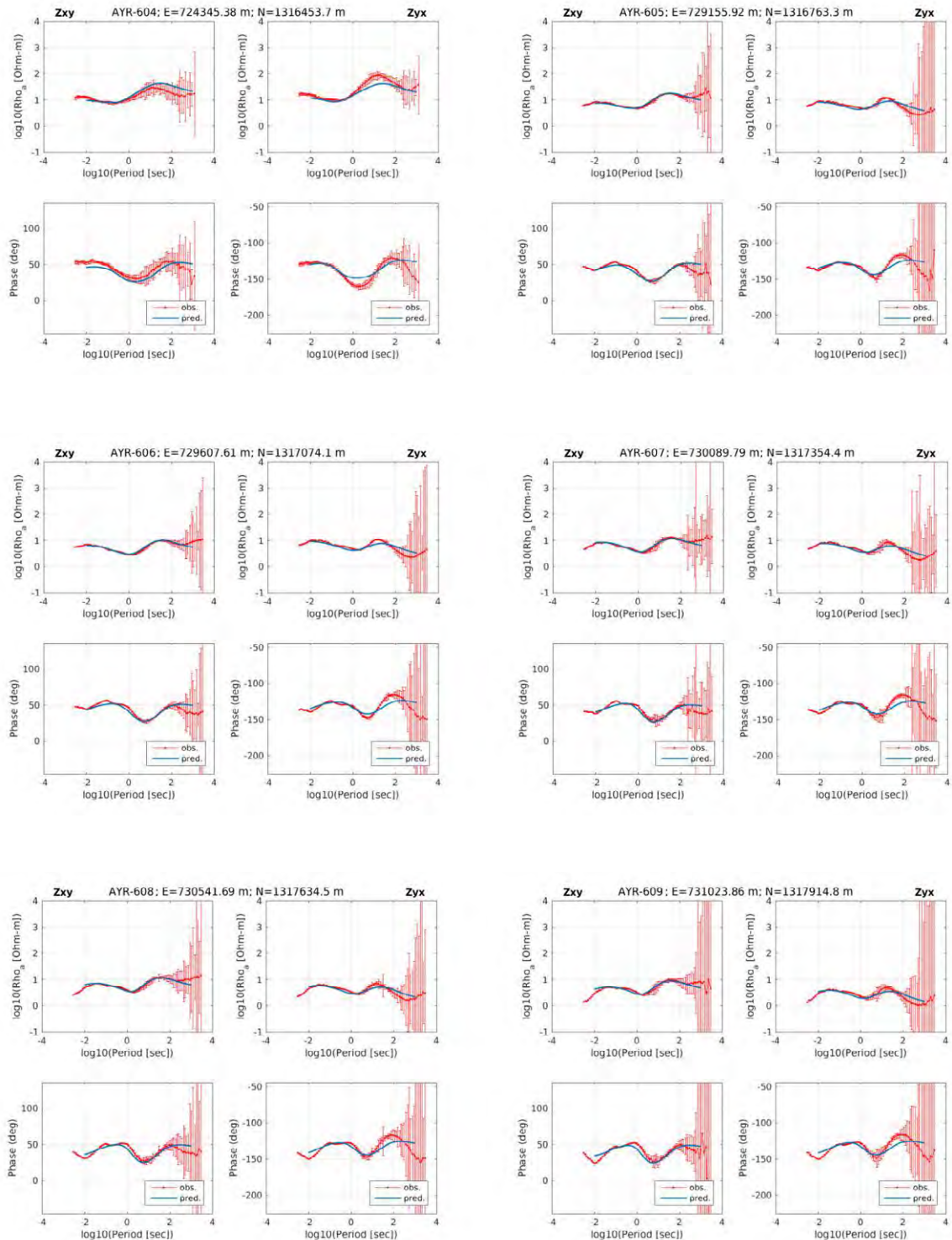
**3D analysis results - Calculated and observed value of apparent resistivity and phase curve (AYR400 2/3)**



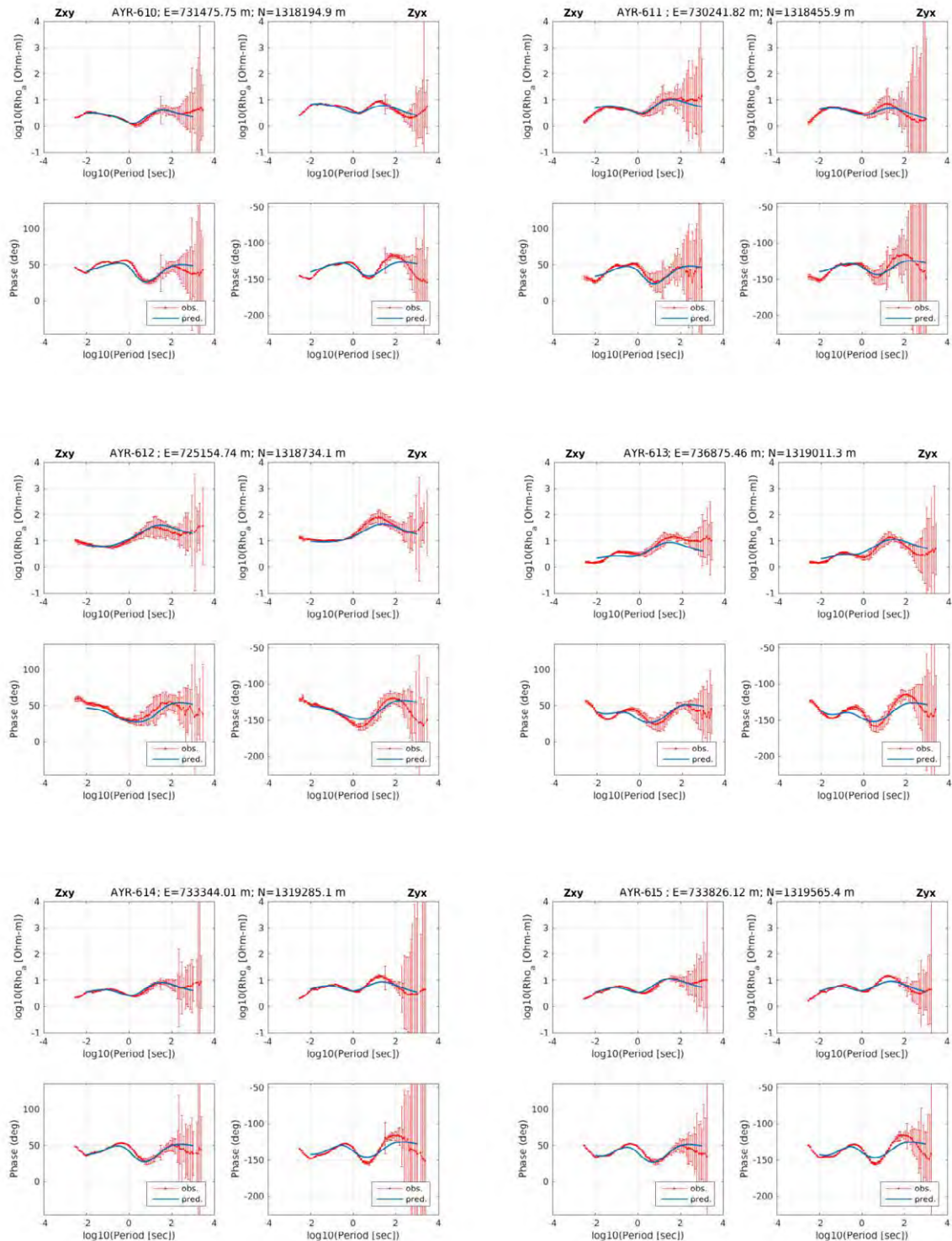
**3D analysis results - Calculated and observed value of apparent resistivity and phase curve (AYR400 3/3)**



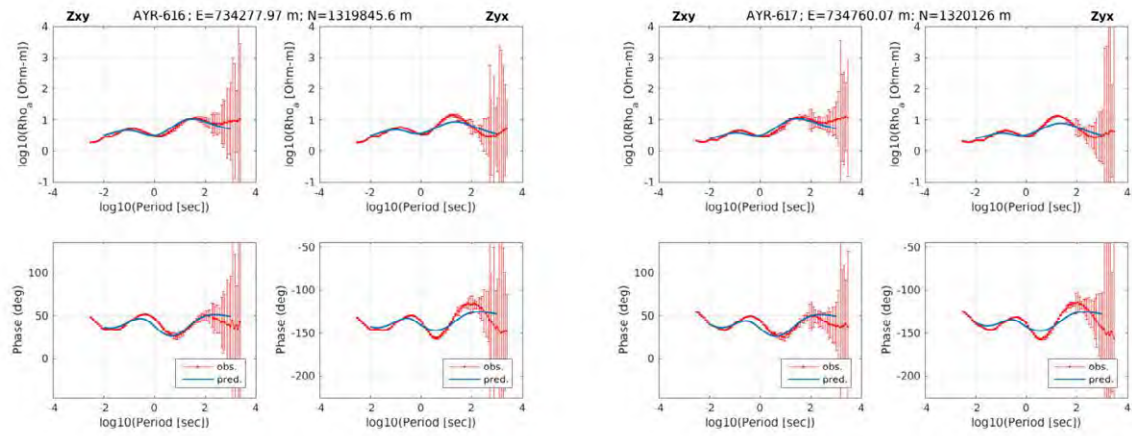
**3D analysis results - Calculated and observed value of apparent resistivity and phase curve (AYR600 1/4)**



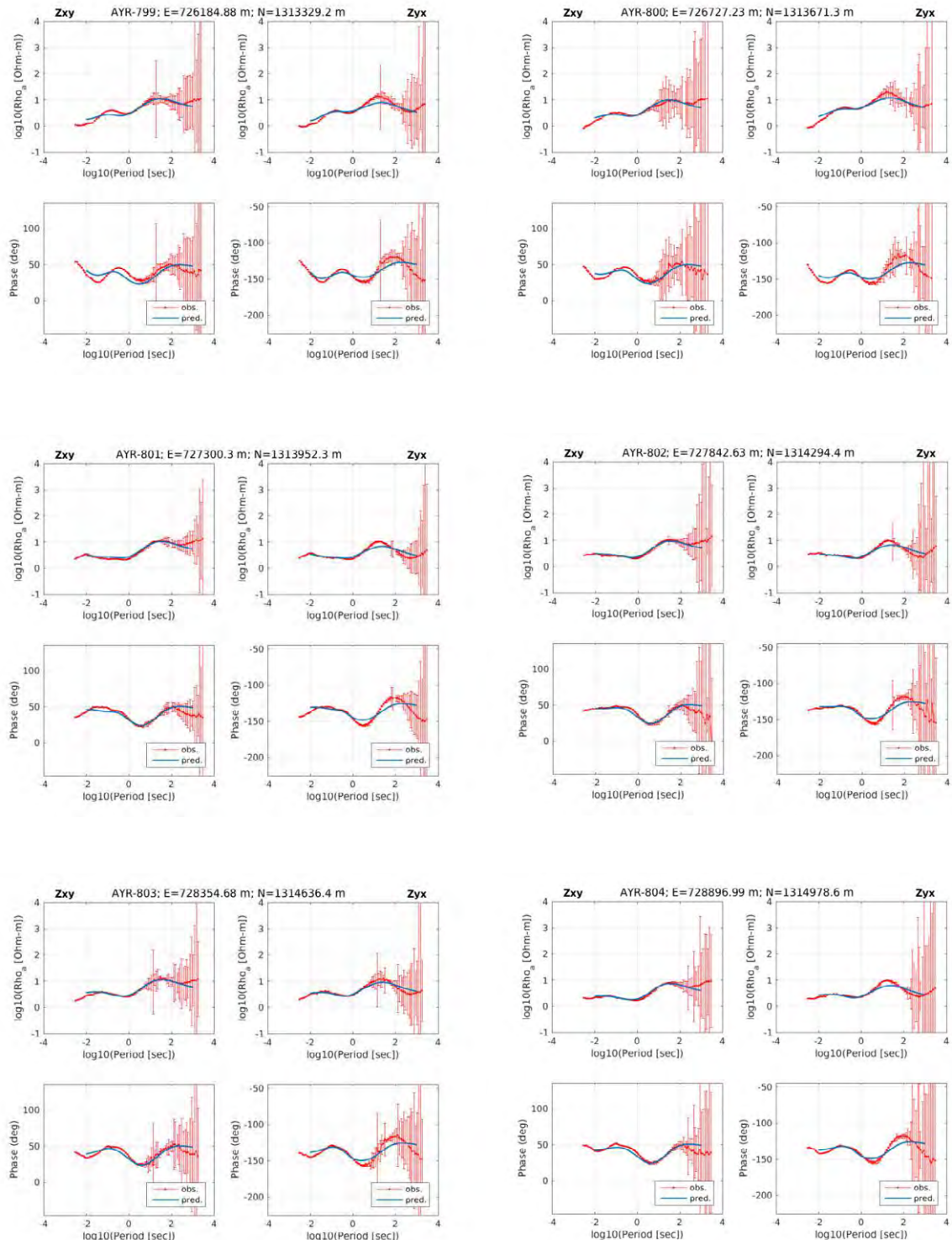
3D analysis results - Calculated and observed value of apparent resistivity and phase curve (AYR600 2/4)



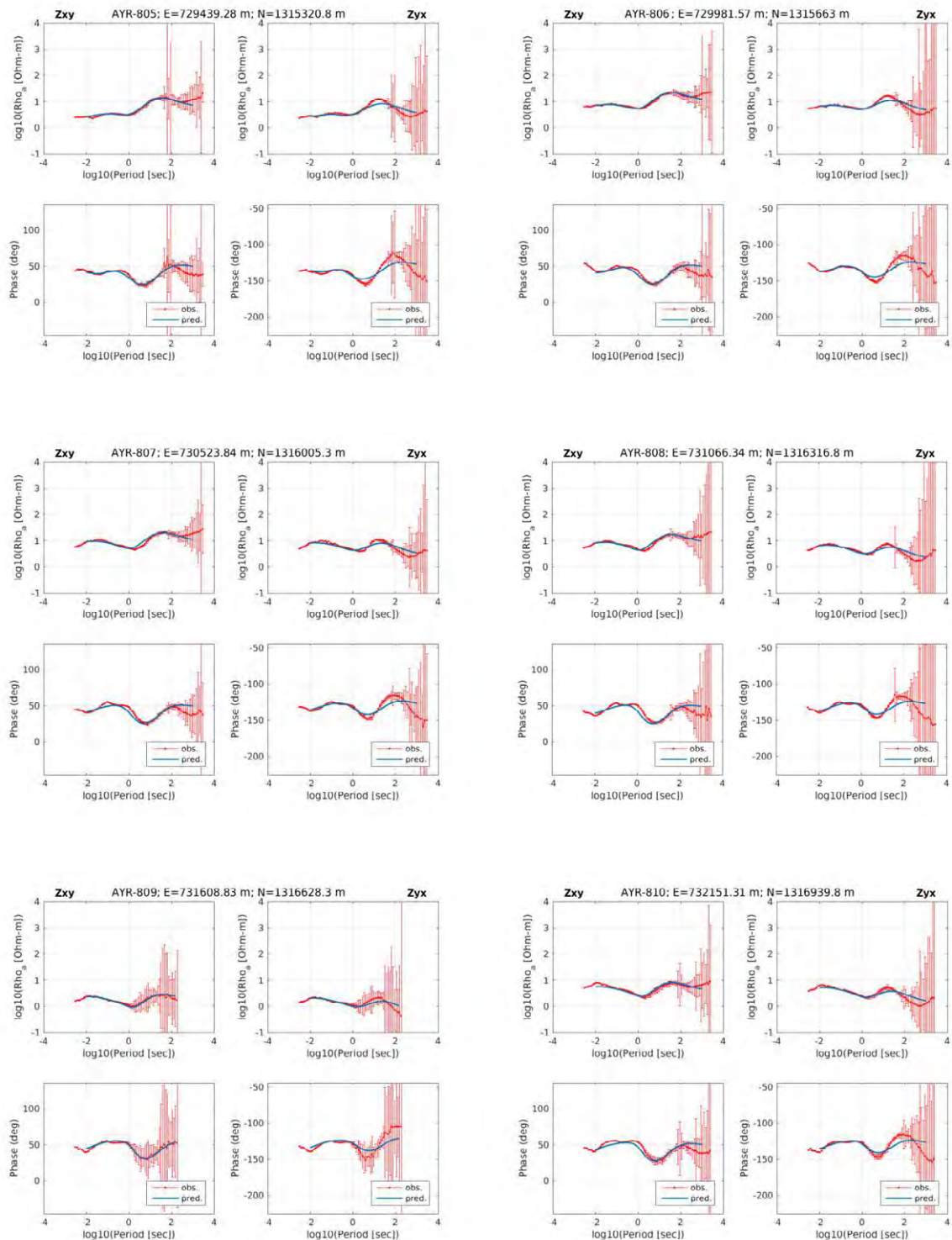
**3D analysis results - Calculated and observed value of apparent resistivity and phase curve (AYR600 3/4)**



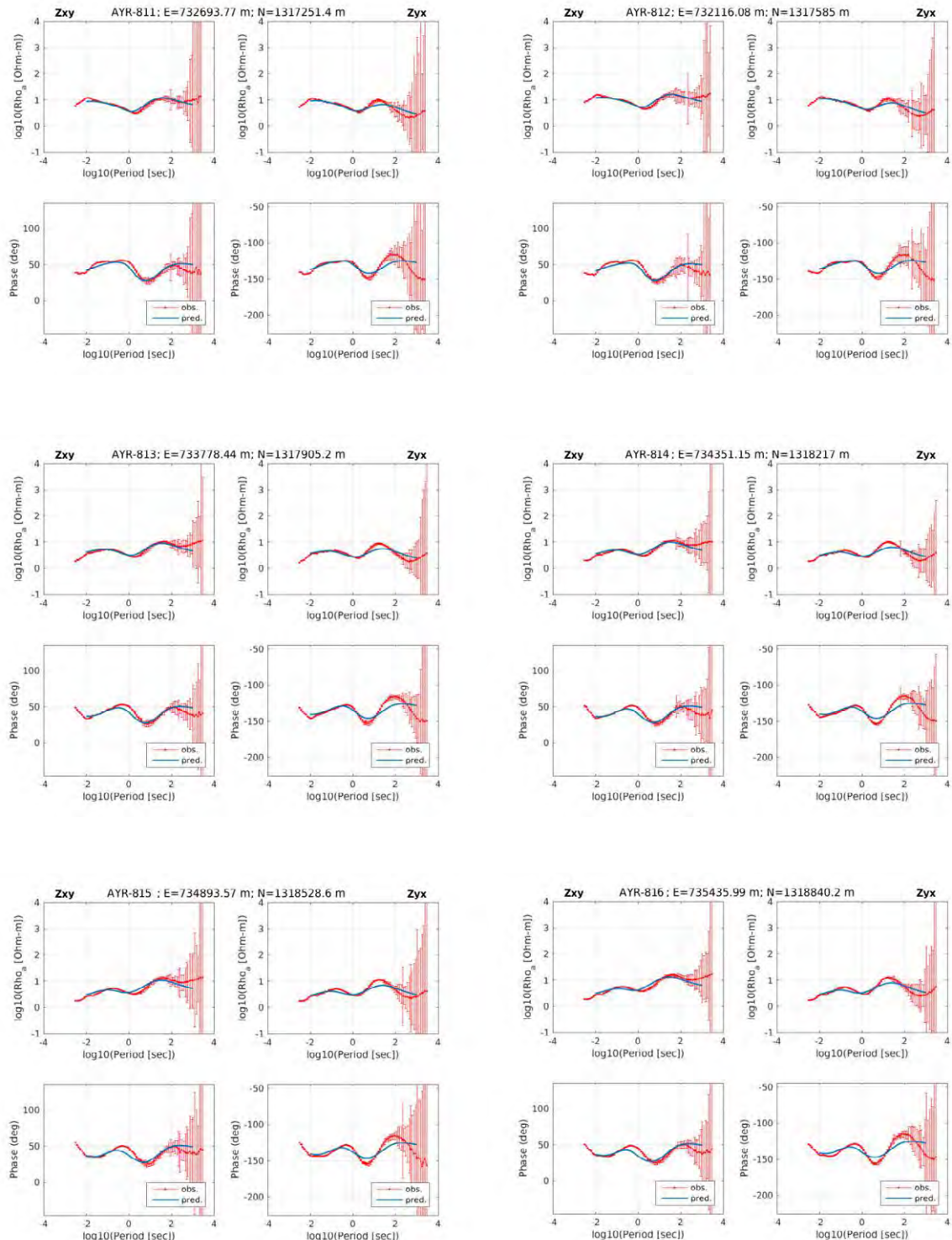
**3D analysis results - Calculated and observed value of apparent resistivity and phase curve (AYR600 4/4)**



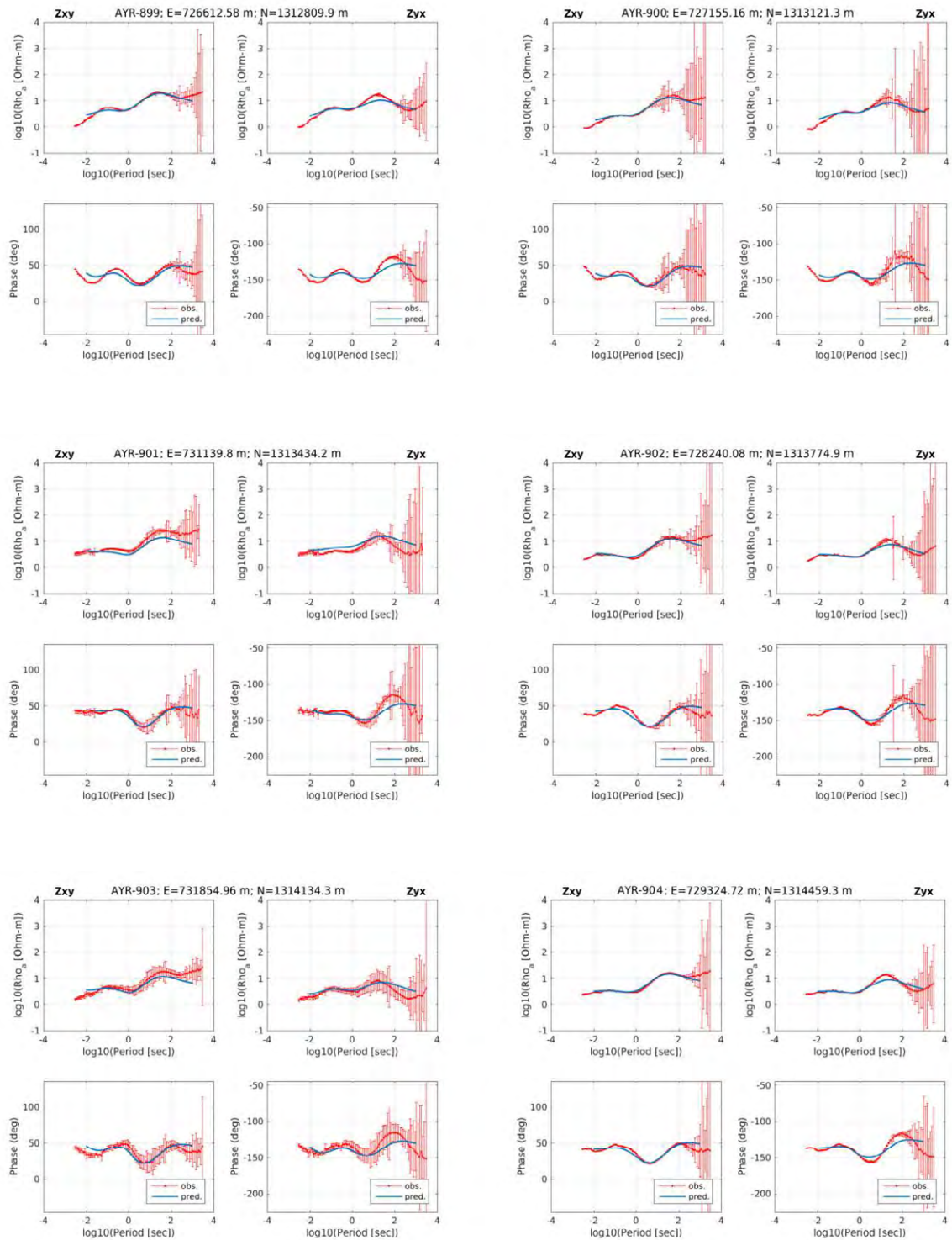
**3D analysis results - Calculated and observed value of apparent resistivity and phase curve (AYR800 1/3)**



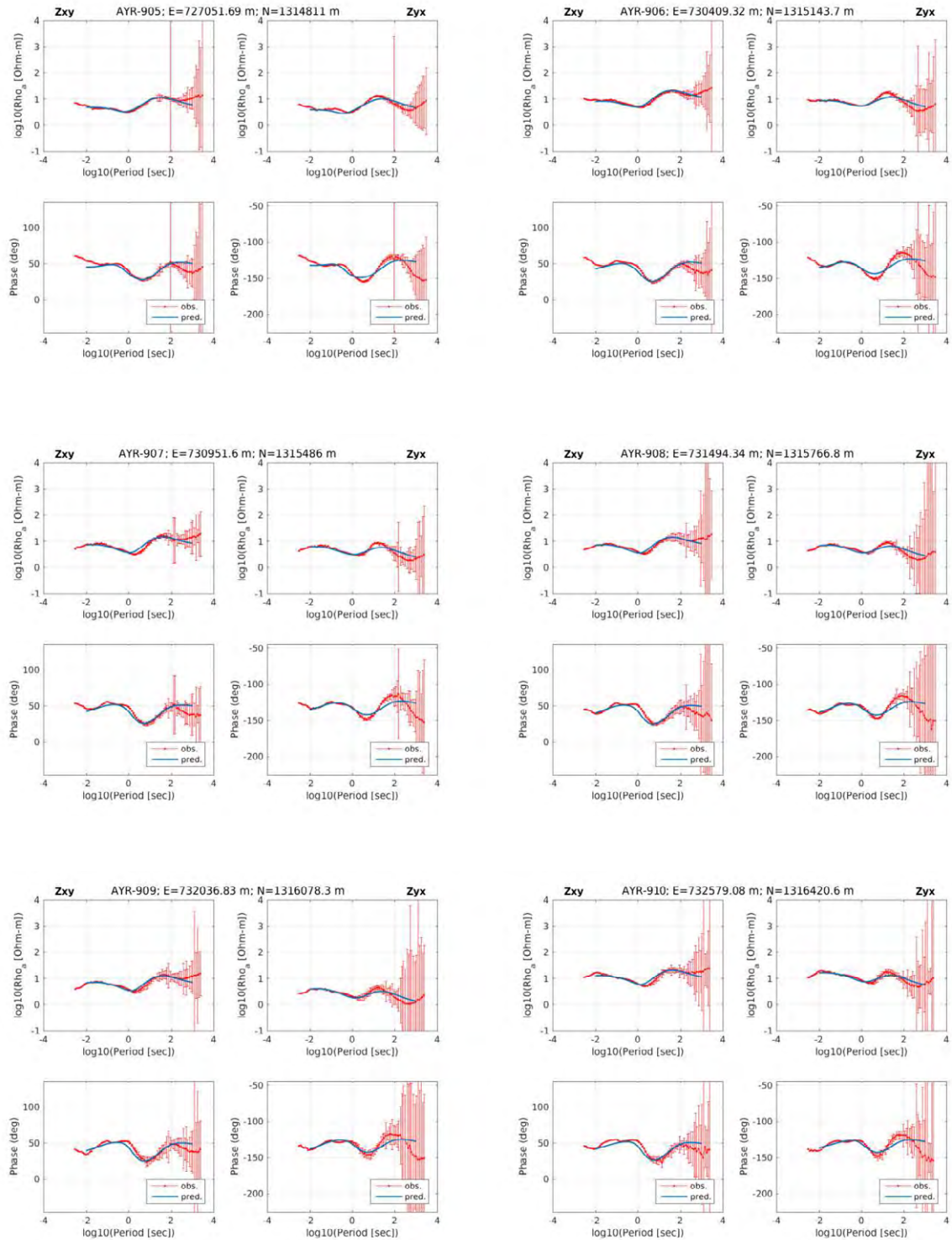
**3D analysis results - Calculated and observed value of apparent resistivity and phase curve (AYR800 2/3)**



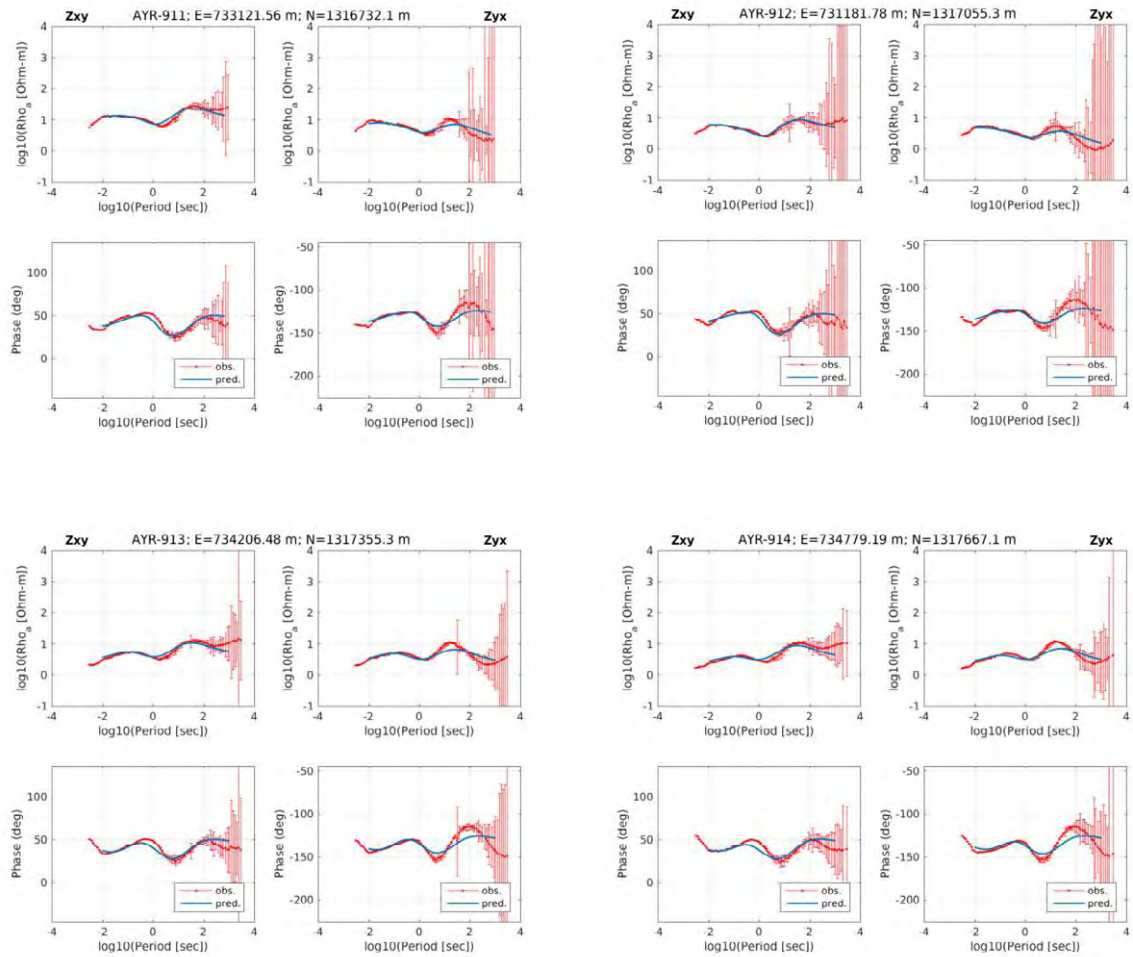
**3D analysis results - Calculated and observed value of apparent resistivity and phase curve (AYR800 3/3)**



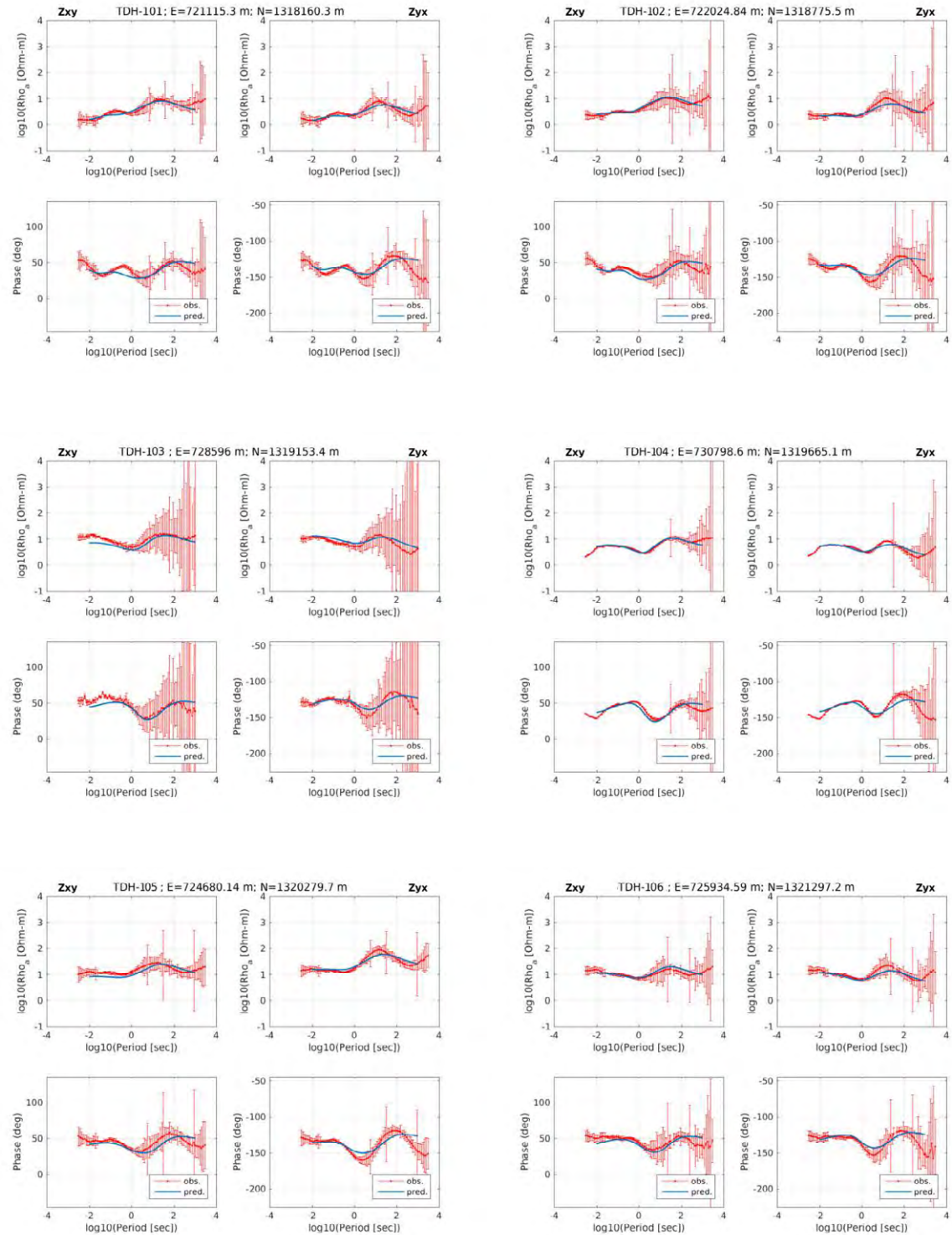
**3D analysis results - Calculated and observed value of apparent resistivity and phase curve (AYR900 1/3)**



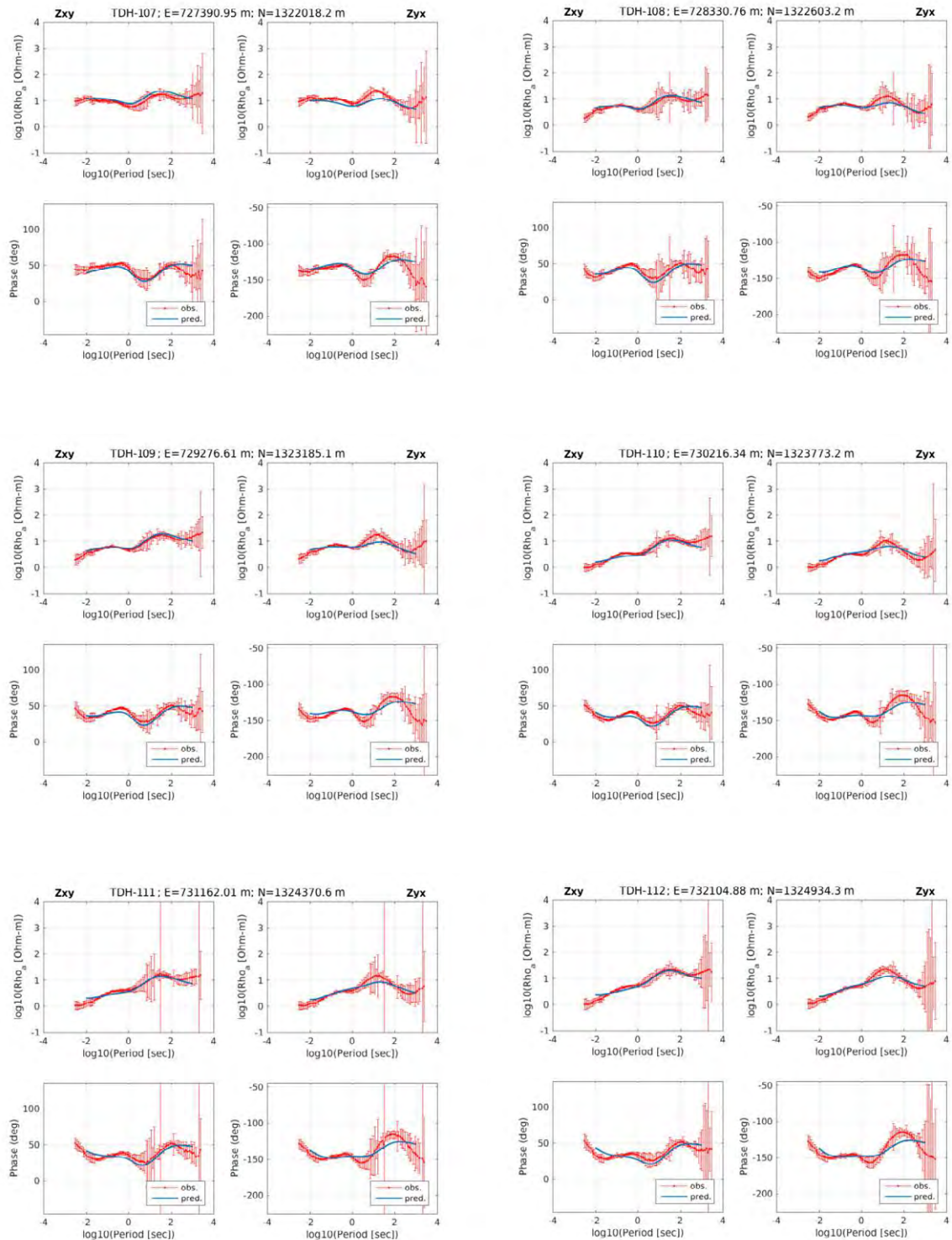
**3D analysis results - Calculated and observed value of apparent resistivity and phase curve (AYR900 2/3)**



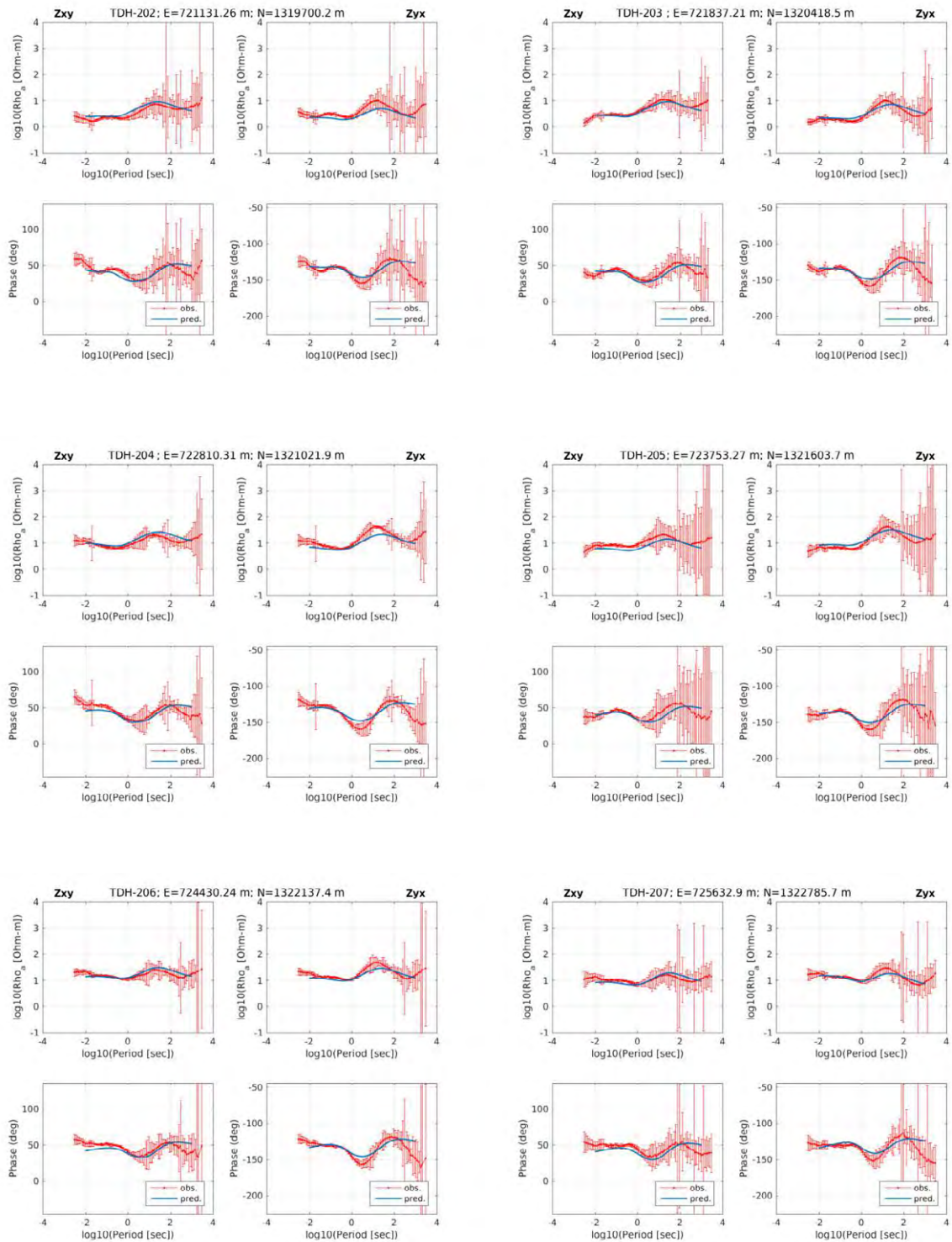
**3D analysis results - Calculated and observed value of apparent resistivity and phase curve (AYR900 3/3)**



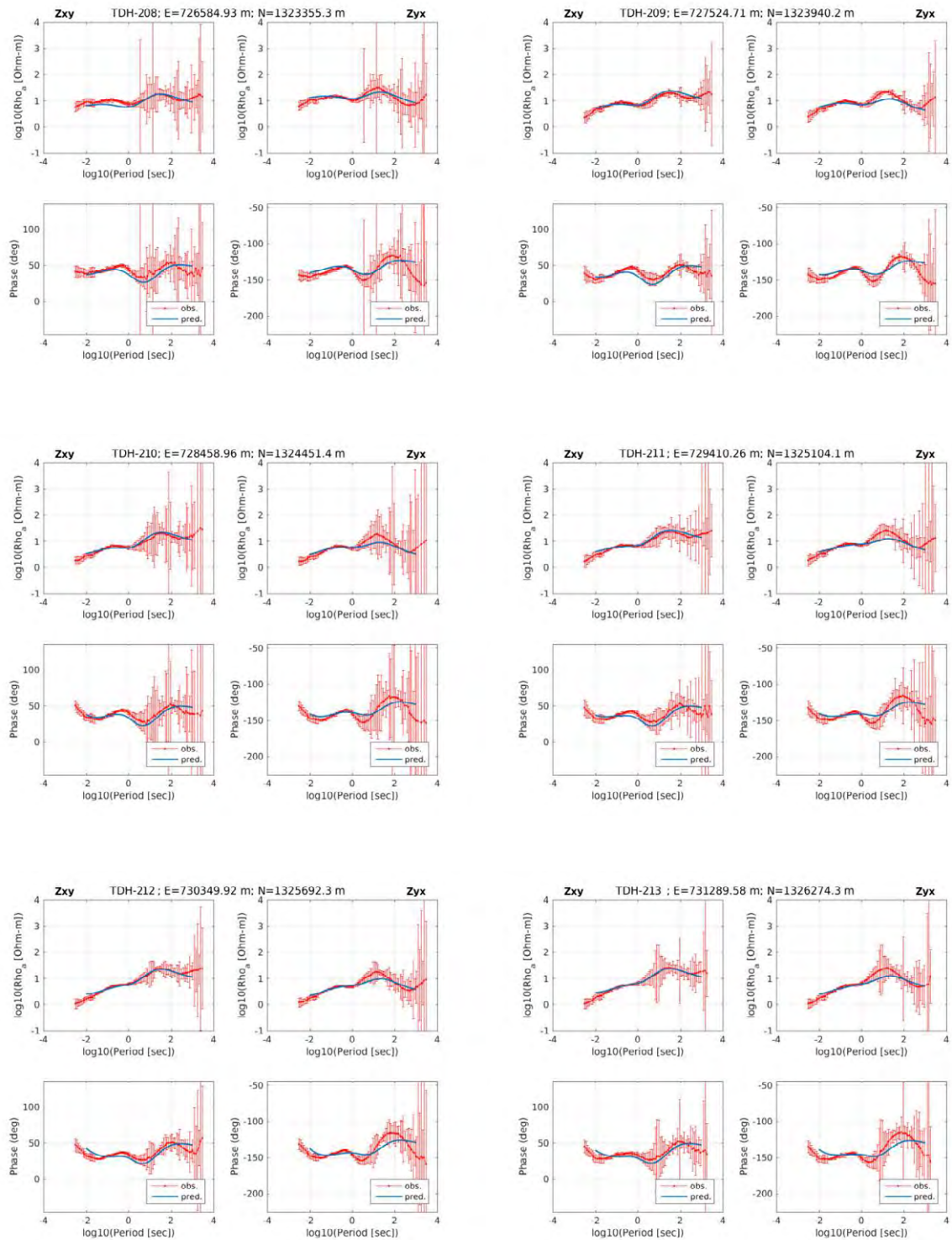
**3D analysis results - Calculated and observed value of apparent resistivity and phase curve (TDH100 1/2)**



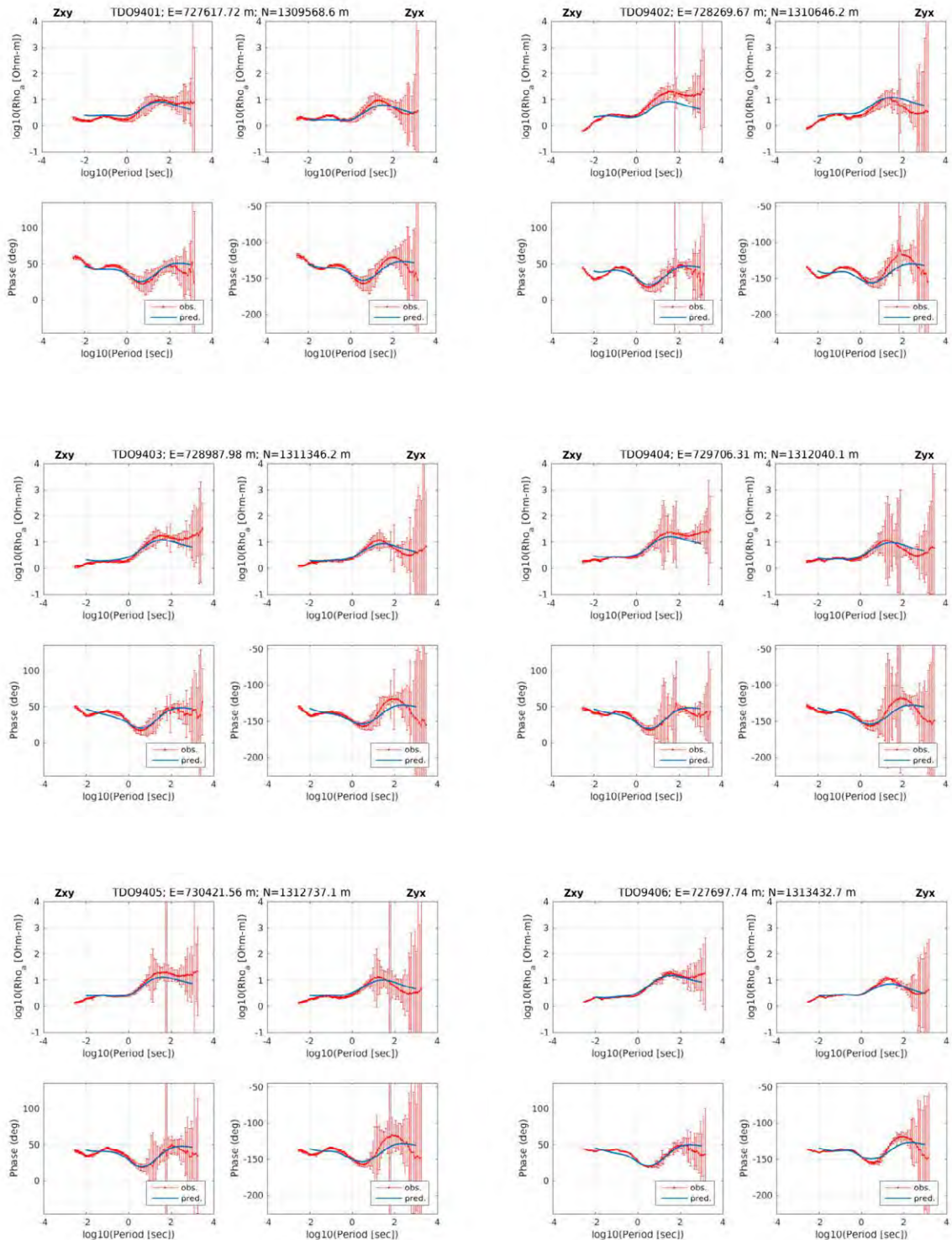
**3D analysis results - Calculated and observed value of apparent resistivity and phase curve (TDH100 2/2)**



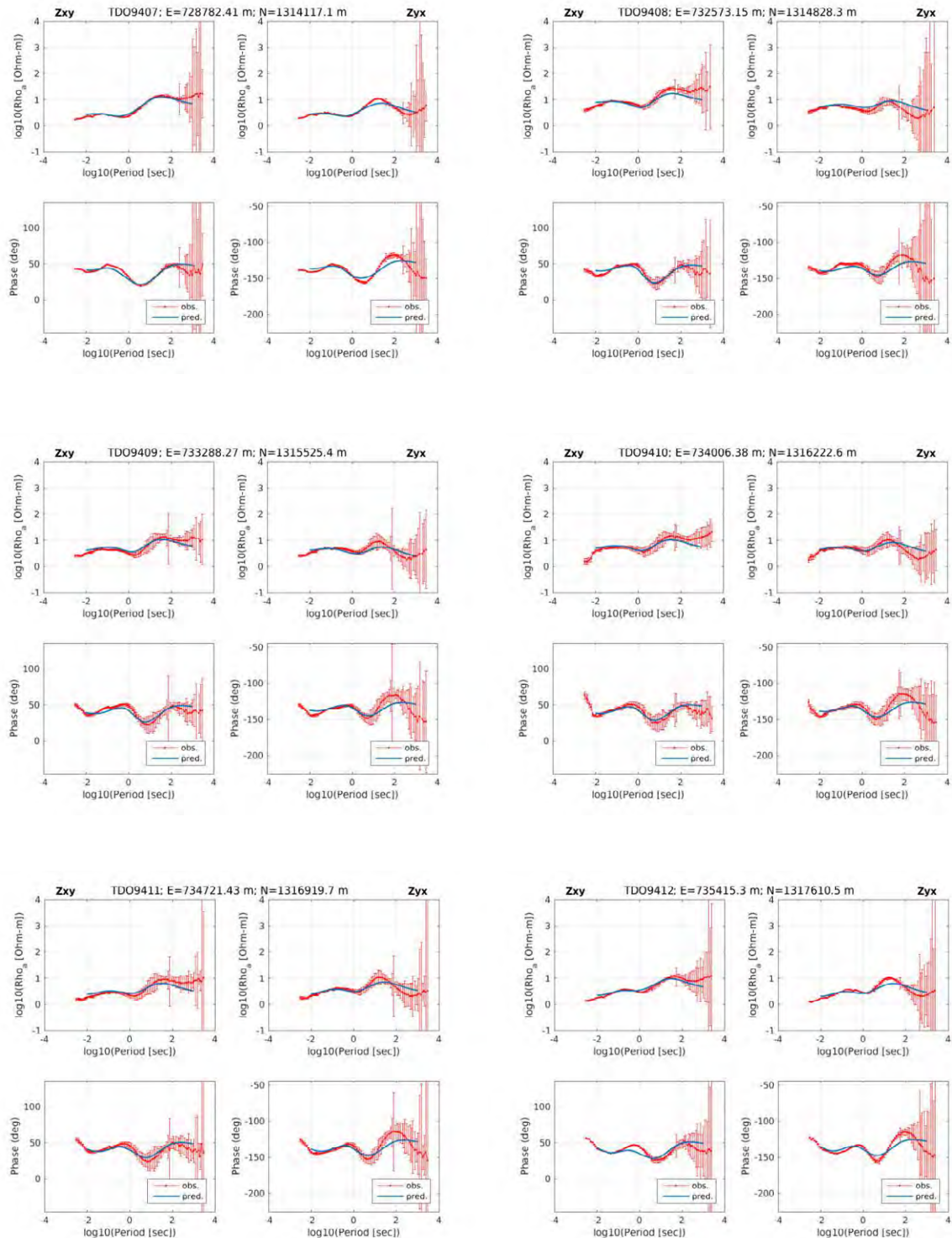
**3D analysis results - Calculated and observed value of apparent resistivity and phase curve (TDH200 1/2)**



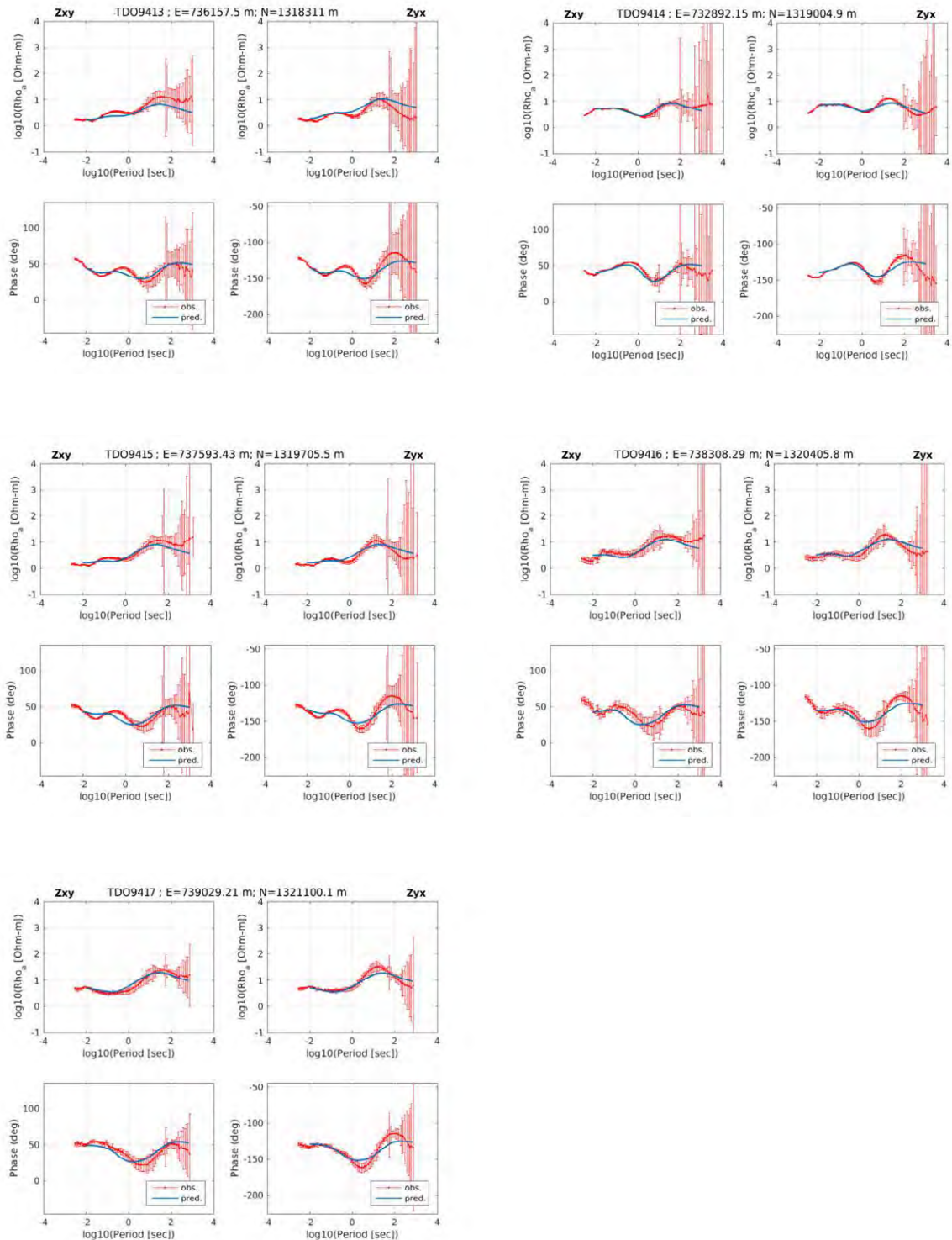
**3D analysis results - Calculated and observed value of apparent resistivity and phase curve (TDH200 2/2)**



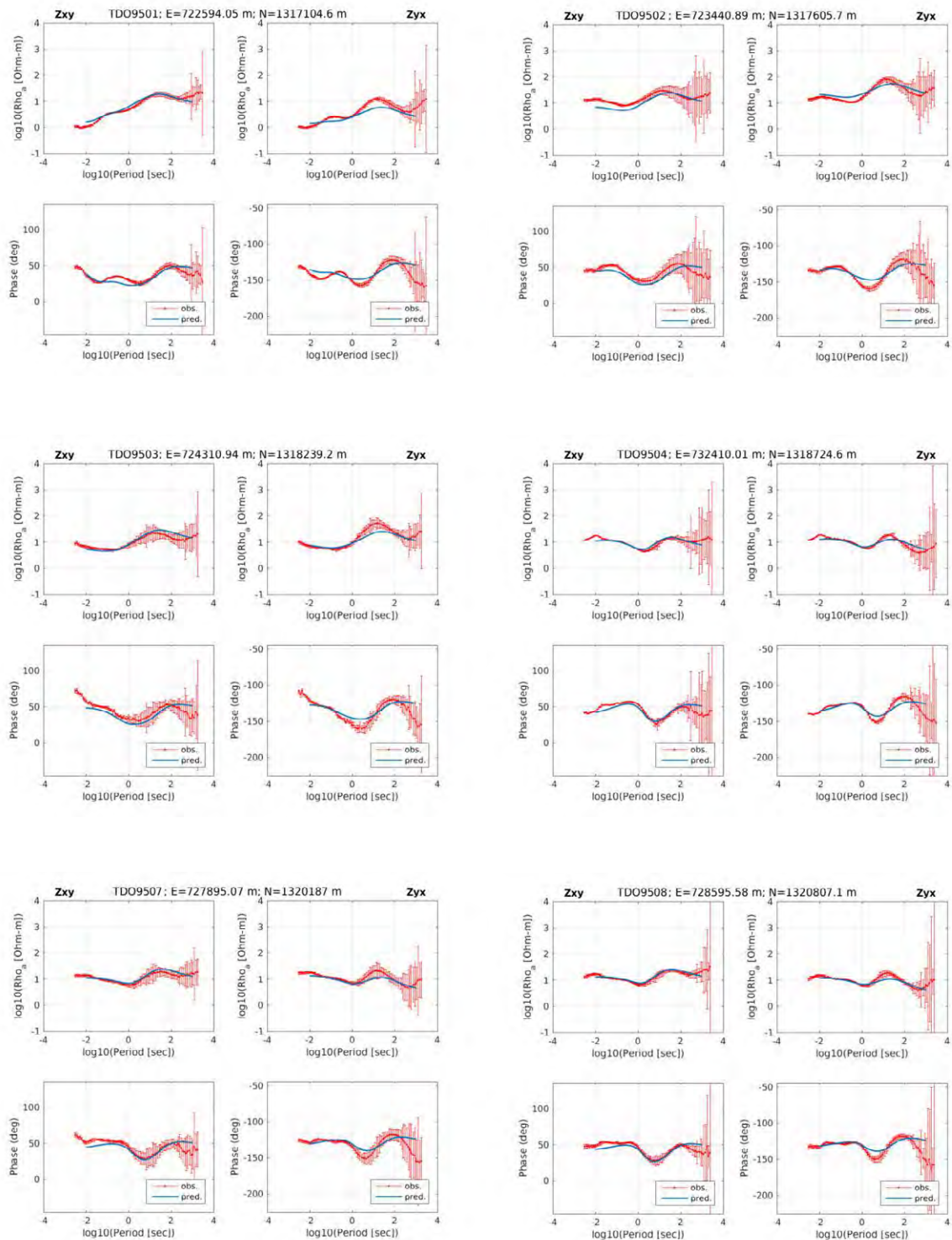
**3D analysis results - Calculated and observed value of apparent resistivity and phase curve (TDO94 1/3)**



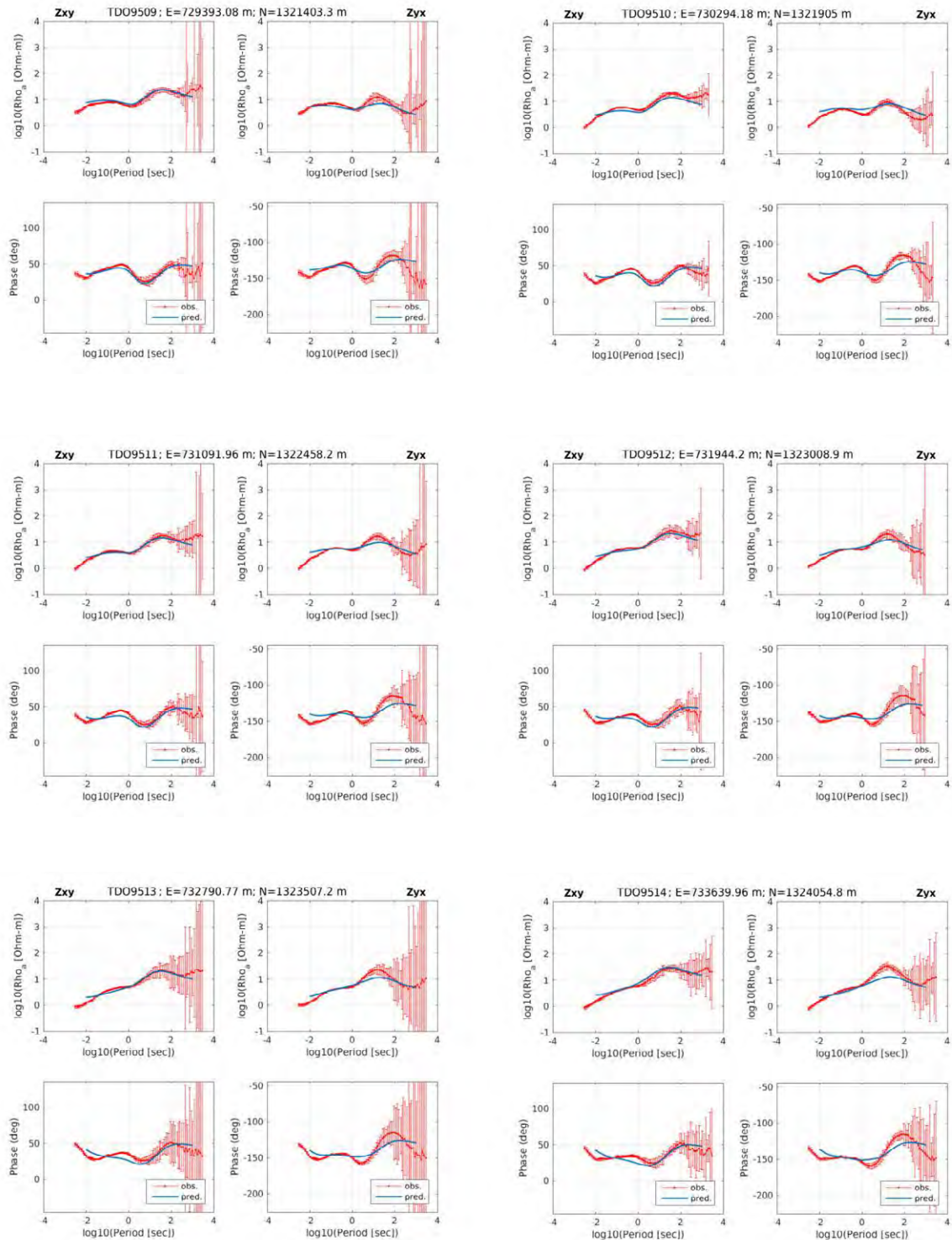
**3D analysis results - Calculated and observed value of apparent resistivity and phase curve (TDO94 2/3)**



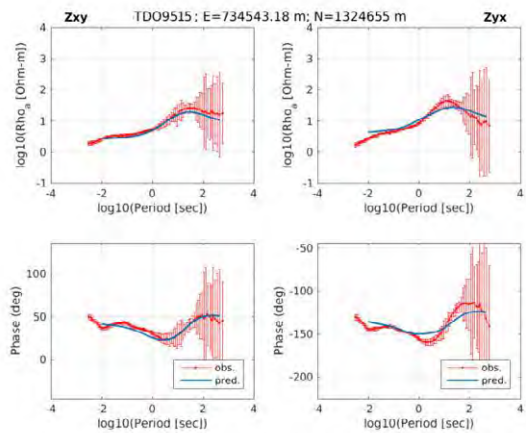
**3D analysis results - Calculated and observed value of apparent resistivity and phase curve (TDO94 3/3)**



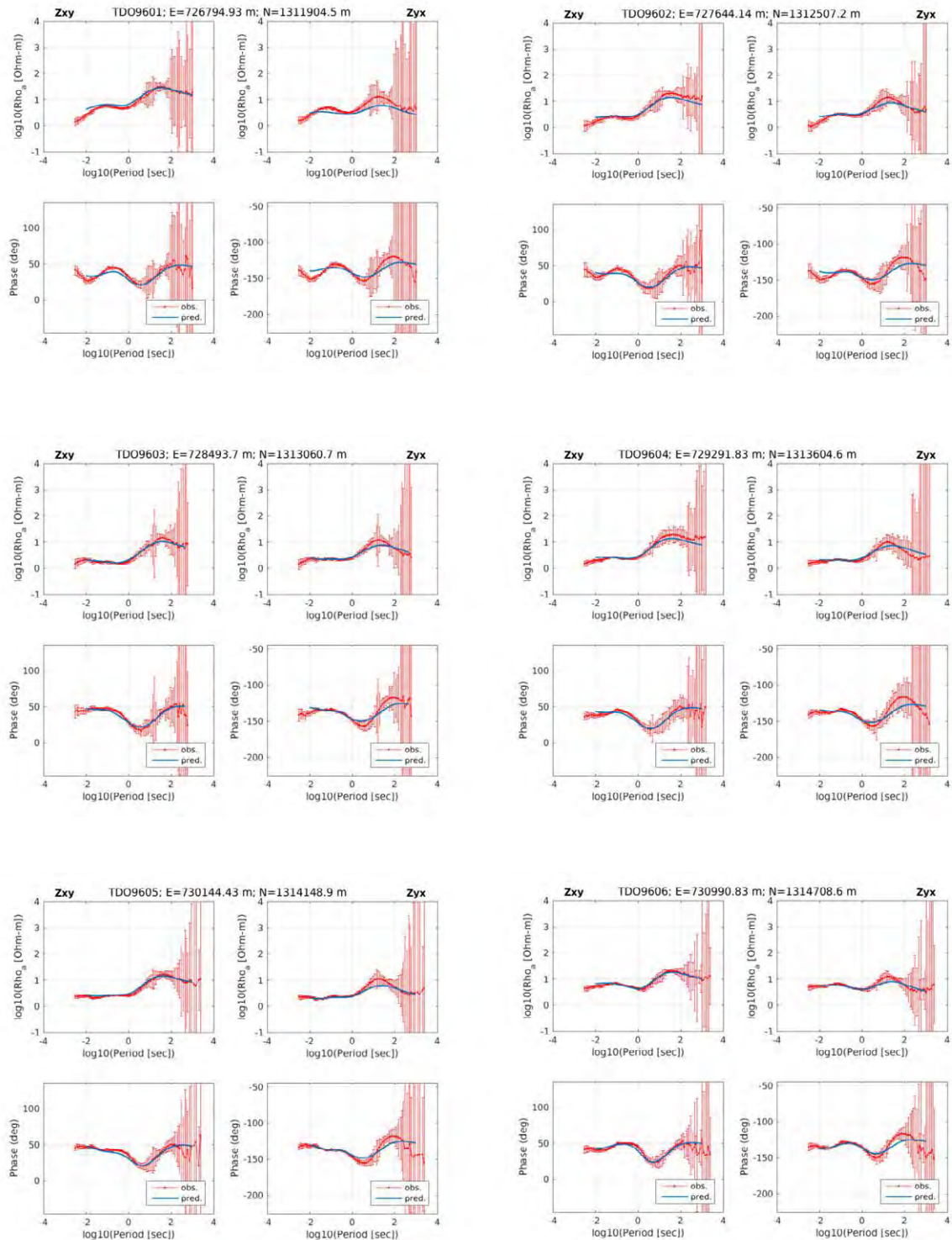
**3D analysis results - Calculated and observed value of apparent resistivity and phase curve (TDO95 1/3)**



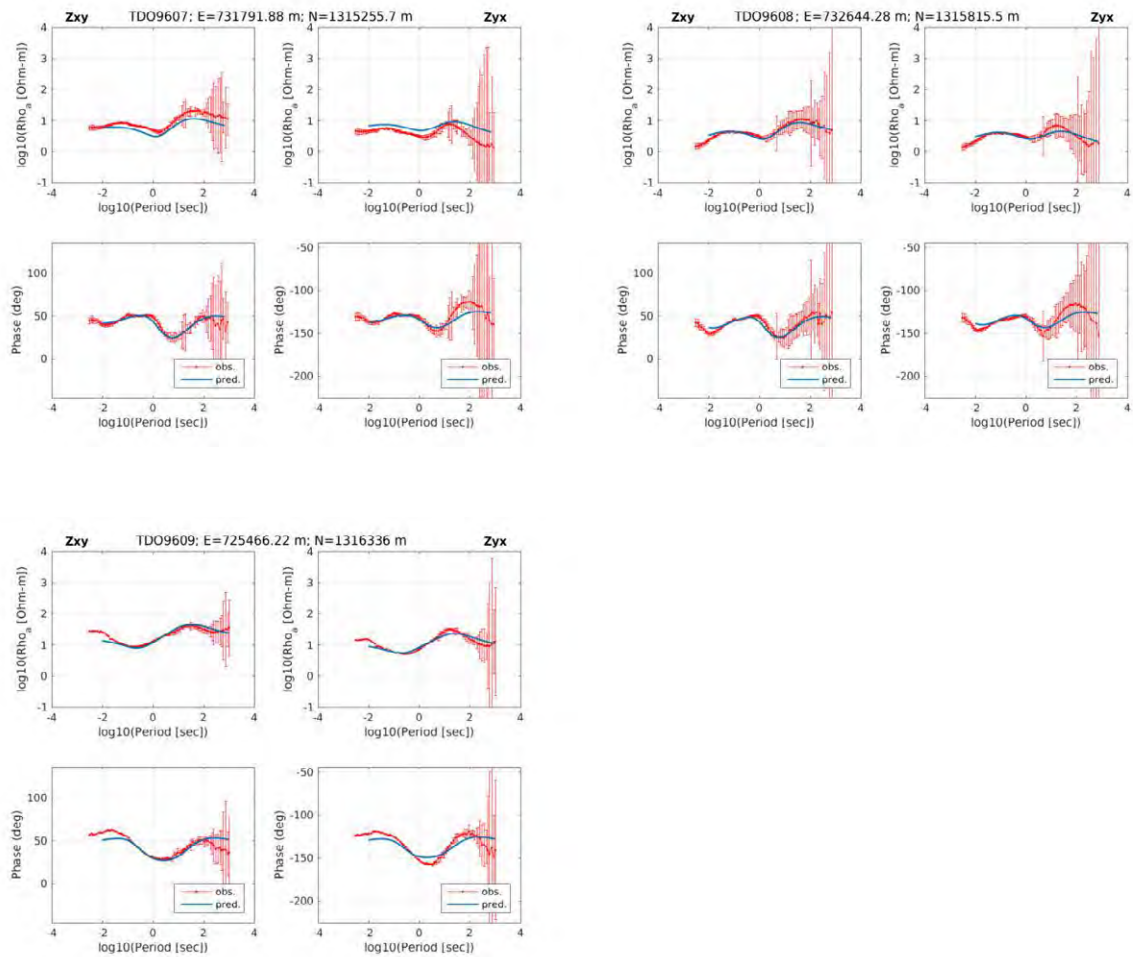
**3D analysis results - Calculated and observed value of apparent resistivity and phase curve (TDO95 2/3)**



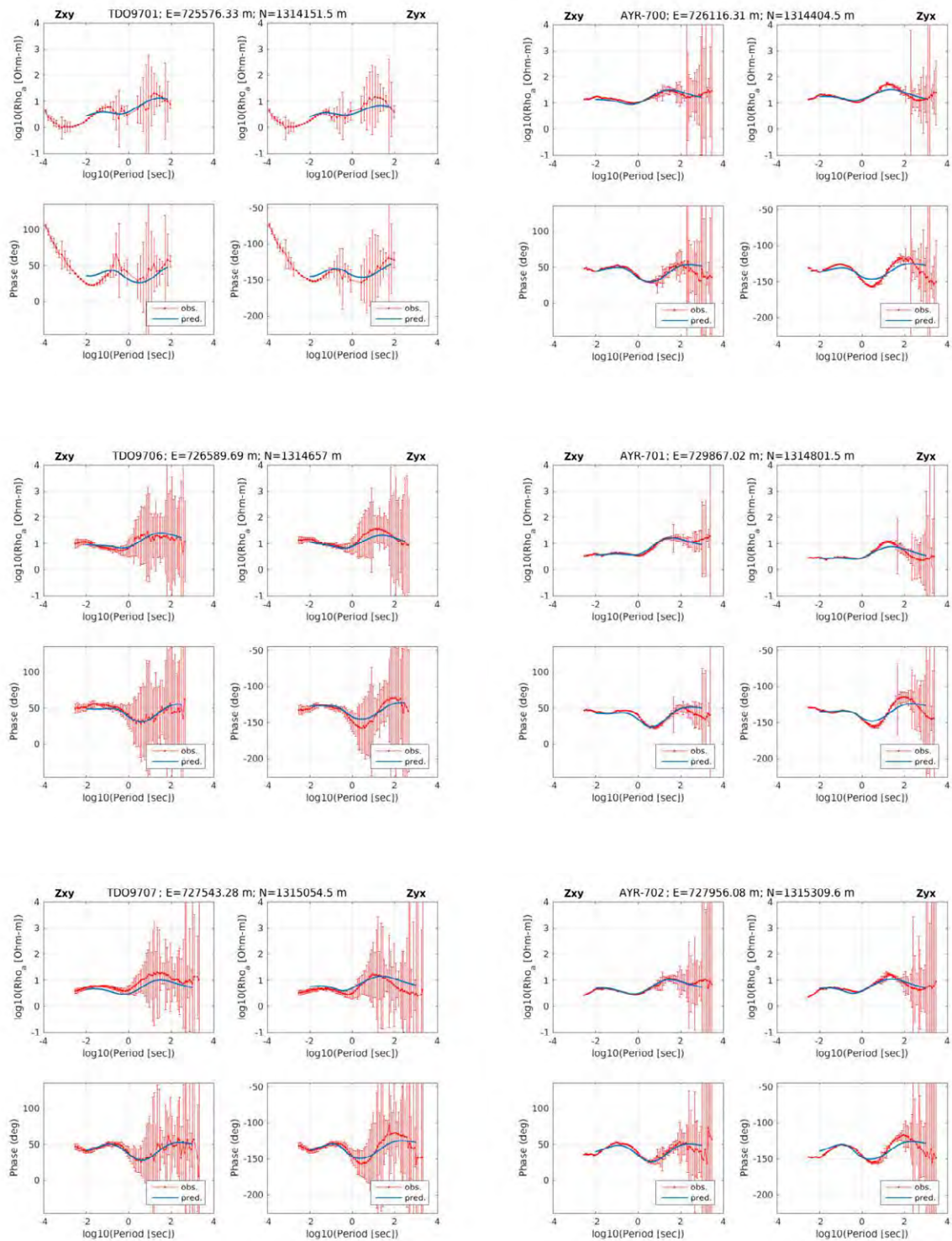
**3D analysis results - Calculated and observed value of apparent resistivity and phase curve (TDO95 3/3)**



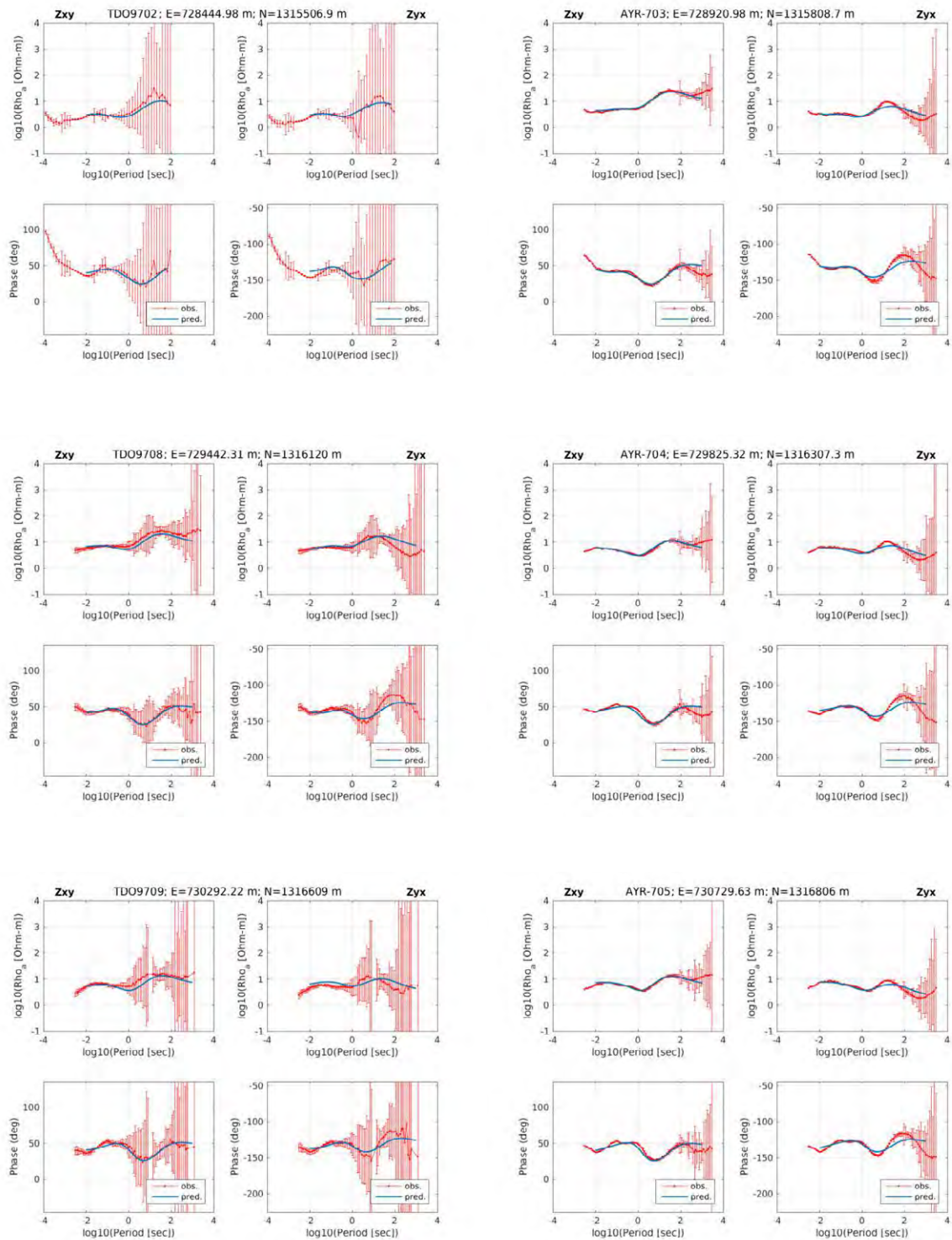
**3D analysis results - Calculated and observed value of apparent resistivity and phase curve (TDO96 1/2)**



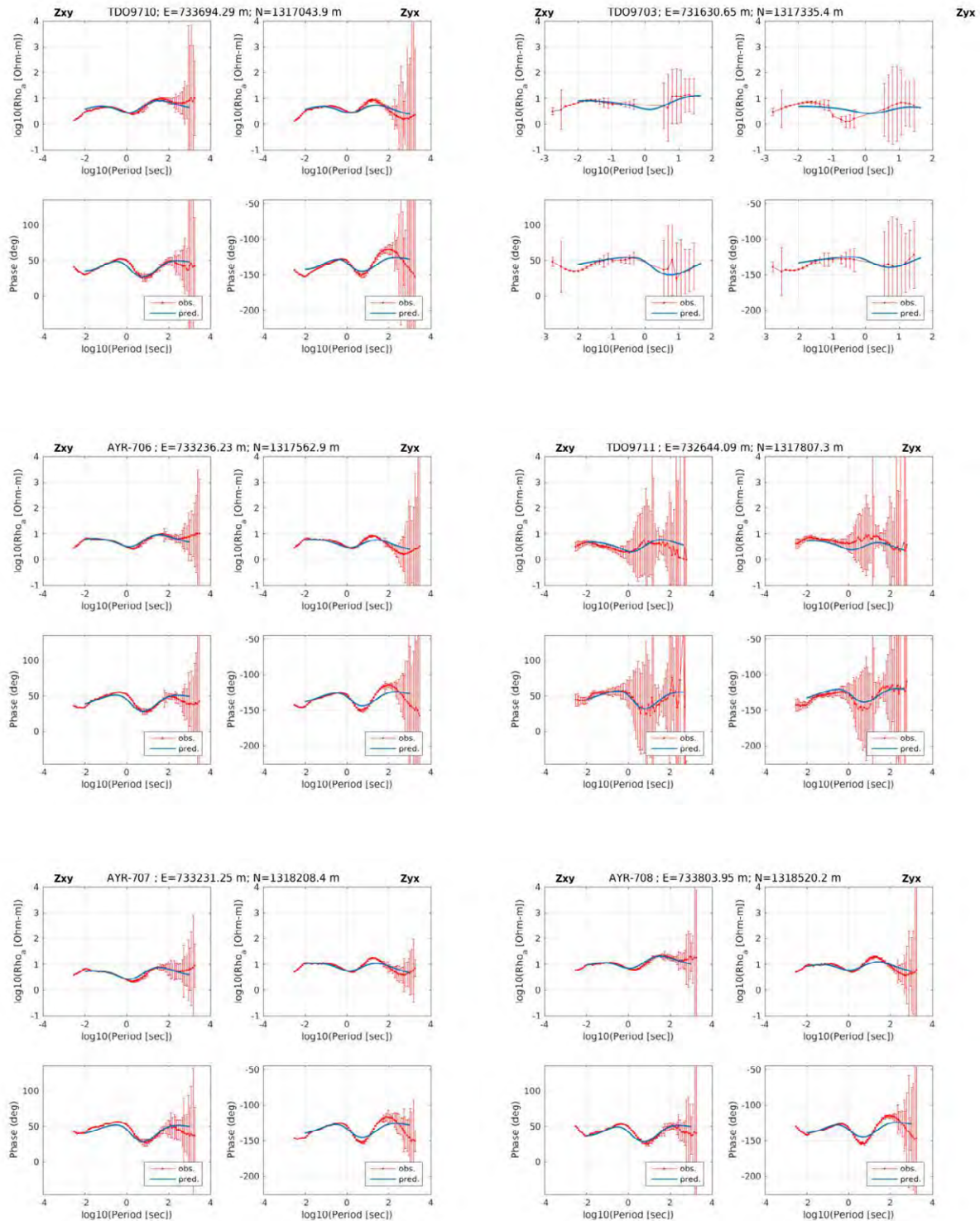
**3D analysis results - Calculated and observed value of apparent resistivity and phase curve (TDO96 2/2)**



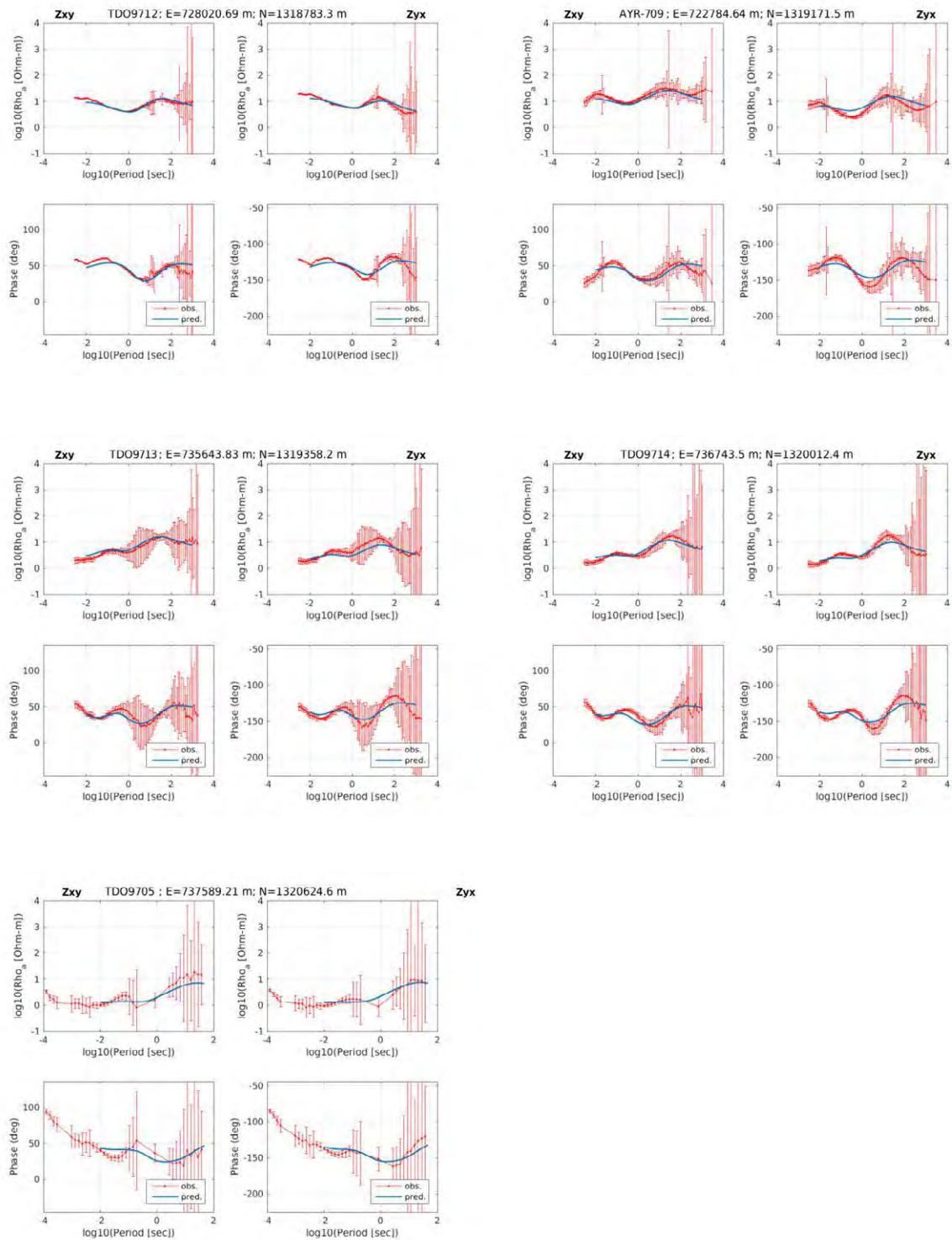
**3D analysis results - Calculated and observed value of apparent resistivity and phase curve (TDO97 1/4)**



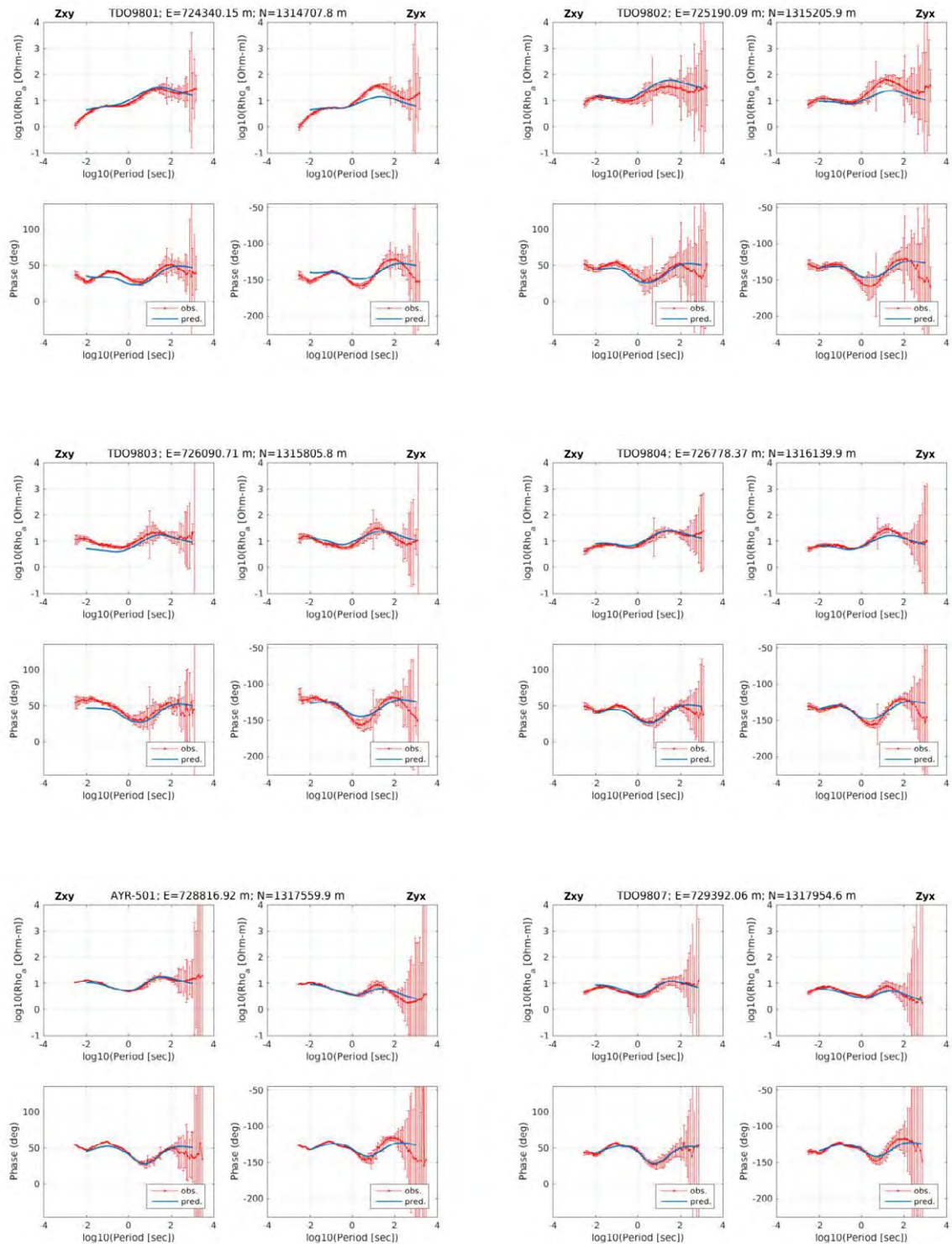
**3D analysis results - Calculated and observed value of apparent resistivity and phase curve (TDO97 2/4)**



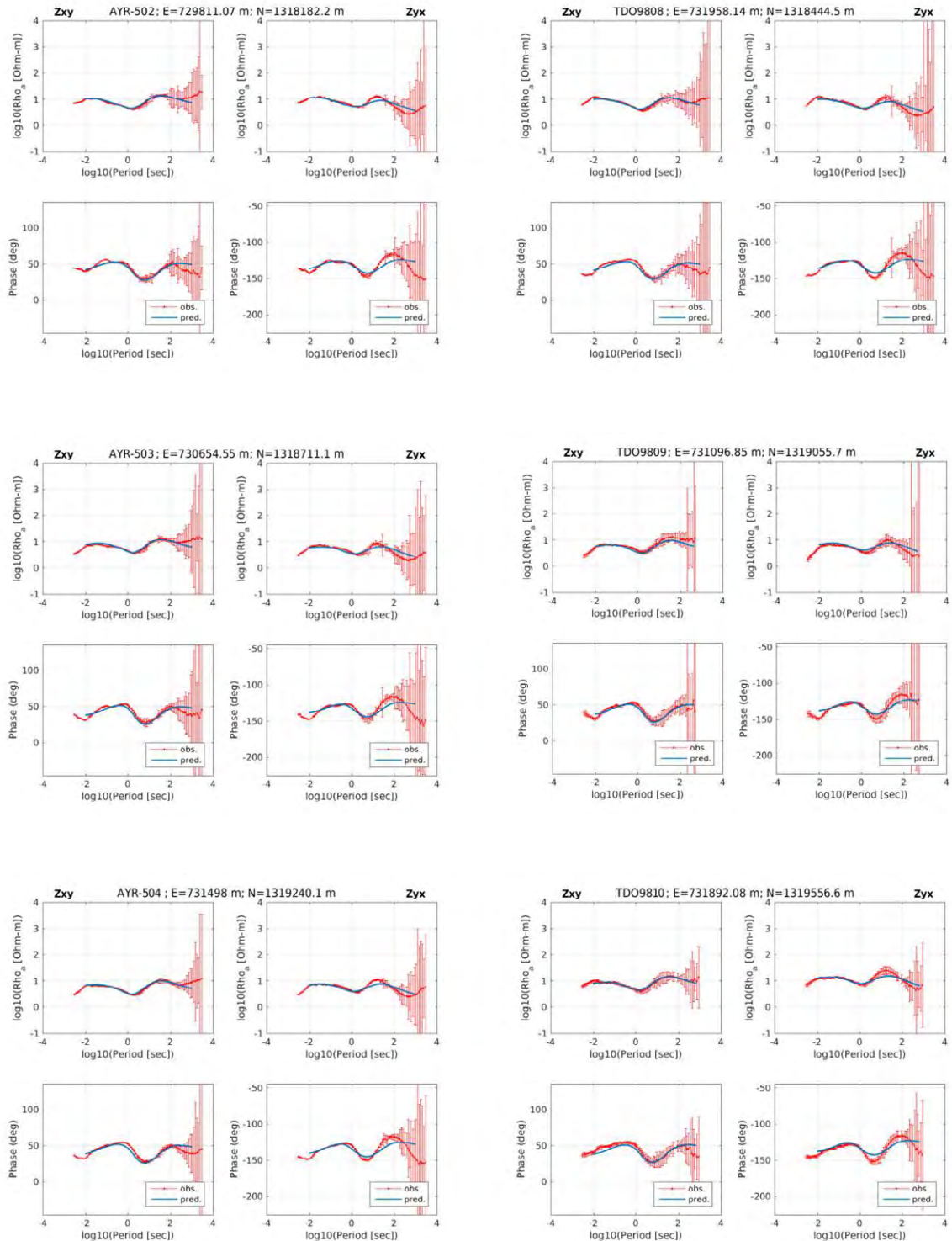
**3D analysis results - Calculated and observed value of apparent resistivity and phase curve (TDO97 3/4)**



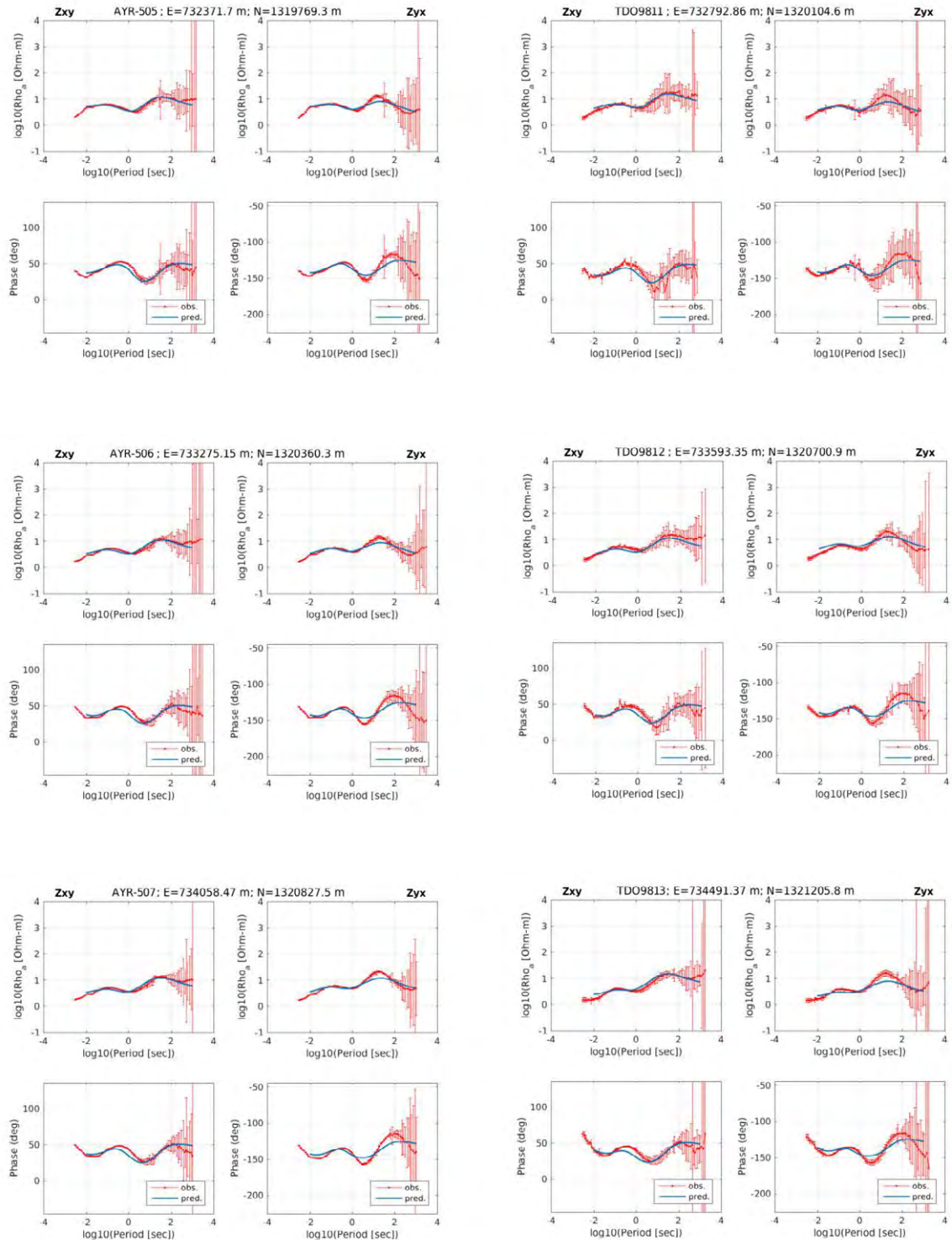
**3D analysis results - Calculated and observed value of apparent resistivity and phase curve (TDO97 4/4)**



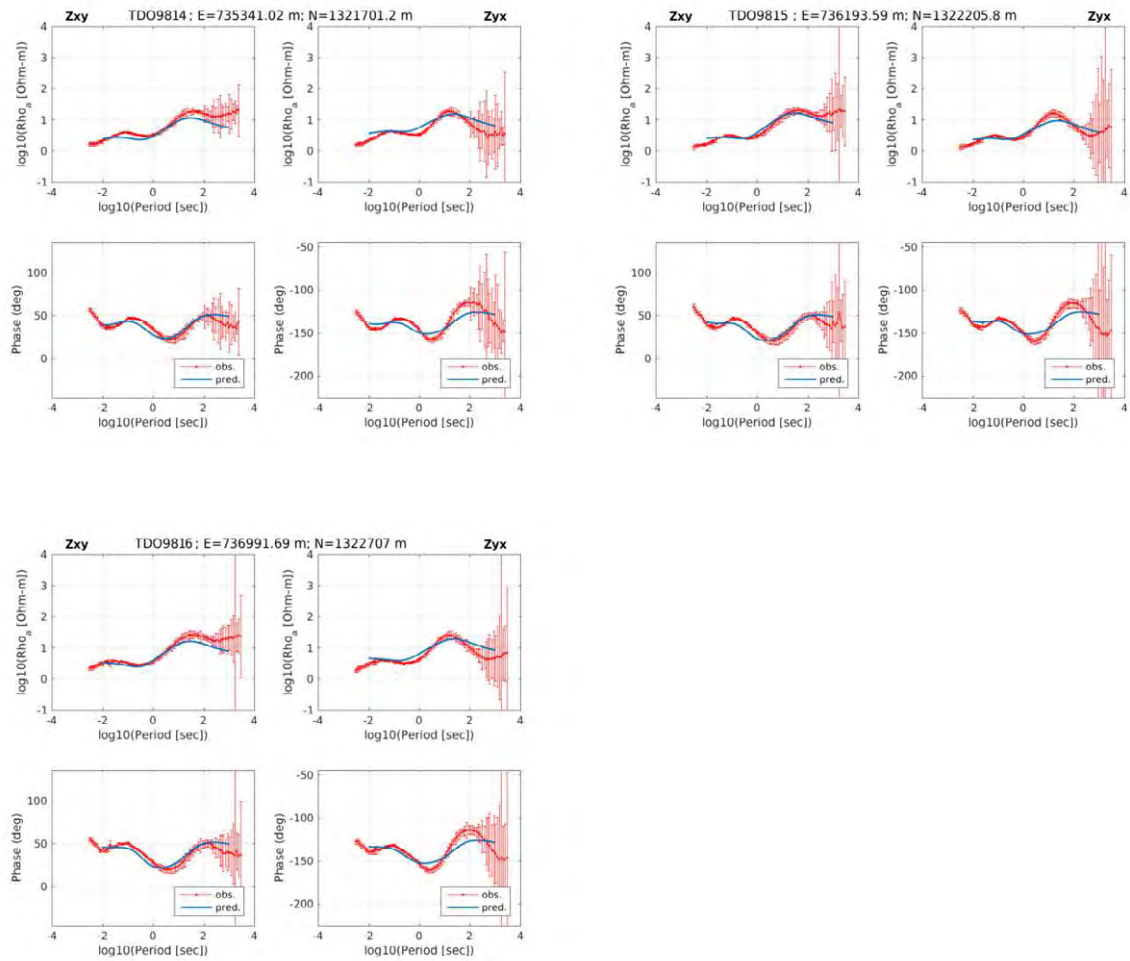
**3D analysis results - Calculated and observed value of apparent resistivity and phase curve (TDO98 1/4)**



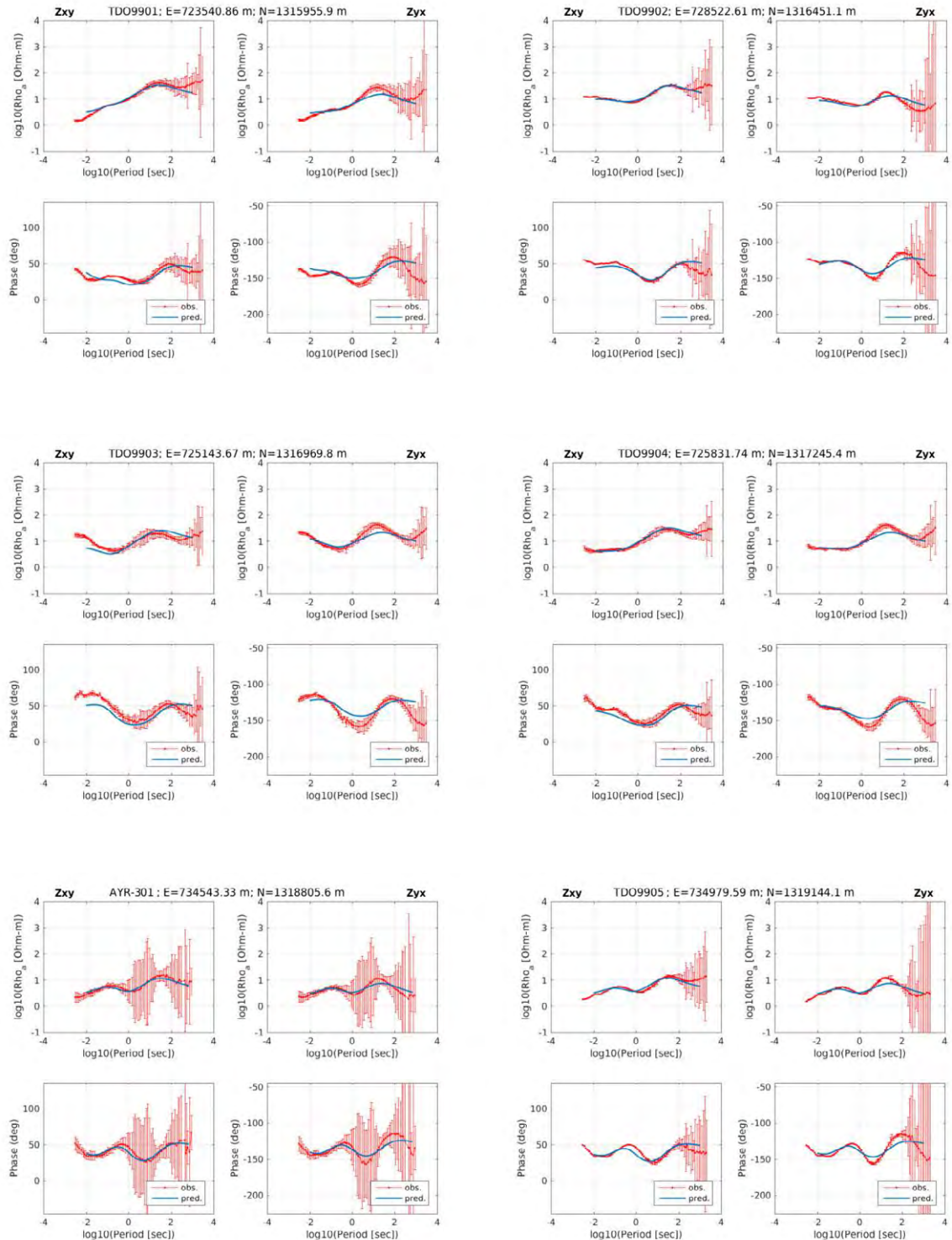
**3D analysis results - Calculated and observed value of apparent resistivity and phase curve (TDO98 2/4)**



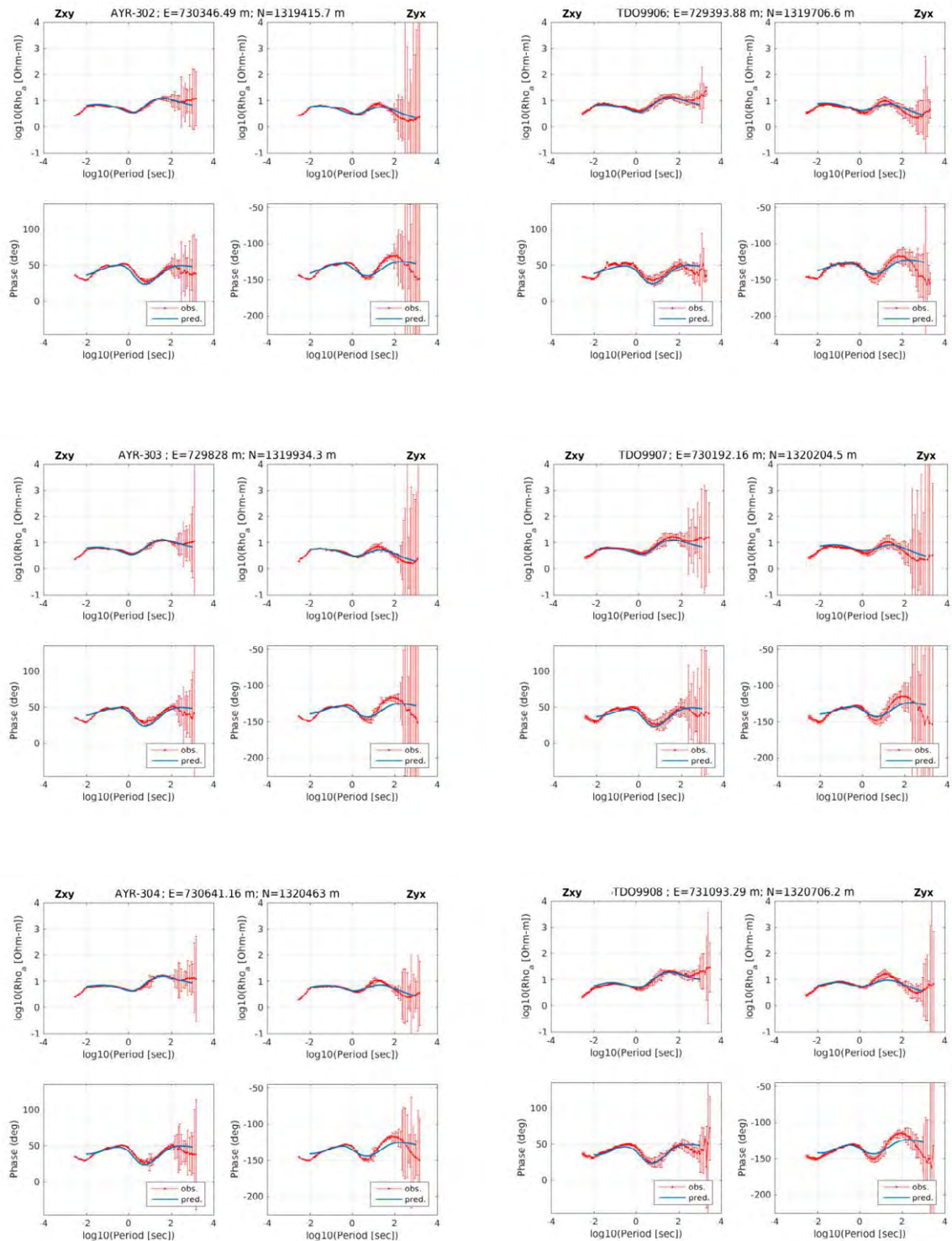
**3D analysis results - Calculated and observed value of apparent resistivity and phase curve (TDO98 3/4)**



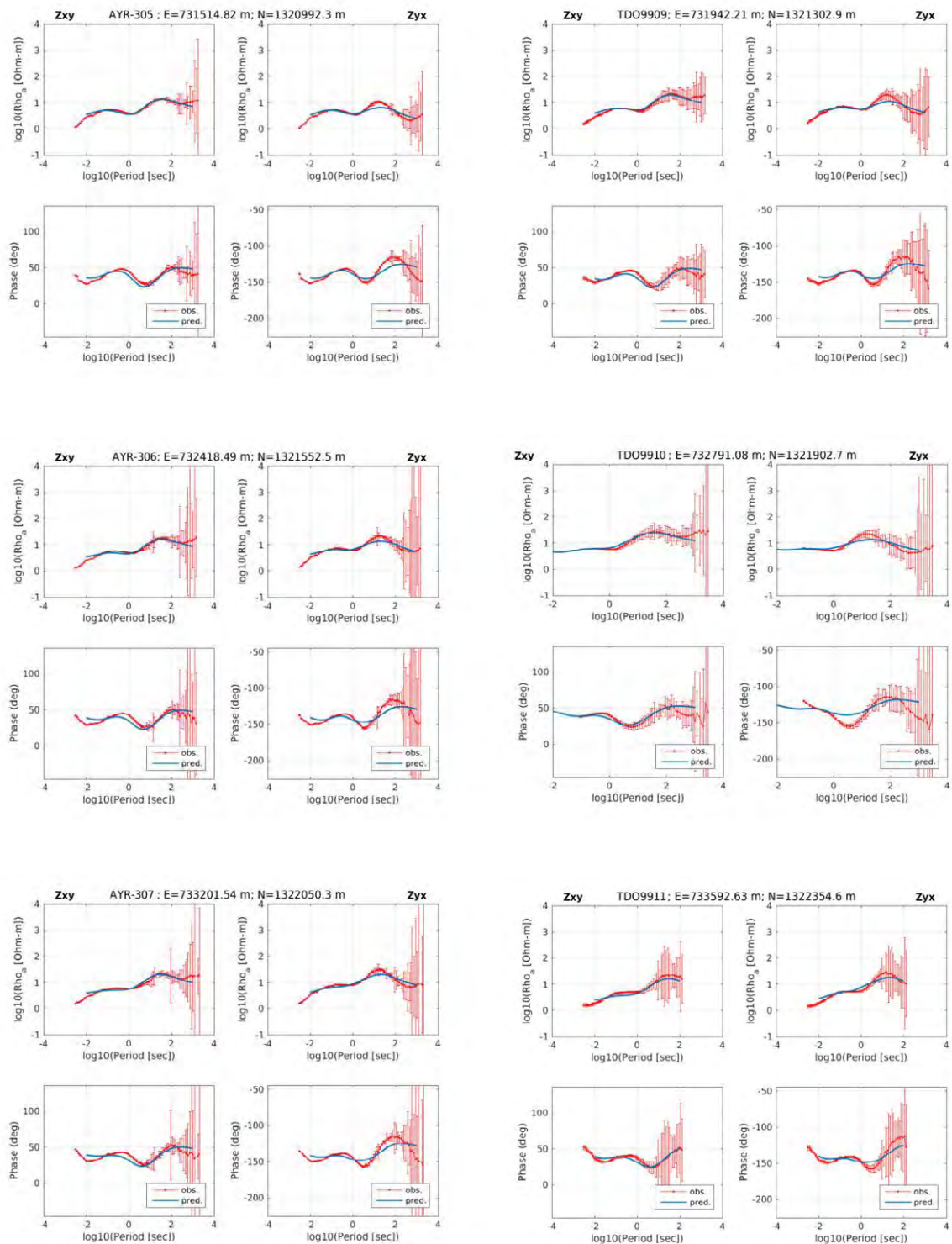
**3D analysis results - Calculated and observed value of apparent resistivity and phase curve (TDO98 4/4)**



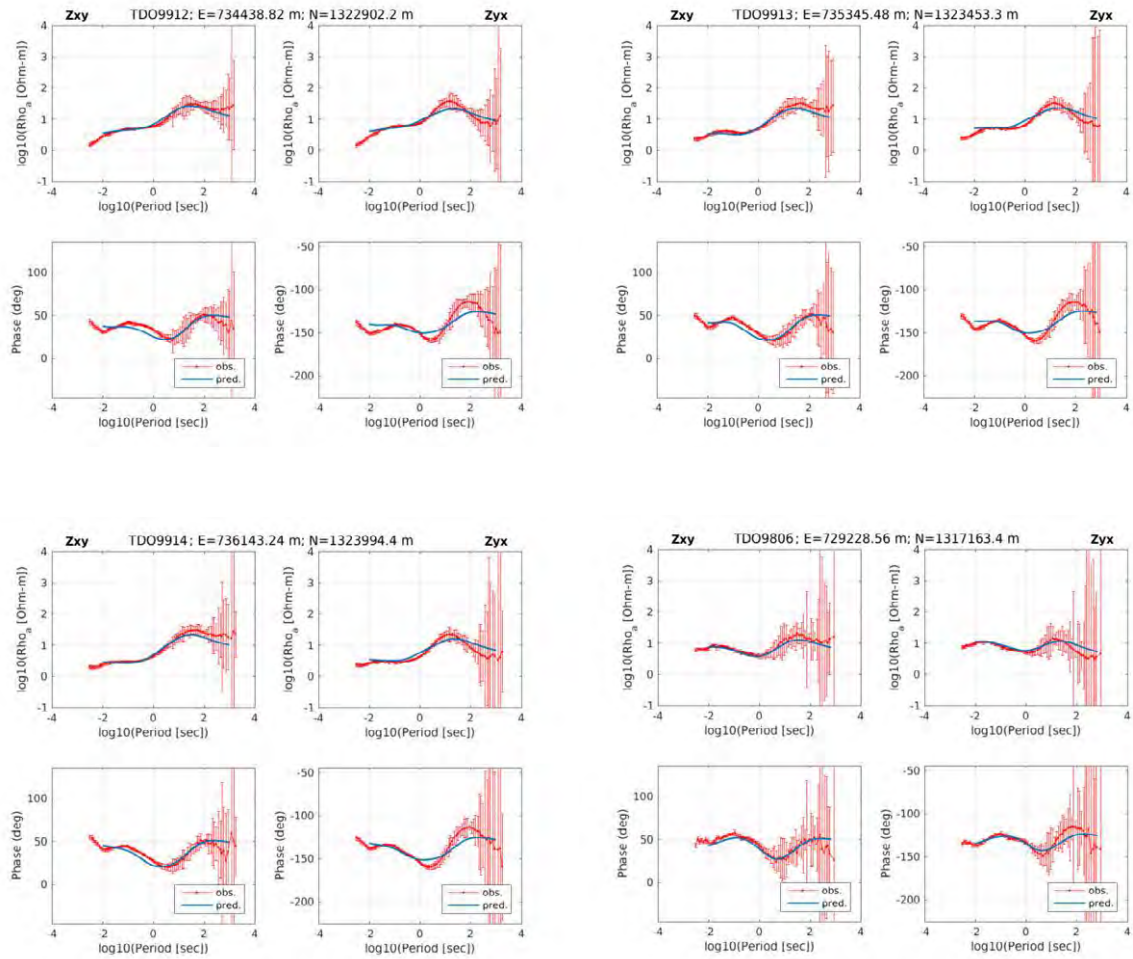
**3D analysis results - Calculated and observed value of apparent resistivity and phase curve (TDO99 1/4)**



**3D analysis results - Calculated and observed value of apparent resistivity and phase curve (TDO99 2/4)**



**3D analysis results - Calculated and observed value of apparent resistivity and phase curve (TDO99 3/4)**



**3D analysis results - Calculated and observed value of apparent resistivity and phase curve (TDO99 4/4)**

## **APPENDIX 3**

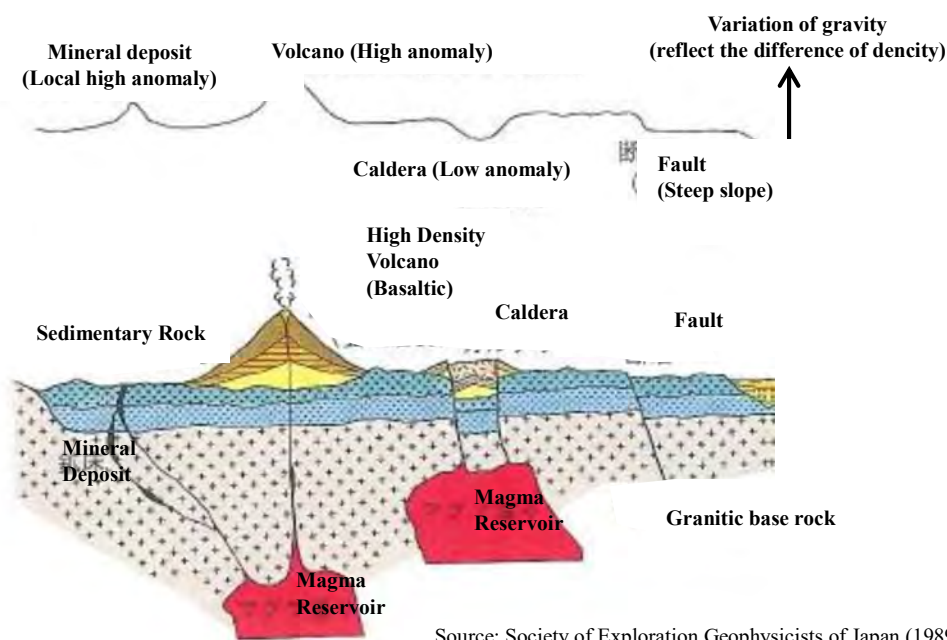
### **Gravity Survey**



## Appendix-3 Methodology and data of gravity survey

### 3.1 Survey Principle

Gravity survey is one of the geophysical survey that estimate subsurface structure using observed weak gravity anomaly caused by the subsurface density distribution. The high gravity anomaly which is observed on the ground is caused by the high density material exist under the ground. In contrast, if the low density material exists under the ground, the gravity anomaly observed on the ground is low. The variation of gravity anomaly is very small compare with the gravity acceleration,  $9.8\text{m/s}^2$  (about  $10^{-4}$  magnifications). On this report, the unit of gravity acceleration and gravity anomaly is expressed by mGal, the unit of density is expressed by  $\text{g/cm}^3$ . Schematic image of gravity anomaly caused by the subsurface structure is shown in Figure.A3.1.1.



Source: Society of Exploration Geophysicists of Japan (1989)

Figure A3.1.1 Relationship Between the Subsurface Structure and the Gravity Anomaly Pattern

### 3.2 Measuring Method

Servo-driven gravimeter "CG-5" of Scintrex was used for the survey. The gravity value of each stations was measured by the relative gravity measurement in closed loop system. On each stations, the reproducibility of measured value is confirmed by repeating measurement, and then, station number, measured date, height of instrument, and topographic cross-section within 20m from the station is mentioned on the note. If the drift value exceeds 0.1mgal, re-measured again. On this survey, there were no available reference station for absolute gravity near the survey area. Therefore, absolute gravity of base station assumed to equal with standard gravity, and measured gravity of each station was calculated.

Together with the gravity survey, leveling survey was conducted to grasp the coordination and elevation in accuracy of several cm. SF-3040 receiver of NavCom was used for the leveling. GNSS leveling was conducted by Static method. The information of gravity base station is as followings.

## Boseti Gravity Base

Station	9999
Latitude (degree, WGS84)	8.527474
Longitude (degree, WGS84)	39.24228
Elevation (m, ellipsoidal)	1689.93
Remarks	Established: February 17, 2016 Kereyu Hill Resort, Adama, Ethiopia

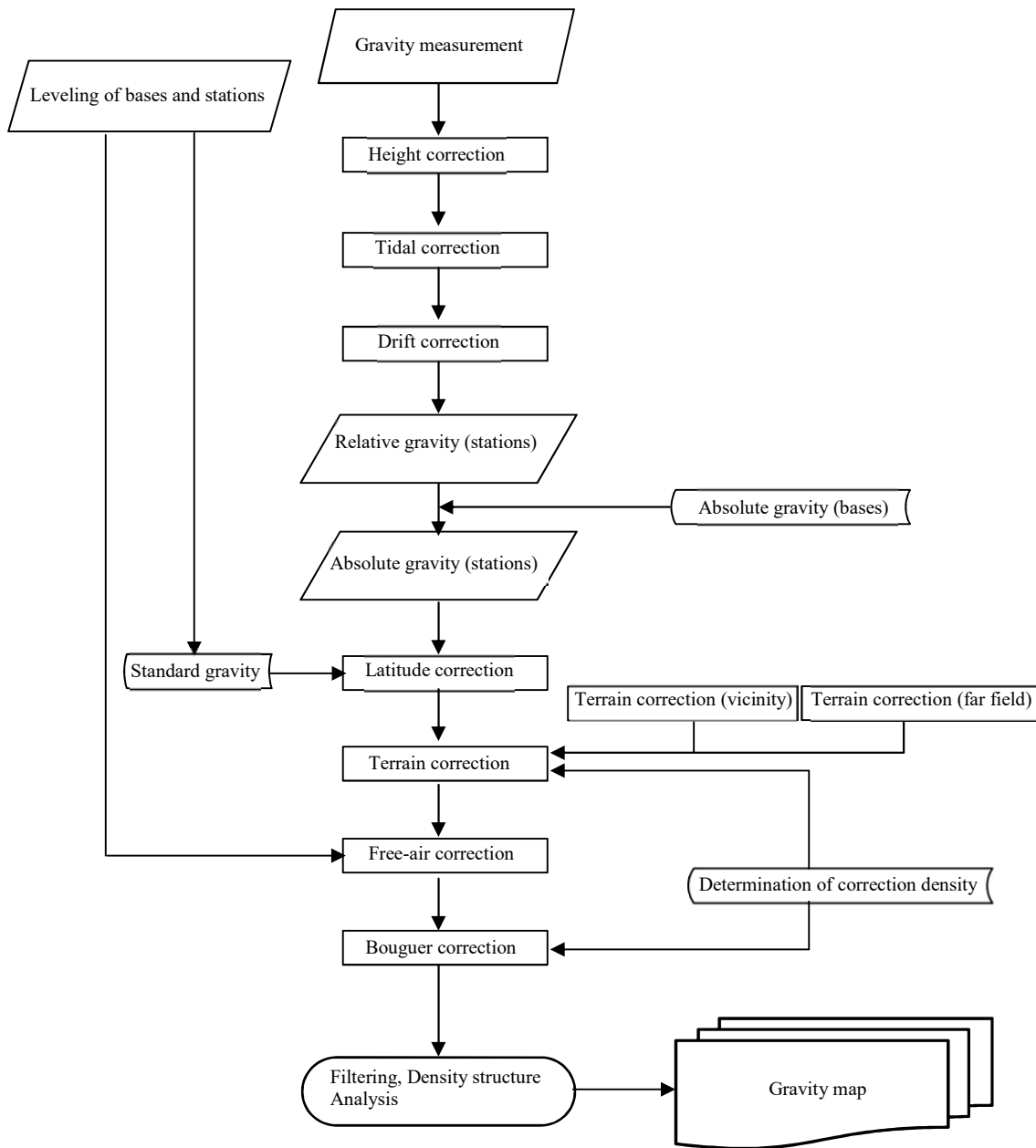


Base was setting in front of the entrance of room 318,Kereyu Hill Resort Hotel (photo).

### 3.3 Data Procedure

#### (1) Calculation of gravity value

Data processing procedure is shown in Figure A3.3.1



Source: JICA Survey Team

**Figure A3.3.1 Data processing procedure of gravity surveys**

Corrected gravity value ( $Gc$ ) is derived by the following equation, applying the correction procedure (described in the following contents A) ~ C)) to gravity value ( $Gr$ ).

$$Gc = Gr + Ghi + Get + Gd$$

$Gr$  : Gravity value at station

$Ghi$  : Instrument height correction

$Get$  : Tidal correction

$Gd$  : Drift correction

#### A) Instrument height correction

Instrument height correction ( $Ghi$ ) is applied by measuring the length between the elevation control point and the top of gravimeter.  $Ghi$  was calculated by the following equation using vertical trend value of the surface of ellipsoid (0.3086mgal/m).

$$Ghi = 0.3086 \times hi$$

$hi$  : height of gravimeter from the elevation control point (m)

#### B) Tidal correction

The gravity values are affected by the attraction of the moon and the sun fluctuating just like the rises and falls of ocean tides.

Tidal correction values ( $Get$ ) are calculated by the following equation.

$$Get = \frac{kma}{\gamma^3} \left\{ 3 \left( \cos \delta \cos \phi \cos \theta + \sin \delta \sin \phi \right)^2 - 1 \right\} \times G$$

$k$  : Gravitational constant       $m$  : Mass of celestial body

$a$  : Equatorial radius of the Earth     $\gamma$  : Distance between the earth and celestial body

$\phi$  : Latitude of point                 $\delta$  : Declination of celestial body

$\theta$  : Hour angle of celestial body     $G$  : G factor (=1.20)

#### C) Drift correction

Measured gravity value shows specific time variations. After applying the instrument height correction and tidal correction for the gravity value on base station, Drift value is estimated in each crossed-loop. Drift correction ( $Gd$ ) is calculated from the drift value which is assumed to be linearly proportional to time.

#### (2) Estimation of bouguer anomaly

Bouguer anomaly ( $\Delta gb$ ) is estimated from the following equation. The method of each correction (A)~D)) is as follows.

$$\Delta gb = Gc - Gsd + \delta G_T + \delta G_F + \delta G_B$$

$G_c$  : Corrected gravity value  
 $G_{sd}$  : Latitude correction  
 $\delta G_T$  : Terrain correction  
 $\delta G_F$  : Free-air correction  
 $\delta G_B$  : Bouguer correction

A) Latitude correction

Latitude correction ( $G_{sd}$ ) is calculated from the standard gravity equation (1980).

$$G_{sd} = 978032.67715 (1 + 0.0052790414 \sin^2 \phi + 0.0000232718 \sin^4 \phi + 0.0000001262 \sin^6 \phi + 0.0000000007 \sin^8 \phi)$$

$\phi$  : Latitude of station

B) Terrain correction

Terrain correction ( $\delta G_T$ ) removes the terrain irregularity of the vicinity of stations. Terrain correction was conducted two correction of “vicinity” and “far-field”. Far-field terrain correction was calculated using 90m grid DEM data of SRTM. And vicinity terrain correction ( $\delta G_{t20}$ ), in the area of 20m, was calculated by the following equation based on the topographical cross-section sketch.

$$\delta G_{t20} = 2G\rho \int_D^R \left\{ \tanh^{-1} \sqrt{\frac{R^2 - X^2}{R^2 + H_0^2}} - \tanh^{-1} \sqrt{\frac{R^2 - X^2}{R^2 + (X \tan \beta + H - H_0 - D \tan \beta)^2}} \right\} dX$$

$G$  : Gravitational constant

$\rho$  : Density

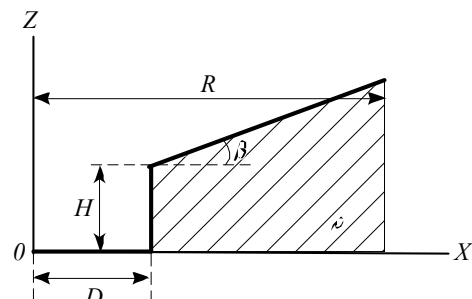
$D$  : Distance between the point and cliff

$H$  : Height of cliff

$\beta$  : Slope angle of cliff

$R$  : Correction area (20m)

$H_0$  : Height of spindle of gravimeter (0.15m)



C) Free-air correction

Free-air correction ( $\delta G_F$ ) removes the gravity difference caused by the difference of elevation.  $\delta G_F$  is calculated by the following equation.

$$\delta G_F = 0.3086h$$

$h$  : Elevation of station (m)

D) Bouguer correction

Bouguer anomaly ( $\delta G_B$ ) is estimated from the following equation. Gravity value measured at the

different elevation varies by the attractive force of rocks which exist in that section.

$$\delta G_B = -0.04192 \gamma h$$

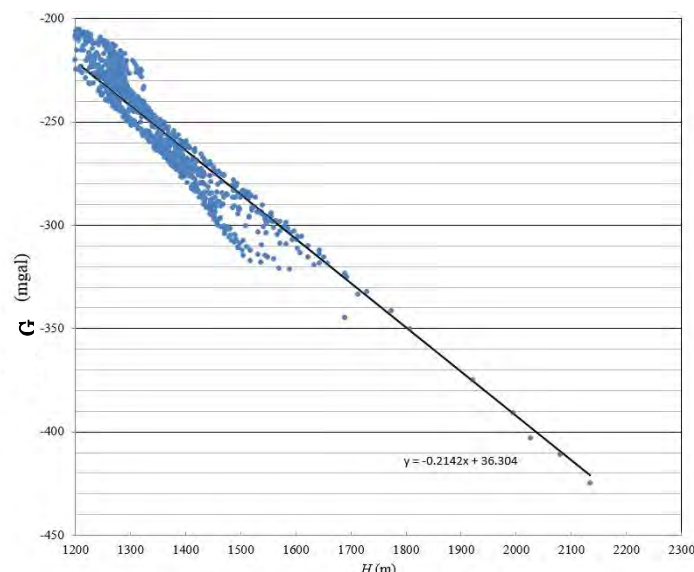
$\gamma$  : Correction density ( $\text{g/cm}^3$ )

$h$  : elevation of station (m)

### (3) Optimum correction density

Optimum correction density was investigated by G-H correlation diagram (Figure A3.3.2) and comparison of bouguer anomaly map applying several correction densities (Figure A3.3.3), in order to create bouguer anomaly map. G-H correlation diagram plots G (see following equation, mGal) against elevation (H) and draw the best fitting linear line in a least squares.

$$G = g_{abs} - g_{nor} + g_{terrain}(\rho)$$



Source: JICA Survey Team

**Figure A3.3.2 G-H correlation diagram**

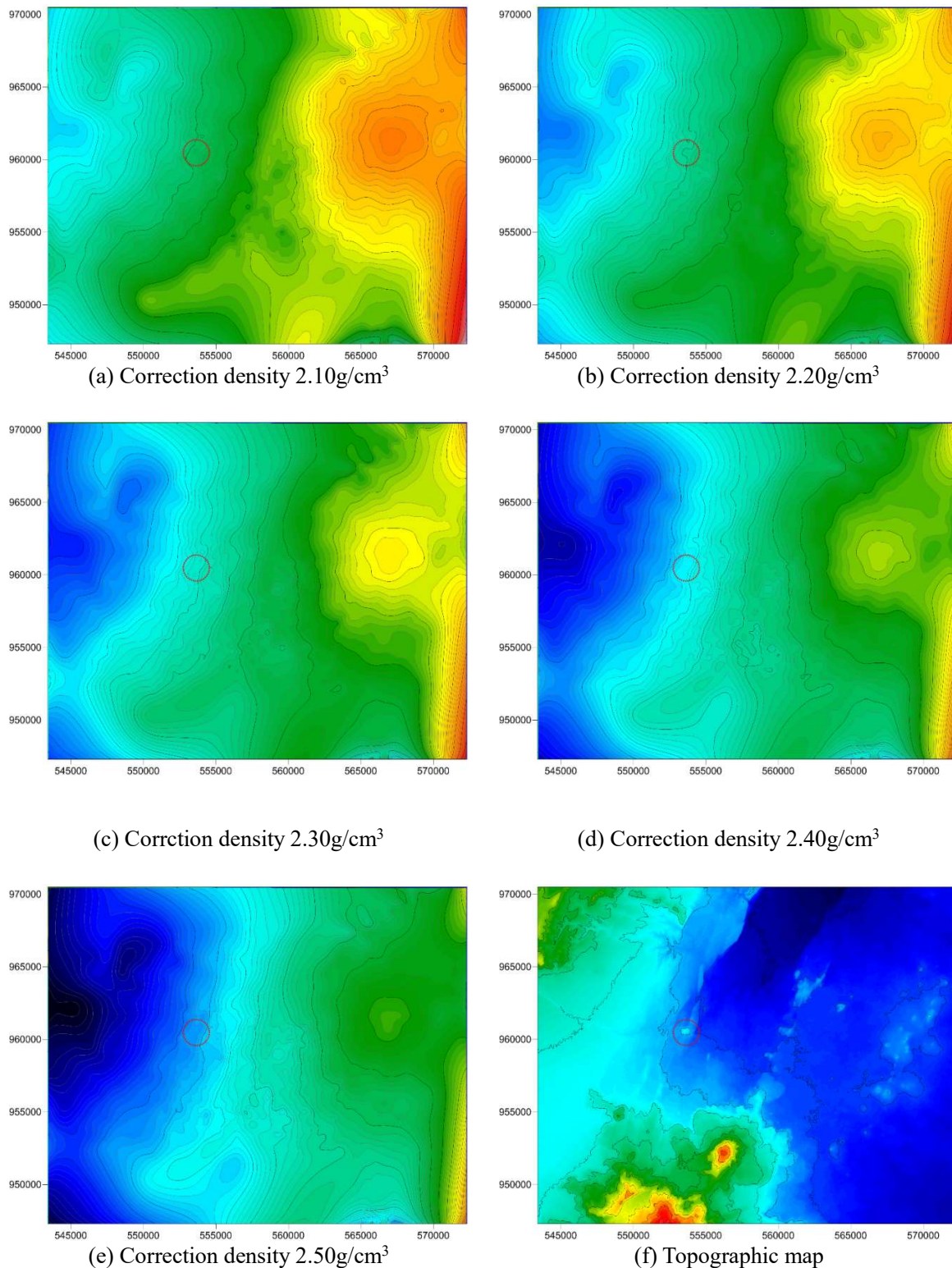
The trend of fitting line (m) is -0.2142. From this value, correction density is estimated about  $2.25 \text{ g/cm}^3$ .

$$\rho = \frac{m + 0.3086}{2\pi K}$$

Where K is gravitational constant,  $\pi$  is the circular constant.

Then, comparing bouguer anomaly map creating by the several correction density between  $2.20 \text{ g/cm}^3$  to  $2.67 \text{ g/cm}^3$  (a~e) with topography map (f). When extracting the base structure, the best density is estimated from that there are no correlation between the pattern of topography and bouguer anomaly map created by that density. From Figure.a3.4, the case of correction density  $2.3 \text{ g/cm}^3$  shows quite small correlation with topographical pattern.

From these results, correction density  $2.30 \text{ g/cm}^3$  was adopted for analysis.



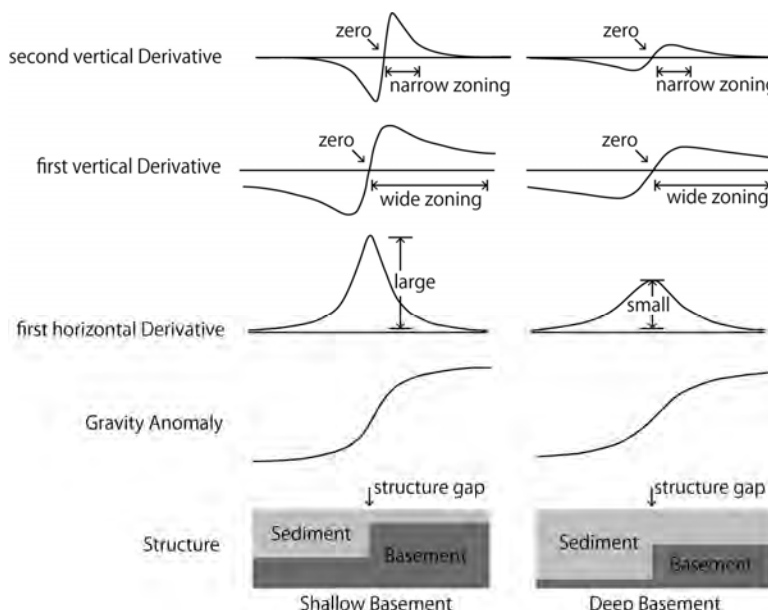
Source: JICA Survey Team

**Figure A3.3.3 The comparison of bouguer anomaly map and topographic map**

### 3.4 Analysis Method

#### (1) Filtering analysis

The filtering analysis was conducted in order to extract several information from Bouguer anomaly distribution. In this survey, filtering analysis was conducted from the 100m grid data made by bouguer anomaly distribution. When considering bouguer anomaly distribution as a kind of wave, short-wavelength anomalies correlating to the gravity anomaly (density information) of the shallow subsurface structure. In this survey, first vertical derivative was adopted in order to extract the subsurface structure shallower than several thousand meter. First vertical derivative distribution could irritably capture the density anomaly structure (Figure A3.4.1). And then, since first vertical derivative value Gzz shows 0 right above the fault, fault line could estimate from this derivative distribution. In addition to the first vertical derivative, filtering analysis of horizontal gradient was conducted. Horizontal gradient is prior to extract the zone which shows significant changes of bouguer anomaly like faults (Figure A3.4.1).



Source: Society of Exploration Geophysicists of Japan (1998)

**Figure A3.4.1 The comparison of first vertical derivative and first horizontal derivative for fault structure**

#### (2) Trend analysis

Bouguer anomaly distribution includes long-wavelength component. In general, long-wavelength component is approximated by high-order polynomial, called trend curve. The difference between bouguer anomaly and trend gravity value on the same point is called residual gravity, it is a kind of low-pass filter. In this survey, trend gravity value ( $gtrend(x, y)$ ) are approximated from bouguer anomaly using least squares method (Figure.a3.6), and trend residual gravity value ( $residual(x, y)$ ) is calculated from the difference between bouguer anomaly value and trend gravity value. 3D density structure analysis, describes in the following contents, was calculated from this trend residual gravity.

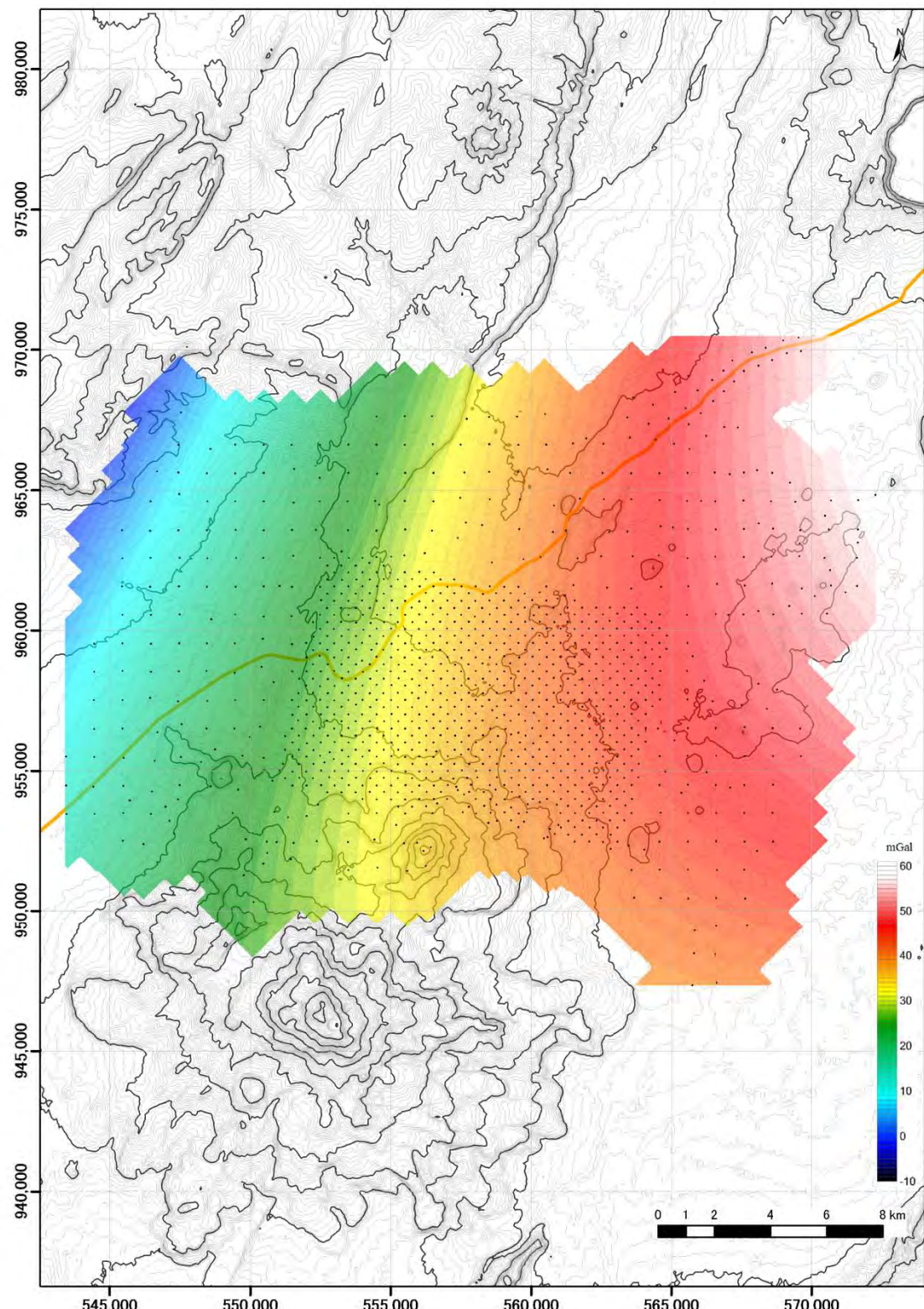
(3) 3D density structure analysis

Gravity value get an influence of attractive force not only below the survey point but also all the surrounding area. But second dimensional inversion is assumed that there is no density change in the vertical direction of cross-section, and differ with actual subsurface structure certainly. Therefore, 3-Dimensional inversion is the best approach to estimate the realistic density structure. In this survey, third dimensional inversion was conducted using VOXIE Earth modeling, which is the gravity analysis module of Oasis montaj (Geosoft).

Input data is terrain data and trend residual gravity data of analysis area.

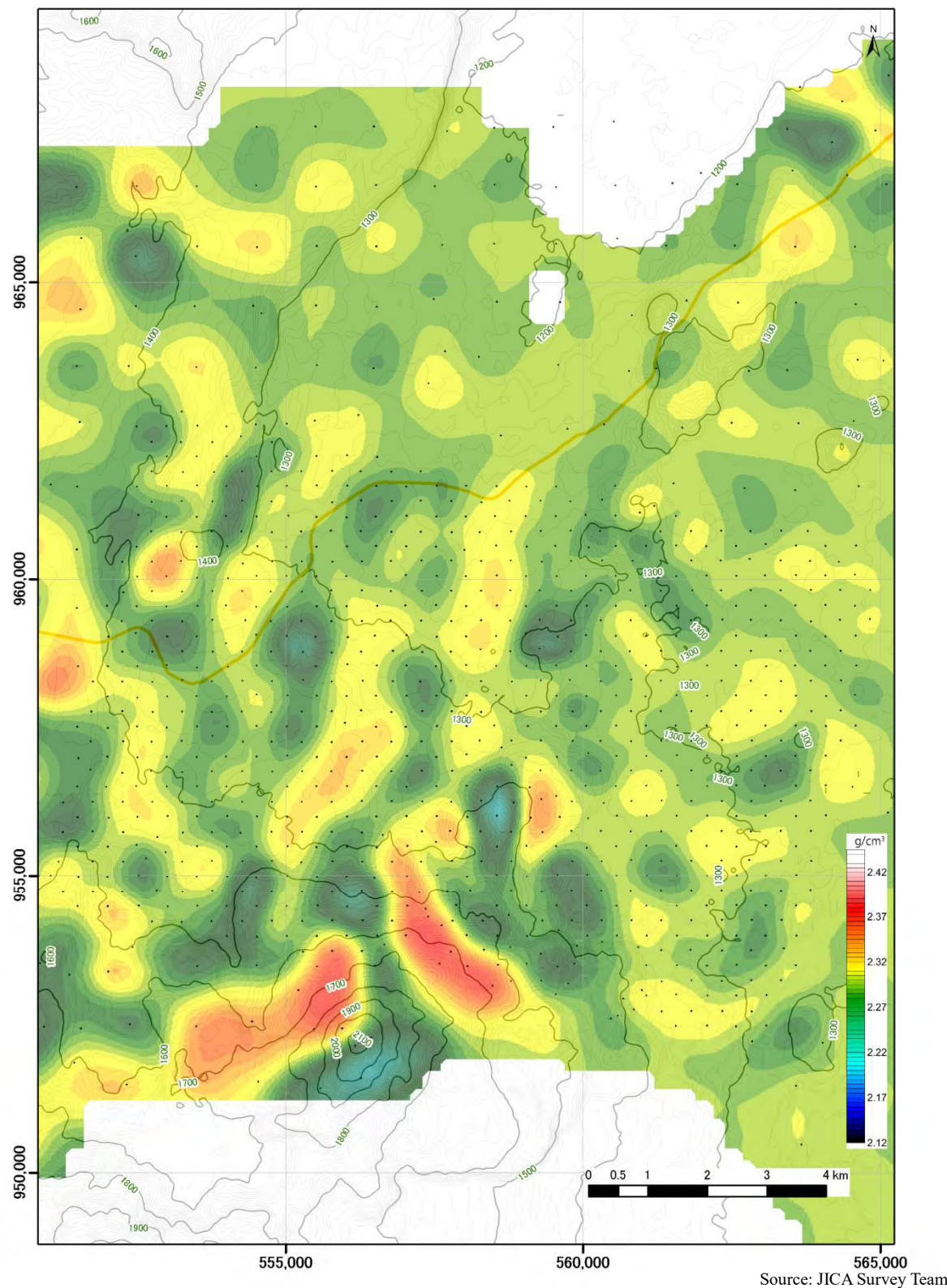
### **3.5 Analysis Method**

Results of gravity survey carried out in this project are shown as below.

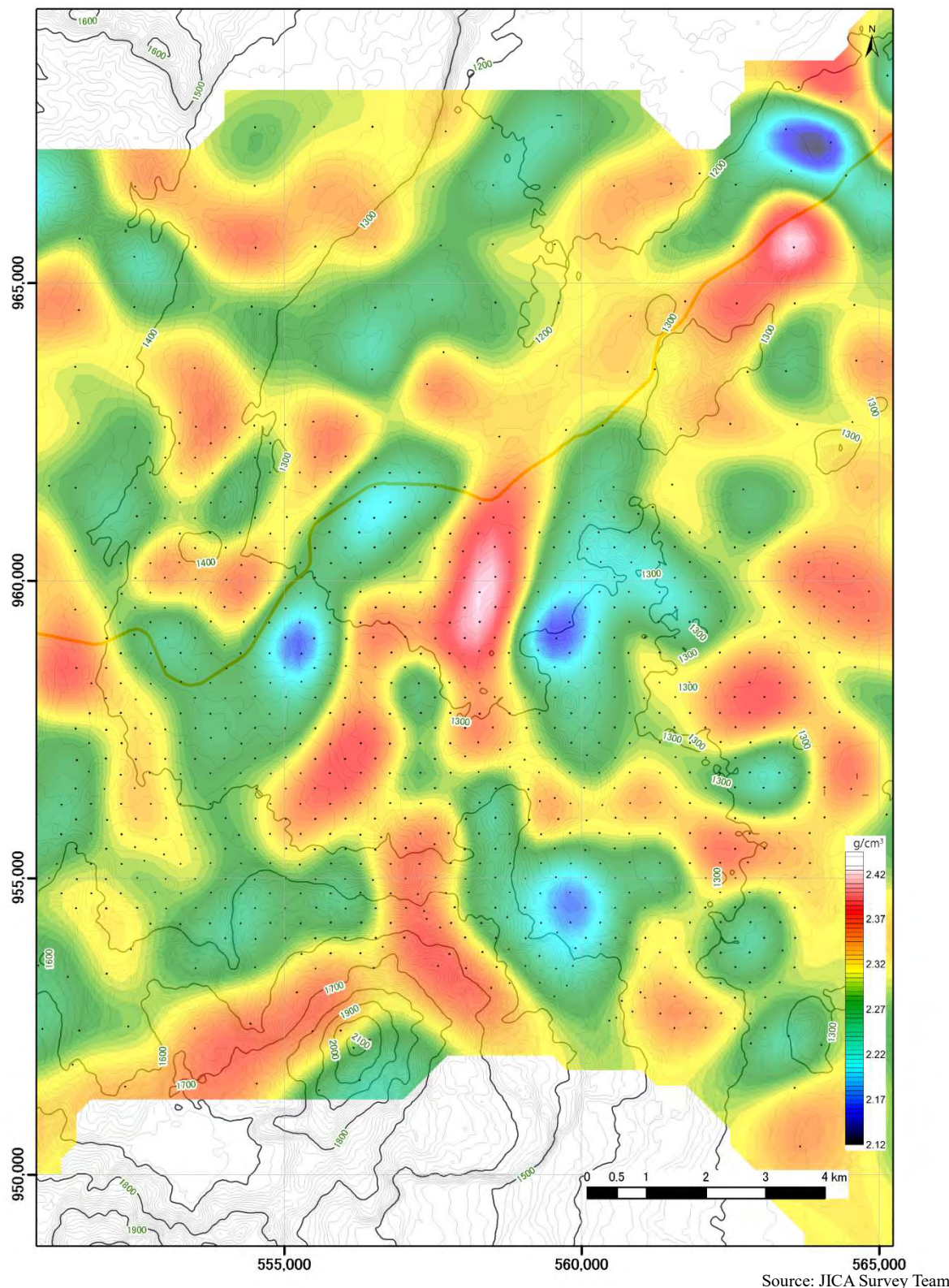


Source: JICA Survey Team

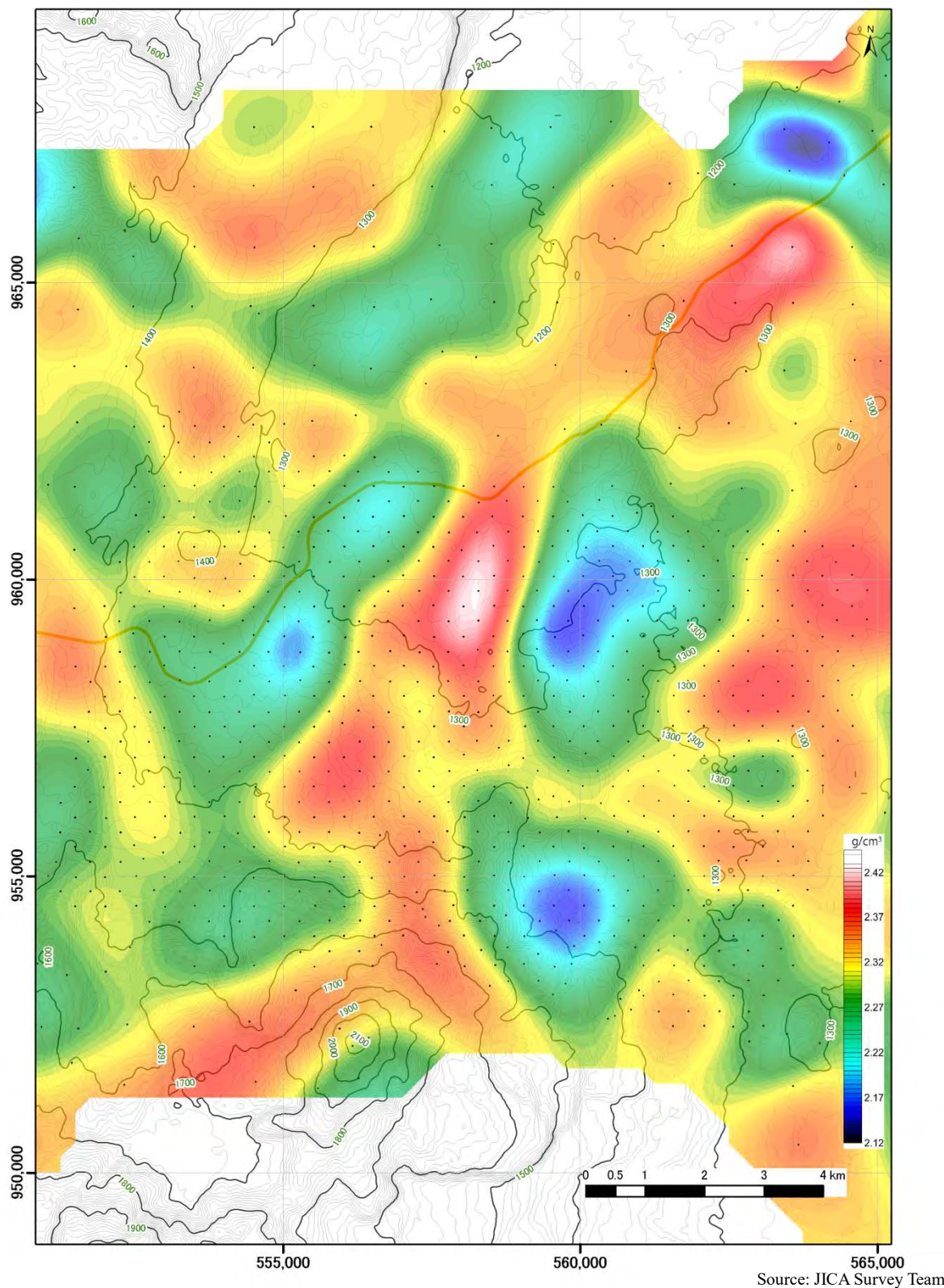
**Secondary trend map**



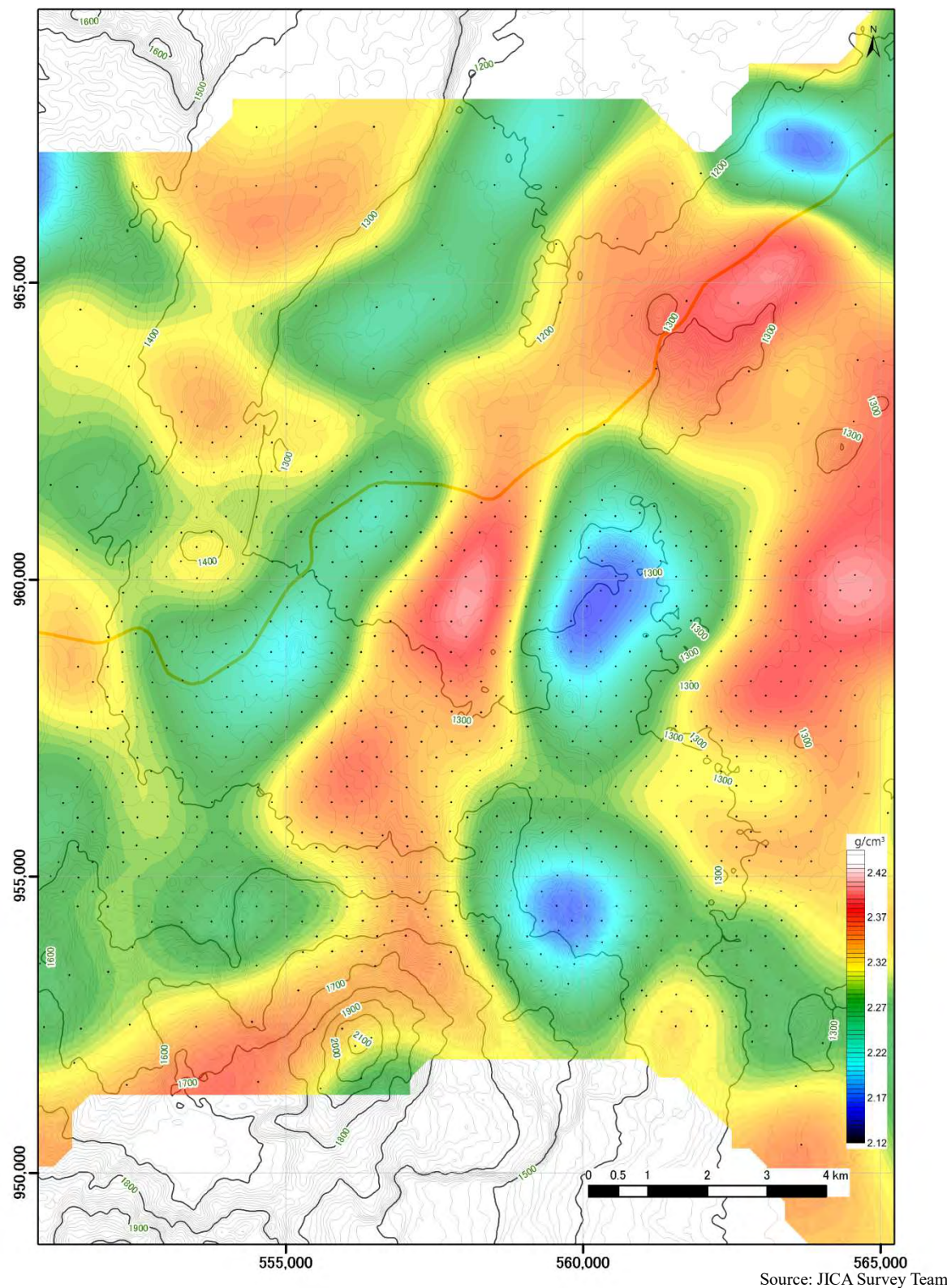
**Density structure map of 3D analysis (1200 m a.s.l)**



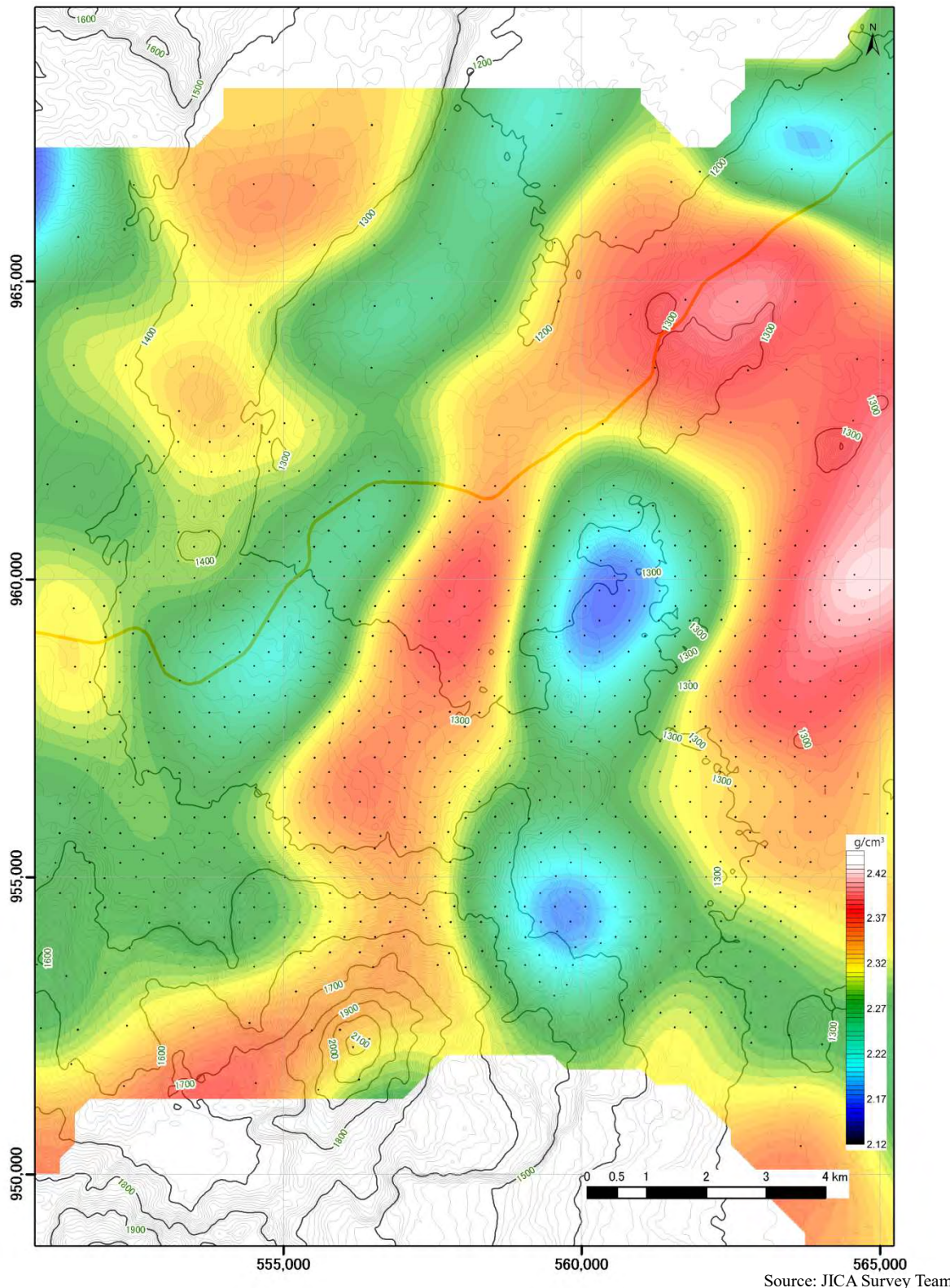
**Density structure map of 3D analysis (500 m a.s.l.)**



**Density structure map of 3D analysis (0 m a.s.l.)**



**Density structure map of 3D analysis (-500 m a.s.l)**



**Density structure map of 3D analysis (-1000 m a.s.l.)**



































